ANALYSIS OF Arabidopsis *AIR12* AND *Brassica carinata CIL1* IN ROOT DEVELOPMENT AND RESPONSE TO ABIOTIC STRESS

A Thesis Submitted to the College of

Graduate Studies and Research

in Partial Fulfillment of the Requirements

for the Degree of Doctor of Philosophy

in the Department of Biology

University of Saskatchewan

Saskatoon

By

Shawn Gibson

PERMISSION TO USE

In presenting this thesis/dissertation in partial fulfillment of the requirements for a Postgraduate degree from the University of Saskatchewan, I agree that the Libraries of this University may make it freely available for inspection. I further agree that permission for copying of this thesis/dissertation in any manner, in whole or in part, for scholarly purposes may be granted by the professor or professors who supervised my thesis/dissertation work or, in their absence, by the Head of the Department or the Dean of the College in which my thesis work was done. It is understood that any copying or publication or use of this thesis/dissertation or parts thereof for financial gain shall not be allowed without my written permission. It is also understood that due recognition shall be given to me and to the University of Saskatchewan in any scholarly use which may be made of any material in my thesis/dissertation.

DISCLAIMER

Reference in this thesis/dissertation to any specific commercial products, process, or service by trade name, trademark, manufacturer, or otherwise, does not constitute or imply its endorsement, recommendation, or favoring by the University of Saskatchewan. The views and opinions of the author expressed herein do not state or reflect those of the University of Saskatchewan, and shall not be used for advertising or product endorsement purposes.

Requests for permission to copy or to make other uses of materials in this thesis/dissertation in whole or part should be addressed to:

Head of the Department of Biology
University of Saskatchewan
Saskatoon, Saskatchewan S7N 5E2
Canada

OR

Dean
College of Graduate Studies and Research
University of Saskatchewan
107 Administration Place
Saskatoon, Saskatchewan S7N 5A2
Canada

ABSTRACT

The development of plants challenged by environmental stress alters plant architecture through several pathways, including those involving plant hormone responses and reactive oxygen species (ROS) production. Auxin, a phytohormone associated with every aspect of development, and abscisic acid (ABA), a phytohormone involved in abiotic stress responses, both interact with ROS. These ROS are used as secondary messengers to activate transcription of abiotic stress genes, and also in developmental responses such as cell elongation. To understand the mechanisms involved in the abiotic stress response and how the response intersects with auxin, ABA, and ROS, I examined *COPPER INDUCED IN LEAVES 1* (*CIL1*) from *Brassica carinata* and its Arabidopsis orthologue, *AUXIN INDUCED IN ROOTS 12* (*AIR12*). Expression of both genes increases in response to auxin and recent work has placed both CIL1 and AIR12 within a family of plant-specific cytochrome *b*561 proteins thought to be involved with transmission of ROS signals. This suggests a link between auxin and ROS production resulting from abiotic stress. Antisense *CIL1 B. carinata* plants produced fewer lateral roots and were resistant to salinity stress during vegetative growth. Mutant *air12* plants showed a 50% reduction in lateral root number, lateral root length, and H_2O_2 root distribution. Growth in the presence of H_2O_2 was able to restore lateral root length to control levels. *In silica* analysis of the CIL1 and AIR12 amino acid sequences detected an attachment site for glucosylphosphatidylinositol, predicting that the protein is targeted to the extracellular leaflet of the plasma membrane where it could be cleaved and released into the apoplast. Subcellular localization using *p35S::GFP-CIL1* and *p35S::GFP-AIR12* translational fusions confirmed that CIL1 and AIR12 localize to the plasma membrane and are released into the apoplast. Organ localization of AIR12 using the *pAIR12::GFP-AIR12* construct in stably transformed Arabidopsis showed fusion protein accumulation in the apex of the primary root and in the vascular tissue. Fusion protein also localized to cells flanking emerging lateral roots. Investigation of *pAIR12::GUS* Arabidopsis showed GUS accumulation in the apex of elongating lateral roots. I demonstrate that AIR12 is an extracellular protein and that *air12* seedlings are susceptible to salt stress, but not osmostic stress and display increased and decreased sensitivity to ABA during germination and primary root elongation, respectively, suggesting that AIR12 acts downstream of abiotic stress recognition.

ACKNOWLEDGEMENTS

I'd like to take this opportunity to express my gratitude and thanks to the droves of people who supported me in the achievement of this degree. Foremost, Dr. Janet Taylor, for allowing me to tackle such an interesting and challenging project that allowed me to develop proficiencies in a wide range of molecular techniques and physiological analyses. Her advice about how to live while completing a science degree, dealing with government, and seeking employment was extremely valuable and helped me learn more than just science over the 6 years we worked together.

My heartfelt thanks also extend to Dr. Christopher Todd, who entered my committee first as a co-supervisor, and then as my primary supervisor after Janet's passing. Without his assistance, guidance, and patient editing, this thesis would have been very different.

Thanks also extend to my external examiner Dr. Elizabeth Schultz for her insightful questions and to my advisory committee: Dr. Peta Bonham-Smith, Dr. Yangdou Wei, Dr. Michele Loewen, and Dr. Pierre Fobert for their comments and suggestions that were instrumental to the completion of this degree. Thanks also extend to both the Department of Biology and PBI for assisting me after Janet Taylor's passing. Numerous colleagues in PBI and the Biology Department are appreciated for their technical and moral support. This includes, but is not limited to, Janet Condie, Carla Barber, Steve Gagne, Devin Polichuk, and Melanie Dauk.

I also wish to thank and acknowledge the support and encouragement of my family and friends. Without them, this degree would have been impossible. Specifically, the members of my immediate family: Dave (dad), Lorraine (mom), Zach, Raelynn, and my two dogs, Douglas and Bergen. Of my friends, Darcy Brower, Christopher Keating, and Mike Urmson deserve special note for being encouraging and not making (too many) jokes at my seemingly perpetual student status. Patricia Vrinten taught me molecular techniques and work ethic that I still possess today, and I thank her for that tumultuous time as her summer student.

Extra-special thanks go to Sharla Lozinsky, the love of my life. Without her encouragement, understanding, and support I would not have been able to complete my degree. Her practicality, precision, and perspicacity aided me greatly whenever I had problems with one experiment or another.

And finally, this thesis is dedicated to my first supervisor, Dr. Janet Taylor, who passed away during my Ph.D. work. When she passed away I lost more than a supervisor and mentor – I lost a treasured friend.

TABLE OF CONTENTS

PERMISSION TO USE i
ABSTRACT ii
ACKNOWLEDGEMENTS iii
TABLE OF CONTENTS v
LIST OF TABLES ix
LIST OF FIGURES x
LIST OF ABBREVIATIONS xiv
1. INTRODUCTION 1
2. LITERATURE REVIEW 2
2.1 What is a plant hormone? 2
2.2 Auxin 2
2.2.1 Auxin influx 4
2.2.2 Auxin efflux 5
2.2.3 Molecular mechanisms of auxin response 8
2.2.3.1 Aux/IAA proteins 8
2.2.3.2 Auxin response elements 11
2.2.3.3 Auxin perception 12
2.3 Abscisic acid 14
2.3.1 Model of ABA action 14
2.3.2 Abscisic acid perception 15
2.3.3 Signaling during abiotic stress 16
2.3.3.1 Water limitation and drought stress 16
2.3.3.2 Salinity 18
2.4 Reactive oxygen species 19
2.4.1 Generation 19
2.4.2 Detoxification 20
2.4.3 Developmental activity 22
2.5 Root development 24
2.5.1 Lateral root development 25
2.6 Glucosylphosphatidylinositol-anchored proteins 28
2.6.1 Biosynthesis 28
2.6.2 Developmental roles 30
2.7 Auxin, ABA, and ROS control root development 32
2.7.1 Auxin and ABA cross talk 32
2.7.2 Hormonal interactions with ROS 33

2.8 The current study 35
3. MATERIALS AND METHODS 37
3.1 Description of lines used 37
3.1.1 Plant material and growth conditions 37
3.1.2 Seed sterilization and growth medium 39
3.1.3 Germination and root measurement 39
3.2 Arabidopsis *air12* lines were generated by Ac/Ds-mediated mutagenesis 40
3.3 Plant transformation 40
3.3.1 Transient infiltrations 41
3.3.2 Selection of transgenic Arabidopsis 41
3.4 *In silica* analysis of AIR12/CIL1 42
3.5 DNA Isolation 43
3.5.1 Small scale DNA preparations 43
3.5.2 RNA sample preparations 44
3.6 Recombinant DNA preparation 44
3.6.1 PCR amplification 45
3.6.2 RT-PCR amplification 45
3.6.3 Cloning of PCR products 47
3.7 Construct assembly 47
3.7.1 Assembly of 35S::GFP-CIL1 50
3.7.2 Assembly of 35S::GFP-AIR12 51
3.7.3 Assembly of 35S::GFP 53
3.7.4 Assembly of pAIR12::GFP-AIR12 53
3.7.5 Assembly of pAIR12::GFP 56
3.8 Identification of detergent insoluble membranes in *Brassica carinata* 57
3.8.1 Electrophoretic analysis of detergent insoluble membranes 57
3.9 Microscopy 58
3.9.1 GUS Staining 58
3.10 Analysis of ROS in *Brassica carinata* 59
3.11 Arabidopsis catalase activity and hydrogen peroxide levels 60
4. RESULTS 62
4.1 *Brassica carinata* antisense *CIL1* plants display altered root growth and response to hormones 62
4.1.1 *CIL1* antisense plants show increased salinity tolerance 62

4.1.2 Reduced steady state reactive oxygen species in *CIL1* antisense plants.....66
4.2 CIL1 is a glucosylphosphatidylinositol-anchored protein (GPI-AP) 68
4.3 Analysis of *Brassica carinata* detergent insoluble membranes did not detect CIL1 .70
4.4 Arabidopsis AUXIN INDUCED in ROOTS12 shows identity with CIL1 72
4.5 Genotypic analysis of Arabidopsis *air12* mutants.....72
4.6 AIR12 and CIL1 localize to the plasma membrane and apoplast 74
4.7 AIR12 localizes to the outer epidermal cell file in stably transformed Arabidopsis..82
4.7.1 AIR12 localization on control medium.....82
4.7.2 GFP-AIR12 localization on medium supplemented with hydrogen peroxide 89
4.7.3 GFP-AIR12 localization on medium supplemented with auxin 92
4.7.4 GFP-AIR12 localization on medium supplemented with KCl 96
4.8 *AIR12* expression is induced by auxin.....101
4.9 Root development is reduced in *air12* seedlings.....106
4.9.1 Effect of treatment on primary root growth 113
4.9.2 Effects of treatment on lateral root number 124
4.9.3 Lateral root elongation is reduced in *air12-1* seedlings.....128
4.10 Catalase activity increased and H_2O_2 concentration decreased in *air12-1* plants ...133
4.10.1 Catalase activity is altered in *air12* mutants 133
4.10.2 Hydrogen peroxide activity is unaffected in *air12-1* seedlings 134
4.11 *air12* seedlings display reductions in extra- and intracellular ROS 140
4.11.1 Imaging of Nössen Arabidopsis.....142
4.11.2 Imaging of Ler Arabidopsis 142
5. DISCUSSION.....150
5.1 *AIR12* and *CIL1* play a role in root development.....150
5.1.1 Action of *AIR12*/*CIL1* during auxin-induced root development.....153
5.1.2 Interplay between auxin and abscisic acid during lateral root development.....157
5.1.3 Involvement of ROS during auxin and ABA-induced lateral growth.....158
5.2 Role of ROS in plant development.....162
5.2.1 The NOX enzyme complex and *air12*/antisense *CIL1* 163
5.3 Induced developmental changes by hormonal or abiotic stress treatment 165
5.4 A model for AIR12/CIL1 GPI-APs in ROS signalling 169
5.5 Significance 176
6. CONCLUSIONS.....177
7. FUTURE DIRECTIONS 179

8. REFERENCES 180

LIST OF TABLES

Table 3.1. Description of Arabidopsis lines used 38
Table 3.2. List of primers used during the present study.....46
Table 4.1. Summary of fluorescence observed in *Ds* and *air12-1 pAIR12::GFP-AIR12* Arabidopsis 83
Table 4.2. Summary of GUS accumulation in *air12-1* Arabidopsis.....102
Table 4.3. Summary of qualitative determination of superoxide accumulation in Nössen and Landsberg *erecta* Arabidopsis ecotypes 141

LIST OF FIGURES

Figure 2.1. Generalized structure of Aux/IAA proteins and auxin response factors 10
Figure 3.1. Vector map of the pER310 binary vector used in this study 48
Figure 3.2. Flowchart outlining the assembly of *GFP-AIR12* 54
Figure 4.1. Diminished lateral roots of AC seedlings 63
Figure 4.2. Response of AC seedlings to auxin and abscisic acid 64
Figure 4.3. *Brassica carinata* control and antisense *CIL1* response to salt stress during germination and vegetative growth 65
Figure 4.4. Analysis of ROS constituents AC plants 67
Figure 4.5. *In silica* analysis of CIL1 69
Figure 4.6. Two-dimensional SDS-PAGE of *Brassica carinata* GPI-APs after digestion with phospholipase C 71
Figure 4.7. Clustal W alignment of the AIR12 and CIL1 amino acid sequences 73
Figure 4.8. Graphical representation of *AIR12 Ac*/*Ds* insertion positions in 4 Arabidopsis lines 75
Figure 4.9. Graphical representation of 4 assembled constructs 76
Figure 4.10. Localization of GFP-CIL1 fusion protein in stably transformed Arabidopsis 78
Figure 4.11. Localization of GFP-CIL1 fusion protein in stably transformed Arabidopsis leaves 79
Figure 4.12. Localization of GFP-CIL1 fusion protein in stably transformed Arabidopsis roots after plasmolysis with 2% NaCl 80
Figure 4.13. Extracellular localization of GFP-CIL1 and GFP-AIR12 in stably transformed Arabidopsis roots following plasmolysis with 800 mM sorbitol 81
Figure 4.14. Localization of GFP-AIR12 in Arabidopsis (*Ds*) stably transformed with *pAIR12::GFP-AIR12* 84
Figure 4.15. Localization of GFP-AIR12 to the cell margins in hypocotyls and leaf epidermis of Arabidopsis (*Ds*) stably transformed with *pAIR12::GFP-AIR12* 85
Figure 4.16. Localization of GFP-AIR12 in primary roots of Arabidopsis (*Ds*) stably transformed with *pAIR12::GFP-AIR12* 87
Figure 4.17. Localization of GFP-AIR12 in lateral roots of Arabidopsis *Ds* and *air12-1* stably transformed with *pAIR12::GFP-AIR12* 88

Figure 4.18. Localization of GFP-AIR12 in roots of Arabidopsis *Ds* and *air12-1* stably transformed with *pAIR12::GFP-AIR12* on H_2O_2 90
Figure 4.19. Localization of GFP-AIR12 in lateral roots of Arabidopsis *Ds* and *air12-1* stably transformed with *pAIR12::GFP-AIR12* on H_2O_2 91
Figure 4.20. Localization of GFP-AIR12 in primary and lateral roots of Arabidopsis *Ds* stably transformed with *pAIR12::GFP-AIR12* on α-NAA 93
Figure 4.21. Localization of GFP-AIR12 in lateral roots of Arabidopsis *Ds* and *air12-1* stably transformed with *pAIR12::GFP-AIR12* on α-NAA 94
Figure 4.22. Localization of GFP-AIR12 to root hairs of Arabidopsis *Ds* and *air12-1* stably transformed with *pAIR12::GFP-AIR12* on α-NAA 95
Figure 4.23. *AIR12* expression after treatment with NaCl using the eFP browser 97
Figure 4.24. Localization of GFP-AIR12 in primary roots of Arabidopsis *Ds* and *air12-1* stably transformed with *pAIR12::GFP-AIR12* on KCl 98
Figure 4.25. Localization of GFP-AIR12 in roots of Arabidopsis *Ds* stably transformed with *pAIR12::GFP-AIR12* on KCl.....99
Figure 4.26. Localization of GFP-AIR12 in lateral roots of Arabidopsis *Ds* and *air12-1* stably transformed with *pAIR12::GFP-AIR12* on KCl 100
Figure 4.27. Transcript accumulation of GUS in *air12-1* Arabidopsis plants.....103
Figure 4.28. Transcript accumulation of GUS in *air12-1* and *air12-3* Arabidopsis seedlings on α-NAA 104
Figure 4.29. X-Gluc-stained *Ds* Arabidopsis on α-NAA 105
Figure 4.30. *Ds* and *air12-1* roots after growth on water-flooded filter paper for 5 days 108
Figure 4.31. Germination frequency of Arabidopsis *Ds* and *air12-1* seeds over a 9 day period on control media, or media supplemented with mannitol, KCl, or nitrate. 109
Figure 4.32. Germination frequency of Arabidopsis *Ds* and *air12-1* seeds over a 9 day period on control media, or media supplemented with α-NAA, 2,4-D, 1 mM H_2O_2 or 3.5% sucrose.....111
Figure 4.33. Germination frequency of Arabidopsis *Ds* and *air12-1* seeds on medium supplemented with abscisic acid over 9 days 112
Figure 4.34. Mean primary root length of vertically grown Arabidopsis *Ds* and *air12-1* seedlings.....114

Figure 4.35. Effect of control medium on vertically grown Arabidopsis *Ds* and *air12-1* mean primary root length....115
Figure 4.36. Effect of mannitol on mean primary root length on vertically grown Arabidopsis *Ds* and *air12-1*....116
Figure 4.37. Effect of KCl on mean primary root length of vertically grown Arabidopsis *Ds* and *air12*-1....117
Figure 4.38. Effect of H_2O_2 on mean primary root length of vertically grown Arabidopsis *Ds* and *air12-1*....118
Figure 4.39. Effect of additional 3.5% sucrose (w/v) on mean primary root length of vertically grown Arabidopsis *Ds* and *air12-1*....119
Figure 4.40. Effect of nitrate (KNO_3 and NH_4NO_3) on mean primary root length of vertically grown Arabidopsis *Ds* and *air12-1*....120
Figure 4.41. Effect of α-naphthaleneacetic acid (α-NAA) on mean primary root length of vertically grown Arabidopsis *Ds* and *air12-1*....121
Figure 4.42. Effect of 2,4-D on mean primary root length of vertically grown Arabidopsis *Ds* and *air12-1*....122
Figure 4.43. Comparison between control and treatments and the effect on primary root growth of Arabidopsis *Ds* and *air12-1* seedlings....123
Figure 4.44. Mean lateral root number of Arabidopsis *Ds* and *air12-1* seedlings....125
Figure 4.45. Comparison between control and treatments and the effect on lateral root production of Arabidopsis *Ds* and *air12-1* seedlings....126
Figure 4.46. Mean lateral root density of Arabidopsis *Ds* and *air12-1* seedlings....127
Figure 4.47. Mean lateral root length of Arabidopsis *Ds* and *air12-1* seedlings....129
Figure 4.48. Mean cumulative seedling lateral root length of Arabidopsis *Ds* and *air12-1* seedlings....130
Figure 4.49. Comparison between control and treatment and the effect on cumulative mean lateral root length of Arabidopsis *Ds* and *air12-1* seedlings....132
Figure 4.50. Catalase activity in Arabidopsis *Ds* and *air12-1* seedlings....136
Figure 4.51. Catalse activity in Arabidopsis Landsberg *erecta* control and *air12-2* seedlings....137
Figure 4.52. Hydrogen peroxide concentration in Arabidopsis *Ds* and *air12-1* seedlings....138

Figure 4.53. Hydrogen peroxide concentration in Arabidopsis Landsberg *erecta* control and *air12-2* seedlings 139
Figure 4.54. Qualitative analysis of extra- and intracellular superoxide in the Arabidopsis Nössen ecotype on control medium 143
Figure 4.55. Qualitative analysis of extra- and intracellular superoxide in the Arabidopsis Nössen ecotype on medium with 400 nM α-NAA 144
Figure 4.56. Qualitative analysis of extra- and intracellular superoxide in the Arabidopsis Nössen ecotype on 1 mM H_2O_2 145
Figure 4.57. Qualitative analysis of extra- and intracellular superoxide in the Arabidopsis Landsberg erecta ecotype on control medium 146
Figure 4.58. Qualitative analysis of extra- and intracellular superoxide in the Arabidopsis Landsberg erecta ecotype on 400 nM α-NAA 148
Figure 4.59. Qualitative analysis of extra- and intracellular superoxide in the Arabidopsis Landsberg erecta ecotype on 1 mM H_2O_2 149
Figure 5.1. Hypothetical model describing interactions between ABA and auxin during lateral root development 170
Figure 5.2. Hypothetical model describing early signaling and downstream signal transduction regulating AIR12/CIL1 during osmotic or nitrogen stress 171
Figure 5.3. Hypothetical model describing early and downstream signaling in response to a salt stress 172

LIST OF ABBREVIATIONS

α-NAA	α-napthaleneacetic acid
2,4-D	2,4-dichlorophenoxyacetic acid
ABA	Abscisic acid
ABI	ABA INSENSITIVE
ABP1	AUXIN BINDING PROTEIN1
Ac	*Association* element
AC	Antisense *CIL1*
ACC	1-aminocyclopropane-1-carboxylic acid
AFB	AUXIN SIGNALING F-BOX
AGP	Arabinogalactan protein
AIR12	AUXIN INDUCED in ROOTS12
ALS	Chlorsulfuron-resistant acetolactate synthase gene
ARE	AUXIN RESPONSE ELEMENT
AREB1	ABSCISIC ACID-RESPONSIVE ELEMENT BINDING PROTEIN1
ARF	AUXIN RESPONSE FACTOR
APX	Ascorbate peroxidase
Asc	Ascorbate
AUX1	AUXIN1
BAR	Biological Array Resource
CAT	Catalase
CDD	Conserved Domain Database
CDK	Cyclin-dependent kinase

CHLH	Magnesium chelatase H subunit
CIL1	COPPER INDUCED in LEAVES1
CT	Control
DAB	Diaminobenzidine
DHAR	Dehydroascorbic acid
DIC	Differential interference contrast
DIG	Detergent insoluble glycolipid-enriched complex
DIM	Detergent insoluble membrane
DRE	DEHYDRATION RESPONSE ELEMENT
DREB	DRE BINDING
Ds	*Dissociation* element
DUF568	Domain of unknown function 568
DZ	Differentiation zone
ERA1	ENHANCED RESPONSE TO ABA1
ER	Endoplasmic reticulum
ERF	ETHYLENE RESPONSE FACTOR
EXP	Expansin
EZ	Elongation zone
FAD7	FATTY ACID DESATURASE7
FCA	FLOWERING TIME CONTROL PROTEIN A
GA	Gibberelic acid
GFP	Green Fluorescent Protein
GPCR	G protein-coupled receptor

GLH17	Glucosyl hydrolase 17
GPI-AP	Glucosylphosphatidylinositol-anchored protein
GR	Glutathione reductase
GTG	GPCR-TYPE G PROTEINS
GUS	β-glucuronidase
H_2DFFDA	(5-(and-6)-carboxy-2',7'-difluorodihydrofluorescein diacetate)
HRP	Horseradish peroxidase
IAA	Indole-3-acetic acid
IAAH	Indole acetamide hydrolase gene
IL	Inner layer
ITN1	INCREASED TOLERANCE to NaCl1
KRP2	KIP-RELATED PROTEIN2
LAX3	LIKE AUX1 3
LB	Left border
Ler	Landsberg *erecta*
LRD2	LATERAL ROOT DEVELOPMENT2
LRR	Leucine-rich repeat
MDA	Monodehydroascorbate
MZ	Meristematic zone
NBT	Nitroblue tetrazolium
NPA	Naphthylphthalamic acid
NPTII	Neomycin phosphotransferase II
NAM	Naphthalene acetamide

NOX	NADPH OXIDASE
OL	Outer layer
ORF	Open Reading Frame
PAT	Polar auxin transport
PCD	Programmed cell death
PCR	Polymerase Chain Reaction
PDK1	3-phosphoinositide-dependent protein kinase 1
PG	Polygalaturonase
PID	PINOID
PIN1,2,4,7	PIN FORMED
PLA2	Pectate lyase 2
PLC	Phospholipase C
PLT	PLETHORA
PP2A	PROTEIN PHOSPHATASE 2A
PYL	PYR-Like
PYR	PYRABACTIN RESISTANCE
RB	Right border
RBOH	RESPIRATORY BURST OXIDATIVE HOMOLOGUE
RCAR	REGULATORY COMPONENTS OF ABA RECEPTORS
RHD2	ROOT HAIR DEFECTIVE2
ROS	Reactive oxygen species
RT-PCR	Reverse Transcription Polymerase Chain Reaction
SAM	Shoot apical meristem

SCF	SKP-Cullin F-Box
SHR	SHORT-ROOT
SOD	Superoxide dismutase
SOS	SALT OVERLY SENSITIVE
SKU5	SKEWED ROOT 5
SLR	SOLITARY ROOT
T-DNA	Transfer DNA
TIR1	TRANSPORT INHIBITOR1
TRH1	TINY ROOT HAIR1
TPL	TOPLESS
Trp	Tryptophan
UTR	Untranslated region
XTR	Xyloglucan:xyloglucosyl transferase

1. INTRODUCTION

Auxin, the most common of which is indole-3-acetic acid (IAA), is a critical regulator of all stages of plant development including embryogenesis, germination, cell differentiation, root and shoot development, vascular tissue patterning, meristem maintenance, and seed dispersal (Weijers et al., 2006; Benjamins and Scheres, 2008; Péret et al., 2009; Sorefan et al., 2009; Vanneste and Friml, 2009). Though these developmental processes require auxin, they are influenced by other regulators during specific stages of development such as seed germination and lateral root development. For example, though seed germination is classically thought to involve antagonism between gibberellins and abscisic acid (ABA), work over the last decade has shown auxin acts synergistically with ABA to repress germination, with both hormones acting through an unknown signaling pathway (Brady et al., 2003). Furthermore, though auxin itself drives root development and forms gradients without the action of other hormones (Grieneisen et al., 2007; Lucas et al., 2008), it requires ABA signaling for proper initiation of lateral roots, despite the antagonistic action of ABA on this developmental process (Brady et al., 2003). Auxin and ABA signals progress through pathways mediated by a class of oxygen-containing molecules known as reactive oxygen species (ROS). Less obvious, and rarely experimentally examined is whether ROS are involved in ABA-auxin signaling cross-talk. The present study examines the effects of auxin, ABA, and ROS on seed germination and lateral root development in *Brassica carinata* and Arabidopsis. The experimental system utilized an uncharacterized gene thought to be involved in lateral root development, Arabidopsis *AUXIN INDUCED IN ROOTS12* (*AIR12*; Neuteboom et al., 1999), and its putative *B. carinata* ortholog, *COPPER INDUCED IN LEAVES1* (*CIL1*; Gibson, 2005). A unique aspect of the current study is the integration of hormonal and reactive oxygen molecules in what appears to be a novel pathway involving extracellular proteins leading to lateral root development.

An overview is presented outlining auxin transport and perception, ROS generation and detoxification, followed by ABA signaling and stress response recognition. A brief description of primary and lateral root development is then integrated with the current knowledge of auxin-ABA cross-talk and ROS signaling.

2. LITERATURE REVIEW

2.1 What is a plant hormone?

Plant hormones are natural compounds that, at very low concentrations, act as signaling molecules to activate physiological processes (Romanov, 2002; Gaspar et al., 2003). Not all signaling molecules act as hormones, and not all hormones act as signaling molecules, however. Plant hormones are set apart from their animal counterparts for two reasons. Plant hormones can be synthesized in any living cell in the plant, though there are generally specific organs that synthesize the majority of a hormone (Gaspar et al., 2003). Hormone response can occur in the plant cell they are synthesized in, or after transport to a target cell. Animal hormones, on the other hand, are synthesized in a specific organ, usually endocrine glands, and travel in the blood to the target cell, which responds to the hormone (Campbell, 1997).

Plant hormones are responsible for a wide range of phenomena that occur during the growth, development, and reproduction of a vascular plant. Historically, there were five classes of phytohormones: indole-3-acetic acid (IAA or auxin), cytokinins, gibberellins, abscisic acid, and ethylene (Taiz and Zeiger, 1998). In the past 10 years several other signaling molecules present at low concentrations throughout the plant have been identified as hormones, such as brassinosteroids, jasmonic acid, and salicylic acid (Reviewed in Santner et al., 2009).

2.2 Auxin

Auxin, derived from the Greek term *auxein*, to increase, was the first of the five classic phytohormones discovered. The action of auxin was described first by Darwin (1880), when he observed that the apex of an oat coleoptile would bend toward a unidirectional source of light. When the shoot apex was excised the coleoptile would grow vertically regardless of the direction of the light source. This coleoptile technique for detecting and observing curvature was perfected and refined by other researchers, who demonstrated that the shoot apex was responsible for sending a chemical signal that directed growth, and that the signal would direct growth even in complete darkness (Boysen-Jensen, 1913; Paal, 1919; Went, 1926).

One of the most recognizable roles of auxin is in apical dominance. Auxin synthesized in the apex of the plant is transported basipetally, and acts on axillary buds to inhibit their growth.

When the shoot apical meristem (SAM) of a dicotyledonous plant is removed, the plant begins to branch extensively. Auxin is also required for cell elongation and expansion (Chen et al., 2001; Braun et al., 2008), having differing effects depending on the organ in which it is present. Auxin stimulates cell elongation in the shoot, but inhibits it in the root (Crozier et al., 2000). In addition to cell elongation, auxin is also involved in phototropism and gravitropism, the processes whereby a plant grows toward light or a root grows towards a gravity source, respectively. Darwin demonstrated phototropism in 1880, while gravitropism was demonstrated later by Went (1926). Auxin also affects the differentiation of vascular tissue and vascular patterning in leaves (Naderi et al., 1997; 1998; Scarpella et al., 2006; Sauer et al., 2006) and formation of phyllotactic patterns (Bainbridge et al., 2008). Auxin is integral in regulating embryogenesis, plant totipotency, and seed dispersal in Arabidopsis (Ribnicky et al., 2002; Sorefan et al., 2009).

The most abundant naturally occurring auxin in plants is indole-3-acetic acid (IAA) (Bartel et al., 2001). IAA is synthesized by two main methods, Trp-independent biosynthesis, a pathway with no identified biosynthetic enzymes, and tryptophan (Trp)-dependent biosynthesis, which uses the amino acid tryptophan as a precursor to generate IAA through indole-3-glycerol phosphate followed by indole-pyruvic acid or indole-3-acetoldoxime (Bartel et al., 2001; Coruzzi and Last, 2000; Crozier et al., 2000; Normanly, 2010). IAA biosynthesis in plants was found to depend on the ambient temperature. In *Lemna gibba*, at a temperature of 15 ^{o}C, Trp-dependent IAA biosynthesis was favored, while at a temperature of 30 ^{o}C Trp-independent biosynthesis was favored (Rapparini et al., 2002). Further, Trp-dependent IAA biosynthesis occurs during periods of high auxin demand such as seed germination, embryo growth, or following wounding. A sustained low amount of IAA is synthesized via the Trp-independent pathway during vegetative growth (Normanly and Bartel, 1999; Bartel et al., 2001). Biosynthesis of IAA in Arabidopsis varies with the age of the plant, with the youngest organs having the highest IAA synthetic capacity, especially the leaves that are less than 0.5 mm in length, while the older organs that have ceased cell division have the lowest capacity (Ljung et al., 2001).

After IAA is synthesized, it is transported throughout the plant by two methods: polar auxin transport (PAT), and phloem transport (Friml and Palme, 2002). Phloem transport is fast and bi-directional. It is used to transport inactive auxin conjugates in addition to physiologically active auxins (Nowacki and Bandurski, 1980). Conversely, PAT is unidirectional, occurring in a cell-to-cell manner and is specific for active free auxins moving in a basipetal or lateral direction

from the auxin source (Friml and Palme, 2002; Friml, 2003). Polar auxin transport is important for flower development and proper patterning of the vascular system in leaves (Naderi et al, 1997; Oka et al., 1999; Dengler and Kang, 2001). A wide range of phenotypic abnormalities occur when PAT is impeded. These abnormalities range from flower aberrations, including petal fusion and reduction, to whole plant effects, such as irregular shaped leaves with abaxial fusions to the adaxial side, and development of additional cotyledons (Naderi et al., 1997; Oka et al., 1999; Friml and Palme, 2002).

Inactivation of IAA occurs through catabolism or conjugation. Conjugated IAA is a source of readily accessible IAA that can be used when required (Bialek and Cohen, 1989). In *Lycopersicon esculentum,* IAA is conjugated through the addition of a glucose residue to the carboxyl group of the IAA side chain to form I-*O*- (indole-3-acetyl)-*B*-glucose (Crozier et al., 2000; Tam et al., 2000). The glucose side chain can be removed through the action of a β-glucosidase. Catabolism, which occurs through amino acid intermediates, irreversibly inactivates IAA and as a result, decreases the total IAA pool (Crozier et al., 2000). The rate of IAA turnover can be calculated through comparison of the amount of IAA catabolites relative to IAA.

2.2.1 Auxin influx

Carrier proteins located in the plasma membrane facilitate the asymmetric distribution of auxin. When auxin distribution is disrupted, phenotypic abnormalities result (Morris, 2000; Tanaka et al., 2006; Vanneste and Friml, 2009). Isolation of carrier proteins involved in auxin distribution began when Arabidopsis seeds were mutagenized with ethyl methanesulfonate and screened for survival on high concentrations of the herbicide and auxin analog, 2,4-dichlorophenoxyacetic acid (2,4-D; Maher and Martindale, 1980). Individuals surviving this treatment were insensitive to 2,4-D and showed wild type primary root lengths even in the presence of inhibitory concentrations of the hormone, produced agravitropic roots, and were named *auxin1* (*aux1*). Later experiments showed *aux1* mutants were resistant not only to auxin but also to the ethylene precursor, 1-aminocyclopropane-1-carboxylic acid (ACC), indicating a possible link between auxin and ethylene during root development (Pickett et al., 1990). *aux1* mutants also displayed a delayed response to inhibitory amounts of exogenously applied IAA (Evans et al., 1994), suggesting that *aux1* mutants were deficient in auxin uptake. Examination of

the AUX1 amino acid sequence showed similarity to plant, fungal, and animal amino acid permeases, a family of proteins involved in amino acid transport (Bennett et al., 1996). Since the structure of IAA is similar to that of tryptophan it was theorized that AUX1 was an auxin transporter. To examine this phenomenon in greater detail, root growth in the mutants was measured after treatment with IAA, 2,4-D, and α-napthaleneacetic acid (α-NAA; Yamamoto and Yamamoto, 1998). Consistent with the hypothesis that AUX1 is required for auxin influx, treatment with α-NAA, which can diffuse through the plasma membrane, rescued the agravitropic root growth of *aux1* plants (Marchant et al., 1999; Morris, 2000). Further examination of the *aux1* mutant revealed that it accumulated less than half the amount of 2,4-D as wild type plants whereas α-NAA accumulation was unaffected (Marchant et al., 1999). Although many studies examined the physiological effects of the *aux1* mutant, biochemical evidence of AUX1-mediated auxin transport was lacking until 2006 when Yang et al. demonstrated that AUX1 was a specific H^+/IAA^- symporter. By expressing *AUX1* in *Xenopus laevis* oocytes, the authors showed that AUX1-mediated IAA uptake was blocked by the same amino acid substitutions that resulted in mutant phenotypes. The same group demonstrated that uptake occurred at physiological concentrations. In addition to AUX1, a root specific influx carrier (Stone et al., 2009), the Arabidopsis genome encodes three other auxin influx carriers (Swarup et al., 2008). Unlike AUX1, LAX1 (LIKE AUX1), and LAX2 (Parry et al., 2001; Bainbridge et al., 2008), the LAX3 auxin influx carrier is specifically present in the cortical and endodermal cells of the primary root. Auxin increases expression of *LAX3* in these cells, causing increases in local auxin uptake, which in turn stimulates the production of cell wall remodeling enzymes, allowing the growing lateral root primordium to emerge from the primary root. Since AUX1 and LAX3 are confined to the roots (Marchant et al., 1999; Swarup et al., 2001; Swarup et al., 2008), the other auxin influx carriers must exist in aerial plant organs. Though this has not yet been described, mutation of auxin influx carrier genes causes aerial phenotypic aberrations (Pickett et al., 1990; Stone et al., 2008), demonstrating the importance of proper auxin distribution by PAT during developmental processes.

2.2.2 Auxin efflux

The auxin efflux carriers are much better understood than the influx carriers. Auxin efflux carriers are believed to be multi-component systems, consisting of transport, catalytic, and

regulatory domains (Morris, 2000). The first identified auxin efflux carrier gene was the Arabidopsis *PIN1* (*PIN*-*FORMED*; Galweiler et al., 1998). In *pin1* mutants, PAT is perturbed in the inflorescences whose pinnate apices develop into only a few, if any flowers. PIN1 is localized to the basipetal region of apical cells, where it is involved in transporting auxin from leaves into the vascular bundle. Two other *PIN* genes (*PIN2* and *PIN3*) were found that function in different organs in Arabidopsis. PIN2 was localized to meristematic and elongating regions of the primary root (Muller et al., 1998) while PIN3 was localized to the columella initial cells of the root tip and on lateral membranes of endodermal cells in young stems (Friml et al., 2002a). PIN4 localizes to developing and mature root apices where it is theorized to have a role in generating an auxin sink used for patterning in development (Friml et al., 2002b). PIN7 localization was found to drive apical to basal auxin gradients in Arabidopsis suspensor cells during embryogenesis. Localization and transport studies demonstrated that PIN proteins export auxin and are responsible for the formation of a graded distribution (gradient) of auxin to drive development (Friml et al., 2003). Further analysis of PIN proteins showed that subcellular localization to the basal or apical pole of cells determines auxin transport routes (Friml et al., 2004), that PINs are necessary for maintenance of the meristem zone in the root (Blilou et al., 2005), and perform a rate-limiting function in auxin efflux (Petrášek et al., 2006). In addition to controlling auxin gradients, PIN proteins are also partially functionally redundant. Double, triple, and quadruple *pin* mutants show additive embryonic defects, ranging from aberrant cotyledon formation in double mutants (*pin4 pin7*), to cotyledon fusion and limited root development in triple mutants (*pin1 pin3 pin4*), to production of globular, malformed inviable embryos in quadruple mutants (*pin1 pin3 pin4 pin7*; Friml et al., 2003).

Since PIN proteins generate critical auxin gradients to drive development, several levels of control exist within plants to manipulate localization of this family of efflux proteins. PLT (PLETHORA) proteins regulate the expression of *PIN* while PIN proteins inhibit the expression of *PLT,* demonstrating the complexity of the interactions necessary for normal vascular patterning to occur. The AUXIN BINDING PROTEIN1 (ABP1) has been examined over the course of several years and was once thought to be a candidate auxin receptor (Bennett et al., 1996; Napier et al., 2002; Napier et al., 2004). It is now known that ABP1 affects PLT gradients to drive auxin efflux (Tromas et al., 2009) and is required for post-embryonic shoot development (Braun et al., 2008). Depending on the concentration of PID (PINOID), a protein kinase that

interacts with 3-phosphoinositide-dependent protein kinase 1 (PDK1; Zegzouti et al., 2006) in Arabidopsis, the localization of PIN within cells switches from basal to apical (Friml et al., 2004) controlling a process termed "polarity". Sub-threshold amounts of PID result in basal localization of PIN while above-threshold amounts result in apical localization of PIN. Counteracting the kinase activity of PID is PROTEIN PHOSPHATASE 2A (PP2A; Michniewicz et al., 2007). Like PID, apical and basal localization of PINs are affected by changing the concentration of PP2A; however PP2A acts in opposition to PID (Michniewicz et al., 2007). In addition to control of phosphorylation status, which in turn controls PIN polarization, polar targeting signals in the PIN amino acid sequence itself affect subcellular localization, and alteration of these signals causes aberrant polarity (Wiśniewska et al., 2006). Additional proteins such as TINY ROOT HAIR 1 (TRH1), a root-specific potassium carrier, are also required for auxin transport (Vicente-Agullo et al., 2004). Plants with reduced TRH1 are impaired in auxin efflux from the stele, resulting in an agravitropic phenotype (Vicente-Agullo et al., 2004).

Control of auxin efflux, and therefore auxin gradient formation, is dependent on subcellular localization of PIN proteins. As previously outlined, polar localization of PINs is determined by phosphorylation status. PIN proteins are mobilized through clathrin-dependent endocytosis, a dynamic and constitutive process used to internalize the efflux proteins into endosomes (Dhonukshe et al., 2007). Following endocytosis, PINs are exocytosed to a specific pole of cell and inserted into the plasma membrane pole, dependent on phosphorylation status. This exocytotic recycling step requires GNOM, an ADP-ribosylation factor GTPase guanine nucleotide exchange factor (ARF-GEF; Geldner et al., 2001). Without functional GNOM, PIN proteins accumulate exclusively within endosomes and no polar auxin gradients form. The constitutive mobilization and re-mobilization of PIN proteins allows plant cells to alter their polar sorting of PIN proteins in response to developmental signals and auxin concentrations (Sauer et al., 2006). Endocytosis of PINs is a rapid process and enables cells to quickly redirect auxin gradients to control development (Tanaka et al., 2006) in situations such as embryonic development (Friml et al., 2002b), tropic responses (Friml et al., 2002a), and in root meristem maintenance (Friml et al., 2002a). Though the complete picture of auxin efflux has not yet been fully described, multiple levels of regulation integrate to rapidly modulate auxin gradients in response to both environmental and endogenous signals to ultimately control auxin distribution within developing organs.

2.2.3 Molecular mechanisms of auxin response

Knowledge of the effects of auxin on both plant development and physiology is abundant, yet it is only within the past ten years that the molecular mechanisms of auxin perception and response have been uncovered. The discovery of a true auxin receptor, TRANSPORT INHIBITOR RESPONSE (TIR1), not only allowed advances in our understanding of how the hormone acts, but also represented the first plant hormone receptor with an elucidated signaling pathway (Ruegger et al., 1997; Ruegger et al., 1998; Dharmasiri et al., 2005a; Kepinski and Leyser, 2005). TIR1 is a member of the F-box protein family; a class of protein motif containing approximately 50 amino acids that functions as a site of protein-protein interaction (Kipreos and Pagano, 1995; Kipreos and Pagano, 2000). Proteins with this motif, including TIR1, are components of the SCF ubiquitin-ligase complex, named after the SKP1, Cullin, and F-box constituents of the complex (Bai et al., 1996). Assembly of this complex is dependent on SKP1, which acts as an intermediate, binding the F-box protein at its C-terminus, while binding Cullin at the N-terminus. The F-box protein associates with SKP1 only after it has bound its specific partner. Following F-box-partner binding, the F-box protein binds SKP1 resulting in recruitment of Cullin, which in turn dimerizes with RBX1, a RING-H2 finger protein that binds zinc (Deshaies, 1999; Freemont, 2000; Moon et al., 2004). The RBX1-Cullin dimer catalyses the transfer of activated ubiquitin from a ubiquitin-conjugating enzyme to the F-box-associated protein, targeting the protein for degradation via the 26S proteasome (Ulmasov et al., 1997a). The pathway to auxin perception and recognition broadly follows this outline; however it deviates at several key points forming a truly elegant signaling mechanism.

2.2.3.1 Aux/IAA proteins

Prior to the discovery of TIR1 as an auxin receptor, several other classes of proteins were isolated that appeared to have some role in auxin response, but the relationship to perception was unclear. The first group of proteins was isolated by Theologis et al. (1985) after examination of auxin-treated pea epicotyls. The authors discovered a specific class of auxin-responsive mRNAs induced within 15 minutes of auxin treatment. Further work showed that there were 29 distinct genes in the Arabidopsis genome coding for transcriptional regulators termed Aux/IAA proteins (Abel and Theologis, 1996; Remington et al., 2004). Generally, Aux/IAA proteins are are denoted as “IAA” proteins and are composed of four highly conserved domains labeled I-IV that

function to regulate auxin signaling along with a second class of proteins, auxin response factors (ARFs; Ulmasov et al., 1997b; Guilfoyle et al., 1998; Ulmasov et al., 1998; Morgan et al., 1999; Ouellet et al., 2001), transcription factors composed of a DNA-binding domain and domains III and IV of Aux/IAA proteins. Aux/IAAs and ARFs are similar in structure in that they share domains III and IV as outlined in Figure 2.1. The first domain, present near the N-terminus of Aux/IAA proteins is required for transcriptional repression (Tiwari et al., 2004), and in Arabidopsis contains an amphiphilic repression, or EAR, motif. This motif interacts with the co-repressor TOPLESS (TPL) through an ETHYLENE RESPONSE FACTOR (ERF), discovered by yeast two-hybrid screening using TPL, a protein critical for embryonic pole identity (Long et al., 2002) as bait (Szemenyei et al., 2008). Analysis of Arabidopsis IAA7 and IAA17 demonstrated that proteins consisting of only domain II are able to interact with TIR1, while short deletions in this domain dramatically decrease the interaction (Gray et al., 2001). Interaction between TIR1 and domain II of Aux/IAA proteins leads to Aux/IAA degradation via the 26S proteasome. Furthermore, auxin stimulates TIR1-Aux/IAA association and is the sole hormone capable of inducing this degradation (Zenser et al., 2001; Zenser et al., 2003). The most C-terminal domains, III and IV are also essential for transcriptional regulation. Domain III contains a βαα fold found in prokaryotic transcriptional repressors involved in dimerization and DNA binding (Abel and Theologis, 1995; Raumann et al., 1994). Investigation of this domain using mutational analysis showed that both domain III, containing the βαα fold, and domain IV are required for both Arabidopsis and pea Aux/IAA proteins to homodimerize, and can even promote heterodimerization between the Arabidopsis and pea Aux/IAA proteins *in vitro* (Kim et al., 1997). Furthermore, these domains mediate heterodimerization between Aux/IAA proteins and another class of transcriptional regulators, the auxin response factors which in turn bind to specific motifs in the promoters of auxin regulated genes, discussed below in section 2.2.3.2.

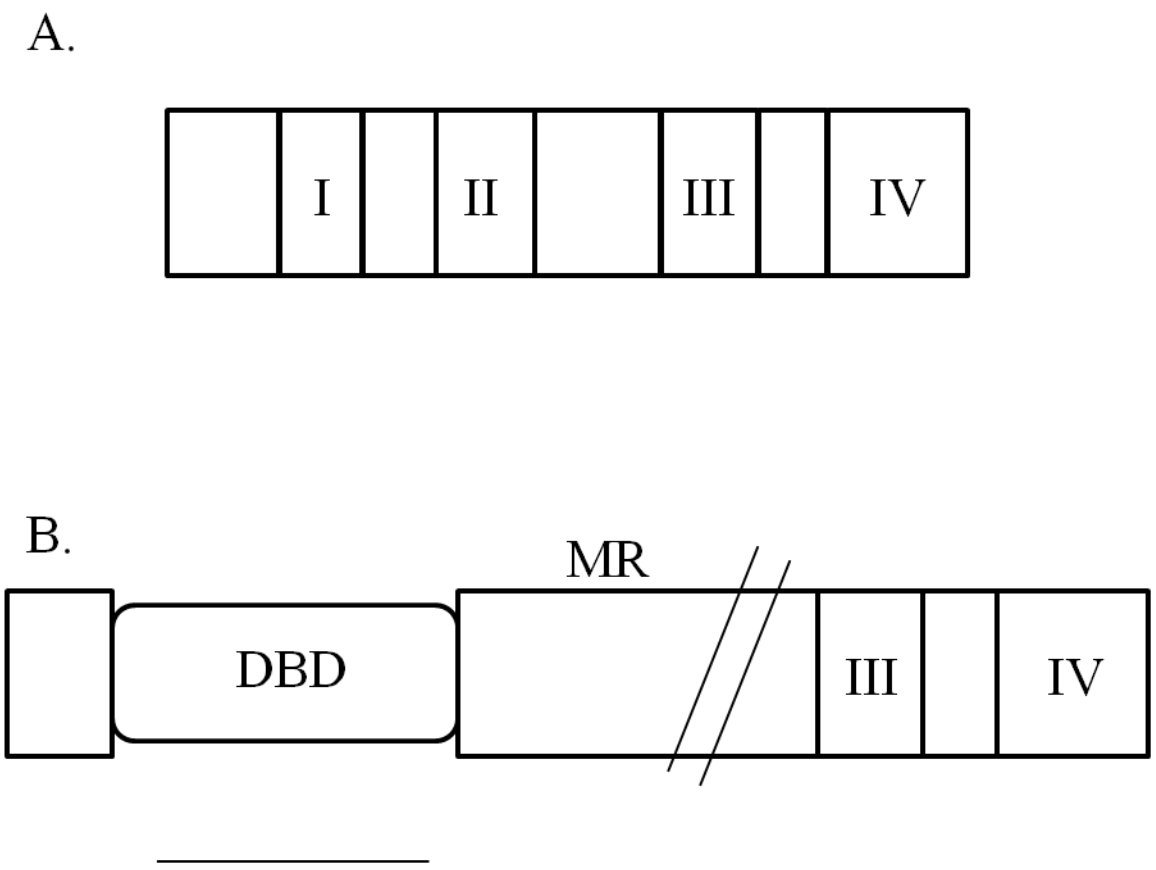

Figure 2.1. Generalized structure of Aux/IAA proteins (A) and auxin response factors (ARF; B). A, Aux/IAA proteins are composed of 4 conserved domains, numbered I-IV. B, ARFs are composed of a DNA-binding domain (DBD), a middle region (MR) of variable length (indicated by the breaks, and the conserved domains III and IV identical to the Aux/IAA proteins. Bar underneath B represents 100 amino acids; figure adapted from Liscum and Reed, 2002.

2.2.3.2 Auxin response elements

Soon after the discovery of *Aux/IAA* genes, putative auxin-responsive elements were discovered in the promoters of auxin-regulated genes, the first of which were *Aux22* and *Aux28*, from soybean (*Glycine max*; Ainley et al., 1988). In both genes, two elements were present upstream of the transcription start site with almost identical spacing between the elements, leading the authors to speculate on their significance. Ballas et al. (1993) identified this promoter element in the early auxin-induced gene *PS-IAA4/5*. Through extensive deletion analysis, a region between -318 bp and -154 bp upstream of *PS-IAA4/5* was discovered that conveyed auxin-inducibility in this gene; without this region, no auxin induction was observed. The defined sequence of this element present in the promoter of auxin-inducible genes was isolated in 1995, when Ulmasov et al. mutated a specific 6-nucleotide motif (TGTCTC) found multiple times in the auxin-responsive region of *GH3*, a soybean gene characterized by rapid, strong induction after auxin treatment (Hagen et al., 1984; Hagen et al., 1991). Further analysis of the TGTCTC domain led Ulmasov et al. (1997b) to develop a synthetic auxin responsive element, termed "DR5". This element consisted of an 11 bp repetitive motif of TGTCTCCCTTT repeated 7 times. The synthesis of this element greatly accelerated auxin research as placing it so that it controls a reporter gene, such as *uidA*, the gene coding for the GUS protein, enabled visualization of auxin patterning *in vivo* for the first time, a system which has only been recently been duplicated with the cytokinins (Müller and Sheen, 2008), and led to the discovery of ARFs.

The ARFs are transcription factors that bind to specific motifs in the promoters of auxin-regulated genes, mediating auxin-dependent gene transcription (Ulmasov et al., 1997b; Ulmasov et al., 1999). The ARFs were initially isolated using yeast one-hybrid assays incorporating four tandem copies of inverted repeats of the TGTCTC element to screen an Arabidopsis cDNA library (Ulmasov et al., 1997b). Auxin response factors contain the same conserved domains III and IV that Aux/IAAs possess, but lack the N-terminal domains (Ulmasov et al., 199b7) limiting these proteins to DNA binding (Tiwari et al., 2003) and homo- and heterodimerization with Aux/IAA proteins (Guilfoyle et al., 1998; Hardtke et al., 2004; Okushima et al., 2007). To date, 23 ARFs have been identified in the Arabidopsis genome (Guilfoyle and Hagen, 2007). Functionally, these proteins function as both positive and negative regulators of auxin-regulated gene transcription (Ulmasov et al., 1999; Tiwari et al., 2003). In Arabidopsis, five of the 23 ARFs (ARF5-8 and 19) are positive regulators of auxin-regulated gene transcription and function

in a wide variety of developmental roles such as embryonic axis formation (ARF5 and 7; Hardtke et al., 2004), hypocotyl phototropism (ARF7; Wang et al., 2005), and in promoting leaf expansion and auxin-induced lateral root formation (ARF7 and 19; Wilmoth et al., 2005). Associations between ARFs and Aux/IAAs have been identified for several combinations, including ARF5/IAA12, which interact in the proembryo to control auxin transport (Weijers et al., 2005; Weijers et al., 2006), Additionally, ARF5 and IAA12/13 or 3 prevent embryonic root formation or seedling growth, in Arabidopsis respectively (Weijers et al., 2005), demonstrating that individual ARFs can pair with more than one Aux/IAA to control development.

2.2.3.3 Auxin perception

The molecular mechanisms of auxin signaling are, as previously outlined, centered on TIR1. Initial examination of the primary amino acid structure of TIR1 revealed a series of leucine-rich repeats (LRR) and the presence of an N-terminal F-box motif, a domain of approximately 50 amino acids that mediates protein-protein interactions in a number of cellular contexts, including ubiquitin-mediated proteolysis by the 26S proteasome. In addition, the F-box domain present in TIR1 displayed high identity to yeast Grr1p and human SKP1 F-box proteins which were implicated in ubiquitin-mediated proteolysis (Bai et al., 1996; Ruegger et al., 1998; Yu et al., 2007), providing the initial evidence that led to elucidation of auxin signaling. Further work examined the effect of mutating either TIR1 or the Arabidopsis components of the SCF^{TIR} complex, ASK and AtCUL1, similar to yeast Skp1p and cdc53p, respectively (Gray et al., 1999). Mutation of any of these proteins resulted in plants with reduced sensitivity to auxin while overexpression of TIR1 increased auxin sensitivity, providing evidence toward auxin-induced proteolysis of the Aux/IAA transcriptional repressors (Ruegger et al., 1998; Gray et al., 1999). TIR1 was not confirmed as an auxin receptor until 2005, when two groups concurrently reported its auxin-binding activity (Dharmasiri et al., 2005a; Kepinsky et al., 2005). Auxin was shown by both groups to directly bind with TIR1 in Arabidopsis and that this binding mediated further interactions with TIR1 and domain II of Aux/IAA proteins. These interactions lead to targeted degradation of the TIR1-Aux/IAA proteins mediated by the 26S proteasome (Kepinsky et al., 2005). Analysis of auxin receptor activity in *tir1* mutants surprisingly showed no difference in recovered copurified protein from wild type plants due to the presence of three other auxin-binding proteins, AUXIN SIGNALING F-BOX (AFB) 1, 2, and 3. Phenotypic characterization of *tir1*, *afb1*, *afb2*, *afb3* quadruple mutant lines showed that these mutants were insensitive to

exogenous auxin and developed a severe embryonic phenotype that was often lethal, indicating that these four proteins are integral for auxin signaling (Dharmasiri et al., 2005a, b). Crystal structure analysis of TIR1 showed the LRR domain contains an inositol hexakisphosphate co-factor that recognizes both auxin and Aux/IAA proteins through a single hydrophobic surface pocket (Tan et al., 2007). Prior to Aux/IAA-TIR1 association, auxin fills the pocket. Binding does not introduce a conformational change; rather, auxin acts as a molecular glue enhancing TIR1-Aux/IAA binding (Tan et al., 2007). The crystallographic evidence presented by Tan et al. (2007) confirmed that TIR1 was an auxin receptor.

To date, auxin signaling represents the most complete plant hormone signaling pathway elucidated. When the cellular concentration of auxin is low, Aux/IAA proteins bind ARFs, an interaction mediated by association of domain I of Aux/IAAs and TPL, repressing transcription of auxin-regulated genes. When cellular auxin concentration increases, auxin binds to the hydrophobic pocket of TIR1/AFB and recruits Aux/IAA proteins, forming the $SCF^{TIR1/AFB}$ complex, causing ubiquitination of Aux/IAAs targeting them for degradation by the 26S proteasome. The TIR1/AFB-Aux/IAA association frees ARFs to bind to auxin-responsive elements in the promoter of auxin-regulated genes, either enhancing or repressing transcription. Although the auxin signaling pathway is short, over 600 possible combinations between ARFs and Aux/IAA proteins potentially exist to control auxin signaling because of the potential for homo- and heterodimerization between the proteins. This suggests possible molecular mechanisms for the ubiquitous involvement of the hormone throughout development. Given the large number of combinations, how do ARFs and Aux/IAA proteins specifically interact to drive development? Limited experimental evidence suggests that associations between an ARF transcriptional repressor-Aux/IAA transcriptional repressor or ARF transcriptional repressor-Aux/IAA transcriptional activator are weaker than ARF activator-Aux/IAA repressor and ARF activator-Aux/IAA activator associations (Tiwari et al., 2003; Hardtke et al., 2004; Guilfoyle and Hagen, 2007). Additionally, after auxin treatment or during periods of auxin-induction, the ARF-AUX/IAA interaction is most likely disrupted through phosphorylation of AUX/IAA (Dharmasiri and Estelle, 2002). Data implies that auxin regulates the degradation of AUX/IAA after dissociation from ARF (Leyser et al., 1993; Zenser et al., 2001). This implies competition between ARF activators or repressors and Aux/IAA proteins. In such a system, ARFs acting as transcriptional activators would require higher concentrations of auxin for release from their

associated Aux/IAA protein than the equivalent repressor-ARF, which may correspond with the large concentrations of auxins found in young organs. Although the mechanisms of auxin signaling are known, further analysis of auxin action during development require focusing on specific pairings of ARF-AUX/IAA proteins with the goal of understanding how these pairings affect plant development.

2.3 Abscisic acid

The compound now known as abscisic acid (ABA) was simultaneously discovered by two groups in the early 1960s. One group named the molecule "abscisin II" (Ohkuma et al., 1963) for its putative role in leaf abscission, (later disproved), and the other group named the molecule "dormin" (Eagles et al., 1964) for its role in bud dormancy. Subsequently, the name "abscisic acid" was given to this phytohormone, despite the fact that ABA has no role in leaf abscission (Addicott et al., 1968). ABA has roles in dormancy, freezing tolerance, drought tolerance, and water flux in the roots. Seed dormancy and desiccation tolerance are also influenced by ABA. Determination of the ABA content in seeds from a dormant ecotype of Arabidopsis, Cape Verde Islands, demonstrated that ABA content was highest in dormant seeds and subsequently decreased under seed-breaking conditions finally reaching a concentration similar to non-dormant seeds (Ali-Rachedi et al., 2004). Unlike auxins and cytokinins, abscisic acid is not an absolute requirement for plant growth and development (Koornneef et al., 1998). However, the loss of ABA sensitivity results in phenotypic aberrations.

2.3.1 Model of ABA action

One of the most well characterised roles of ABA is negative regulation of stomatal opening during periods of low water potential. Water flux in plants is perceived in the roots (Mantyla et al., 1995). Specifically, the interruption in water uptake is sensed in lateral roots and root hairs and induces ABA transport through the xylem to the photosynthetically active leaves (Hetherington, 2001; Schroeder et al., 2001). The ABA concentration in the xylem sap increases from approximately 1-15 nM to 3 μM in *Helianthus annulus* plants when water uptake is interrupted (Schurr et al., 1992). In leaves, ABA enters the guard cells and triggers a series of signal cascades that lead to loss of turgor pressure and stomata closure (Schroeder et al., 2001). A model summarizing the current knowledge of ABA-induced stomatal closure was presented by Li et al. (2006), incorporating theoretical and experimental information from Arabidopsis and

other plants. Guard cell closure is a phenomenon initially involving a series of protein phosphatases and kinases that act as signal transducers, relaying the ABA signal to enzymes and membrane transporters. These signals culminate in the accumulation of Ca^{2+} from intracellular stores, increasing pH within the guard cells, promoting closure (Li et al., 2001). Intracellular increases in Ca^{2+} are mediated both by influx from outside of the cell and release from internal stores, stimulated by phospholipase C (Hunt et al., 2003) and inositol hexakisphosphate (Lemtiri-Chlein et al, 2003), both of which are synthesized in response to ABA treatment (Garcia-Mata et al., 2003). Increases in cytosolic pH cause the opening of anion efflux channels (Li et al., 2006). This enhances K^+ export, which drives cell volume changes leading to cell closure (Miedema and Assmann, 1996; Blatt and Grabov, 1997; Wang et al., 2001). Guard cell closure halts transpiration and gas exchange, allowing plants to conserve water during periods of high heat or low water availability.

2.3.2 Abscisic acid perception

The search for true ABA receptors has been one wrought with false positives. As early as 2006, FLOWERING TIME CONTROL PROTEIN A (FCA), an Arabidopsis nuclear RNA-binding protein was identified by Razem et al. as an ABA receptor; however this was later disproven by Risk et al. (2008) after demonstrating that the actual binding capacity of FCA to ABA was substantially reduced compared to what was originally reported. The same year FCA was reported as an ABA receptor, an Arabidopsis magnesium chelatase H subunit (CHLH) was reported as an ABA receptor (Shen et al., 2006). Again, later work reported that ABA treatment did not affect barley CHLH activity and furthermore, CHLH did not bind ABA (Müller and Hansson, 2009). However, recent work by Wu et al. (2009) showed that the Arabidopsis CHLH did in fact, bind ABA and that ABA-binding is specific to the C-terminal end of the protein and not the N-terminus as was originally reported. A third ABA receptor was reported by Liu et al. (2007) as a member of the G protein-coupled receptor (GPCR) family in Arabidopsis. GCR2 was proposed to mediate all documented ABA responses in Arabidopsis. Like the other putative receptor proteins, later work proved that ABA did not bind GCR2 (Risk et al., 2009).

Recent work has uncovered one putative and one experimentally validated ABA receptor. Two novel GPCRs possessing intrinsic GTP-binding and GTPase activity were isolated and named GPCR-TYPE G PROTEINS (GTG1 and GTG2; Pandey et al., 2009). Mutational analysis of *gtg1 gtg2* Arabidopsis show hyposensitivity to ABA and that the GTG proteins relay an ABA

signal when the protein is bound to GDP but not GTP, acting as a membrane-bound receptor (Pandey et al., 2009). The second receptor protein was discovered simultaneously by two groups, and represent members of a protein family called PYRABACTIN RESISTANCE (PYR; Park et al., 2009) and REGULATORY COMPONENTS OF ABA RECEPTORS (RCAR; Ma et al., 2009). One group found that ABA binds PYR1 to inhibit ABI1, a PP2C that acts as a negative regulator required for ABA signaling (Park et al., 2009), while another group showed that PYL9 binds ABA and interacts with ABI1 and ABI2 (Ma et al., 2009). Later work showed the PYR/PYR-Like (PYL)/RCAR family of proteins are stimulated by ABA and that *pyr1*/*pyl1*/*pyl2*/*pyl4* quadruple mutants are insensitive to ABA during stomatal closure assays (Nishimura et al., 2009).

2.3.3 Signaling during abiotic stress

2.3.3.1 Water limitation and drought stress

In conditions of transient low water availability, plants close their stoma to prevent water loss through transpiration. Prolonged periods of drought stress result in loss of turgor pressure within plant cells, changing the membrane potential, which leads to cellular collapse (Beck et al., 2007). To avoid detrimental physiological changes, a series of signal cascades are initiated that promote the biosynthesis of compounds to adjust the osmotic concentration of plant cells. In Arabidopsis the biosynthesis of proline has a major role in osmotic adjustment (Voetberg and Sharp, 1991). Synthesis of large amounts of proline raises the osmotic concentration of cells resulting in the water potential becoming more negative and temporary rehydration. In addition to proline, sugars such as galactose, sugar alcohols such as D-ononitol, and polyamines such as putrescine are generated to alter cellular osmotic concentration (Seki et al., 2007). Increased drought tolerance was observed in tobacco plants overexpressing a myo-inositol *O*-methyltransferase from the ice plant (*Mesembyanthemum crystallinum*), increasing the biosynthesis of D-ononitol (Vinocur and Altman, 2005), while overexpression of a stress-inducible arginine decarboxylase from *Datura stramonium* in *Oryza sativa* caused increased drought resistance due to the large accumulation of putrescine (Capell et al., 2004).

In Arabidopsis, drought stress is sensed by a membrane-bound two-component histidine kinase which is activated by increased cellular osmotic concentration, a process that occurs as a plant cell loses water (Beck et al., 2007). The two-component histidine kinase activates a signal transduction pathway leading to the biosynthesis of phospholipase C (Hirayama et al., 1995),

causing release of cellular Ca^{2+} reserves (Mahajan and Tuteja, 2005; Cousson, 2009). Increased intracellular Ca^{2+} promotes transcription of genes containing a dehydration response element (DRE; Yamaguchi-Shinozaki and Shinozaki, 1994) and an ABA-responsive element (ABRE) in their promoters (Narusaka et al., 2003; Huang et al., 2007; Huang et al., 2008). Transcriptional increases in such genes are promoted by binding of transcription factors to these motifs. Two transcription factors that displayed specific binding to DREs were identified by yeast one-hybrid screening and named DRE BINDING1A (DREB) and DREB2A (Liu et al., 1998). Though both DREBs bind the DREs during the stress response, only DREB2A is involved with drought stress (Liu et al., 1998); DREB1A mediates resistance to freezing stress. Curiously, overexpression of DREB1A using the CaMV35S promoter or expression under the control of the promoter of *RD29A*, a gene involved in the drought response, greatly increased stress tolerance to freezing, salt, and drought (Kasuga et al., 1999). This implies that there is some overlap or crosstalk during the abiotic stress response.

The ABSCISIC ACID-RESPONSIVE ELEMENT BINDING PROTEIN1 (AREB1) is a basic leucine zipper transcription factor that binds to ABREs and activates transcription during drought, increasing tolerance to this stress (Fujita et al., 2005). An additional family of transcription factors, the *ABA INSENSITIVE* (*ABI*) genes influence plant responses to both ABA and drought (Finkelstein and Somerville, 1990). Examination of *abi1* mutants showed a decrease in proline accumulation in response to drought, indicating that ABI1 is a positive regulator of protein accumulation (Verslues and Bray, 2006). *ABI4*, on the other hand, is a negative regulator of proline accumulation in response to drought (Verslues and Bray, 2006) indicating a possible mechanism for feedback regulation of ABA-induced proline biosynthesis. Later experiments using microarray analysis discovered 1300 ABA-regulated drought-responsive genes with increased expression 3 hours after re-watering drought stressed plants (Huang et al., 2008). Furthermore, evidence suggests that intergenic regions of Arabidopsis contain drought-responsive motifs (Matsui et al., 2008). These studies highlight the importance of ABA in acclimation to drought tolerance. Further research focusing on integration of transcriptome data with classical genetic and physiological studies will allow a complete picture of the plant drought response to be formed.

2.3.3.2 Salinity

Like dehydration stress, high soil salinity requires the plant to make osmotic adjustments, optimizing water uptake to prevent water loss. However, unlike periods of drought, which can be solved by rehydration, soil salinity adaptation requires a long-term metabolic adjustment. Salt in the environment is generally encountered as NaCl, and originates from weathering of rock or the deposition of oceanic salts in rainwater (Munns and Tester, 2008). Dissolved salts in rain or groundwater decrease the water potential, making water more difficult to extract. Furthermore, excess Na^+ ions in the water are toxic to cells because excess salt causes an imbalance in ionic homeostasis (Zhu, 2002). When challenged with increasing Na^+ concentrations, plants employ a variety of methods to adapt, involving both ABA-dependent and -independent mechanisms.

The precise pathway for ABA-dependent response to salt stress has not yet been fully developed, though there is evidence for overlap between two pathways. Research examining transcriptional increases after abiotic stress in *Medicago sativa* resulted in the discovery of a new annexin-like protein, AnnMs2 (Kovács et al., 1998). Annexins compose a family of structurally related proteins that bind to negatively-charged phospholipids in a Ca^{2+}-dependent manner. Initial transcriptional analysis showed annexin expression increases after salt, osmotic, and ABA treatment (Kovács et al., 1998). Proteomic analysis of salt-treated Arabidopsis demonstrated that this class of annexins belongs to a family of Ca^{2+}-dependent membrane salt stress-responsive proteins (Lee et al., 2004). Further work showed that Arabidopsis annexin1 (AtAnn1) has a role in regulating oxidative stress following ABA treatment through an unknown mechanism (Konopka-Postupolska et al., 2009).

Experimentation with a double mutant Arabidopsis line containing a nonsense mutation in the *FATTY ACID DESATURASE7* (*FAD7*) gene and an uncharacterized gene led to the discovery of *INCREASED TOLERANCE to NaCl1* (*ITN1*; Sakomoto et al., 2008). Mutation of *ITN1* resulted in Arabidopsis plants that displayed a high degree of salt resistance. *ITN1* encodes a transmembrane protein containing an ankyrin-repeat motif. Proteins containing this motif have been implicated in the involvement of signal cascade transmission (Sakomoto et al., 2008).

Transciptional investigation of *itn1* showed suppression of *RBOHC* and *RBOHD,* genes coding for the reactive oxygen species (ROS)-producing NADPH oxidase (NOX) enzyme complex, as well as suppression of an ABA-inducible gene *RESPONSIVE TO DESICCATION29A* (*RD29A*). Interestingly, expression of an additional ABA-inducible gene,

RD22 was unaffected, implying there is an ABA-dependent mechanism that mediates ROS production, and that *ITN1* indirectly affects specific components of ABA signaling leading to salt tolerance in Arabidopsis. The interplay between components of ABA signaling and ROS raises the possibility that similar mechanisms exist to control development in addition to salinity responses.

2.4 Reactive oxygen species

A consequence of aerobic life and the use of molecules containing oxygen for respiration, photosynthesis, and other metabolic functions is the generation of reactive oxygen species (ROS). In the chloroplast the major site of ROS production is within the photosystems. Excited chlorophyll in the triplet state within the reaction centre of photosystem II can transfer excess energy to O_2 to form singlet oxygen while an excess of energy in photosystem I can cause photoreduction of O_2 to H_2O_2 ($^1O_2$; Asada, 2006). This toxic by-product of photosynthesis results in the generation of reactive oxygen species such as superoxide ($O_2^{\cdot-}$) through step-wise, single electron reduction of oxygen. Reactive oxygen species (ROS) derive their "reactive" nature from the unpaired electrons residing in their pi orbitals (Halliwell, 2006). For example, ground state O_2, through a series of reduction reactions, adding one electron at each step, proceeds through singlet oxygen with unpaired electrons ($^1O_2$), superoxide (O_2^-), hydrogen peroxide H_2O_2, the hydroxyl radical ($OH^{\cdot}$), and finally, H_2O.

2.4.1 Generation

In plants, molecular oxygen is produced during photosynthesis in the chloroplast and is utilized in the mitochondria during respiration. In these organelles, two ROS can join their unpaired electrons forming covalent bonds, reducing nearby compounds. Subsequent reactions with other compounds initiate a chain of redox reactions, potentially damaging proteins, lipids, and DNA (Alscher et al., 1997). It is also possible for reactive oxygen species to pair with non-radical compounds, resulting in a new free radical molecule (Scandalios, 2005).

Reactive oxygen generation, particularly superoxide, often occurs on the electron transport chain in the mitochondria and chloroplasts (Salin, 1991). Transition metals such as Fe^{2+} and Cu^+ are able to auto-oxidize oxygen, forming the superoxide radical. The superoxide radical has the potential to cause cellular damage, not because it itself is damaging, but because of the downstream molecules derived from it. Hydrogen peroxide can cause DNA breakage as well as

inhibition of thiol-containing molecules by reducing disulfide bonds. Interaction between oxygen-containing molecules and transition metals can also form the hydroxl radical ($OH^{\cdot}$). The hydroxyl radical modifies proteins, making them more vulnerable to proteolysis (Charles and Halliwell, 1981; Hagar et al., 1996; Casano et al., 1994). These modified proteins are also capable of reacting with nearby proteins, initiating a cascade of redox reactions, generating free radicals very quickly. Membrane-lipid peroxidation also occurs, such as when $OH^{\cdot}$ oxidizes carbonate, resulting in the carbonate radical. A series of reactions can then occur leading to the generation of peroxyl radicals which in turn initiates a chain reaction of oxidation and reduction reactions, results in lipid peroxidation and potentially causing severe cellular damage (Li and Trush, 1993; Halliwell, 2006). The danger of lipid peroxidation is two-fold: a reactive radical such as $OH^{\cdot}$ can receive a proton from a C-H bond, leaving a $C^{\cdot}$ radical behind that will quickly react with O_2, generating peroxyl radicals (Halliwell, 2006). These peroxyl radicals will oxidize other C-H bonds propagating the reactive oxygen species initiating a chain reaction. This series of lipid peroxidations not only results in a membrane with oxidized lipids and membrane proteins, but also an increase in membrane permeability. At this point, the membrane is no longer able to maintain the proper gradients necessary for cellular function and cell death will result.

2.4.2 Detoxification

The reactive and potentially damaging properties of ROS require specific methods to either detoxify or spatially isolate these molecules to prevent cellular damage from occurring. At physiological pH, the superoxide radical exists in equilibrium with its conjugate acid, the hydroperoxyl radical (Baker and Orlandi, 1995). The hydroperoxyl radical is more lipophilic than superoxide and capable of lipid peroxidation. Two methods of inactivating superoxide and hydroperoxyl radicals exist: Natural dismutation, and enzyme-assisted dismutation. At neutral or slightly acidic pH, superoxide and the hydroperoxyl radical spontaneously dismutate to hydrogen peroxide and oxygen. During periods of increased abiotic or biotic stress however, spontaneous dismutation will be insufficient to protect the plant from increased O_2^{-} levels because of the increase in ROS resulting from the stress.

Superoxide dismutases (SODs) are metallo-enzymes that function to detoxify superoxide and hydroperoxyl radicals. SODs contain different metals at their active site depending on their location in the cell (Fink and Scandalios, 2002). The SODs are able to catalyze the dismutation

of O_2^- and hydroperoxyl radicals, with a rate of conversion of $3x10^9\ M^{-1}\ s^{-1}$ (Fink and Scandalios, 2002). The SODs containing a Cu-Zn core are prevalent in a wide range of locations including the cytosol, chloroplast, apoplast, and nucleus. Mitochondrial and peroxisomal SODs, on the other hand contain a Mn core (Drążkiewicz et al., 2007). A third type of SOD containing a Fe core is also present in the chloroplasts of plants. Unlike animals, plants have multiple isoforms of each SOD gene, raising the possibility that each *SOD* gene codes for a protein to deal with a specific subset of oxidative stressors (Kliebenstein et al., 1998). Additionally, the hydrophilic nature of superoxide prevents it from crossing membranes, increasing the need for local production of SOD.

Hydrogen peroxide results after a stepwise addition of two electrons to molecular oxygen (O_2) and two protons. Superoxide is capable of spontaneous dismutation into hydrogen peroxide (H_2O_2) and oxygen. A common method for H_2O_2 formation is through the dismutation of O_2^- either spontaneously or catalyzed by SOD. Hydrogen peroxide also arises during photorespiration from glycolate in the peroxisome by glycolate oxidase during β-oxidation. During this process electrons released from fatty acid oxidation are transferred to oxygen forming hydrogen peroxide (Buchanan et al., 2000). Unlike O_2^-, H_2O_2 is membrane-diffusible (Henzler and Steudle, 2000), stable and is able to react with molecules in an area of the cell spatially separate from where it is generated. In the presence of a transition metal, such as Fe^{3+} or Cu^{2+}, Fenton and Haber-Weiss reactions occur, yielding the highly reactive $OH^{\cdot}$ in the following reaction:

$$Fe^{3+} + O_2^- \rightarrow Fe^{2+} + O_2 \quad (1.1)$$

$$Fe^{2+} + H_2O_2 \rightarrow Fe^{3+} + OH^{\cdot} + OH^- \quad (1.2)$$

The same reaction is also possible using Cu^{2+} instead of Fe^{3+}, resulting in the production of the highly reactive $OH^{\cdot}$. Hydrogen peroxide is also potentially damaging to organic molecules, generally occurring through reactive by-products of peroxidases (Scandalios, 2005).

The membrane-diffusibility of H_2O_2 combined with its ability to form additional reactive molecules has resulted in the evolution of a number of detoxification pathways and methods of preventing interactions. Since transition metals are required for the formation of $OH^{\cdot}$ from H_2O_2, these metals are generally sequestered in the vacuole bound to another molecule, such as a metallothionein (Evans et al., 1992; Zhigang et al., 2006). This places the metal into a state that

is incapable of interacting with H_2O_2, halting the conversion of H_2O_2 to $OH^{\cdot}$, protecting the cell. Several different methods exist to detoxify hydrogen peroxide including catalase, ascorbate, peroxidases, and ascorbate peroxidases.

Catalases are found most predominantly in the peroxisome and catalyze the conversion of H_2O_2 into water and oxygen:

$$H_2O_2 + H_2O_2 \rightarrow 2H_2O + O_2 \quad (1.3)$$

Catalase is a unique reactive oxygen-scavenging enzyme. It does not become reduced during the conversion of the substrate H_2O_2 and does not need to be regenerated by a reducing molecule, such as NADPH. Catalase also exists as a dual-functional enzyme. In high concentrations of substrate, catalase uses H_2O_2 as both the electron donor and acceptor during the reaction, while at low concentrations, catalase has peroxidase activity, using intermediate compounds such as ascorbate, to inactivate H_2O_2 (Scandalios, 2005).

An alternate method for hydrogen peroxide detoxification is through the use of ascorbate peroxidases (APX). APX is a heme-containing enzyme that uses intermediate compounds to convert H_2O_2 into H_2O. The ascorbate peroxidase class of enzymes utilizes porphyrin, ascorbate (Asc) and monodehydroascorbate (MDA) as a source of the reducing cation, reducing substrate, and oxidizing substrate, respectively (Smith and Veitch, 1998). During the peroxidase reaction step-wise oxidations and reductions occur on the heme core of APX and on porphyrin using Asc as an electron donor. Ascorbate regeneration represents a pathway where perturbations in amounts of antioxidants, either increased or decreased, can alter the survival of a plant (Bowler et al., 1991). APX activity results in the conversion of H_2O_2 into H_2O through 2 free-radical intermediate complexes (Scandalios, 2005). Since Asc is oxidized to MDA during this reaction it will contain unpaired electrons and can act as a weak reducing agent. To regenerate Asc, MDA can spontaneously dismutate to dehydroascorbate which then reacts with glutathione to produce ascorbate and oxidized glutathione. Oxidized glutathione is converted to reduced glutathione by glutathione reductase, using NADPH as an electron source (Mittler, 2002). Alternatively, ascorbate can be regenerated in plastids using MDA reductase with the requirement of NADPH as an electron donor.

2.4.3 Developmental activity

Though ROS are generally viewed as toxic molecules, produced in response to biotic or abiotic stressors, at low concentrations they act as signaling molecules, influencing development.

A number of key studies have found a central class of enzymatic complexes that mediate response to both biotic and abiotic challenges and produce a ROS burst, but are also responsive to hormones and other developmental signals, producing comparatively small concentrations of ROS. Plant respiratory burst oxidative homologs (rboh) are homologous to the human neutrophil pathogen-gene *gp91phox*. The $gp91^{phox}$ represents one of the two constituents of the mammalian NADPH oxidase (NOX) plasma membrane-associated protein. These proteins are involved in the generation of extracellular reactive oxygen species (ROS) from molecular oxygen in response to biotic stress (reviewed in Baker and Orlandi, 1995). The first report of a role for ROS in plant physiology came with the discovery by Levine et al. (1994) that hydrogen peroxide from an oxidative burst triggered a hypersensitive disease resistance response. Reactive oxygen species are also major contributors to the gibberellic acid (GA_3) induced programmed cell death (PCD) of barley aleurone cells (Bethke and Jones, 2001). In hormone signaling, Joo et al. (2001) found that auxin treatment or gravistimulation induced the asymmetric distribution of ROS in maize roots. Additionally, abscisic acid (ABA) induction of ROS in guard cells of Arabidopsis and *Vicia faba* is necessary for stomatal closure (Pei et al., 2000; Zhang et al., 2001a). Recently, involvement of extracellular ROS in plant development and architecture was examined in tomato plants (Sagi et al., 2004). Antisense *Lycopersicon esculentum respiratory burst oxidative homologue1* (*rboh1*) and *whitefly-induced1* (*wfi1*; another *L. esculentum* RBOH) plants showed reduced hydrogen peroxide accumulation compared to wild type plants, as well as overproliferation of secondary shoots and abaxial leaf curling.

Interaction of ROS and ABA during control of stomatal aperature function has been well documented. ROS, specifically hydrogen peroxide (H_2O_2), produced downstream of ABA treatment is able to inhibit K^+ transport, promoting cytosolic Ca^{2+} accumulation in Arabidopsis and bean (*Vicia faba*) guard cells, accelerating stomata closure during drought stress (Pei et al. 2000; Zhang et al. 2001b).Production of *RBOH1* was also increased by treatment with ABA, IAA, benzylaminopurine, a cytokinin, and ACC, an ethylene precursor (Sagi et al., 2004). The use of ROS as a signal requires careful regulation.

Too much ROS and cell death can occur, not enough and proper cellular development will be impaired. The redox state of a plant is a tightly regulated system that requires all molecules in the system present at amounts that are appropriate for the plant's developmental stage and stress level.

As in mammals, extracellular ROS that regulate plant development are produced by NOX that generate O_2^-. The cytoplasmic NADPH in the NOX complex donates an electron to extracellular oxygen, reducing it to superoxide (Reviewed in Sagi and Fluhr, 2006). Extracellular ROS are associated with cross-linking of cell wall components (Schopfer, 2001), differentiation of vascular tissue (Nakanomyo et al., 2002), and suberization in wounded potato (Razem and Bernards, 2003). Auxin was previously shown to promote the production of superoxide in the outer epidermis of maize coleoptiles (Schopfer, 2001). Auxin-induced cell wall elongation was shown to require the hydroxyl radical as a cell wall loosening factor. These factors may be responsible for the developmental changes often seen in transgenic plants with altered ROS production.

2.5 Root development

Critical to the understanding of root development *in planta* is an accurate description of the cellular components of this organ. The primary root of Arabidopsis is a relatively simple structure consisting of 4 radial layers, each one cell thick. From the outside they are the epidermis, cortex, endodermis, and pericycle (Dolan et al., 1993). The stele includes the pericycle, which forms the outermost layer of the stele, and the central region of the primary root containing the vascular tissue (phloem and xylem) as well as stele parenchyma cells (Dolan et al., 1993). As the primary root develops, each cell type forms a vertical file of cells visualized in the transverse plane. Every individual cell file can be traced to meristematic initials, which are responsible for maintaining proper cellular organization of the root in the root apical meristem (Malamy and Benfey, 1997) and are established during embryogenesis (Scheres et al., 1994). Upon mitotic division of meristematic initial cells, a new initial is regenerated followed by the addition of one cell to the vertical cell file. Repeated mitotic division results in vertical growth of the primary root. In Arabidopsis, 4 sets of meristematic initials have been identified: i) cells differentiating into the epidermal and lateral root cap; ii) cells differentiating into the columella root cap; iii) one producing the cortical and endodermal layers; and iv) one producing the stelar tissues (Dolan et al., 1993).

As the primary root develops, several regions of the root form, and are typified by the types of cells and stage of development. The meristematic zone (MZ) encompasses the meristematic initials, representing a region of great mitotic activity and constitutes the distal 250

μm of the primary root (Dolan et al., 1993). Proximal to the MZ is the elongation zone (EZ), a region containing cells undergoing elongation. Following the EZ is the differentiation zone (DZ), the region of the primary root that contains fully elongated cells that mature into differentiated tissue. The distal region of this zone can be identified by locating cells with initiated root hairs. A more precise region of the root, lying between the MZ and DZ is the basal meristem, an area characterized by cells undergoing both cell division and cell elongation (Beemster et al., 2003; Péret et al., 2009).

Root development is a dynamic process guided by the positional flow of auxin (De Smet et al., 2007; Grieneisen et al., 2007; Dubrovsky et al., 2008; Péret et al., 2009; Vanneste and Friml, 2009). Distribution of auxin mediated by PAT is responsible for the formation of gradients, driving root development. Using a combination of computational modeling and experimental validation, maps of auxin distribution were described, allowing Grieneisen et al. (2007) to examine pattern formation and the formation of discrete root zones. Auxin is transported basipetally down the stele of the primary root in a cell-to-cell manner by the influx carrier AUX1 and the efflux PIN proteins (Gälweiler et al., 1998; Friml et al., 2002a; Friml et al., 2002b; Friml et al., 2003). At the meristem, PINs redirect the flow of auxin outward to the epidermis where it is transported acropetally through the lateral root cap (Leyser, 2005). This system of auxin redistribution resembles a reverse fountain where auxin is transported down the stele of the root towards the root tip, then redirected to the epidermis and transported upward. Further, the flow of auxin through these cell files is sufficient to generate local auxin maxima and gradients, defining the MZ, EZ, and the development of lateral roots.

2.5.1 Lateral root development

Following the formation of auxin gradients and zonation of the root, cells in the DZ begin to differentiate into their programmed tissue or organ. Of these organs, the lateral root is of special interest. Lateral roots enable plants to expand in a plane perpendicular to the primary root. Large numbers of lateral roots can be produced down the entire length of the cylindrical primary root, greatly enhancing a plant's water and ionic uptake potential.

In Arabidopsis, lateral roots develop from the pericycle, which until recently was thought to be a layer composed of a single cell type. Recent cytological analysis showed the pericycle is actually composed of two distinct cell types, xylem associated cells, which display strong competence to undergo cell division after specific stimuli, and phloem associated cells which

remain quiescent (Parizot et al., 2008). Together, the xylem and phloem associated cells differentiate to form the diarch stele characteristic of Arabidopsis, however lateral roots develop exclusively from the xylem associated cells. Although all xylem associated cells remain competent to undergo cell division, few will form lateral roots.

Prior to the formation of lateral roots, xylem associated cells in the basal meristem known as xylem pole pericycle cells are "primed" toward lateral root development, a process regulated by auxin (De Smet et al., 2007). Lack of auxin, caused either by application of a transport inhibitor such as *N*-1-naphthylphthalamic acid (NPA) or by mutation of the *PIN* efflux transporters blocks or inhibits lateral root formation (Himanen et al., 2002; De Smet et al., 2007; Laskowski et al., 2008). High auxin levels in the basal meristem, detected using the *DR5::GUS* reporter construct correlate with future sites of lateral root initiation. Furthermore, the amount of auxin in the basal meristem oscillates under constant light, reaching a maximum every 15 hours (De Smet et al., 2007). This temporally and spatially specific auxin maximum correlates with and is capable of stimulating lateral root initiation. Exogenous local application of auxin is also sufficient to induce lateral root formation (Boerjan et al., 1995; Dubrovsky et al., 2008), and the oscillatory action of auxin maxima explains that though every xylem pole pericycle cell is capable of forming a lateral root, not all are fated to become primordia. This oscillatory action also causes regular spacing of lateral roots, a mechanism unknown until recently. Initiation of lateral roots involves *SOLITARY-ROOT* (*SLR*), an Arabidopsis gene encoding IAA14, a transcriptional repressor within the Aux/IAA protein family (Fukaki et al., 2002). Gain-of-function *slr* plants, generated by mutating specific amino acids within the coding region of the gene and therefore stabilizing the repressor protein, completely lack lateral roots and are insensitive to applied auxin. Like other Aux/IAA proteins, IAA14 represses transcription of auxin-regulated genes by dimerizing with specific ARFs, identified as ARF7 and ARF19, both of which are transcriptional activators (Fukaki et al., 2005). In the presence of root-derived auxin (Bhalero et al., 2002), IAA14 is targeted to the 26S proteasome by SCF^{TIR1}-mediated ubiquitination freeing the ARFs to activate auxin-regulated gene transcription, allowing lateral root initiation to proceed.

Primed xylem pole pericycle cells are known as pericycle founder cells and are competent to initiate a lateral root. Lateral roots initiate from pairs of pericycle founder cells flanked by unprimed xylem pole pericycle cells (Blaikely et al., 1982; Malamy and Benfey,

1997; Dubrovsky et al., 2008) with the initial event marked by an anticlinal and asymmetrical division of the founder cells (Malamy and Benfey, 1997). At the cellular level, xylem pole pericycle cells are regulated from G1-to-S transition by the cyclin-dependent kinase (CDK) protein KIP-RELATED PROTEIN2 (KRP2; Himanen et al., 2002). In the absence of auxin, KRP2 acts as a checkpoint inhibitor, preventing cells from entering S phase of mitosis. Auxin appears to be a transcriptional regulator of *KRP2*, decreasing *KRP2* expression when auxin is present, providing a cellular mechanism for the requirement of auxin for the formation of lateral roots.

Following initiation, lateral roots proceed through seven discrete stages, outlined by Malamy and Benfey (1997). The "domed" structure of lateral root primordia is formed by asymmetric division of the 4 cells comprising the lateral root initial. The founder cells divide and expand radially while the flanking cells do not. A series of anti- and periclinal divisions creates four discrete layers in the growing primordia, outer layer (OL) 1, and OL2 followed by inner layer (IL) 1 and IL2 (Malamy and Benfey, 1997). Further division and radial expansion pushes the primordia first through the endodermal layer (stage 4), the cortex (stage 5), and the epidermis (stage 6). Stage 6 marks the first appearance of cells adopting the shape of vascular elements with the differentiation of the stele following. In the final stage, the lateral root primordia is pre-emergent and is just below the outer epidermis of the primary root.

Lateral root emergence presents an interesting challenge: how does the root pierce the epidermis without water loss or pathogen exposure? Prior to root emergence, auxin originating from developing lateral roots creates local auxin maxima near the primordia (Swarup et al., 2008). These local maxima, in turn, activate expression of *LAX3*, an auxin influx carrier and homologue of *AUX1* in the cortical and epidermal cells overlying the growing primordia (Swarup et al., 2008). Accumulation of auxin in the cortical and epidermal cells resulting from LAX3-mediated auxin influx activates expression of cell wall remodeling enzymes. Furthermore, activation of these enzymes is spatially restricted to cell layers overlying the growing primordia (Swarup et al., 2008). Several classes of remodeling enzyme displayed increases in expression during lateral root emergence including a subtilisin-like protease, pectate lyase 2 (PLA2), polygalacturonase (PG), xyloglucan:xyloglucosyl transferase (XTR), expansin 17 (EXP17), and glucosyl hydrolase 17 (GLH17; Swarup et al., 2008). Many of these enzymes have documented effects on cell wall loosening. Expansins loosen cell wall polysaccharides allowing for turgor

pressure-driven cell expansion (Cosgrove, 2000). Pectate lyases catalyse cleavage of de-esterified pectin, a component of cell walls (Marin-Rodriguez et al., 2002). Polygalacturonases are involved in cell separation processes (González-Carranza et al., 2007) while XTR enzymes also have a role in cell expansion, localizing to expanding tissue (Vissenberg et al., 2005). Until auxin flux in pre-emergent lateral roots was examined the mechanism for emergence was unknown. Auxin's involvement in lateral root development pervades every step and is integral for initiation and emergence. Following emergence, the lateral root continues to elongate and is composed of similar cell layers as the primary root (Dolan et al., 1993).

2.6 Glucosylphosphatidylinositol-anchored proteins (GPI-APs)

Glucosylphosphatidylinositol-anchored proteins are post translationally modified plasma membrane proteins present in low abundance (less than 0.5 % total cell proteins) that are integrated into the outer plasma membrane bilayer, linked to the membrane by lipids or lipid-like moieties (Elortza et al., 2006). The amino acid sequence of all GPI-APs share some common structural features: Absence of transmembrane domains, the presence of a cleavable N-terminal hydrophobic signal, an 8-20 amino acid hydrophobic region in the C-terminus, and a hydrophobic spacer region preceding the hydrophobic region in the C-terminus, the ω-site (Elortza et al., 2006; Borner et al., 2002; De Groot et al., 2005). The GPI anchor is a signal that targets proteins to the outer leaflet of a cell's plasma membrane. Unfortunately, existence of the GPI anchor does not convey information regarding a specific protein function.

2.6.1 Biosynthesis

Post-translational processing of proteins possessing a GPI modification site begins in the cytosolic side of the endoplasmic reticulum (ER) where the complete GPI anchor is assembled prior to attachment to a protein (Chatterjee and Mayor, 2001). The molecular mechanisms for anchor biosynthesis and attachment are highly conserved among eukaryotes, including animals (Chatterjee and Mayor, 2001), plants (Lalanne et al., 2004) and fungi (Fontaine et al., 2004). In mammals, biosynthesis of the anchor occurs on the cytosolic side of the ER and the first step involves GPI-*N*-acetylglucosaminyltransferase (GPI-GnT), an enzyme consisting of at least seven proteins (Kinoshita and Inoue, 2000; Chatterjee and Mayor, 2001; Maeda et al., 2007). The GPI-GnT adds acetylglucosamine to phosphotidylinositol, followed by a deacetylation reaction (Hooper, 2001). Subsequent steps involve translocation across the ER membrane

followed by sequential additions of mannose units and an ethanolamine phosphate to the glucosamine-phosphatidylinositol (Kinoshita and Inoue, 2000; Boccuni et al., 2000). Once the GPI anchor is completed it is attached to proteins by GPI transamidase, which cleaves the GPI attachment signal peptide from the protein and links it to the GPI anchor (Maeda et al., 2007).

Prior to GPI anchor attachment, a protein undergoes several steps of post-translational processing in the ER. During processing the amino terminal signal peptide is cleaved by the N-terminal signal peptidase (Udenfriend and Kodukula, 1995). Following cleavage of the N-terminal signal peptide, the C-terminal hydrophobic signal peptide is cleaved by a C-terminal signal peptidase. Cleavage of the C-terminal signal peptide exposes the site of anchor attachment of the future GPI-AP. The completed GPI is then transferred to the protein's anchor attachment site, mediated by a GPI transamidase consisting of at least two ER membrane proteins, GAA1 and GPI8 (Meyer et al., 2000; Ohishi et al., 2000). After GPI attachment, the proteins are transported to Golgi bodies where additional sugars are added to the mannose (Lalanne et al., 2004). The proteins are subsequently sorted and transported to the outer leaflet of the plasma membrane via the secretory system (Chatterjee and Mayor, 2001) where the GPI binds to the lipids on the membrane. The GPI anchor is composed of unsaturated fatty acids, and it has been hypothesized that the composition of the anchor targets GPI-anchored proteins to lipid rafts, or microdomains that exist within the plasma membrane composed of sphingolipids and cholesterols (Peskan, 2000; Bhat and Panstruga, 2005; Maeda eta l., 2007). A second hypothesis suggests that the lipid portion of the GPI anchor is remodeled to predominantly saturated rather than unsaturated fatty acids for insertion into non-raft regions of the plasma membrane (Elortza et al., 2006; Maeda et al., 2007).

An interesting feature of GPI-APs is that they can exist as either membrane associated proteins, linked to the membrane through the GPI moiety, or the proteins can be released from the GPI anchor by specific phospholipases, generally phospholipase C and D (Borner et al., 2003; Elortza et al., 2006; Lalanne et al., 2004). In mammals cleavage of the GPI anchor by phospholipases releases the protein into the extracellular matrix in response to developmental signals (Gillmor et al., 2005). Similarly, plants and fungi have GPI-APs that are membrane associated. However upon release of the protein by phospholipase digestion, the protein localizes to the cell wall, where it has influence on a number of developmental activities (Gillmor et al., 2005; Jones et al., 2006; Sun et al., 2004; De Groot et al., 2005; Damveld, 2005). In mammals,

GPI-APs have the ability to transfer from one cell surface to the plasma membrane of an adjacent cell in a mechanism known as protein painting (Premkumar et al., 2001). It is unknown if a similar activity occurs in plants.

2.6.2 Developmental roles

In addition to the GPI anchor targeting GPI-APs to the outer leaflet of the plasma membrane, lipid rafts have been hypothesized to bind GPI-APs, possibly having a role in membrane targeting, though this has not been demonstrated experimentally (Munro, 2003). In mammals, lipid rafts are hypothesized to be small regions in the outer leaflet of the plasma membrane enriched in cholesterol and sphingolipids that are associated laterally with one another, possibly through weak interactions between the carboxy heads of the lipids (Simons and Ikonen, 1997; Martin et al., 2005). Lipid rafts are thought to function as sorting platforms for proteins destined to the plasma membrane (Borner et al., 2005), accumulating GPI-APs, transmembrane proteins, and doubly acylated tyrosine kinases of the Src family (Borner et al., 2005). The tight association of sphingolipids in rafts results in the formation of detergent insoluble glycolipid-enriched complexes (DIGs). Interactions with lipid rafts also confer detergent insolubility on a GPI-AP and the association of GPI-APs with DIGs is affected by the cholesterol and sphingolipids present in the raft (Simons and Ikonen, 1997). Some signaling molecules cluster in DIGs (Parton and Simons, 1995; Anderson, 1993; Lisanti et al., 1994) such as Arabidopsis hypersensitive response regulators (Borner et al., 2005), and *Nicotiana tabacum* NOX enzyme complexes and G protein regulators; the lateral association of lipids on lipid rafts may lead to clustering of membrane associated molecules, such as GPI-APs in a similar fashion. The clustered GPI-APs may be involved in signal transduction, either through a flippase activity followed by phospholipase digestion of the GPI-AP, resulting in a free cytosolic protein that can act as a secondary messenger, or by the clustered GPI-APs interacting with signaling proteins on the cytosolic leaflet of the plasma membrane (Simons and Ikonen, 1995).

In yeast, the *SPI1* gene coding for a GPI-AP was found to be involved in resistance to the highly lipophilic auxin analog 2,4-dichlorophenoxyacetic acid (2,4-D; Simoes et al., 2003). When incubated on 0.3 mM 2,4-D, wild type *Saccaromyces cerevisiae* cell walls became resistant to β-1,3-glucanase digestion. *S. cerevisiae spi1* cells, on the other hand, lost viability and were susceptible to digestion with β-1,3-glucanase. β-1,3-glucan is a major constituent of the yeast cell wall. SPI1 may mediate a decrease in diffusion of lipophilic acids across the cell wall.

Unlike the mammalian and yeast systems where much research has been conducted to elucidate the function of various GPI-APs in development (Hooper, 2001; Udenfriend and Kodukula, 1995; Brown and Rose, 1992; Meyer et al., 2000; Faure et al., 2006), comparatively little research has been done in plants (Borner et al., 2002). The first steps of GPI biosynthesis have been described in plants by examining disruptants of the PIG-A subunit of GPI-GnT, *SETH1* and *SETH2* (Lalanne et al., 2004). Disruption of *SETH1* in Arabidopsis prevented male gametophyte transmission, while *seth1* and *seth2* disruptants had diminished pollen tube germination and growth. Forty-seven GPI-AP genes were identified that have functional relevance to pollen, and the mutant phenotype suggests that at least one of the 47 genes is affected by the disrupted GPI-GnT (Lalanne et al., 2004). The *L. esculentum* AGP-1 arabinogalactan protein (AGP) has been identified as a GPI-AP (Zhao et al., 2002; Sun et al., 2004a). Once LeAGP-1 reaches the plasma membrane, it is cleaved by a phospholipase and the free protein localizes to the cell wall where it may have roles in cellular signaling and matrix remodeling (Sun et al., 2004a; Sun et al., 2004b). Additional AGPs have been identified, and the arabinogalactan may target a released GPI-AP to the cell wall where these proteins are involved in a variety of developmental important processes ranging from cell wall synthesis, cell differentiation, and cell-cell recognition, to programmed cell death (Nothnagel, 1997; Showalter, 2001; Gillmor et al., 2005).

GPI-anchored proteins have been implicated in plant development, where research has examined the role of proteins anchored to the plasma membrane and their interactions with auxin. *SKU5* was isolated by mutation; mutant plants grew skewed roots (curled and twisted counterclockwise; Sedbrook et al., 2002). SKU5 is a GPI-AP and was localized to the plasma membrane and cell wall, and may modify linkages between cell wall structural components effecting turgor driven cell extension. The authors also found that *SKU5* was a member of a multigene family and is structurally related to multiple copper oxidases (Sedbrook et al., 2002). The C-teminus of ABP1 (CBP1) is freed from the plasma membrane association after phospholipase C digestion demonstrating that it is likely a GPI-AP (Shimomura, 2006). CBP1 is a copper-binding protein that likely contributes to directional cell growth in the cell wall and is homologous to *SKU5,* possibly acting in a similar pathway. The *PMR6* pectate lyase-like gene was determined to be a loss of function mutation that resulted in powdery mildew resistance in Arabidopsis (Vogel et al., 2002). Interestingly, this gene is also a GPI-AP and represents a novel

form of pathogen resistance. *pmr6* mutation causes an increase of pectins in the cell wall, decreasing the nutrients available to pathogens.

2.7 Auxin, ABA, and ROS control root development

Initiation, emergence, and elongation of lateral roots is believed to involve the action of multiple hormones including auxin (Malamy and Benfey, 1997; Casamiro et al. 2001; Himanen et al. 2002; Dubrovsky et al. 2008), cytokinins (Dasharath et al. 2004; Laplaze et al. 2007), and more recently, abscisic acid (ABA; De Smet et al. 2003; Deak and Malamy, 2005; Guo et al. 2009) and ROS (Joo et al., 2005; Li et al., 2006).

2.7.1 Auxin and ABA cross talk

As previously outlined, ABA is a key regulator of stomatal function and response to abiotic stressors including drought, cold, and heat. An example of this crosstalk is illustrated by *AUXIN RESPONSE FACTOR 10* (*ARF10*), a gene normally regulated by microRNA160, causing mRNA cleavage of the transcript (Jones-Rhodes et al., 2006). Expression of *ARF10* resistant to negative regulation by microRNA160 caused hypersensitivity to ABA, greatly reducing germination frequency in mutant Arabidopsis seeds grown on the hormone (Liu et al. 2007). Additionally, when grown a medium containing both auxin and ABA, germination of Arabidopsis is inhibited, indicating some degree of cross talk between the two hormones (Brady et al., 2003).

ABA is involved in lateral root development. Initiation and elongation of lateral roots requires ABA signaling through *LATERAL ROOT DEVELOPMENT 2* (*LRD2*), acting as an antagonist to auxin (Deak and Malamy, 2005). Examination of lateral root development in mutant *abi3* loss-of-function Arabidopsis plants showed that while exogenous application of IAA correlated with increased lateral root initiation in both wild type and *abi3* mutant plants, the mutants required a higher concentration of IAA to reach wild type initiation levels (Brady et al., 2003). That an ABA-insensitive mutant requires increased auxin for root initiation implies a convergent pathway downstream of both. Furthermore, mutation of Arabidopsis *ENHANCED RESPONSE TO ABA1* (*ERA1*) increased the lateral root initiation rate (Fukaki and Tasaka, 2009). This indicates that while ABA appears to act as a repressor of lateral root development, some component of ABA signaling may be required for proper development, mediated through ERA1, followed by ABI3 and LRD2 (De Smet et al., 2006a; Fukaki and Tasaka, 2009).

Microarray analysis of salt stress-regulated genes in Arabidopsis plants led to the discovery of *AtNAC1* (He et al., 2005), a member of the *NAC* gene family encoding proteins that contain a specific helix-turn-helix domain that binds DNA (Aida et al., 1997). Overexpression of *AtNAC1* in Arabidopsis caused proliferation of lateral roots. Expression analysis of *AtNAC1* showed transcript accumulation in the roots and flowers. Specific induction by ABA, auxin, and ACC, the stable precursor to ethylene, was also shown (He et al., 2005). Though induced by ABA treatment, salt induction of *AtNAC1* in *abi2*, *abi3*, and *abi4* mutant Arabidopsis plants was not affected, suggesting that the salt stress response does not require the ABI family of transcription factors. Though not tested, it is possible that ABA induction of *AtNAC1* is a secondary effect of auxin, ACC, or even salt stress signaling pathways.

Evidence also suggests that ABA-mediated repression of lateral root development can proceed through an auxin-independent pathway using the Arabidopsis catalytic subunit of protein phosphatase 2A (PP2Ac-2; Pernas et al. 2007). These studies point toward both auxin-dependent and -independent ABA signaling pathways operating during development. Although specific genes involved in lateral root development have been identified (Deak and Malamy, 2005; Swarup et al., 2008), the transduction mechanism for auxin and ABA signals are unknown.

2.7.2 Hormonal interactions with ROS

Evidence has recently surfaced implicating ROS in downstream auxin signal transmission. During auxin-stimulated cell elongation, the concentration of extracellular $OH^{\cdot}$ and other ROS increase (Schopfer, 2001; Schopfer et al., 2002; Liszkay et al., 2004). This increase is directly dependent on auxin. Application of ROS scavengers blocks auxin-induced cell elongation, and the inhibition can be rescued by further application of H_2O_2 (Schopfer, 2001). Further evidence of ROS-mediated transmission of auxin signals is present during root gravitropism. The mechanical gravitropic response is dependent on not only auxin gradients in the developing roots but also on local concentrations of ROS (Joo et al., 2005). Similar to cell elongation, blocking auxin transport inhibits gravitropism, and tropism can be restored by applying H_2O_2 to specific regions of the root. For proper root hair development, the *ROOT HAIR DEFECTIVE2* (*RHD2*) gene, an Arabidopsis gene coding for a NOX subunit must be present to stimulate Ca^{2+} influx during root hair elongation (Foreman et al., 2003). It has been hypothesized that ROS involved in root development may originate from NOX (Joo et al., 2005). In the

absence of RHD2, extracellular ROS accumulate at very low concentrations and root hair elongation does not occur, demonstrating a critical role of ROS as a signal molecule in root hairs.

The ABA-independent response to salt stress appears to focus on altering the osmotic concentration of cells and removal of the Na^+ ion. Similar to the response to drought, when plants encounter high salt concentrations they begin increasing the cellular concentration of the sugar alcohol D-ononitol (Vinocur and Altman, 2005) and the amino acid proline (Borsani et al., 2005; Seki et al., 2007). Interestingly, a component of proline-mediated salt tolerance in Arabidopsis involves a pair of overlapping genes, a Δ^1-pyrroline-5-carboxylase dehydrogenase (*PSCDH*), involved in proline catabolism and *SRO5*, a salt-inducible gene with no described function (Borsani et al., 2005). In the Arabidopsis genome, both genes are in opposing orientation, and generate a convergent transcript that contains an overlapping 760 nucleotide region. In response to salinity, but only when both genes were present, an endogenous short interfering RNA (siRNA) transcript is produced and promotes cleavage of *PSCDH* transcript resulting in decreased proline catabolism and increased salt tolerance (Borsani et al., 2005). Removal of Na^+ ions is mediated by the SALT OVERLY SENSITIVE (SOS) regulatory pathway (Zhu, 2001). Three proteins have been identified in this pathway; SOS1, an Na^+/H^+ antiporter (Shi et al., 2000), SOS2, a serine/threonine protein kinase (Liu et al., 2000), and SOS3, a Ca^{2+} sensor (Liu and Zhu, 1998). Salt elicits an increase in cellular Ca^{2+}, likely as a consequence of phospholipase C-mediated release from cellular reserves (Hirayama et al., 1995) and is sensed by SOS3, which activates SOS2 (Zhu, 2001). *SOS1* mRNA is unstable under normal growing conditions (Chung et al., 2008). When challenged with salt, other ionic, drought, or oxidative stress, mRNA stability increases. Furthermore, both SOS2 and SOS3 regulate the expression of *SOS1* and are required for its activity (Shi et al., 2000). Once activated, SOS1 exports Na^+ while importing H^+, elevating the extracellular pH, which in turn is thought to activate ROS synthesis via the NOX enzyme complex (Chung et al., 2008). The ROS generated by NOX create a positive feedback, stabilizing *SOS1* mRNA, leading to further Na^+ export. Localization studies showed that SOS1 controls Na^+ transport from the root to shoot via the xylem (Shi et al., 2002) and in Arabidopsis plants overexpressing *SOS1*, plants have increased salt tolerance and reduced cellular Na^+ content (Shi et al., 2003). No direct effect of ABA on either the SOS or ITN1 pathway has been identified to date, however since both regulatory

pathways take advantage of ROS generated by NOX, there may be some overlap between ABA-mediated and stress-mediated ROS generation.

Though a large body of work examining ROS production in response to ABA has focused on guard cells as a model, limited evidence suggests that H_2O_2 is also involved in mediating the ABA-repressive effect on primary root growth in Arabidopsis (Liang et al. 2007). The effect of ABA-mediated H_2O_2 generation during root development contrasts with increasing evidence of auxin-regulated ROS production. Indole-3 acetic acid (IAA) treatment of maturing maize embryos, germinating seeds, or true leaves correlated with an increase in catalase gene expression (Lingqiang and Scandalios, 2002), possibly as the result of increased ROS within the embryos. Auxin-induced growth inhibition of maize roots is mediated through the reduction of superoxide (O_2^-), a precursor of the hydroxyl radical ($OH^·$), causing cell wall loosening and allowing cell expansion to occur (Schopfer, 2001; Liszkay et al. 2004). In growing Arabidopsis roots, auxin-induced gravitropic responses are promoted by the asymmetrical distribution of ROS through the action of phosphatidylinositol 3-kinase and its putative association with the NADPH oxidase (NOX) enzyme complex (Joo et al., 2005). Demonstration of positive regulation between ABA and auxin signaling with NOX (Foreman et al. 2003; Kwak et al. 2003; Li et al. 2005; Lin et al. 2009) suggests this enzyme complex may represent a point of convergence between the two hormones, and that ROS produced by this complex may be involved in transmitting signals from these hormones during development. Though auxin and ABA proceed through separate signaling pathways, these signals could converge on NOX, causing increases or decreases in extracellular ROS production to drive root development through an uncharacterized pathway.

2.8 The current study

The objective of this dissertation was to characterize the function of a copper-induced gene *COPPER INDUCED in LEAVES1* (*CIL1*) from *Brassica carinata* and its putative ortholog from Arabidopsis, an auxin-regulated gene, *AUXIN INDUCED in ROOTS12* (*AIR12*). The study was focused on understanding how these genes, and the proteins they code for, are involved in ABA, auxin, and ROS signaling during lateral root development. Lateral root development was examined in response to abiotic stressors or hormone treatment using a combination of phenotypic quantification, protein subcellular localization, and enzymatic assays.

Germination, primary root elongation, lateral root production, and lateral root elongation was quantified in both control and mutant lines by comparing these traits on control medium and medium supplemented with mannitol, KCl, and nitrogen. As well, the response to auxin and ABA was examined.

Light and confocal laser-scanning microscopy was utilized to determine transcript and protein subcellular localization, respectively. Localization of transcript was examined under control conditions and after growth on auxin. Protein localization was visualized under control conditions, and after growth on auxin, H_2O_2, and KCl using an *AIR12* fusion with *GFP* under the control of the *AIR12* promoter. Subcellular localization was accomplished using an *AIR12* or *CIL1* fusion with *GFP* under the control of the constitutive overexpressing *35S* promoter to confirm extracellular localization.

Enzyme assays were completed to examine the effect of *AIR12* mutation and *CIL1* expression reductions. The major focus of the qualitative assays was the fluorescent determination of extracellular and intracellular superoxide. Quantitative assays were completed to examine total root catalase activity and H_2O_2 concentration. These assays, combined with the other data, help build a picture of how AIR12 and CIL1 may act in controlling lateral root development of Arabidopsis and *B. carinata*.

3. MATERIALS AND METHODS

3.1 Description of lines used

Throughout this study two plant species were used: *Brassica carinata* (A. Braun) and *Arabidopsis thaliana* (L.) Heynh (Arabidopsis). The *B. carinata* lines used were previously described (Gibson, 2005). The *Brassica carinata* breeding cultivar C90-1163 from Agriculture and Agri-Food Canada Research Station (Saskatoon, Saskatchewan, Canada) was used as the wild type and transformation recipient plant material. Z. Zheng (PBI/NRC) and T. Uchacz (University of Saskatchewan) produced the antisense *CIL1* transgenic plants (Zheng et al., 2001). Antisense expression was driven by the cauliflower mosaic virus duplicated-enhancer 35S-promoter (Kay et al., 1987) and leader sequence from alfalfa mosaic virus RNA4 (Datla et al., 1993). This construct was cloned into the plant binary vector RD400 (Datla, et al., 1992) and was used to transform *B. carinata*, according to Babic et al. (1988). Plants from individual transformation events were allowed to self-pollinate and the copy number of the antisense cassette was determined (Gibson, 2005). Homozygous antisense *CIL1* line 6 (AC6) was used in experiments involving *B. carinata*.

Experiments involving Arabidopsis used the Nossen, Landsberg *erecta*, and Columbia ecotypes. In addition to control plants from each ecotype a description of mutant plant lines used is summarized in Table 3.1.

3.1.1 Plant material and growth conditions

Both *B. carinata* and Arabidopsis seeds were sown in Sunshine 3 germinating mix (Sun Gro Horticulture, Vancouver, B.C., Canada). *Brassica carinata* plants were grown in a Conviron C1010 growth chamber with a 16 h photoperiod, a light intensity of 102 μmol s^{-1} m^{-2} and a constant temperature of 21^{o}C. Arabidopsis plants were grown in a Foster growth chamber with a 16 hour photoperiod, a constant temperature of 24 ^{o}C and light intensity of 73 μmol s^{-1} m^{-2}. Light was provided by Sylvania 215 W cool white fluorescent tubes in both chambers. After germination, plants were thinned to 4 plants per pot (*B. carinata)*, or one plant per pot (Arabidopsis*)* and grown until senescence.

Ecotype	Line Number	Institute	Reference and/or source
Nossen	CS3081 (Wild type)	ARBC	Keith Davis, Arabidopsis Biological Resource Centre
	CS8518 (*Ds* Parent)	ARBC	Fedoroff and Smith, 1993; Smith et al., 1996
	CS8538 (*Ac* Parent)	ARBC	Fedoroff and Smith, 1993; Smith et al., 1996
	54-4309-1 (*air12-1*)	RIKEN	Ito et al., 2002
Landsberg *erecta*	Wild type	AAFC	Isobel Parkin, Agriculture and Agri-Food Canada
	ET8602 (*air12-2*)	CSHL	Martienssen, 1998; Sundaresan et al., 1995
	ET13878 (*air12-3*)	CSHL	Martienssen, 1998; Sundaresan et al., 1995
	GT16870 (*air12-4*)	CSHL	Martienssen, 1998; Sundaresan et al., 1995

Table 3.1. Description of Arabidopsis lines used.

3.1.2 Seed sterilization and growth medium

A solution containing 15% bleach (v/v), 0.01% Silwet L-77 (v/v; Lehle Seeds, Round Rock, TX, USA) was added to *B. carinata* or Arabidopsis seed and incubated on a rotary shaker for 20 minutes. The seed was centrifuged at 6,000*g* for 1 minute, the bleach solution was pipetted off and the seed washed with water. The seed was again centrifuged, the water pipetted off and replaced with 70% ethanol followed by continuous shaking for one minute. The seed was centrifuged, the ethanol pipetted off and replaced with water. The seed was centrifuged, the water was pipetted off and replaced with fresh water and repeated 4 additional times. After the final water wash, seed was transferred to media using forceps (*B. carinata*) and placed in a Conviron 01114 growth chamber or pipetted onto the media (Arabidopsis), incubated for 3 days at 4 ^{o}C in the dark (Arabidopsis) and placed in a Conviron 01114 growth chamber at 23^{o}/18^{o} C with a 16/8 day night photoperiod, respectively. Seed germination and root growth was monitored in response to different abiotic stressors. Control medium was composed of ½ Murashige and Skoog basal salts (Sigma-Aldrich, St. Louis, MO, USA) supplemented with 1% sucrose (w/v; Sigma-Aldrich, St. Louis, MO, USA) and either 1.2% (w/w) or 0.8% (w/w) phytagar (Caisson Laboratories, North Logan UT, USA). The medium was then autoclaved, followed by the addition of abiotic stressor chemicals or hormones. Media containing abiotic stressors were composed of the control medium supplemented with one of 60 mM mannitol, 30 mM KCl, 40 mM nitrate (composed of 20 mM KNO_3, 20 mM NH_4NO_3; Fisher Scientific, Fair Lawn, NJ, USA), 400 nM α-napthaleneacetic acid (α-NAA; Sigma-Aldrich, St. Louis, MO, USA), 100 nM 2,4-dichlorophenoxyacetic acid (2,4-D; Sigma-Aldrich, St. Louis, MO, USA), 1 mM H_2O_2 (EMD Chemicals, Gibbstown, NJ, USA), 3.5% sucrose (w/v), 3.5 μM ± abscisic acid (ABA; Sigma-Aldrich, St. Louis, MO, USA), 5 μM ± ABA, or 3.5 μM ± ABA and 400 nM α-NAA.

3.1.3 Germination and root measurement

Germination and root assays all utilized 3 biological replicates with 10 seeds per replicate per line. Germination of Arabidopsis seeds was monitored for eight days beginning one day after placement in the growth chamber. One observation was made per day, 4 hours into the "day" portion of the photoperiod. Seeds were examined under a dissecting microscope and were scored as "germinated" once radicle protrusion from the seed could be observed.

After 13 days of growth, primary root length, lateral root number, and mean lateral root length were determined. Primary root length was measured under a dissecting microscope with a ruler. Lateral root number was manually counted under a dissecting microscope. Similarly, lateral root length of all seedlings was manually measured under a dissecting microscope using a ruler. Seedlings grown on 400 nM α-NAA, 100 nM 2,4-D, or 3.5 μM ± ABA could not be scored for lateral root number and mean lateral root length because of the high density of roots (α-NAA and 2,4-D) or lack of roots (ABA). Because auxin often causes a loss of primary root identity (Figures 3.49, 3.50) the longest root was assigned as the "primary root" and measured.

3.2 Arabidopsis *air12* lines were generated by *Ac*/*Ds*-mediated mutagenesis

Four Arabidopsis *Ac/Ds* insertion lines were used to elucidate the function of *AIR12*. Of these four lines, one originated from the accession Nössen (No-0), from the RIKEN Bioresource Center's Experimental Plant Division (Koyadai,Tsukuba-shi, Ibaraki Japan) while the remaining three are of the accession Landsberg *erecta* (Ler) and originate from the Cold Spring Harbor Laboratory (New York, USA). All four mutant lines are the result of *Association*/*Dissociation* (*Ac/Ds*)-mediated mutagenesis described by Fedoroff and Smith (1993; used by RIKEN) and Martienssen and Springer (1998; used by Cold Spring Harbor Laboratory). The lines were designated *air12-1*, to *air12-4*, respectively (Table 3.1). The mutagenesis cassettes used by RIKEN were assembled by the Fedoroff lab (Fedoroff and Smith, 1993).

3.3 Plant transformation

Flowering Arabidopsis plants were transformed according to Clough and Bent (1998) with modifications. Briefly, Arabidopsis plants were grown until flowering and the first bolts were clipped to encourage proliferation of secondary bolts. Five days after clipping, plants were transformed using the construct of interest in *Agrobacterium tumefaciens* GV3101 containing the Ti plasmid pMP90.

Prior to transformation, 1 L of *A. tumefaciens* containing the construct of interest was grown at 28 ^{o}C for 16 hours in 2xYT medium supplemented with the appropriate antibiotics. Cells were pelleted by centrifugation at 4,500*g* for 20 minutes and resuspended in a freshly prepared 5% sucrose (w/v) solution to an OD_{600} of 0.8. To the resuspended cells 0.05% Silwet L-77 (v/v) was added and the solution mixed. The above-ground parts of the plants were

submerged in the solution with gentle agitation for 15 seconds. Transformed plants were then placed on their side under a dome and in the dark at room temperature for 24 hours. Afterward, plants were returned to the growth chamber until they completed their life cycle and seeds were collected.

3.3.1 Transient infiltrations

Four to six week old *N. benthamiana* plants were used for transient infiltration. Infiltration was completed according to Sparkes et al. (2006) with one modification. To prevent viral induced gene silencing, the p19 protein of the bushy stunt virus was co-infiltrated with the construct of interest according to Voinnet et al. (2003). Briefly, 5 mL of LB supplemented with the appropriate antibiotic was inoculated with *A. tumefaciens* carrying the construct of interest and grown overnight at 28 ^{o}C. An additional 5 mL of LB was supplemented with 100 μg/mL kanamycin and inoculated with *E. coli* expressing the p19 protein and grown overnight at 37 ^{o}C. The following day, fresh infiltration medium (0.5% sucrose [w/v], 50 mM MES, 2 mM Na_3PO_4, 100 μM acetosysingone) was prepared, and the cells were centrifuged at 2,500*g* for 10 minutes, collected, resuspended in water and centrifuged again for 10 minutes. The *A. tumefaciens* culture was diluted to an OD_{600} of 0.7 in 2 mL infiltration buffer while *E. coli* containing p19 was diluted to an OD_{600} of 1.0 in 10 mL infiltration buffer. A mixture of cultures was made, containing 0.75 mL of each and approximately 1 mL was injected into the abaxial surface of mature, turgid *N. benthamiana* leaves using a syringe. The area infiltrated was then marked for reference. After two days, leaves were examined for fluorescence using a Zeiss Meta510 laser-scanning confocal microscope.

3.3.2 Selection of transgenic Arabidopsis

Prior to plating, seeds were incubated for 20 minutes with gentle rotation in a solution of 15% (v/v) bleach and 0.01% (v/v) Silwet L-77 (Lehle Seeds, Round Rock, TX, USA). The seeds were allowed to settle and the bleach solution was poured off and replaced with sterile H_2O. Seeds were mixed with the water, allowed to settle, the water was then poured off and replaced with 75 % ethanol (v/v). Seeds were vigorously shaken for 45 seconds and the ethanol was poured off, followed by 5 sterile water rinses.

Following sterilization, approximately 25 seeds were plated on medium containing ½ Murashige and Skoog (MS) salts (Sigma-Aldrich, St. Louis, MO, USA), 1% sucrose (w/v), and

0.8% Phytagar (Caisson Laboratories, North Logan, UT, USA) supplemented with either 20 μg/L hygromycin (*air12-1*) or 50 mg/L kanamycin (all other transgenic lines) and kept at 4 ^{o}C for 3 days. Plates were placed in a Conviron C1114 growth chamber with a constant temperature of 24 ^{o}C, a photoperiod consisting of 16/8 hours of light/dark, and a light intensity of 45 μmol s^{-1} m^{-2}. Light was provided by Sylvania 215 W cool white fluorescent tubes.

For selection of Arabidopsis transformed with the pER310 backbone, seed was sprinkled on top of wetted Sunshine 4 mix (Sun Gro Horticulture, Vancouver, B.C., Canada), incubated for 3 days at 4 ^{o}C in the dark, and grown in conditions listed above. After the appearance of the second true leaf, plants were sprayed with a BASTA solution containing 667 μL of 60 g/L glufosinate ammonium, 0.01% (v/v) Silwet L-77, diluted to a final volume of 500 mL H_2O. Plants were sprayed three times every other day.

3.4 *In silica* analysis of AIR12/CIL1

Five separate programs were used to analyze the primary amino acid and nucleotide sequences of AIR12 and CIL1. The Conserved Domain Database (CDD; http://www.ncbi.nlm.nih.gov/sites/entrez?db=cdd, Marchler-Bauer et al., 2003; first accessed August, 2006) was used to identify conserved domains within AIR12 and CIL1, comparing these sequences to those in the CDD database. WoLF PSORT (http://wolfpsort.org/, Horton et al., 2006; Horton et al., 2007; first accessed September, 2007) was used to predict subcellular localization of AIR12 and CIL1. To reinforce WoLF PSORT predictions, SignalP (http://www.cbs.dtu.dk/services/SignalP/, Nielsen et al., 1997; Nielsen and Krogh, 1998; Bendtsen et al., 2004; first accessed August, 2006) was used to predict signal peptides in the N-termini of AIR12 and CIL1, utilizing both Neural Networks and Hidden Markov Models. To determine the presence of sequence order and disorder, PDISORDER (http://linux1.softberry.com/berry.phtml?topic=pdisorder&group=programs&subgroup=propt, Penkner et al., 2007; first accessed January, 2008) and disEMBL (http://dis.embl.de/, Linding et al., 2003; first accessed August, 2006) were used.

Prediction of DNA motifs in isolated promoter regions of AIR12 and CIL1 defined as 1,000 bp upstream of the transcription start site was accomplished using PLACE (http://www.dna.affrc.go.jp/PLACE/signalscan.html, Higo et al., 1999; first accessed August,

2006) and the Berkeley Drosophila Genome Project's Neural Network Promoter Prediction (http://www.fruitfly.org/seq_tools/promoter.html, Reese, 2001; first accessed December, 2006).

Finally, the presence of a site for glucosylphosphatidylinositol anchor attachment on AIR12/CIL1 was predicted using the big-PI Plant Predictor (http://mendel.imp.ac.at/gpi/plant_server.html, Eisenhaber et al., 1998; Eisenhaber et al., 1999; Eisenhaber et al., 2000; first accessed July, 2006) and GPI-SOM (http://gpi.unibe.ch/, Fankhauser and Mäser, 2005; first accessed June, 2008).

3.5 DNA isolation

3.5.1 Small scale DNA preparations

Genomic DNA from Arabidopsis and *B. carinata* was isolated according to Dellaporta (1983) with slight modifications. Approximately 200 mg fresh weight of leaf tissue was frozen in liquid nitrogen in a 1.5 mL microcentrifuge tube and ground with a pestle to a fine powder. The powder was then homogenized in 500 µL extraction buffer (100 mM Tris-HCl pH 8.5, 50 mM EDTA, 500 mM NaCl, 10 mM β-mercaptoethanol), 35 µL of 20% (w/v) SDS was added, the tube was inverted four times and incubated at 65 ^{o}C for 5 min, 160 µL of 5 M potassium acetate was added and samples were mixed by inverting. Samples were incubated on ice for 10 min, followed by centrifugation at 4 ^{o}C in a microcentrifuge at 16,000*g*. After centrifugation, the supernatant was transferred to a fresh 1.5 mL microcentrifuge tube and 100 µL of 3 M sodium acetate was added. The DNA was precipitated with 640 µL isopropyl alcohol, recovered by centrifugation and then dissolved in 50 µL TNE buffer (50 mM Tris-HCL pH 7.5, 140 mM NaCl, 5 mM EDTA). The samples were treated with 15 µg RNAse A at 37 ^{o}C for 10 min. The reactions were extracted with 1:1 phenol:chloroform, pH 8.0, and the DNA was precipitated with 300 µL isopropyl alcohol. The DNA was recovered by centrifugation at 16,000*g* and washed once with 70% (v/v) ethanol. After drying, the DNA was dissolved in sterile deionized H_2O and used immediately or stored at –20 ^{o}C.

Isolation of Arabidopsis genomic DNA for PCR-based screening of mutagenized lines was completed using a heavily modified Dellaporta method. Approximately 200 mg (fresh weight) of leaf tissue was placed in a 1.5 mL microcentrifuge tube and ground with a pestle for approximately 10 seconds. Four hundred µL of extraction buffer (200 mM Tris-HCl [pH 8.0], 250 mM NaCl, 25 mM EDTA, 0.5% SDS) was added and the sample was ground for another 30

seconds. Samples were vortexed for 30 seconds and centrifuged at 16,000*g* for 5 min. To a clean 1.5 mL tube containing 300 μL isopropyl alcohol, 400 μL supernatant was added. Tubes were inverted 3 times, incubated at 4 ^{o}C for 20 minutes, and centrifuged at 16,000*g* for 5 minutes. The pellet was washed with 1 mL 70% ethanol for 5 minutes at 16,000*g*, dried and dissolved in 50 μL 1 X TE buffer (10 mM Tris-HCl, 1 mM EDTA [pH 8.0]). Two microlitres of isolated genomic DNA was used for PCR analysis.

3.5.2 RNA sample preparations

RNA for RT-PCR analysis was isolated using Trizol (Invitrogen, Carlsbad, CA, USA) following the manufacturer's directions. The extractions were performed with 200 mg fresh weight of plant material. Material was frozen in liquid nitrogen and ground with a pestle to a fine powder prior to extraction, followed by the addition of 800 μL Trizol. The ground material was resuspended using the pestle followed by the addition of 200 μL chloroform. Samples were mixed by inverting several times, incubated at room temperature for 5 minutes and centrifuged at 12,000*g* for 15 minutes. The aqueous phase was transferred to a fresh tube and 500 μL cold isopropanol was added to precipitate the RNA followed by centrifugation at 16,000*g* at 4 ^{o}C. The pellet was washed with 70% (v/v) ethanol for 2 minutes at 16,000*g* and dried. The RNA was dissolved in DEPC-treated H_2O and stored at –80 ^{o}C. RNA used in cDNA library construction was isolated from 1 g fresh weight of plant material using a cold phenol method (Maes and Messens, 1997).

Quantification of RNA and DNA was achieved using a Nanodrop 8000 Spectrophotometer (Thermo Fisher Scientific, Wilmington, DE, USA). Absorbances were measured at 320, 280, 260 and 230 nm wavelengths.

3.6 Recombinant DNA preparation

Primers used for polymerase chain reaction (PCR) and reverse transcriptase polymerase chain reaction (RT-PCR) were designed by eye in most cases, using SeqBuilder version 1.0 (DNAStar Inc. Madison, WI, USA) to visualize DNA sequences. Primers were designed manually to add specific restriction site adaptors to the 5' end of a forward or reverse primer. Restriction site adaptors were composed of the specific recognition sequence of a restriction enzyme with an additional 3 nucleotides upstream of the recognition site to promote complete digestion (Table

3.2). Primers used for PCR and RT-PCR were designed using Primer Design version 1.0 software (Scientific and Educational Software, 1990). The criteria for primer design in the selected primers between 17 and 20 bp in length with a GC content between 40 and 50%. The primers were also specified to have a T_m between 50 and 65 ^oC. Primers containing runs of bases, secondary structure, or primer interactions involving the 3' end were discarded. Primer sequences were checked using NetPrimer (http://www.premierbiosoft.com/netprimer/netprlaunch/netprlaunch.html, first accessed October, 2002). Prior to ordering, primer sequences were checked by BLASTN queries to determine if there were any similarities to other plant genes. The DNA Technologies unit at the National Research Council Plant Biotechnology Institute, Saskatoon, Saskatchewan, Canada synthesized all primers. The primers used during this study are summarized in Table 3.2.

3.6.1 PCR amplification

Polymerase chain reactions used for general screening purposes consisted of final concentration: 2 mM $MgCl_2$, 1 X *Taq* polymerase buffer, 1 U *Taq* polymerase (Invitrogen, Carlsbad, CA, USA), 0.25 pmol/μL forward and reverse primers, and template DNA. The reaction conditions consisted of an initial denaturation at 94 ^oC for 30 s, subsequently 30 cycles of 94 ^oC for 30 s, annealing at the Ta of the primer set for 30 s, and 72 ^oC for 1-2 min (depending on product size) were performed. A final extension of 72 ^oC for 2 min was followed by an indefinite hold at 4 ^oC.

Amplification of products for cloning reactions consisted of the same primer concentration, but used Advantage 2 PCR buffer at 1X concentration containing 3.5 mM $MgCl_2$ and the Advantage 2 Polymerase mix, composed of TITANIUM Taq polymerase and a small amount of an undisclosed proofreading enzyme (Clontech, Mountain View, CA, USA) at 1X concentration. Reaction conditions consisted of an initial denaturation at 95 ^oC for 1 m followed by 30 cycles of 95 ^oC for 15 s, T_a of the primer pair for 30 s, and 68 ^oC for 1-2 m depending on resulting PCR amplicon size. A final extension at 68 ^oC was followed by an indefinite hold at 4 ^oC.

3.6.2 RT-PCR amplification

Reverse transcriptase-polymerase chain reaction (RT-PCR) was used to analyse the expression of *AIR12* in mutant Arabidopsis lines. The RT-PCR protocol presented was found to

Primer	Sequence (5'- 3')	Size	T_a	Use
SG1	CACCGCAATGGCTTCAAACGCTTCTCTC	28	59	*CIL1* Forward
SG2	TCAGAATATGAAAACTGAAGC	21	50	*CIL1* Reverse
SG3	TTTGTTAACGTGAGCAAGGGCGAGGAGCTG	30	67	*GFP* Forward
SG4	TTTAGGCCTCTTGTACAGCTCGTCCATGCC	30	61	*GFP* Reverse
SG5	GAACGGACCGGCGGAGTTCAAGTTCTGTGATTTGCA***GTTAAC***AGC	45	67	*AIR12* site-directed mutagenesis (*Hpa* I)
SG6	CCAATGTCCCTGTGTCTTAAAATACCT	21	64	*AIR12*-F
SG7	CAT***CGGACCG***TCAGAAAATAAAAATAGAACCCAACAA	37	61	*AIR12*-R (*Rsr* II)
SG8	TCCACTGACGTAAGGGATGAC	21	57	*35S*-F
SG9	ATATATTAAAGCAGAGAGAATTGCGGG	27	63	*pAIR12*-F
SG10	TGGTTTGTTATAATTAAAAGTCGGAGG	27	63	*pAIR12*-R
SG11	CATGGCGTAATGTCTCGGGTT	21	62	pER310-F
SG12	TTT***AAGCTT***ATATATTAAAGCAGAGAGAATTGC	33	53	*pAIR12*-F (*Hind* III)
SG13	TTT***CTGCAG***TGGTTTGTTATAATTAAAAGTCGG	33	56	*pAIR12*-R (*Pst* I)
GW1	GTTGCAACAAATTGATGAGCAATGC	25	58	Gateway-F
GW2	GTTGCAAACAAATTGATGAGCAATTA	26	58	Gateway-R
M13F	GTAAAACGACGGCCAG	16	58	pCR2.1-F
M13R	CAGGAAACAGCTATGAC	17	58	pCR2.1-R

Table 3.2. List of primers used during the present study. Annealing temperatures (T_a) of primers calculated using Netprimer (http://www.premierbiosoft.com/netprimer/netprlaunch/netprlaunch.html, first accessed October, 2002). Restriction sites within primers are bolded and italicized.

produce optimal results. Prior to the RT reaction, 200 ng RNA was treated with 1 U of RNase-free DNase I (Amersham, Little Chalfont, Buckinghamshire, UK) and 40 U of RNase OUT (Invitrogen, Carlsbad, CA, USA), 10 µl of 5X first-strand buffer (Invitrogen, Carlsbad, CA, USA) at 37 ^{o}C for 15 min. Reverse transcription was carried out using Superscript II (Invitrogen, Carlsbad, CA, USA) according to supplier's directions. Subsequently, 500 nL of the RT reaction was added to the corresponding PCR amplification. The PCR amplifications contained: 0.25 pmol/µL each of *AIR12*-specific primers, 2 mM $MgCl_2$, 1X PCR buffer (Invitrogen, Carlsbad, CA, USA), 0.20 mM dNTPs, and 1.0 U of *Taq* polymerase (Invitrogen, Carlsbad, CA, USA).

3.6.3 Cloning of PCR products

Cloning of PCR products was accomplished using the TOPO TA cloning system (Invitrogen, Carlsbad, CA, USA) following the manufacturer's directions. Chemically competent *Escherichia coli* TOP10 strain with genotype - F '- *mcr*AΔ(*mrr-hsd*RMS-*mcr*BC) Φ80*lac*ZDM15 Δ*lac*X74 *rec*A1 *ara*D139Δ (*ara-lea*)7679 *gal*U *gal*K *rps*L (Str^{R}) *end*A1 *nup*G was used for transformation. For chemical transformation, the directions from the manufacturer were followed (Invitrogen, Carlsbad, CA, USA). Plasmid DNA was recovered from clones using the QIAprep miniprep kit (Qiagen, Hilden, Germany) according to manufacturer's instructions. Polymerase chain reaction using product-specific primers and DNA sequencing were used to verify the identity of the PCR products. The DNA was submitted for sequencing to the DNA Technologies Unit (NRC-PBI), sequenced with M13 forward and reverse primers using an ABI Prism 377 DNA Sequencer (Applied Biosystems, Foster City, CA, USA). Unless otherwise specified, clones using *pCR2.1* or *pCR8/GW* vector backbones were sequenced using the universal and reverse primer set. Sequences were analysed using the SeqMan and SeqBuilder programs (DNASTAR Inc., Madison, WI, USA).

3.7 Construct assembly

All constructs generated during this study used the pER310 binary vector (donated by Raju Datla, assembled by Eddy Risseeuw), shown in Figure 3.1. This vector utilizes the Gateway recombination system (Invitrogen, Carlsbad, CA, USA) and contains R1 and R2 destination sites that recombine with the L1 and L2 entry sites during a recombination event. All Gateway recombinations were completed according to the manufacturer's instructions. Initial cloning of PCR products was completed using the pCR8GW/TOPO TA vector (Invitrogen, Carlsbad, CA,

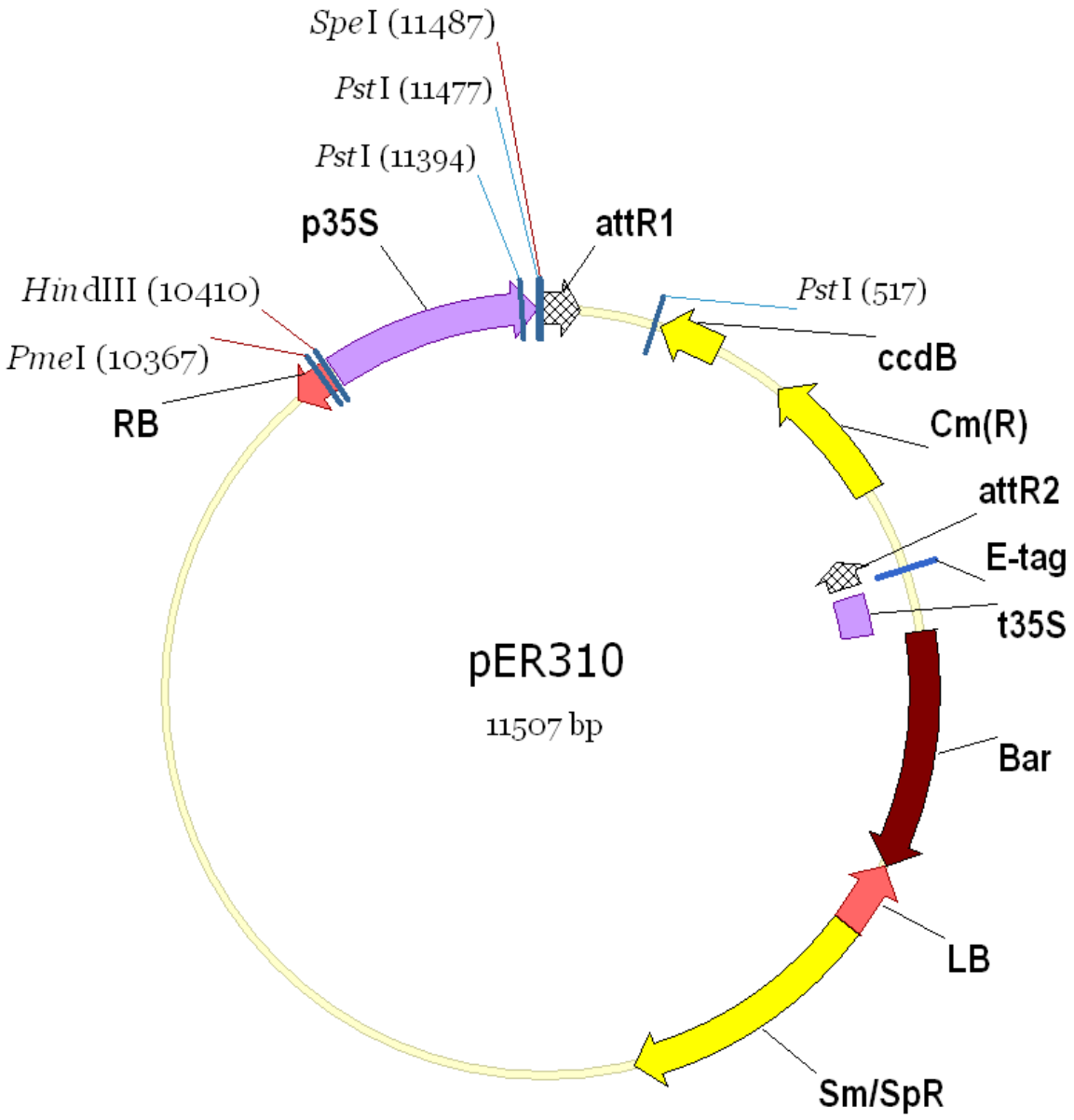

Figure 3.1. Vector map of the pER310 binary vector used in this study. Restriction sites used for promoter cloning are indicated along with positional information. RB and LB, right and left borders, respectively; p35S, cauliflower mosaic virus *35S* promoter (CaMV35S); attR1 and attR2, Gateway recombination sites for homologous recombination with attL1 and L2 sites; *ccd*B, gene coding for a toxic protein used for negative selection; Cm(R), chloramphenicol resistance gene; E-tag, C-terminal epitope tag (portion of a molecule an antibody binds to); t35S, CaMV35S terminator; Bar, gene conveying phosphothricin resistance to transformed plants, Sm/SpR, Streptomycin/spectinomycin resistance gene.

USA) following the manufacturer's instructions. In some cases, PCR product was cloned using the pCR2.1 TOPO TA system. Clones were analyzed using either plasmid isolation followed by restriction enzyme digestion or by colony PCR. For colony PCR, single colonies of *E. coli* were picked using a toothpick and placed in a 0.2 mL thin-walled PCR tube containing 10 μL H_2O. The toothpick was twisted several times and then streaked on a replica plate with the appropriate antibiotic. The thin-walled tubes were then heated at 94 ^oC for 5 minutes. Afterward, 1 μL of the heated cells was added to the PCR mix and amplified as determined by the primer T_a. Unless otherwise specified, all restriction enzyme digestions were completed by incubation at 37 ^oC for one hour. When required, dephosphorylation of DNA was completed after restriction enzyme digestion by adding 1 U calf intestinal alkaline phosphatase (CIAP; Invitrogen, Carlsbad, CA, USA) to the sample followed by incubation at 37 ^oC for 1 hour. Gel electrophoresis of PCR product and restriction enzyme digestions was completed in 0.7% agarose gels with 1 X Gel Red (Biotium, Hayward, CA, USA) unless otherwise specified. DNA was visualized using a UV transilluminator at 302 nm wavelength. If required, bands of interest below 10 kb were excised and purified using a QIAquick gel extraction kit (Qiagen, Hilden, Germany), according to the manufacturer's instructions. For purification of fragments greater than 10 kb, the QIAEX II Gel Extraction kit (Qiagen, Hilden, Germany) was used, according to the manufacturer's directions. For purification of PCR product a QIAquick PCR Purification Kit was used, following the manufacturer's instructions. Sequencing of cassettes in pCR2.1 and pCR8/GW/TOPO was completed using the M13 forward and reverse primers unless otherwise indicated. Restriction enzyme digestions were always completed using 10 U of enzyme in 1 X reaction buffer. During the present study both cohesive and blunt-ended ligations were performed. For ligations involving cohesive-ended fragments, the Rapid DNA Ligation Kit (Roche, Waukesha, WI, USA) was used with either a molar ratio of 5:1 insert:vector or 3:1 and was completed according to the manufacturer's instructions. Briefly, the combined insert and vector was diluted in DNA dilution buffer to a final concentration of 1 X, followed by addition of 10 μL DNA Ligase Buffer and 1 μL T4 DNA Ligase. The ligation was incubated for 30 minutes at room temperature and 2 μL was used to transform chemically competent *E. coli*. When required, restriction fragments with recessed 3' ends were filled in using the large fragment of Klenow polymerase (Invitrogen, Carlsbad, CA, USA). Briefly, following restriction enzyme digestion the reactions were transferred to thin-walled 0.2 mL tubes followed by the addition of 0.2 mM dNTPs and 2 U large

fragment of Klenow polymerase. Reactions were mixed and incubated at 24 ^{o}C for 10 minutes followed by inactivation at 75 ^{o}C for 10 minutes. One unit of CIAP was then added to the reactions and incubated at 37 ^{o}C for 1 hour.

3.7.1 Assembly of 35S::GFP-CIL1

The putative GPI-anchoring of CIL1 requires intact N- and C- termini for the signal peptide and anchoring site of the GPI moiety, respectively. To preserve the termini, the open reading frame of the gene coding for emerald green fluorescent protein (GFP) was fused in-frame downstream of the *CIL1* sequence coding for the N-terminal signal peptide, similar to the work of Zhao et al. (2002). The signal peptide in the *CIL1* ORF extends 69 nucleotides from the start codon. An additional nine nucleotides downstream an *Oli I* restriction site is present. Digestion with *Oli I* (CACNN|NNGTG) is in frame with the *CIL1* ORF and represents an ideal position for ligation of *GFP*.

Primers were designed to amplify the full-length *CIL1* ORF (SG1 and SG2) with a conserved translational initiation sequence (Kozak, 1984), by PCR using Advantage 2 Polymerase Mix with wild type *B. carinata* genomic DNA as template. The product was cloned using the pCR8/GW/Topo vector. Clones were screened by colony PCR using the original primer set, plasmid was isolated from clones with the correct product (810 bp) and sequenced. Clones with sequence matching *CIL1* were designated *pCR8-CIL1*.

To clone GFP, primers were designed to amplify the entire *GFP* ORF lacking the start and stop codons (SG3 and SG4). These primers were designed to add an *Hpa* I adaptor directly upstream of the ORF on the 5' end and a *Stu I* adaptor directly downstream of the ORF on the 3' end. *GFP* was amplified using Advantage 2 Polymerase Mix with pTH15-2 *GFP* (Teerawanichpan et al., 2007) plasmid as template. The amplified product was subsequently cloned using the pCR2.1 vector. Clones were screened by colony PCR using the original primer set, plasmid was isolated from clones with product of the correct size (720 bp) and sequenced. Clones with sequence matching *GFP* were designated *pCR2-GFP*.

Following sequence confirmation, 2 μg of *pCR8-CIL1* was digested with *Oli* I (Fermentas, Burlington, ON, Canada) in buffer R, treated with CIAP and separated on an agarose gel. The linearized *pCR8-CIL1* was excised and gel extracted. Concurrently, 2 μg of *pCR2-GFP* was restriction enzyme digested with *Hpa* I (GTT|AAC) and *Stu* I (AGG|CCT) in NeBuffer 4 (New England Biolabs, Ipswich, MA, USA). The approximately 800 bp band was gel extracted.

The *GFP* fragment was ligated to linearized pCR8-CIL1 at a 5:1 insert:vector molar ratio using a Rapid DNA Ligation Kit (Roche, Basel, Switzerland) according to the manufacturer's instructions. The ligation was extracted with phenol:chloroform, ethanol precipitated, and the DNA dissolved in 10 μL H_2O. Electrocompetent XL-1 Blue *E. coli* was transformed with 4 μL of the purified ligation. Colony PCR was used to confirm directional insertion of the *GFP* fragment, using the forward *GFP*-specific primer (SG3) and reverse *CIL1*-specific primer (SG2). Plasmid was isolated from clones with product of the correct size (1460 bp). The clones were sequenced with the PCR primers, and were designated *pCR8-GFPCIL*. Alignments between the predicted *GFP-CIL1* and sequenced *pCR8-GFPCIL* were completed to confirm the ligation.

pCR8-GFPCIL was digested with *Xba* I and *Bgl* I, in NeBuffer 3 (New England Biolabs, Ipswich, MA, USA) to excise the spectinomycin promoter and resistance gene prior to Gateway recombination. The 3.5 kb fragment containing the vector backbone and *GFPCIL* cassette, but lacking the selectable marker was gel extracted and used in a Gateway recombination reaction. The recombination reaction was performed between the digested pCR8-GFPCIL entry vector and the pER310 binary destination vector (Figure 3.1) according to the manufacturer's instructions using 150 ng of each vector. Chemically competent Top10 cells (Invitrogen, Carlsbad, CA, USA) were transformed with 2 μL of the Gateway reaction. Confirmation of the Gateway recombination was completed by colony PCR using the vector-specific *35S* forward primer and the cassette-specific *CIL1* reverse primer. Clones with approximately 1600 bp product were sequenced to confirm successful recombination and designated *perGFPCIL*.

3.7.2 Assembly of 35S:GFP-AIR12

Like CIL1, AIR12 contains an N-terminal signal peptide and a putative C-terminal GPI-anchoring site. Downstream 34 nucleotides of the *AIR12* sequence coding for the signal peptide there is a *Rsr* II restriction site, however digestion with this restriction enzyme results in a frame shift in the ORF. To remedy this, *AIR12* was mutagenized by introducing an *Hpa* I restriction site in frame 12 nucleotides downstream of the sequence coding for the signal peptide by PCR (SG5). A series of primers were designed to amplify the sequence coding for the signal peptide with the introduced *Hpa* I site (175 bp from start; SG6), and to amplify full length *AIR12* including a *Rsr* II site on the 3' end of the gene (832 bp from start; SG7). Genomic Arabidopsis DNA was amplified using the primer sets and Advantage 2 Polymerase Mix. Product from the PCR was purified and both PCR products were cloned using the pCR2.1 vector. Colony PCR

was completed using the original primers; plasmid was isolated from clones with the correct sized amplicon and sequenced. Clones with sequence aligning to the *AIR12* signal and *AIR12* ORF were designated pCR2-AS and pCR2-AO, respectively.

Next, pCR2-AS was digested with *Hpa* I followed by treatment with CIAP. The reaction was separated on a 0.7% agarose gel and the linearized pCR2-AS was gel extracted and quantified. *GFP* digested with *Hpa* I and *Stu* I was ligated to linearized pCR2-AS using a Rapid DNA Ligation kit and a molar ratio of 5:1 insert:vector for 30 min. The ligation reaction was phenol:chloroform extracted, ethanol precipitated, and the DNA was dissolved in 10 μL H_2O. Electrocompetent XL-1Blue *E. coli* was transformed with 2 μL of the purified ligation. Colonies were screened by colony PCR using the SG6 and SG4 primer set to confirm ligation. Plasmid was isolated from clones with the correct product (850 bp) and sequenced. Clones with the correct sequence were designated pCR2-ASG.

To complete the GFP-AIR12 construct, the *ASG* cassette was combined with the pCR8/GW/Topo vector. Since pCR8/GW/Topo is supplied in a linearized form prevented from circularizing by topoisomerase (Invitrogen, Carlsbad, CA, USA) and the flanking regions of the TA cloning site contain *Eco*R I recognition sequences, 2 μg of previously assembled pCR8-GFPCIL was digested with *Eco*R I in 1X React 3 buffer (Invitrogen, Carlsbad, CA, USA). The digestion was treated with CIAP and separated on an agarose gel. The linearized vector (2.9 kb) was excised, gel extracted and quantified. Concurrently, 2 μg pCR2ASG was digested with *Eco*R I. The 850 bp ASG fragment was excised, gel extracted and quantified. The ASG fragment was ligated to the pCR8/GW/Topo vector using a Rapid DNA Ligation kit with a 3:1 insert:vector molar ratio followed by phenol:chloroform extraction and ethanol precipitation. The DNA was dissolved in 10 μL H_2O and 2 μL was used to transform electrocompetent XL-1Blue *E. coli* cells. Orientation of the ligation was confirmed by colony PCR using the vector-specific GW1 forward primer (Invitrogen, Carlsbad, CA, USA) and a cassette-specific *GFP* primer. Clones with PCR product of 950 bp were cultured and plasmid DNA was isolated followed by sequencing. Clones with sequence aligning to *in silica*-prepared cassettes were designated pCR8-ASG.

To assemble the complete cassette, 2 μg each of pCR2-AO and pCR8-ASG were digested with *Rsr* II followed by CIAP treatment of pCR8-ASG. Products of both restriction enzyme digestions were separated on an agarose gel. The 650 bp band corresponding with *AO*

and the linearized pCR8-ASG band was excised, gel extracted and quantified. The *AO* fragment was ligated to the pCR8-ASG fragment and 2 μL was used to transform electrocompetent XL-1Blue *E. coli* cells. Colony PCR was used to screen clones with the full-length *AIR12* forward and reverse primers. Clones with PCR product of the desired size (1500 bp) were cultured in LB. Plasmid was isolated from these clones and were sequenced. Clones with the correct sequence were designated pCR8-ASGO.

Finally, 2 μg pCR8-ASGO was digested with 10 U each of *Xba* I and *Xho* I. The 3.3 kb band was excised, gel extracted, quantified and used for a Gateway reaction with per310 as previously described. *ASGO* in pER310 clones were screened by colony PCR using a vector-specific forward *35S* primer (SG8) and cassette-specific reverse *GFP* primer (SG4). Clones with PCR product of 1,000 bp were cultured in LB, followed by plasmid isolation and sequencing using the *35S* forward primer, reverse *GFP* primer, and reverse *AIR12* ORF primer. Clones with the correct sequence were designated per-ASGO. A flowchart describing assembly of this construct is presented in Figure 3.2.

3.7.3 Assembly of 35S:GFP

To assemble this construct, a Gateway recombination reaction was performed with 100 ng each of *GFP* in pENTRD-TOPO (Invitrogen, Carlsbad, CA, USA; a gift from Dr. Gopalan Selvaraj's lab) and pER310. Clones were screened by colony PCR using a vector-specific *35S* forward primer and *GFP*-specific reverse primer. Clones with PCR product of 700 bp were cultured. Plasmid was isolated, and sequenced. Sequence information was aligned and matching clones were designated pERGFP.

3.7.4 Assembly of pAIR12:GFP-AIR12

Using publicly available sequence information on chromosome 3 of Arabidopsis, primers were designed to amplify a region spanning 1,000 bp upstream of *AIR12* (SG9 and SG10 for forward and reverse primers, respectively). This 1,000 bp fragment would act as the *AIR12* promoter, and contains predicted transcription start sites at 764 bp and 501 bp, predicted by both PLACE and the neural network predictor. This promoter would control expression of the *GFP-AIR* construct. The promoter region was amplified by PCR using Advantage 2 Polymerase Mix followed by separation on an agarose gel, extraction of the 1,000 bp product, and cloning the product into pCR2.1. Colony PCR was used to confirm ligation/transformation and plasmid was

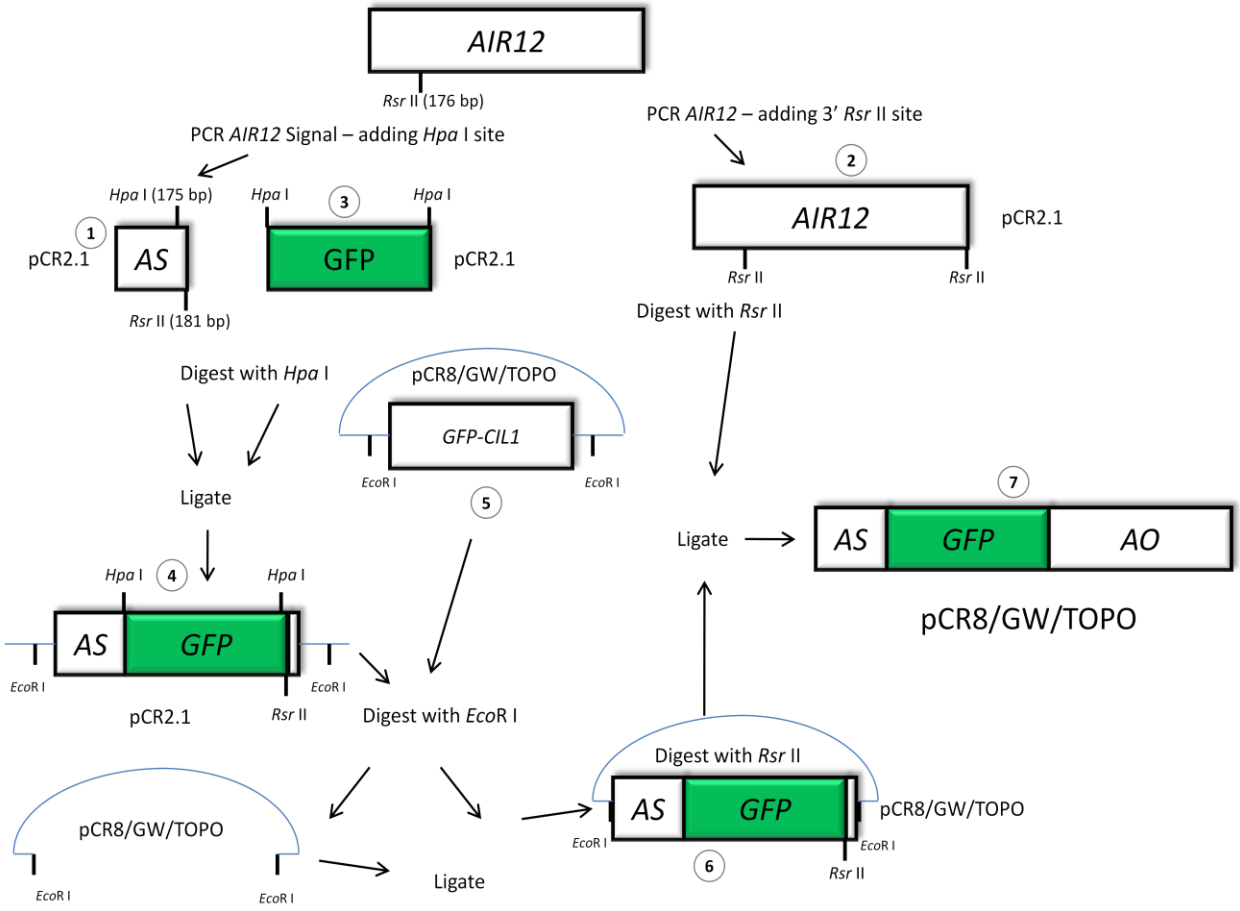

Figure 3.2. Flowchart outlining the assembly of *GFP-AIR12*. *AIR12* possesses an *Rsr* II site 176 bp after the transcription start site. A primer set was designed to add an *Hpa* I site directly upstream of *Rsr* II. This primer set was used to amplify the first 181 bp of the reading frame which includes the signal peptide (1; *AIR Signal; AS*) and the fragment was cloned using pCR2.1. Next, the full length *AIR12* open reading frame was amplified using a primer set designed to add an *Rsr* II site directly downstream of the transcription stop site (2). Previously cloned *GFP* in pCR2.1 with 5' and 3' *Hpa* I sites (3) and (1) were digested with *Hpa* I. The two fragments were ligated, resulting in *AS-GFP* (4). Next, previously cloned *GFP-CIL* in pCR/GW/TOPO (5) and (4) were digested with *Eco*R I. This digestion excised both constructs from their cassettes. The linearized pCR8/GW/TOPO and *AS-GFP* fragments were purified and ligated, resulting in *AS-GFP* in pCR8GW/TOPO (6). Finally, (2) and (6) were digested with *Rsr* II and ligated, generating *AS-GFP-AO*, or *GFP-AIR12* (7). The lines with *Eco*R I sites in (4) and (5) represent the vector sequence of pCR2.1 and pCR8/GW/TOPO flanking the construct.

isolated from clones with PCR product of the desired size (1,000 bp) followed by sequencing. Sequence was aligned using BLAST (Altschul et al., 1990). Clones with the desired sequence were designated pCR2-APro. A restriction enzyme digestion using *Eco*R V (Invitrogen, Carlsbad, CA, USA), 2 μg pCR2-APro and 1X REact 2 was completed followed by the addition CIAP. Concurrently, 2 μg pCR8-ASGO was digested with *Eco*R I. A ligation reaction was initiated between the ASGO and the linearized pCR2-APro. Clones were screened by colony PCR, using the forward SG9 and reverse SG7 primer to confirm directional ligation of the insert. Plasmid was isolated from clones with PCR product of the desired size (1,200 bp) and sequenced. Sequence information was aligned with *in silica*-prepared data and matching clones were designated pCR2-AP::ASGO. pCR2-AP:ASGO was digested with *Not* I and *Hind* III. Two μg *pCR8-GFPCIL* was digested using *Eco*R I. Following the incubation, the recessed ends were filled in using Klenow. The reaction was mixed and incubated at 24 ^{o}C for 10 min, followed by 75 ^{o}C for 10 min and the addition of CIAP to the reaction. Both restriction enzyme digestions were separated on a 0.7% agarose gel, gel extracted and quantified. A ligation reaction was initiated between the *AP::ASGO* insert and the pCR8/GW/TOPO vector using T4 DNA Ligase (Invitrogen, Carlsbad, CA, USA) at a molar ratio of 5:1 insert:vector.Colony PCR using the GW1 vector-specific forward primer (GW1) and the cassette-specific *AS* reverse primer (SG7) was completed to confirm ligation in the desired orientation. Plasmid was isolated from clones with PCR product of the desired size (1,400 bp) and sequenced. Sequence information was aligned and matching clones were designated pCR8-AP::ASGO. Next, 2 μg of pER310 was digested with *Bgl* II and *Pme* I in buffer to excise the *35S* promoter. After 1 hour incubation at 37 ^{o}C, the *Bgl* II end was filled in as previously described using Klenow fragment. The 10 kb band was excised and gel extracted using a QIAEX II Gel extraction kit (Qiagen, Hilden, Germany). An intra-molecular ligation reaction was initiated to recircularize the binary vector. The reaction contained 1 U T4 DNA Ligase, 1X T4 DNA Ligase Buffer, 100 ng pER310 blunted vector and H_2O to 20 μL. The ligation reaction was incubated at 16 ^{o}C overnight. The following day, one vial of ccdB survival cells (Invitrogen, Carlsbad, CA, USA) was transformed with 4 μL of the ligation, according to the manufacturer's instructions. Plasmid was isolated from clones and screened for the absence of the *35S* promoter by digesting with *Stu* I, an internal restriction site in *35S* and *Xho* I, a restriction site found outside of the *35S* promoter. The digestions were completed using 10 U of each enzyme in One Phor All buffer at 37 ^{o}C for 1 hour followed by

separation on a 0.7% agarose gel. Absence of the *35S* promoter was indicated by a single band on the gel representing linearized per310. These clones were designated "per35-".Prior to recombination with per35-, 2 μg pCR8-AP:ASGO was digested with *Eco*R V and *Xho* I restriction enzymes to remove the spectinomycin resistance promoter and gene. The reaction was separated on an agarose gel and the band corresponding to 5.4 kb was excised, gel extracted, and quantified. A Gateway recombination reaction was performed between digested pCR8-AP:ASGO and per35- using 100 ng of each vector according to the manufacturer's instructions. Top 10 cells were transformed with 1 μL of the reaction. Clones were screened using a vector-specific forward primer (SG11) and the *AS* reverse primer (SG7). Plasmid was isolated from clones with PCR product of the desired size (1,500 bp) and sequenced. Clones with the correct sequence were designated perAPAG.

3.7.5 Assembly of pAIR12::GFP

To generate this construct, primers were designed to add *Hind* III and *Pst* I adaptors to the 5' (SG12) and 3' (SG13) end of the *AIR12* promoter, respectively. The promoter was PCR amplified using Advantage 2 Polymerase Mix and the product was cloned using the TOPO TA Cloning Kit. Clones containing the desired adaptors with sequence matching the region 1,000 bp upstream of *AIR12* were designated pCR2-HAP. Following sequence confirmation, 2 μg pCR-HAP was digested with *Hind* III and *Pst* I. The 1000 bp band corresponding to *HAP* was gel extracted using a QIAquick Gel Extraction kit.

Previously assembled perGFP was digested with *Hind* III and *Pst* I to excise the *35S* promoter. After separation on a 0.7% agarose gel the 10 kb band was gel extracted using a QIAEX II Gel Extraction kit.

The gel extractions were quantified and a ligation reaction between *HAP* and perGFP was initiated using a molar ratio of 3:1 insert:vector. Ten percent of the ligation mix was used to transform chemically competent Top10 Cells. Colony PCR using the *HAP* forward (SG12) and *GFP* reverse (SG4) primers was completed to confirm ligation. Clones with the correct sequence were designated perAPG.

3.8 Identification of detergent insoluble membranes in *Brassica carinata*

To prepare total cell membranes, 40 g of leaf tissue from 3 week old *B. carinata* was suspended in 200 mL of cold homogenization buffer (12 % [w/v] sucrose, 1 mM EDTA, and 100 mM Tris-HCl [pH 8.0]). The preparation of detergent insoluble membranes was completed according to Borner et al. (2003) with slight modifications. Twenty-five milligrams of total membrane protein was processed for a single experiment. Membrane preparations were resuspended in 2% (v/v) Triton X-114/TNE at 37 ^{o}C and centrifuged at 11,300*g* for 5 minutes and 4 ^{o}C to remove insoluble material. Phase separation was induced by incubating membranes at 37 ^{o}C. The detergent phase was then washed three times by repartitioning with Tris-buffered saline (10 mM Tris-HCl [pH 7.4] and 150 mM NaCl) at 37 ^{o}C. The membranes were diluted 20-fold in Tris-buffered saline, split into two equal parts and phospholipase C (Pi-PLC; Sigma-Aldrich, St. Louis, MO, USA) was added to one sample at a final concentration of 1.5 U mL^{-1}. Both samples were incubated at 37 ^{o}C for 1 h and 30 min. The aqueous phases were separated and washed twice with fresh Triton X-114. The samples were concentrated using Centriprep Centifugal Devices (Millipore, Billerica, MA, USA) with a molecular weight cutoff of 10,000 Da, followed by precipitation of proteins with 80% (w/v) acetone at -20 ^{o}C overnight. Proteins were air dried and resuspended in AUT sample buffer (10 mM Tris-HCl [pH 8.5], 7 M urea, 2 M thiourea, and 2% [w/v] amino-sulfobetaine detergent [ASB14]) for two-dimensional electrophoresis and in SDS sample buffer for one-dimensional electrophoresis.

3.8.1 Electrophoretic analysis of detergent insoluble membrane proteins

Two-dimensional electrophoresis was completed using an 11-cm pH 3 to 10 IPG strip on a PROTEAN IEF Cell (Bio-Rad, Hercules, CA, USA). The IPG strip was rehydrated for 12 hours with rehydration buffer (2 mg mL^{-1} dithiothreitol, 1% [w/v] IPG buffer, 7 M urea, 2 M thiourea, and 2% [w/v] ASB14) followed by the addition of sample for a final volume of 250 µL. Focusing was carried out for a total of 35,000 V h. Separation in the second dimension was completed using a 12.5% (w/v) Criterion Precast Gel (Bio-Rad, Hercules, CA, USA). Silver stain (Bio-Rad, Hercules, CA, USA) was used to visualize proteins. Pi-PLC-treated and control fractions were separated simultaneously. Bands with different migration patterns on the Pi-PLC gel compared to the control gel were excised and analyzed by LC-MS/MS according to Borner et al. (2002).

3.9 Microscopy

Throughout the course of this study a number of microscopic techniques were used. Primary and lateral root length, as well as lateral root number was determined using a M3C dissecting microscope (Wild Leitz, Heidelberg, Germany). X-gluc stained seedlings were viewed using a Laborlux S compound microscope (Wild Leitz, Heidelberg, Germany) and images were recorded using a Leica DMR compound microscope (Leica Microsystems GmbH, Wetzar, Germany) equipped with an Optronics Microfire camera (Goleta, CA, USA).

To visualize the AIR12/CIL1-GFP fusion proteins and GFP in stably transformed Arabidopsis organs, fluorescence microscopy was performed using a Carl Zeiss Meta510 laser-scanning confocal microscope. Six independent lines and at least 20 seedlings per line were examined for fluorescence localization in *p35S::GFP-AIR12*, *pAIR12::GFP-AIR12*, and *p35S::GFP-CIL1*. GFP was detected using an argon laser with a 488 nm excitation filter and an emission range of 505-530 nm. The red fluorescent dye propidium iodide was detected using a HeNe laser with an excitation of 543 nm and an emission of 617 nm. Data were captured by the Carl Zeiss LSM 510 software. For some experiments, roots were plasmolysed with 0.8 M sorbitol or 2% NaCl for 5 minutes immediately prior to imaging.

To visualize ROS accumulation in Arabidopsis roots, the fluorescent dyes H_2DFFDA (5-(and -6)-carboxy-2',7'-difluorodihydrofluorescein diacetate; carboxy-H_2DFFDA) and Oxyburst green H_2HFF (dihydro-2',4,5,6,7,7' hexafluoroflurescein)-BSA; both Invitrogen, Carlsbad, CA, USA) were used at 20 μM (in DMSO) and 100 μg mL^{-1}, respectively. Roots were incubated in one of the two dyes for 15 minutes in the dark, followed by immediate visualization on the previously mentioned confocal microscope for no more than 10 minutes. Fluorescence was detected using an argon laser with a 488 nm excitation filter and a long pass emission range of wavelengths greater than 505 nm. Consistent image capture settings were used for every ROS confocal image.

3.9.1 GUS Staining

Staining for GUS accumulation in Arabidopsis was accomplished by immersing entire seedlings, or organs of interest in a 1.5 mL microcentrifuge tube containing pre-chilled 90% acetone. The tissue was incubated in 90% acetone at room temperature for 20 minutes. The acetone was then decanted and the tissue was rinsed with chilled water. Following the water

rinse, chilled X-gluc stain (50 mM 1M sodium phosphate, 10% Triton X-100, 0.1 M ferrocyanide, 0.1 M ferricyanide, and 100 mM X-gluc [pH 7.2]) was added to cover the tissue. The tube was then covered in foil and incubated at 37 ^{o}C for 16 hours in the dark.

The following day the tissue was processed through an ethanol series comprising 25% (v/v), 50% (v/v), 70% (v/v), and 90% (v/v) for 20 minutes each with low agitation. Following the 90% ethanol incubation the seedlings or organs were observed under a compound microscope and stored in 100% ethanol.

To examine *AIR12* expression in a mutant background, heterozygous *AIR12*/*air12-1* or *AIR12*/*air12-3* seedlings were stained.

3.10 Analysis of ROS in *Brassica carinata*

The following section regarding ROS determination was completed by Janet Taylor and Alyx Conway. Determination of O_2^- production was completed according to Able et al., (1998). Leaves were harvested from 41-day old *B. carinata* plants and 1 g (fresh weight) of leaf pieces were homogenized in 5 ml of 50 mM Tris-HCL (pH 7.5) and centrifuged at 5,000*g* for 10 min. The reaction mixture contained 50 µg of leaf supernatant protein, 0.5 mM XTT, and 50 mM Tris-HCL (pH 7.5) to 1 mL. The reduction of XTT was followed at 470 nm for 5 min. Corrections for background were performed with 50 units SOD. Rates of O_2^- generation were calculated using an extinction coefficient of $2.16x10^4$ M^{-1} cm^{-1}.

Hydrogen peroxide levels were determined according to Shi et al. (2005), with slight modifications. Leaves were harvested from 41-day old *B. carinata* plants and 0.5 g (fresh weight) of leaf pieces were homogenized in liquid nitrogen. After homogenization 5 mL 0.1% (w/v) trichloroacetic acid was added. The homogenate was centrifuged at 12,000*g* for 15 min followed by combining 0.5 mL of supernatant with 0.5 mL K-phosphate buffer (pH 7.0) and 1 mL 1 M KI. The content of H_2O_2 was calculated by measuring the absorbance at 390 nm based on a standard curve.

Prior to determination of glutathione content, leaves of 41-day old *B. carinata* plants were harvested and 1 g of leaf pieces was homogenized according to DeRidder et al. (2002). Glutathione crude extract was then prepared for use for spectrophotemetric detection of glutathione and glutathione disulfide (Griffith, 1980).

To determine ascorbic acid content, leaves were collected from 56-day old *B. carinata* and flash-frozen in liquid N_2. Frozen leaf material (0.5 g) was prepared according to Kampfenkel et al. (1995), with modifications. To the homogenized material 10 mL 5% trichloroacetic acid was added and ground into the powdered leaf material. The homogenate was centrifuged at 15,600*g* for 5 min at 4°C and the supernatant was colourimetrically assayed for ascorbate (Arakawa et al., 1981).

To determine NAD+, NADH, NADP+, and NADPH content, leaf pieces (1 g) of 56-day old *B. carinata* was ground in liquid nitrogen and were extracted and assayed according to Queval et al. (2007) with slight modifications. For NAD+ and NADH, alcohol dehydrogenase (ADH) was freshly dissolved in 0.1 M HEPES and 2 mM EDTA (pH 7.5) to a concentration of 2,500 U mL^{-1}. To a cuvette containing 100 μL neutralized supernatant, 0.5 mL of 0.1 M HEPES, 2 mM EDTA (pH 7.5), 100 μL 1.2 mM DCPIP, 50 μL of 20 mM PMS, 125 μL water, and 50 μL ADH. The reaction was initiated by the addition of 75 uL absolute ethanol. After shaking, the decrease in A_{600} was recorded for 5 min. Contents were calculated by reference to a constructed standard curve. To assay NADP+ and NADPH glucose 6-phosphate dehydrogenase (G6PDH) was freshly prepared by centrifugation of a $(NH_4)_2SO_4$ suspension and resuspension of the pellet to 200 U mL^{-1} in 0.1 M HEPES, 2 mM EDTA (pH 7.5). To a cuvette containing 150 μL neutralized supernatant, 0.5 mL 0.1 M HEPES, 2 mM EDTA (pH 7.5), 100 μL 1.2 mM DCPIP, 50 μL of 20 mM PMS, 50 μL glucose 6-phosphate, and 150 μL of water were added. The reaction was initiated with the addition of 50 μL G6PDH. After shaking, the decrease in A_{600} was recorded for 5 min and contents were calculated by reference to a constructed standard curve.

3.11 Arabidopsis catalase activity and hydrogen peroxide levels

Catalase activity of *air12-1*, the wild type equivalent, *Ds*, *air12-2*, and wild type L*er* was analysed using an Amplex Red Catalase Assay kit (Invitrogen, Carlsbad, CA, USA). Prior to analysis, seeds were sterilized as previously described and plated on control medium, or control medium supplemented with 400 nM α-NAA or 1 mM H_2O_2. After 13 days, total roots were harvested. Roots were placed in 1.5 mL tubes, weighed, and flash frozen in liquid nitrogen. The frozen roots were manually ground in 1.5 mL eppendorf tubes using a pestle for 30 seconds, 200 mL sodium phosphate buffer (20 mM, pH 7.4) was added and the roots were ground for a

further 30 seconds and placed at room temperature while the remaining samples were processed. The samples were vortexed for 3 minutes using a IKA-VIBRAX-VXR automatic vortexer with a Typ VX2E adaptor (Janke and Kunkel, Germany) and centrifuged for 5 minutes at 14,000*g*. The supernatant was placed in a clean tube and 50 μL was used for the catalase assay. The remaining sample was frozen.

The catalase assay was completed according to the product manual using a Victor3v 1420 Multilabel Counter with excitation and emission filters at 530 and 615 nm (Perkin Elmer, Waltham, MA, USA), respectively. For each assay replicate a new standard curve was constructed using the catalase concentrations, 0, 6.25, 250, 500, 1000, 2000 mU mL^{-1}. In total, 3 biological replicates per line were completed. Within each biological replicate, 3 technical replicates were completed. Each replicate used pooled roots from at least 10 seedlings.

Steady state levels of Arabidopsis H_2O_2 was determined using an Amplex Red Hydrogen Peroxide Assay kit (Invitrogen, Carlsbad, CA, USA). The remaining supernatant from the sodium phosphate-extracted Arabidopsis roots (100 μL) was used for this assay, and was completed according to the manual using the same plate reader and excitation/emission settings as previously described. A standard curve was conducted for each biological replicate using the H_2O_2 concentrations, 0, 1, 4, 6, 8, and 10 μM. These concentrations were empirically determined from prior assays. As for the catalase assay, 3 biological replicates were completed per line with 3 technical replicates per biological replicate per sample.

4. RESULTS

4.1 *Brassica carinata* antisense *CIL1* plants display altered root growth and response to hormones

Control and antisense *CIL1* (AC) seeds were surface-sterilized and incubated on ½ MS plates oriented vertically for 8 days. At this time the lateral root number was counted and lengths of the primary root and all lateral roots were measured. AC seedlings produced approximately 50% fewer lateral roots than control (Fig. 4.1A), but showed no significant difference in primary root length (Fig. 4.1B, C). Since auxin and ABA act antagonistically during lateral root development I examined the effects of auxin and ABA on root elongation of *B. carinata* seedlings. When germinated on medium containing ½ MS, 400 nM α-NAA, control seedlings developed a shorter primary root and produced additional lateral roots (Fig. 4.2A). While AC seedlings showed similar proliferative lateral root development, unlike wild type seedlings they retained primary root identity and developed a conspicuous primary root. The high density of lateral roots of both control and AC seedlings prevented accurate measurements from being recorded at this stage of development. When germinated on plates containing ½ MS and 3.5 μM ABA, control seedlings germinated, but showed reduced primary root elongation compared to AC seedlings, while the primary root of AC seedlings appeared to be partially insensitive to ABA and elongated (Figs. 4.2B, C). On media containing both 400 nM α-NAA and 3.5 μM ABA germination of wild type seedlings was completely abolished while AC seedlings were able to germinate and develop a primary root that was shorter than when ABA alone was added to the medium (Fig. 4.2D), which was in turn shorter than the primary root of AC seedlings grown on control medium. Since no lateral roots developed during this assay, the measurements were not completed.

4.1.1 Antisense *CIL1* plants show increased salinity tolerance

The ABA insensitivity displayed by AC *B. carinata* and the involvement of ABA in abiotic stress responses led me to question how environmental stressors would affect the germination of these seeds. First, I tested the ability of control and AC *B. carinata* to germinate in the presence of NaCl under a short-day photoperiod (Figure 4.3A). Seeds were placed in a sealed petri-plate with a 1% NaCl (w/v) solution on filter paper on the bench top. Four days after initiating the assay, 80% of the AC seedlings had unfolded cotyledons, compared to 20% of

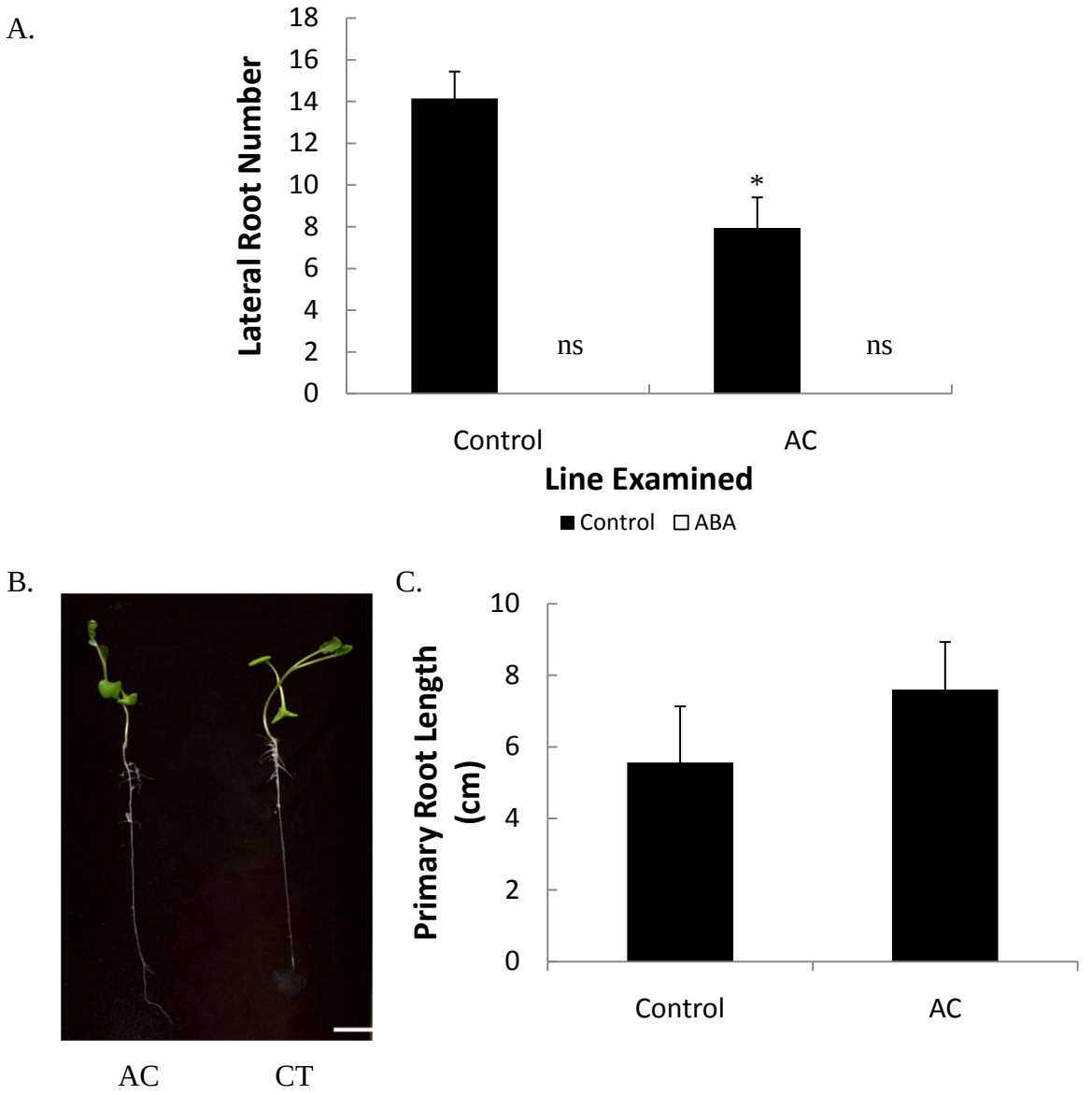

Figure 4.1. Diminished lateral root development of antisense *CIL1 Brassica carinata* seedlings. Antisense *CIL1* (AC) root development was compared to control (CT) after 8 days growth on vertical plates containing half strength MS medium or medium containing 3.5 μM ± ABA. A, Mean lateral root number of *B. carinata* seedlings, "ns" represents "none seen"; * $p<0.05$, as compared to genotype lateral root number using a two-tailed Student's t-test; n=3, bars represent standard error. B, Representative image of AC and CT seedling primary root, scale bar represents 1 cm. C, Graph of primary root length, bars represent standard error.

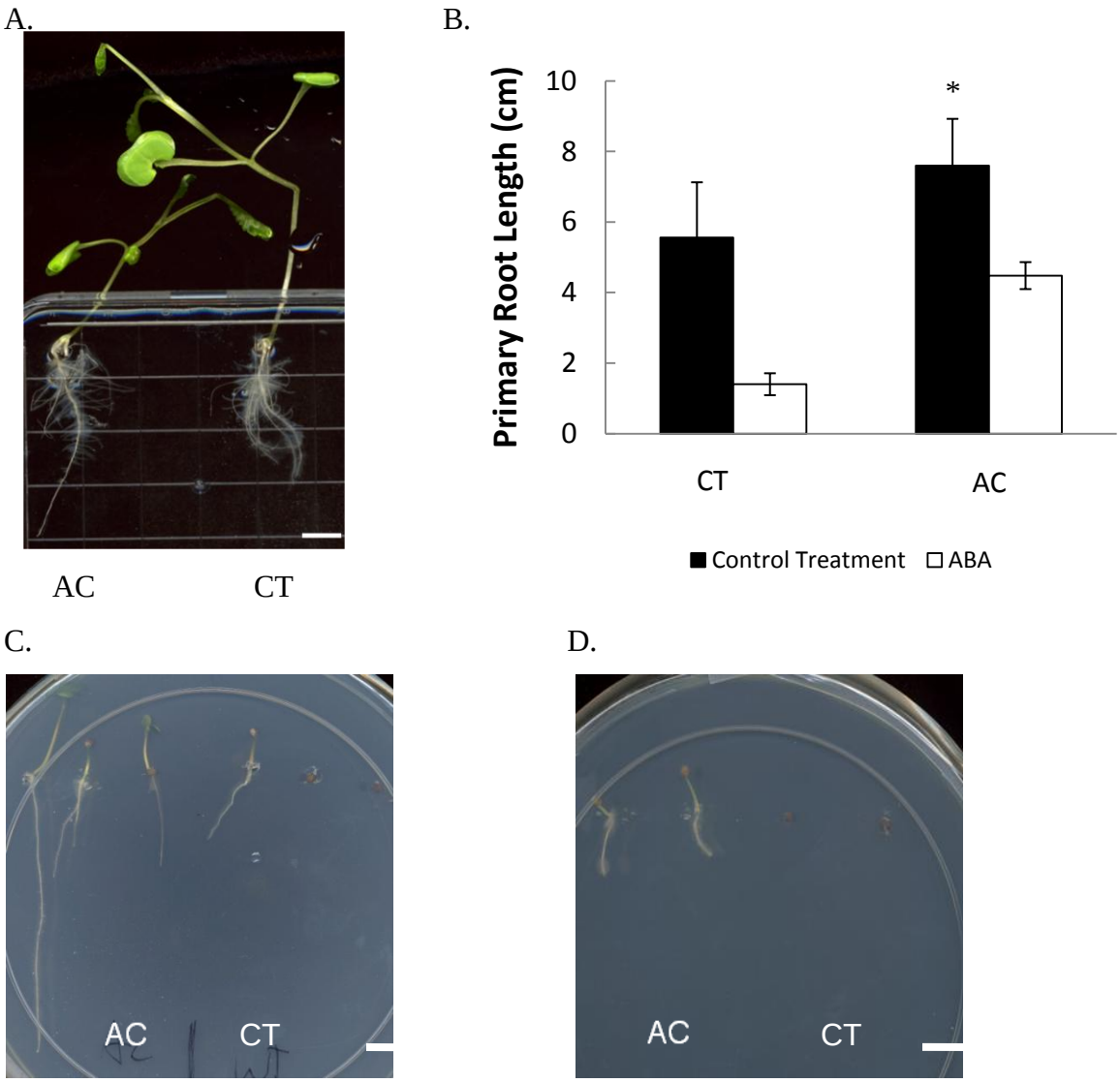

Figure 4.2. Response of antisense *CIL1 Brassica carinata* (AC) and control plants (CT) to auxin (α-NAA) and abscisic acid (ABA). A, Primary and lateral roots of seedlings grown for 13 days on half strength MS supplemented with 400 nM α-NAA. B, Primary root length of seedlings grown on half strength MS supplemented with 3.5 μM ± ABA for 13 days; * $p<0.005$, as compared to control on the same medium using a two-tailed Student's t-test on control medium or medium with ABA; n=3, bars represent standard error. C, Primary root length of seedlings grown for 13 days on medium containing half strength MS supplemented with 3.5 μM ± ABA. D, Germination of seedlings after 13 days on medium containing 400 nM α -NAA and 3.5 μM ± ABA. Scale bars in all figures represents 1 cm.

A.

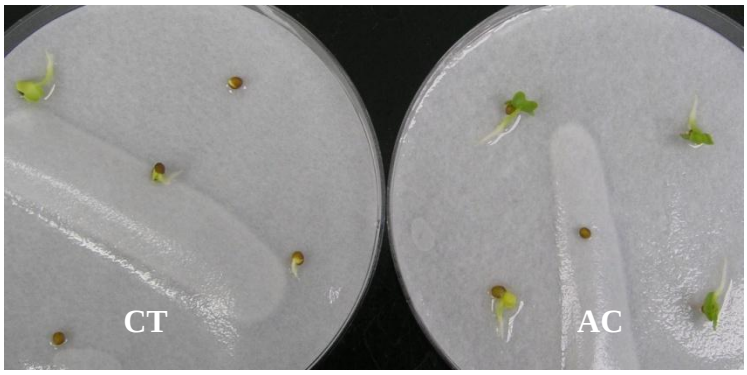

B.

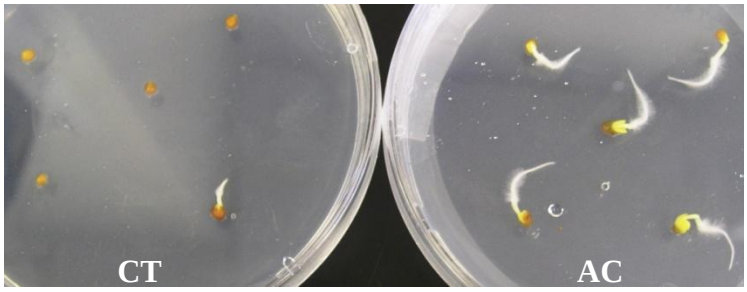

C.

Figure 4.3. *Brassica carinata* control (CT) and antisense *CIL1* (AC) response to salt stress during germination and vegetative growth. A, Seedlings after four days on filter paper containing 1% (w/v) NaCl under a 8 hour day/16 hour night photoperiod. B, Seedlings on medium containing ½ MS, 1% NaCl (w/v) after 4 days in the dark. C, Four week old plants, 4 hours after watering with 100 mL of 5% NaCl (w/v).

control seedlings. Because *CIL1* exhibits photoperiodicity (Gibson, 2005), I placed both control and AC seeds on ½ MS, 1% (w/v) NaCl in the dark. After 4 days, all AC seeds had germinated and cotyledons were unfolding, compared to 20% wild type seeds germinated with no unfolded cotyledons (Figure 4.3B). Based on this information, a preliminary experiment was completed to examine the effects of salt treatment on plant survival during vegetative growth. After 4 weeks of growth with equal watering for 1 week, plants were watered with either 100 mL of a 5% (w/v) NaCl solution or water. After 16 hours, the AC plants remained turgid and appeared unaffected by the salt treatment. In contrast, the wild type plants demonstrated signs of severe salt stress (Figure 4.3C). No differences were seen in the control treatment for either genotype.

4.1.2 Reduced steady state reactive oxygen species (ROS)

Since ROS accumulate in response to auxin and because AC plants showed mildly reduced apical dominance, as well as increased branching during reproductive growth (Gibson, 2005), the steady state levels of redox molecules in AC plants was examined. Leaves were harvested from 56-day old *B. carinata* plants, homogenized and used in assays to determine the reactive activity of eight enzymes involved in the generation and turnover of ROS: NADPH oxidase (NOX), superoxide dismutase (SOD), catalase (CAT), ascorbate peroxidase (APX), glutathione reductase (GR), ascorbate oxidase (AOX), dehydroascorbate reductase (DHAR), and glutathione peroxidase (GPX). Enzyme activity in AC plants was normalized to control, setting the control activity at 1. Of the enzymes examined, CAT, SOD, and NOX activity was greater in AC and GR activity was reduced (Figure 4.4A). The abundance of constituents of the ROS generation/detoxification pathway: superoxide, hydrogen peroxide, total glutathione, ascorbate, dehydroascorbate, NADP+, NADPH, NAD+, and NADH were also determined. Although not significant, NADP+ and NADPH concentration showed decreasing trends with increased NOX activity. Reductions in superoxide and hydrogen peroxide concentration were detected in AC, while the concentration of ascorbate was increased compared to wild type *B. carinata* (Figure 4.4B). The change in GR activity did not result in a decrease in total (oxidized and reduced) glutathione, however the method used could not differentiate between the two forms of glutathione. Increased SOD activity corresponded with a decrease in superoxide concentration. However, the increase in catalase activity did not result in a proportional decrease in hydrogen

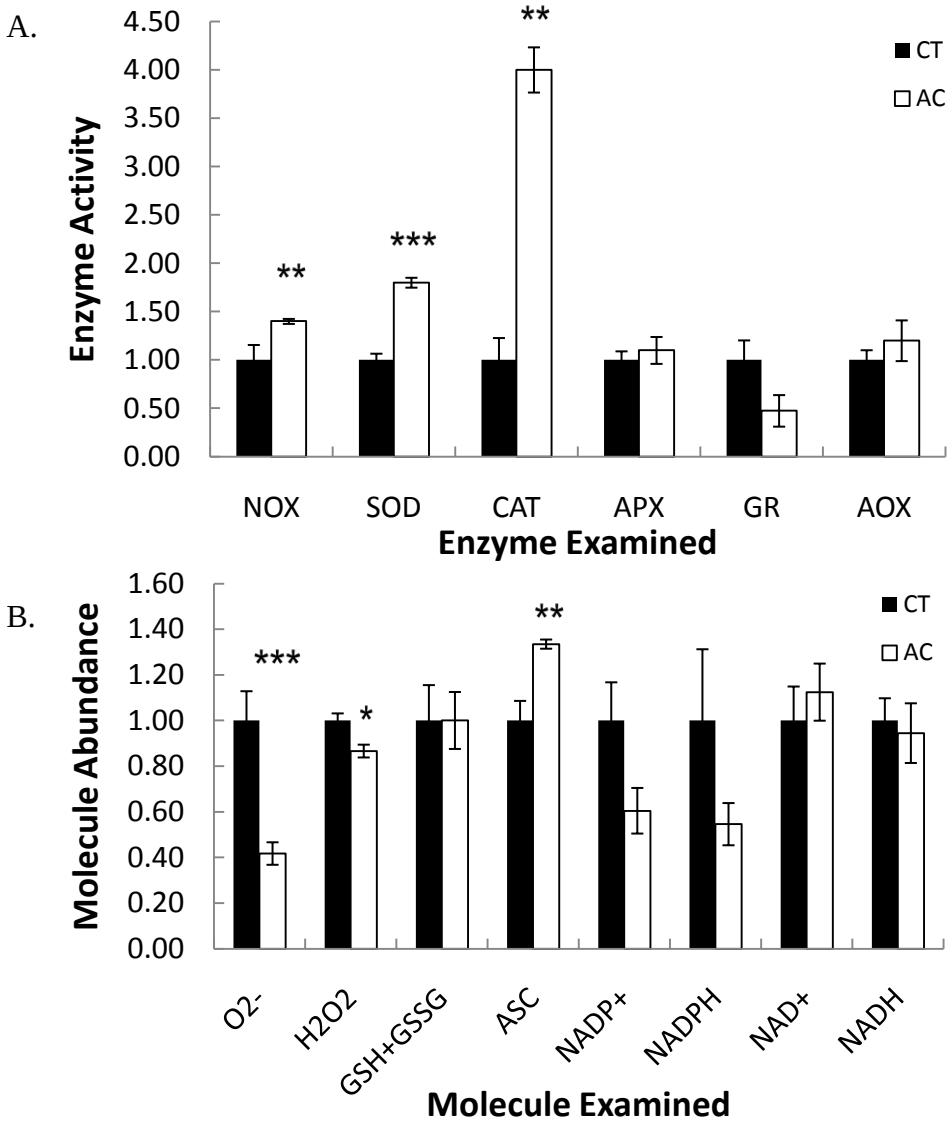

Figure 4.4. Reactive oxygen constituent analysis of 56 day old *Brassica carinata* control (CT) and antisense *CIL1* (AC) plants. A, Steady-state activity of enzymes involved in generation and elimination/turnover of ROS. NOX: NADPH oxidase; SOD: superoxide dismutase; CAT: catalase; APX: ascorbate peroxidase; GR: glutathione reductase; AOX: ascorbate oxidase; DHAR: dehydroascorbate reductase; GPX: glutathione peroxidase. B, Relative steady-state abundance of molecules involved in generation and elimination of reactive oxygen species (ROS). GSH+GSSG: oxidized and reduced glutathione; ASC: ascorbate; DHASC: dehydroascorbate. For all graphs: bars indicate SE, n=3. *$P < 0.05$, **$P < 0.005$, ***$P < 0.0005$, as compared to control plants using a two-tailed Student's t-test.

peroxide concentration, suggesting that increased catalase activity may be a consequence of elevated H_2O_2.

4.2 CIL1 is a glucosylphosphatidylinositol-anchored protein (GPI-AP)

In silica analysis of *CIL1* using Big-PI and GPI-SOM revealed a signal peptide, identity to the DOMON superfamily of domains including DoH, a conserved domain present at the amino-terminal end of the dopamine-beta hydroxylase protein in mammals. Additionally, a domain of unknown function 568 (DUF568) was detected using a combination of SignalP and the conserved domain database (Marchler-Bauer et al., 2009). The carboxy terminus of CIL1 consists of disordered amino acids, detected using DisEMBL (Linding et al., 2003). Hydrophobicity plots using neural networks and transmembrane Hidden Markov Method found a hydrophobic region approximately 30 amino acids long at the amino-terminus and a 26 amino acid hydrophobic region at the carboxy-terminus, but did not predict either of these regions as transmembrane. Furthermore, the entire protein was predicted as extracellular (Figure 4.5A). I hypothesized CIL1 was an extracellular protein either: 1) targeted for secretion by the signal peptide, or 2) targeted for localization by the signal peptide and anchored into a membrane. WolfPSORT predicted CIL1 localizes extracellularly, supporting both hypothesized models. The presence of a signal peptide and a short hydrophic C-terminal domain are properties of glucosylphosphatidylinositol-anchored proteins (GPI-AP). Big-PI was used to examine whether CIL1 contains a GPI signal. This program predicted two potential sites for GPI modification, at amino acids 243 and 244 corresponding with N and A residues, respectively, with scores of 14.09 and 8.66, respectively (Figure 4.5B). Predicted sites are considered significant if the score is greater than 2. These predicted anchor attachment sites match the C-terminal hydrophobic region predicted by the TMHMM program.

A.

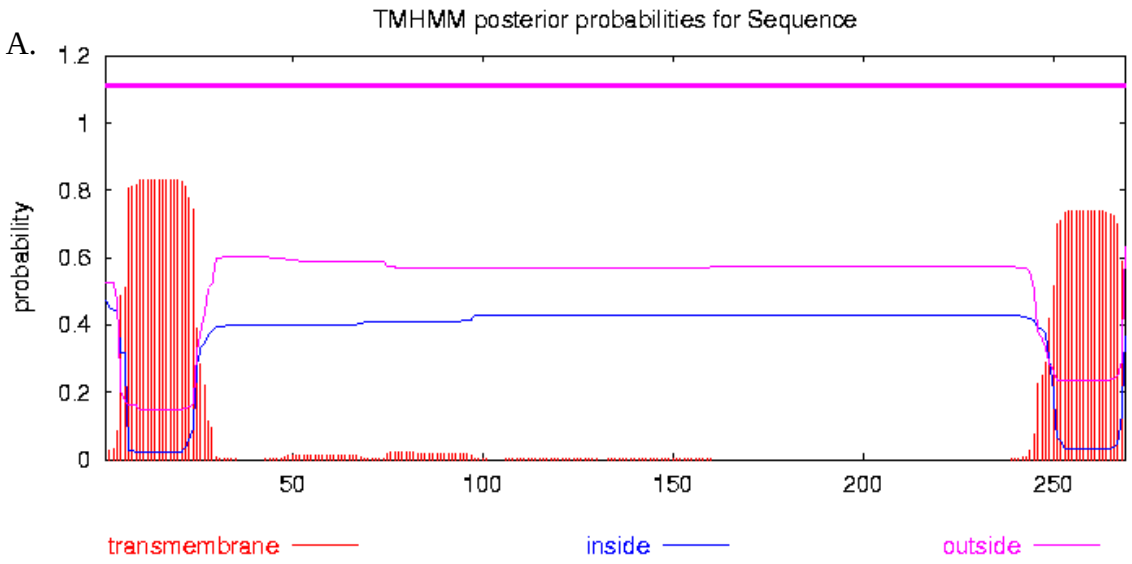

B.

MASNASLTLVLAVACFVSLISPAISQTCSTQNVTGDFKNCMDLPV**LDSFLHYTYDAANSSLSVAFVAT** 69

PPRSGDWVAWGINPTGTKMIGSQAFVAYSPRAGARPEVNTYNISSYSLSAGRLTFDFWNLRAESMAGN 136

RIVIYTSVKVPAGADSVNQVWQIGGNVTGGRPGPHPMTPANLASTRMLRLTGSDAPSSAPGSAPSSGP 205

GSAPSSGPGSAPGSVPGSAEGPTTPDASTTPGQAGSPGNA*GSMTTSVNFGVNFGILVMLASVFIF* 269

Figure 4.5. *In silica* analysis of CIL1. The presence of transmembrane domains and GPI anchoring sites using the TransMembrane Hidden Markov Method (TMHMM; A, http://www.cbs.dtu.dk/services/TMHMM/) and the Big-PI GPI modification site predictor (B, http://mendel.imp.ac.at/gpi/plant_server.html) were examined. CIL1 contains two highly probable transmembrane regions, from amino acids 1-30 and 243-269, corresponding to the signal peptide (1-30), and GPI modification site of the CIL1 amino acid sequence (B) predicted by Big-PI. The location of the signal peptide (underlined), DoH domain (bold), DUF568 domain (highlighted yellow), primary GPI modification site (highlighted red), secondary GPI modification site (highlighted blue), and GPI modification region (italics) are indicated on the amino acid sequence.

4.3 Analysis of *Brassica carinata* detergent insoluble membranes did not detect CIL1

Borner et al. (2002) described a method for detection of GPI-APs present at the plasma membrane of plant cells, often associated with detergent insoluble membranes (DIM). The method exploits the activity of the phospholipase C enzyme that cleaves an anchored protein from its GPI anchor (Chatterjee and Mayor, 2001). Plasma membrane fractions were isolated from 3-week old control *B. carinata* leaves according to Borner et al. (2003). The fractions were then enriched for DIMs and split into two equal parts. One part was untreated while the second part was treated with phospholipase C. Afterward, the fractions were washed several times by phase separation with Triton X-114. Both fractions were then separated using 2-D gel electrophoresis and unique spots on the treated gel were excised and analysed by mass spectrometry by comparison of protein sequences to the NCBI non-repetitive database (2007) using Mascot Daemon (Boston, MA, USA) software.

In total, 58 unique spots were excised from the 2-D gel and examined by mass spectrometry (Figure 4.6). The protein sequences recovered using this method were predominantly subunits of ATP synthase and ribulose 5,6-bisphosphate. Other confirmed GPI-APs SKU5 (Sedbrook et al., 2002) and FLA7 (Borner et al., 2003) were recovered from a spot at pH 4.7 and approximately 60 kDa. Interestingly, several thioredoxin isoforms were detected at approximately pH 3.3 and 45 kDa. No CIL1 was detected in any spot examined.

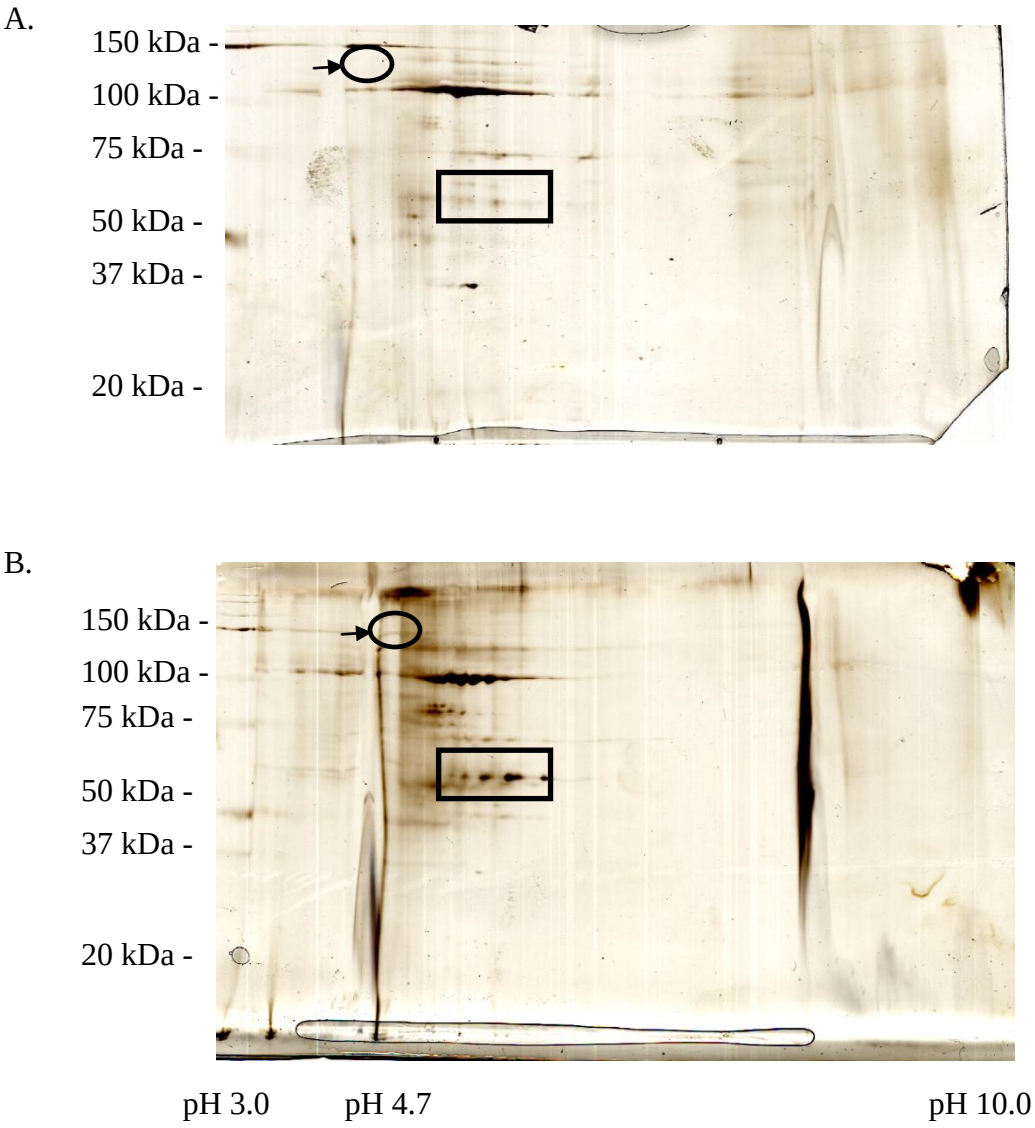

Figure 4.6. Two-dimensional SDS PAGE used to examine the presence of glucosylphosphatidylinositol-anchored proteins (GPI-APs) in purified *Brassica carinata* plasma membranes before (A) and after (B) digestion with phospholipase C. Proteins were first separated on an IEF strip with a pH range of 3-10 followed by separation in the second dimension (SDS-PAGE). Unique dots were excised and examined by mass spectrometry. The dot indicated by the arrow contained 2 confirmed GPI-APs present at pH4.7, FLA7 and SKU5. The dots indicated by the box did not contain proteins that conformed to any known GPI-AP.

4.4 Arabidopsis AUXIN INDUCED in ROOTS 12 (AIR12) shares amino acid sequence with CIL1

The CIL1 amino acid sequence is defined by several domains, outlined previously. Analysis of CIL1 using BLAST identified one amino acid sequence with 64% identity to CIL1, AUXIN INDUCED in ROOTS 12 (AIR12; NP_566306), isolated in 1999 from a subtractive cDNA library of auxin treated Arabidopsis roots (Neuteboom et al., 1999). The AIR12 amino acid sequence is characterized by the presence of 4 distinct domains identical to those present in CIL1. In order of appearance, from the N-terminus to the C-terminus, these domains in the AIR12 amino acid sequence are: 1) the signal peptide (amino acids 1-47); 2) the DOMON superfamily including DoH, a domain of unknown function, DUF568 (amino acids 112-212); 3) a disordered region (amino acids 198-273), and; 4) a site for GPI anchor attachment (amino acids 247-273). Alignment of the proteins shows moderate differences in primary amino acid composition between regions with high identity within the conserved domains (Figure 4.7). To continue characterizing AIR12 and CIL1, Arabidopsis T-DNA insertion lines were obtained.

4.5 Genotypic analysis of Arabidopsis *air12* mutants.

Prior to analysis, *air12* mutants were ordered from the RIKEN institute. The mutagenesis system used by RIKEN involved crossing the parental lines available from the Arabidopsis Biological Resource Center (ARBC), *Ac* (CS8538) and *Ds* (CS8518). The *Ac* parent is phenotypically normal; during the initial transformation, this cassette integrated into a non-coding region of the Arabidopsis genome. The *Ds* parent, on the other hand, is phenotypically a dwarf. The dwarf phenotype was caused by integration of the cassette into the coding region of At5g66210, annotated as a calcium dependent protein kinase; CDPK (Ito et al., 2002). As a result, the *air12-1* No-0 plants are, in fact, double mutants. Attempts were made to identify a plant that was either homozygous for the *Ds* cassette within *air12* and heterozygous at the At5g66210 locus or heterozygous at both loci. Over 100 heterozygous *AIR12/air12* plants were PCR screened with no success at identifying heterozygous At5g66210 plants. Therefore, for the remainder of the study the *Ds* parent (dwarf) was used as a comparator to this allele, designated *air12-1*. The remaining three Arabidopsis *Ac*/*Ds* insertion lines are in the Landsberg *erecta* background. The parents used in the crosses to generate these three lines contained the *Ac*

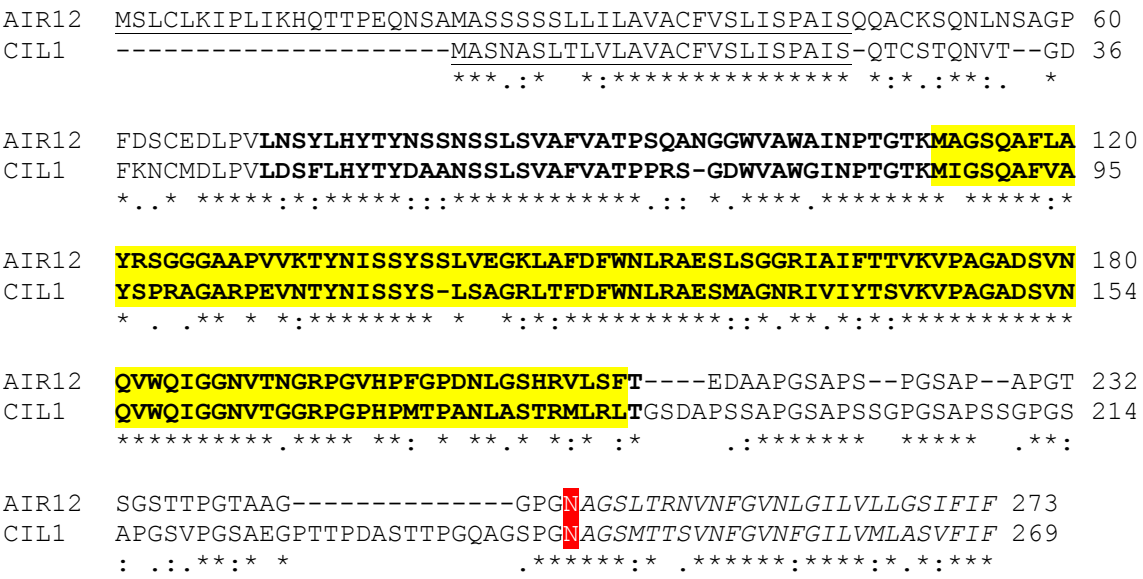

Figure 4.7. Clustal W alignment of the AIR12 and CIL1 amino acid sequences. The symbols "*", ":", and "." below each line represent exact matches, conserved substitutions, and semi-conserved substitutions, respectively. Regions of similarity between the two sequences are prominent throughout the alignment, with strong similarities present at the beginning, middle, and end or the proteins, corresponding with the signal peptide (underlined), DoH (bold), DUF568 (highlighted yellow), primary GPI modification site (highlighted red), and GPI anchor region (italics), respectively.

or *Ds* cassette in non-coding regions (http://genetrap.cshl.org/TrParentalLines.html). Seed from homozygous *air12* plants, as determined by PCR, using one 5' *AIR12* primer, one 3' *AIR12* primer, and one *Ds*-specific primer have been collected for two lines, *air12-2*, and *air12-4*, while homozygous individuals have not been isolated from *air12-3* to date. The position of *Ds* integration into *AIR12* is shown in Figure 4.8.

4.6 AIR12 and CIL1 localize to the plasma membrane and apoplast

Both the AIR12 and CIL1 amino acid sequences contain a signal peptide, targeting these proteins for secretion as predicted by WolfPSORT and SignalP. Additional support for secretion includes specific hydrophobic residues near the C-termini of both proteins, making this region the likely target of GPI anchor attachment as predicted by Big-PI. Prior to anchor attachment, immature proteins containing a GPI target site are post-translationally modified. The C-terminus is cleaved at specific hydrophobic residues while the anchor is covalently attached, targeting the protein for Golgi-mediated secretion (Brown and Rose, 1992; Elortza, 2006). The C-terminus, in essence, acts as an additional signal peptide. The double signal peptides present in GPI-APs presented challenges for the assembly of a fusion protein to confirm localization. The fusion must be made downstream of the N-terminal signal peptide, and upstream of the C-terminal signal peptide. I wanted to confirm the predicted subcellular localization of AIR12 and CIL1 using GFP-fusion proteins and confocal laser-scanning microscopy. The designed fusion constructs incorporated the predicted signal peptides, both N- and C-terminal. To generate these constructs, the gene coding for emerald GFP (Teerawanichpan et al., 2007) was placed in-frame directly downstream of the N-terminal signal peptide and upstream of the open reading frame of the mature protein. The resulting fusion proteins contained the consensus transcriptional start site followed by the N-terminal signal peptide, the open reading frame of GFP followed by the remaining open reading frame of *AIR12* or *CIL1* (Figure 4.9). After assembly of the two constructs in a Gateway entry vector (pCR8/GW/TOPO), they were recombined with the Gateway destination binary vector pER310 containing a CaMV 35S promoter. The constructs were used to stably transform *Ds*, *air12-1*, Ler, and *air12-2* Arabidopsis plants by floral dipping.

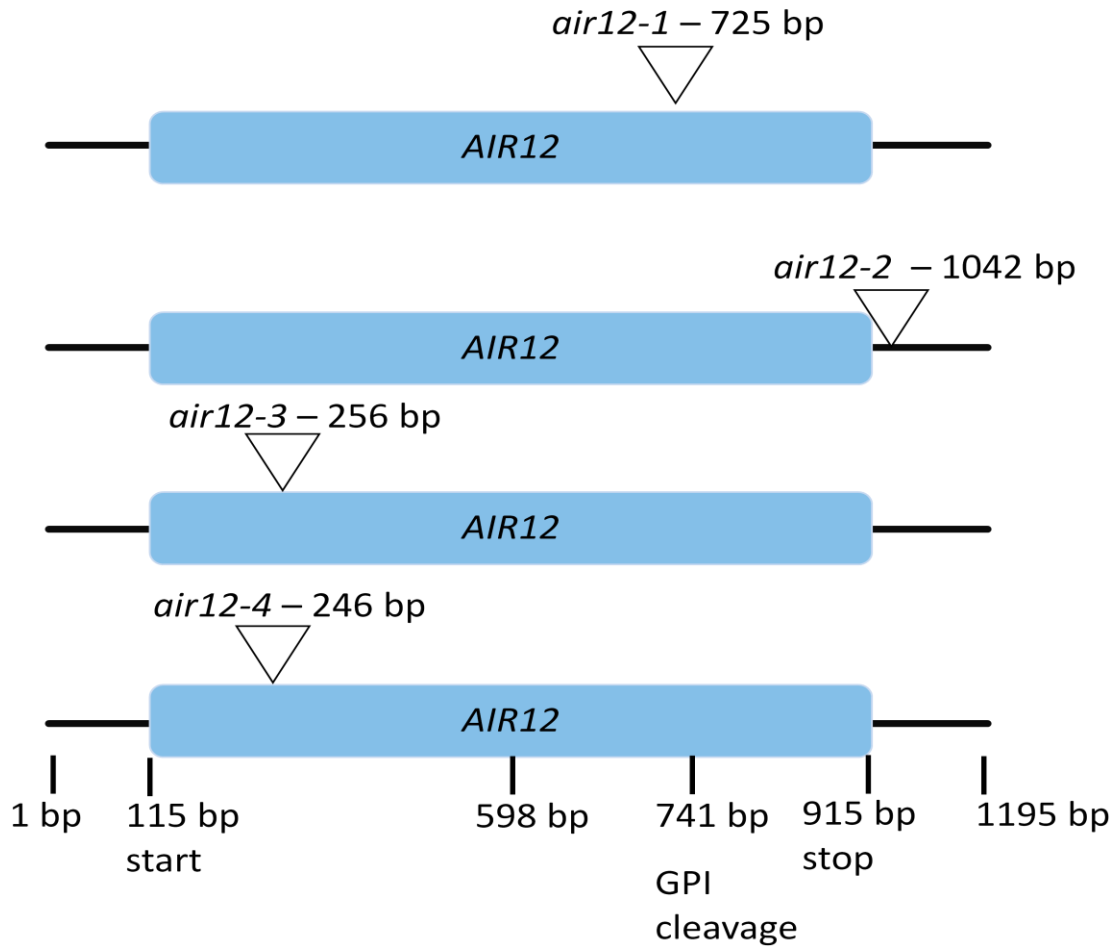

Figure 4.8. Graphical representation of *AIR12 Ac*/*Ds* insertion position in 4 Arabidopsis lines. *air12-1* is in the Nössen *Ds* background while *air12-2*, *air12-3*, and *air12-4* are in the Landsberg *erecta* background.

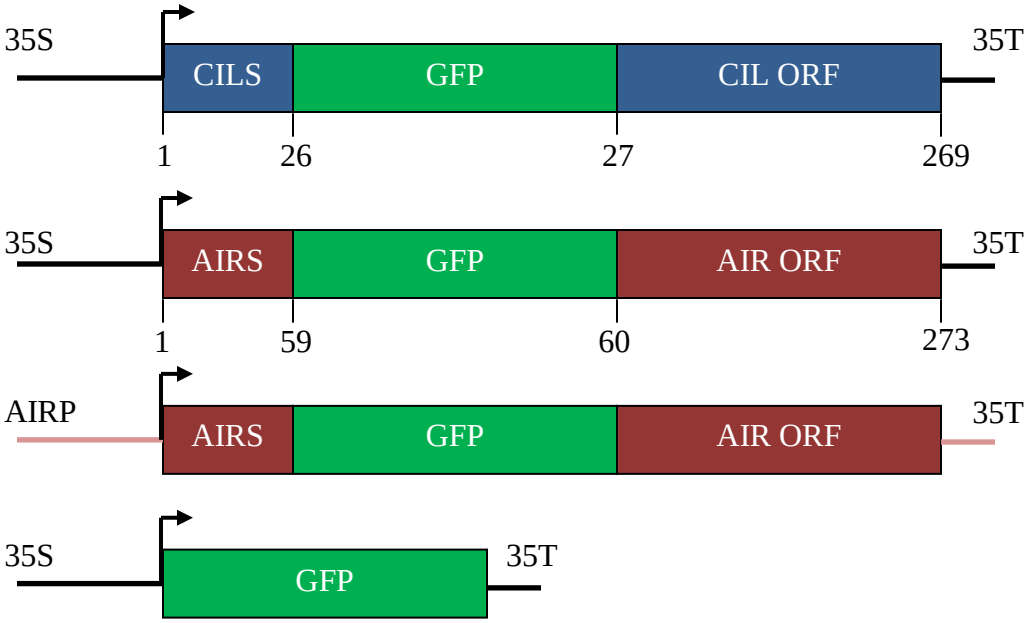

Figure 4.9. Graphical representation of 4 assembled constructs. The first three constructs are under the control of the CaMV 35S promoter (35S) or the *AIR12* promoter (AIRP) and were assembled by placing the gene coding for green fluorescent protein (GFP) directly downstream of the signal peptide. The fourth construct was used as a fluorescence control. With all constructs, transcription was terminated using the 35S terminator (35T). Amino acid positions of GFP-AIR12 and –CIL1 constructs indicated below diagram. Amino acid positions are identical for the two GFP-AIR12 constructs.

Seed collected from floral-dipped plants were germinated and sprayed with a BASTA solution once the second leaves were visible. Surviving plants were grown for an additional 2 weeks at which point DNA was isolated from harvested leaf material. The presence of the *GFP-AIR12/CIL1* fusion was confirmed using PCR with primers that bridged the 35S promoter (SG8) and *AIR12* (SG7) or *CIL1* (SG2). Leaves of PCR-positive plants were examined using a confocal laser-scanning microscope. Visualization of *p35S::GFP-AIR12 Ds* or *air12-1* (Data not shown) were the same as *p35S::GFP-CIL1* showed similar patterns; localization to cell margins in both root (Figure 4.10A) and leaf Arabidopsis tissue (Figure 4.10B). Both AIR12 and CIL1 were predicted as GPI-anchored proteins localized to the plasma membrane. When incubated in water, plant cells remain turgid making it difficult to differentiate the plasma membrane from the apoplast. To view the plasma membrane independent of the cell wall, stably transformed *p35S::GFP-CIL1* plants were plasmolyzed with 2% NaCl (w/v) for 5 minutes and examined using confocal laser-scanning microscopy. In plasmolyzed leaves, CIL1 localized to both the plasma membrane and the apoplast (Figure 4.11A, B). To allow for definitive differentiation of the plasma membrane from the cell wall, tissue was first stained with the red fluorescent dye propidium iodide (PI), a cell wall stain, for 2 minutes followed by plasmolysis with 2% NaCl (w/v) as before. In plasmolyzed roots, the same plasma membrane/apoplastic CIL1 localization was seen (Figure 4.12A) with the addition of red fluorescence localizing to the cell wall and nucleus. In addition, green fluorescence was also seen in specific regions surrounding the nucleus, likely the endoplasmic reticulum. Strands of plasma membrane or hechtian strands were also visible spanning the width of cells (Figure 4.12B). Although PI is generally cell wall specific, nuclear localization of the dye can be seen in dead or severely injured cells. In this case, the nuclear localization of PI is likely due to the plasmolysis treatment. In many cases the plasmolysis of cells was so severe that clear images could not be acquired. To remedy this, instead of plasmolyzing with a 2% NaCl (w/v) solution, 800 mM sorbitol was used to apply an osmotic plasmolysis for 5 minutes. Fluorescence was clearly localized to the plasma membrane and apoplast versus the red fluorescence of the cell wall, and in some cases, the nucleus (Figure 4.13).

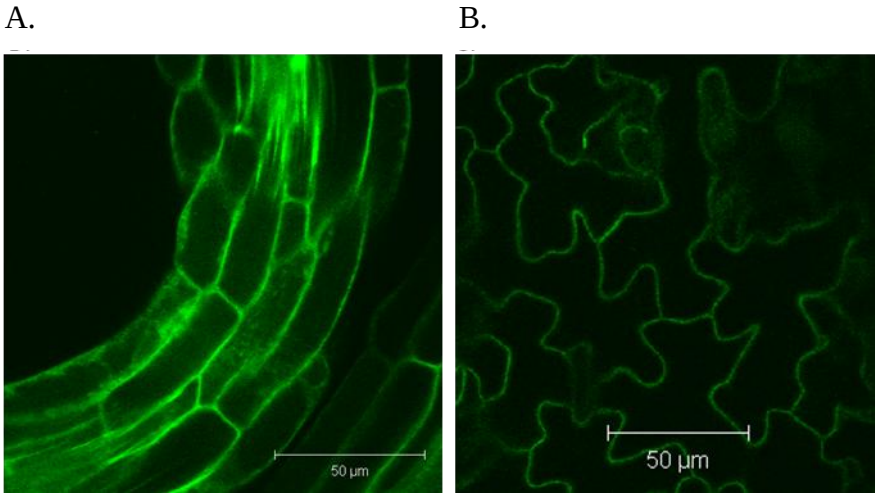

Figure 4.10. Localization of GFP-CIL1 (*p35S::GFP-CIL1*) fusion in stably transformed Arabidopsis. A and B, localization of GFP-CIL1 in Arabidopsis root and leaf epidermis, respectively. Identical capture settings were used for both images.

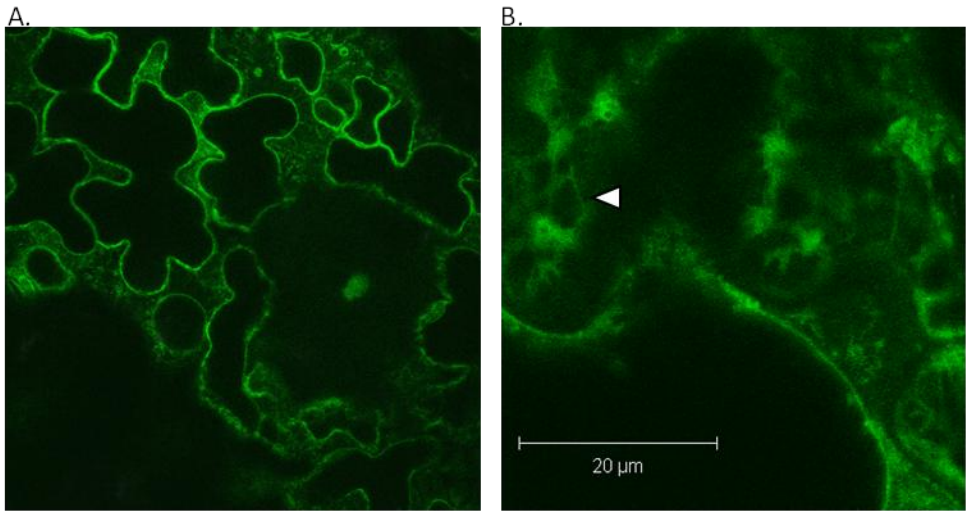

Figure 4.11. Localization of GFP-CIL1 (*p35S::GFP-CIL1*) fusion in the leaves of stably transformed Arabidopsis. A, Arabidopsis leaves plasmolyzed with 2% NaCl (w/v) and immediately imaged. GFP-CIL1 is evident in both the apoplast and cell margins. B, magnification showing margin localization and hechtian strands (arrowhead). Identical capture settings were used for both images.

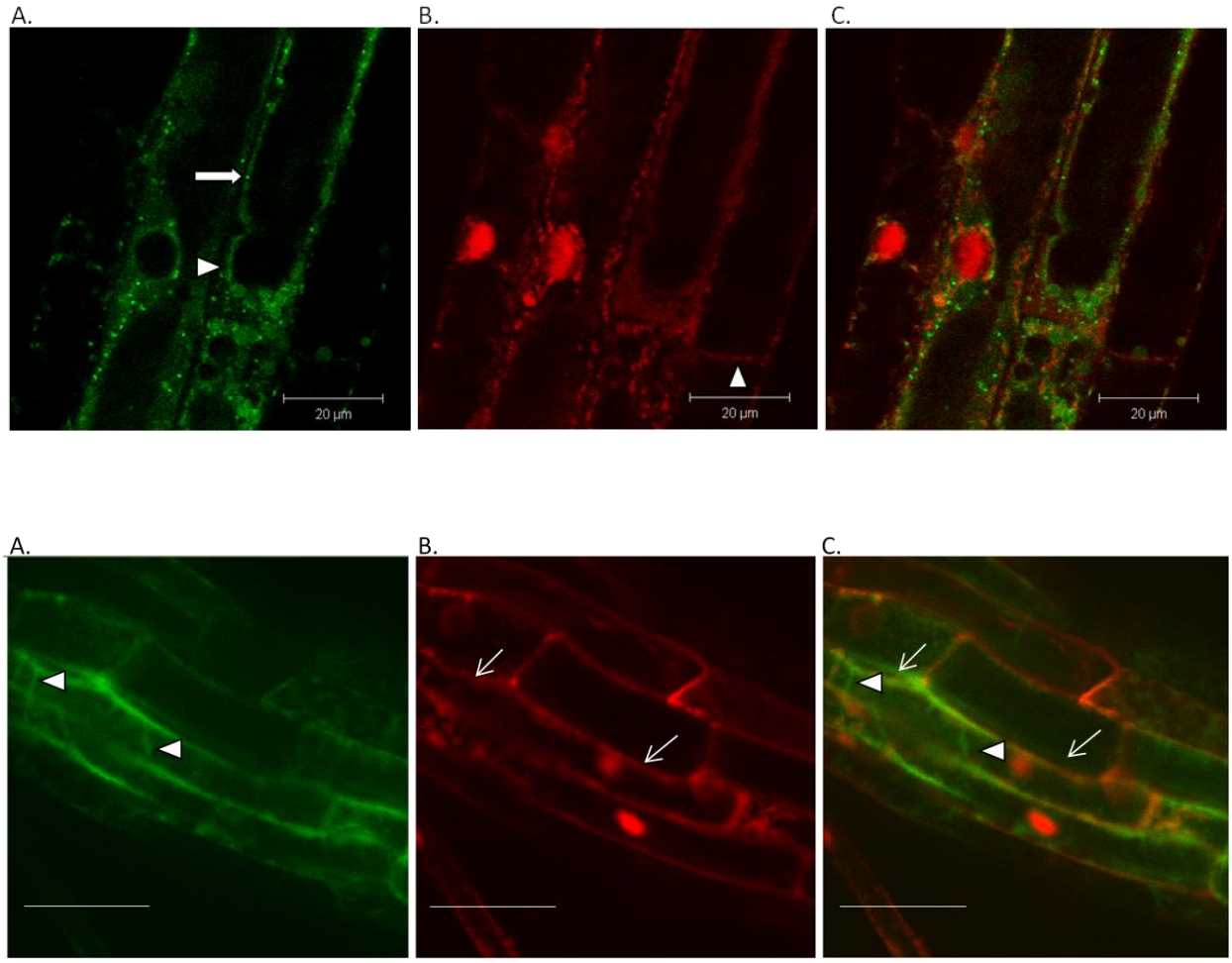

Figure 4.12. Localization of GFP-CIL1 fusion protein together with propidium iodide in roots of stably transformed Arabidopsis roots after plasmolysis with 2% NaCl. Top panel, apoplastic localization of GFP-CIL1. Bottom panel, localization of GFP-CIL1 to hechtian strands. A, GFP-CIL1 localizes to the plasma membrane (arrow) and apoplast (arrowhead) of plasmolyzed cells. B, Propidium iodide stains the cell wall (open arrow) and nucleus of plasmolyzed plant cells. C, merged image of A and B. Identical capture settings were used for all images.

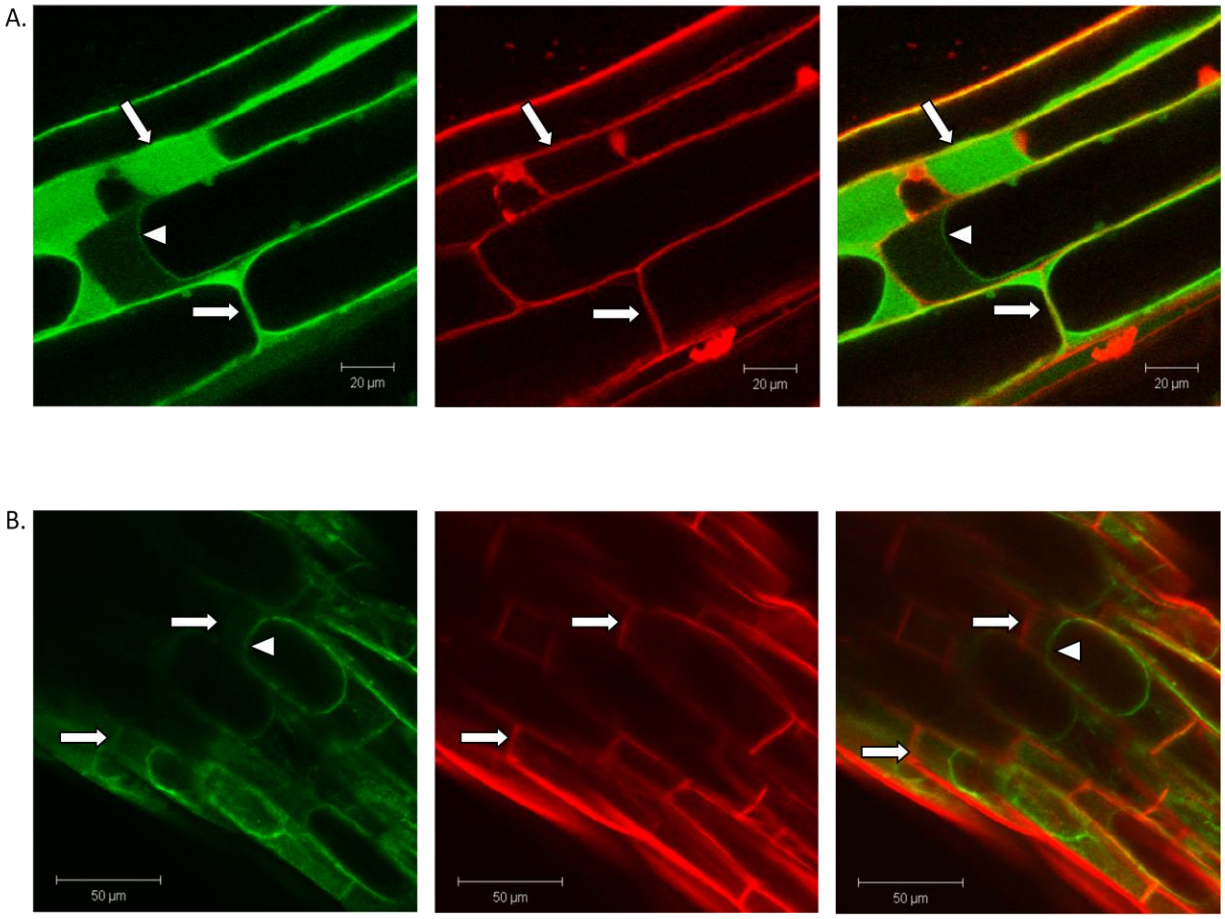

Figure 4.13. Localization of GFP-CIL1 (A) and GFP-AIR12 (B) together with propidium iodide in Arabidopsis roots following plasmolysis with 800 mM sorbitol. Left, Localization of the fusion proteins to the apoplast (arrows) and plasma membrane (arrowheads), in green. Middle, Localization of propidium iodide to the cell wall (arrow), in red. Right, Merged image of green and red channels. Images shown are representative of 3 independently transformed lines. Pinhole diameter and gain for the green channel were 397 µm and 9.0%, respectively, and 294 µm and 8.1% for the red channel, respectively in A, and 306 µm and 25.8% (green), respectively, and 454 µm and 21.8% respectively (red) in B.

4.7 AIR12 localizes to the outer epidermal cell file in stably transformed Arabidopsis roots

To ascertain the distribution of AIR12 *in vivo*, a construct was designed consisting of the *AIR12* promoter controlling a fusion between *GFP* and *AIR12* (*pAIR12::GFP-AIR12*). This cassette was used to stably transform Arabidopsis *Ds* and *air12-1* plants. T_2 seedlings from at least 3 independent transformation events were germinated on media containing ½ MS, 1% sucrose ([w/v]; control medium) or control media supplemented with 1 mM H_2O_2, 400 nM α-NAA, or 30 mM KCl. After 8 days of growth seedlings were visualized using confocal laser-scanning microscopy.

4.7.1 AIR12 localization on control medium

GFP-AIR12 localization driven by the *pAIR12::GFP-AIR12* construct in both the *Ds* and *air12-1* backgrounds are summarized in Table 4.1. In the *Ds* seedlings, fluorescence was visible both in the tip of elongating lateral roots and in the primary root tip. Fusion protein was predominantly localized to the epidermal cell file in these organs and was consistently present in a "scattered" pattern (Figure 4.14A). In all cases, fluorescence was absent from one side of the elongating primary root tip. Fluorescence remained cellular from the primary root tip 400 μm basipetally. Approximately 600 μm from the primary root tip, the fusion protein shifted from the cell margins to the vascular tissue of the root (Figure 4.14B). The intensity of the vascular fluorescence increased as the distance from the root tip increased until approximately 1,200 μm from the root tip, where fluorescence reached a maximal intensity (Figure 4.14C) and remained at this intensity through 5 mm of a 10 mm root (Figure 4.14D). GFP-AIR12 fusion protein was also visible in cell margins in the hypocotyl and leaf epidermis (Figure 4.15A, B).

During lateral root emergence, adjacent pericycle cells separate allowing the primordium to grow out from the endodermal cell file (Casamiro et al., 2001; Himanen et al., 2002). These lateral roots also contain a file of vascular tissue connected to the vascular tissue of the primary root. Since I observed localization of the GFP::AIR12 fusion protein in vascular tissue, I hypothesized it would be present in the vascular tissue of emerging or elongating lateral roots.

		Ds	*air12-1*
Control	Primary root	(++) CM of epidermal cells in a scattered pattern	(+) 2 epidermal files and root cap, within cytoplasm
	Emerging or elongating LR	(+) CM of 1 cell in pericycle flanking either side of LR	(-)
	Lateral root	(++) CM of epidermis in a scattered pattern CM	(+) Cytoplasm of 2 epidermal files and at root cap
	Stele	(++) Throughout vasculature	(-)
	Root hairs	(-)	(+) Cell Margins
+ α-NAA	Primary root	(++) CM of epidermal cells in the MZ	(+) Near root cap in cytoplasm of cells
	Emerging or elongating LR	(++) CM of multiple cells in pericycle flanking either side of LR	(-)
	Lateral root	(++) CM of elongating LR. In older LR, within stele	Fluorescence near root cap, present in cytoplasm of cells (+)
	Stele	(+++) Fluorescence throughout vasculature	(-)
	Root hairs	(+) Fluorescence present at CM	(+) Cell Margins
+ KCl	Primary root	(++) CM of epidermal cells in the MZ	(+) Cytoplasm of cells near root cap and in MZ
	Emerging or elongating LR	(++) CM of 1 cell in pericycle flanking either side of LR	(-)
	Lateral root	(+++) CM of epidermal cells in MZ	(++) Within cytoplasm of cells of 2 epidermal files
	Stele	(+) Throughout vasculature	(-)
	Root hairs	(-)	(+) Present at CM
+ H_2O_2	Primary root	(++) CM of epidermal cells in MZ, (dns)	(+) Cytoplasm of 2 epidermal files and root cap
	Emerging or elongating LR	(+) CM near lateral roots	(-)
	Lateral root	(+++) CM of epidermal cells in MZ	(+) Epidermal cells, present within cytoplasm
	Stele	(+) Near lateral roots at CM	(-)
	Root hairs	(+) Cell Margins	(-)

Table 4.1. Summary of GFP-AIR12 fluorescence observed in Arabidopsis stably transformed with *pAIR12::GFP-AIR12 Ds* or *air12-1*; CM, cell margins; LR, lateral root; MZ, meristematic zone; dns, data not shown. Intensity of GFP-AIR12 fluorescence on control medium, and medium supplemented with 400 nM + α-NAA, 30 mM KCl, and 1 mM H_2O_2 is indicated for each background and organ; no fluorescence seen (-), faint (+), present (++), and intense (+++).

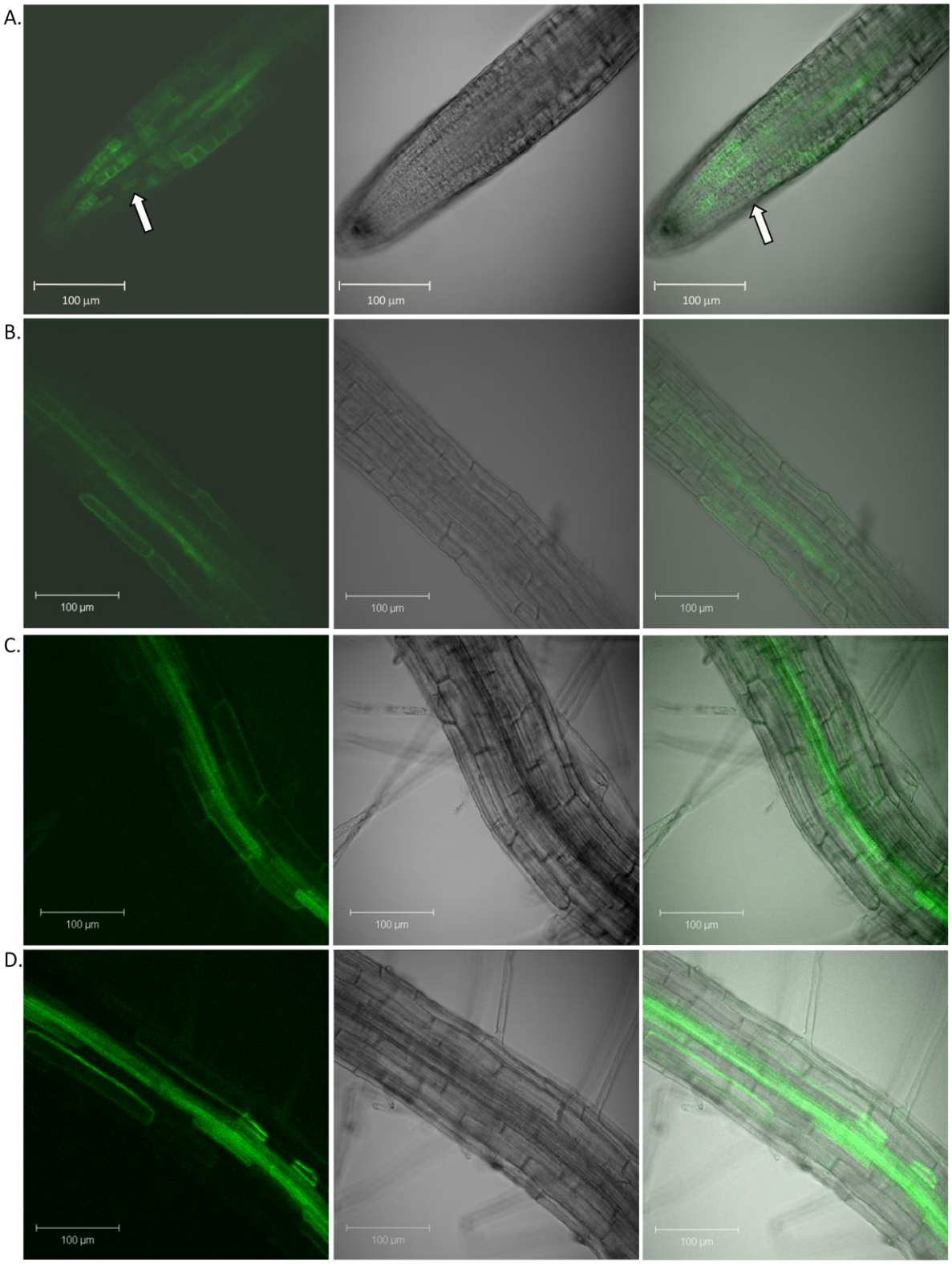
A.
B.
C.
D.
100 µm

Figure 4.14. Localization of GFP-AIR12 in Arabidopsis (*Ds*) stably transformed with *pAIR12::GFP-AIR12*. Seedlings were grown on ½ MS, 1% sucrose (w/v) for 8 days shown in fluorescence (left), DIC (middle), and merged images (right). A, GFP-AIR12 fusion localization to the cell margins of the epidermis with a small zone of fluorescence exclusion (arrow) and vascular tissue in primary roots. B, Vascular localization extends from approximately 200 μm from the apex toward the base of the primary root. Fluorescence intensity increases proportionally with the distance from the root apex. Noticeable increases in fluorescence were observed at 600 μm (B), 1000 μm (C), and maximal intensity was observed at 1400 μm (D). Identical capture settings were used for all images.

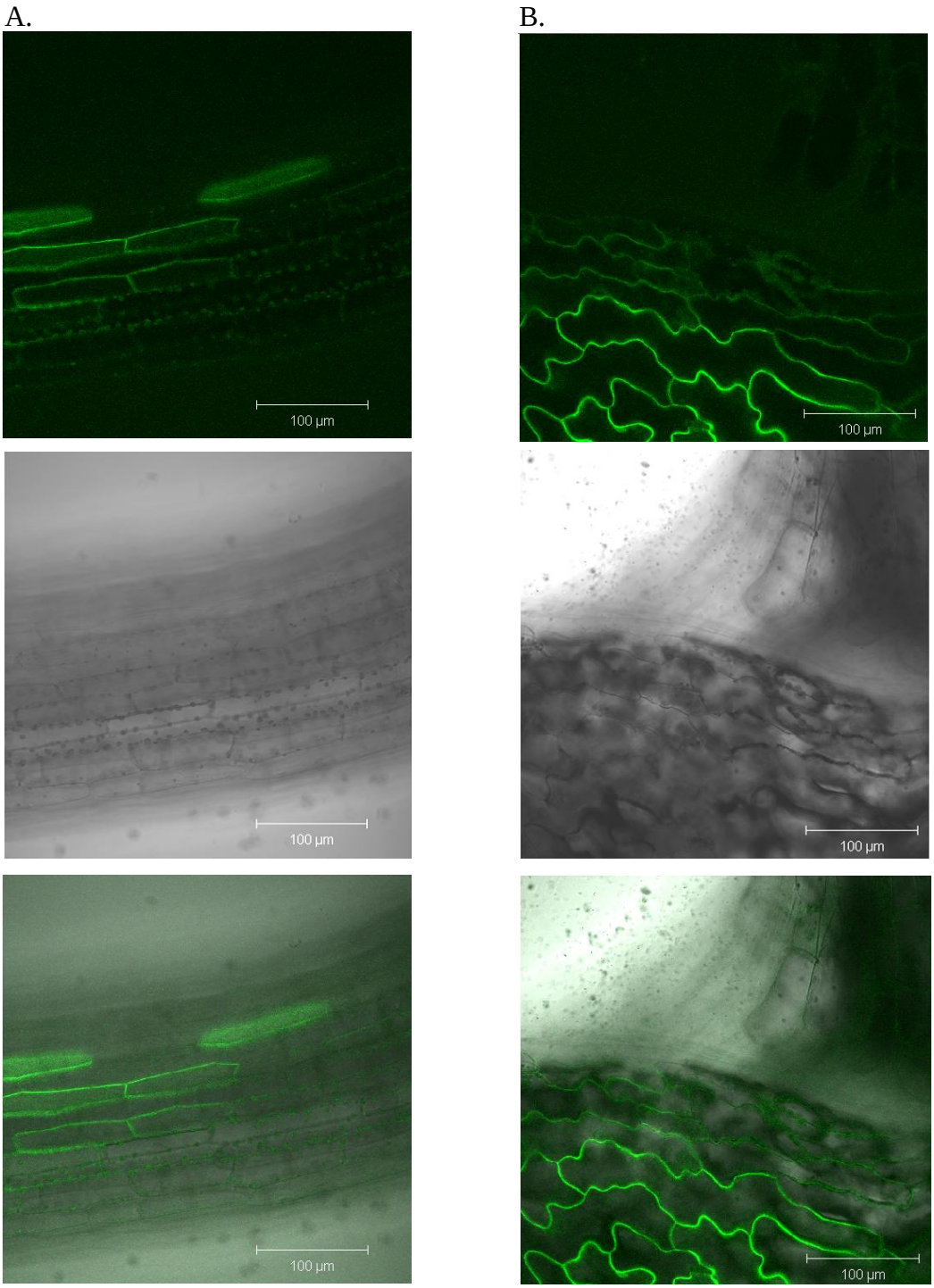

Figure 4.15. Localization of GFP-AIR12 at the cell margins in hypocotyl (A) and leaf epidermis (B) of Arabidopsis (*Ds*) stably transformed with *pAIR12::GFP-AIR12*. Seedlings were grown on ½ MS, 1% sucrose (w/v) medium for 8 days. Top panel, fluorescence channel; middle panel, DIC; bottom panel, merged image. Identical capture settings were used for all images.

Surprisingly, no fluorescence was visible in cells of emerging lateral roots, yet in most cases a single fluorescent cell flanked each side of the lateral root (Figure 4.16A). These single cells, likely endodermal in origin separate as the growing primordium expands. Post-emergence, lateral roots develop defined vasculature resembling the primary root. Examination of lateral roots between 300 and 600 μm did not detect a high degree of fluorescent signal, though the flanking cells endodermal in origin were still visible (Figure 4.16B). Mature lateral roots showed fluorescence in the MZ (Figure 4.17A) and a small degree of vascular fluorescence near the base (Figure 4.16B) but did not show the same transition to vascular localization as seen in primary roots.

Seedlings transformed with *pAIR12::GFP-AIR12* in the *air12-1* background were germinated and grown under identical conditions to *Ds* seedlings. Patterns of fluorescence from two independently transformed lines differed in intensity but retained similar localization to equivalent lines in the *Ds* background. Epidermal localization of the fusion protein was obvious in the lines examined, present both at the lateral root tip and distal to the elongation zone. However, the scattered pattern was absent (Figure 4.17B). Additionally, fluorescence did not completely envelop the cells and appeared almost punctate, localizing to the basipetal pole of these cells. Post-emergence, lateral root primordial contained weak fluorescence. Curiously, near these primordia in the primary root, fluorescence was predominantly present at the cell margins and also localized to root hairs, a phenomenon not seen in any *Ds* lines examined (Figure 4.17 C).

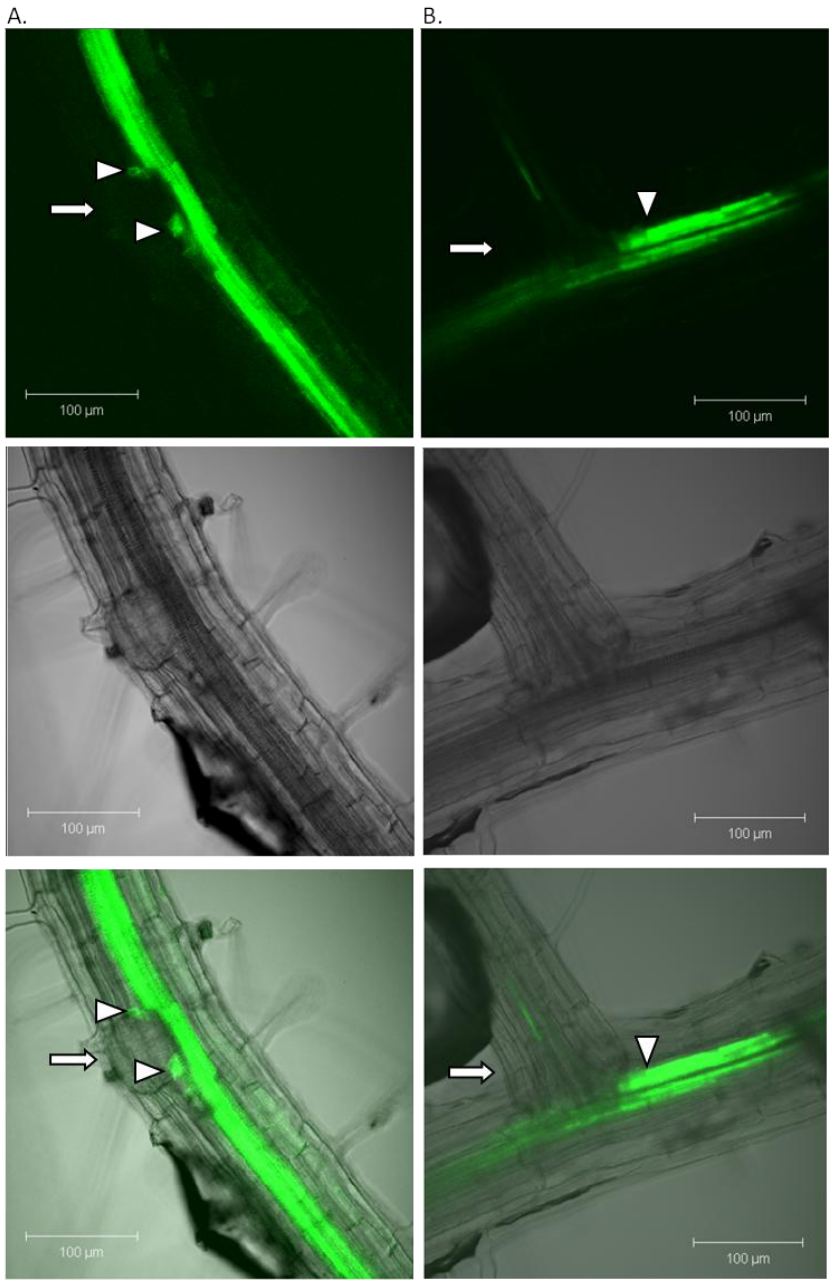

Figure 4.16. Localization of GFP-AIR12 in Arabidopsis (*Ds*) stably transformed with *pAIR12::GFP-AIR12*. Seedlings were grown on ½ MS, 1% sucrose (w/v) for 8 days. A, GFP-AIR12 localizes to the vacular tissue and in cells flanking (arrowheads), but not within emerging lateral roots (arrow). B, GFP-AIR12 fusion protein (arrowhead) extends into vascular tissue of elongating lateral root (arrow). Top panel, fluorescence channel; middle channel, DIC; bottom channel, merge. Identical capture settings were used for all images.

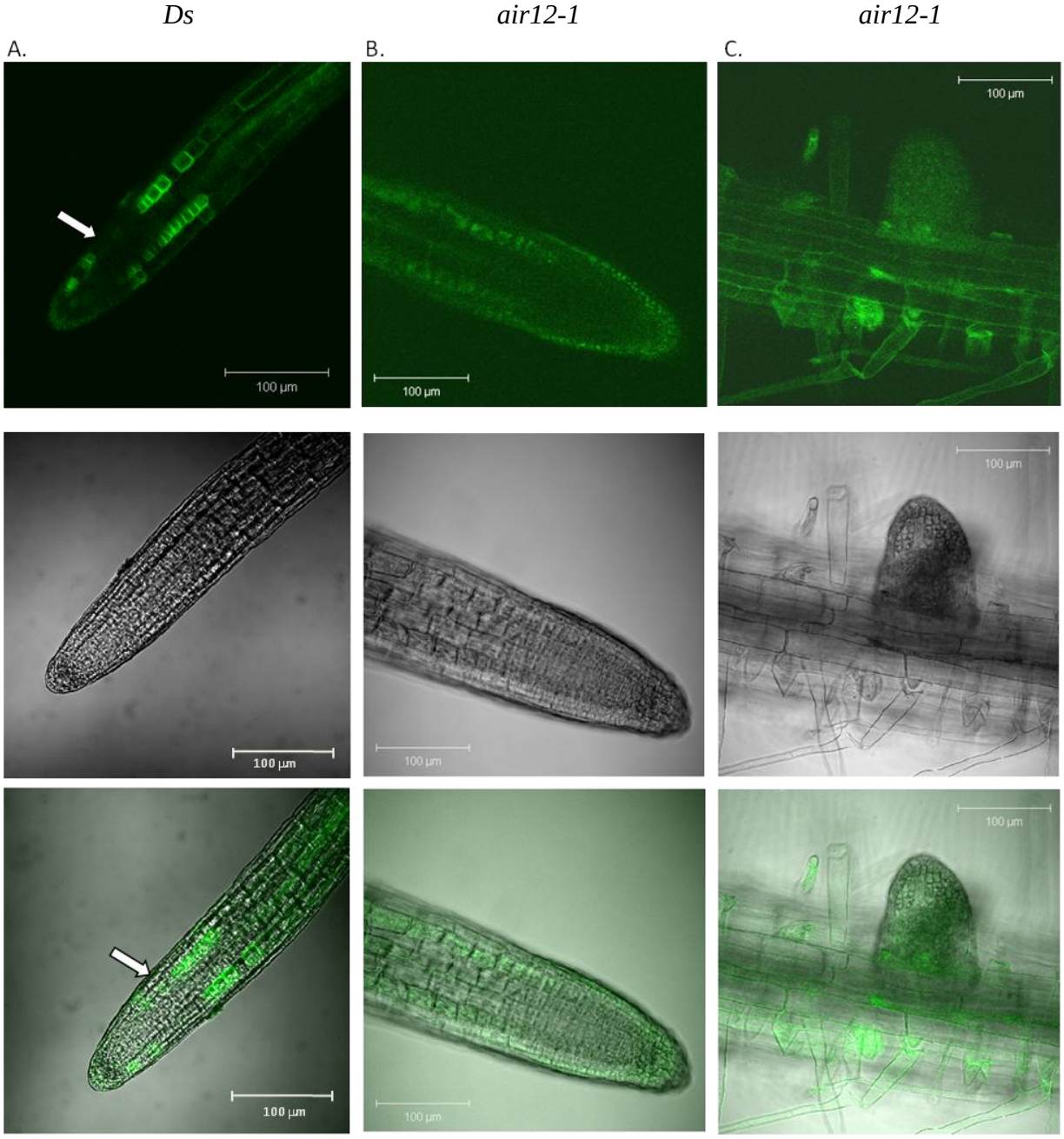

Figure 4.17. Localization of GFP-AIR12 in Arabidopsis *Ds* (A) and *air12-1* (B, C) stably transformed with *pAIR12::GFP-AIR12*. Seedlings were grown on ½ MS, 1% sucrose (w/v) for 8 days. GFP-AIR12 localized to to the cell margins of the epidermis in *Ds* lateral roots (A; arrow), to the cytoplasm of cells within the epidermal file of *air12-1* lateral roots (B), and to the cell margins of root hairs and post-emergent lateral roots (C). Top panel, fluorescence channel; middle panel, DIC; bottom panel, merged image. Identical capture settings were used for all images.

4.7.2 GFP-AIR12 localization on medium supplemented with hydrogen peroxide

The DUF568 present in AIR12 was theorized as a domain involved in electron transport or redox regulation (Iyer et al., 2007; Preger et al., 2009). I decided to test the localization of the GFP-AIR12 fusion protein after growth on a medium containing H_2O_2, examining the *Ds pAIR12::GFP-AIR12* lines first.

At the interface between primary/lateral and lateral/second-order lateral roots grown on H_2O_2, fusion protein was visible at cell margins (Figure 4.18A). One line with exclusive epidermal GFP-AIR12 localization also showed specific subcellular localization to all but the apical poles in the lateral roots (Figure 4.18B). At lateral root tips fusion protein was confined to the epidermal cell layers in lines 1 and 2 (Figure 4.19A), and present almost uniformly throughout the tip in line 3 (Figure 4.18B) with a small area of exclusion, similar to the pattern seen on control medium (Figure 4.17A). Like the control medium-grown seedlings, the strength of the fluorescent signal was proportional to the distance from the lateral root tip. After 300-600 um from the root tip, no fluorescent signal was detected (Data not shown).

Next, I examined *pAIR12::GFP-AIR12* lines in the *air12-1* background. In both lines, faint GFP-AIR12 was present near the elongation zone of lateral root tips. In these small cells, GFP-AIR12 appeared intracellular, causing the entire cell to appear green (Figure 4.18C). Just basipetal of the elongation zone, GFP-AIR12 localized to the epidermal cell file. Similar to the *Ds* lines and *air12-1* lines grown on control medium, subcellular localization of GFP-AIR12 was absent from the cell edge adjacent to the cortex (Figure 4.19B).

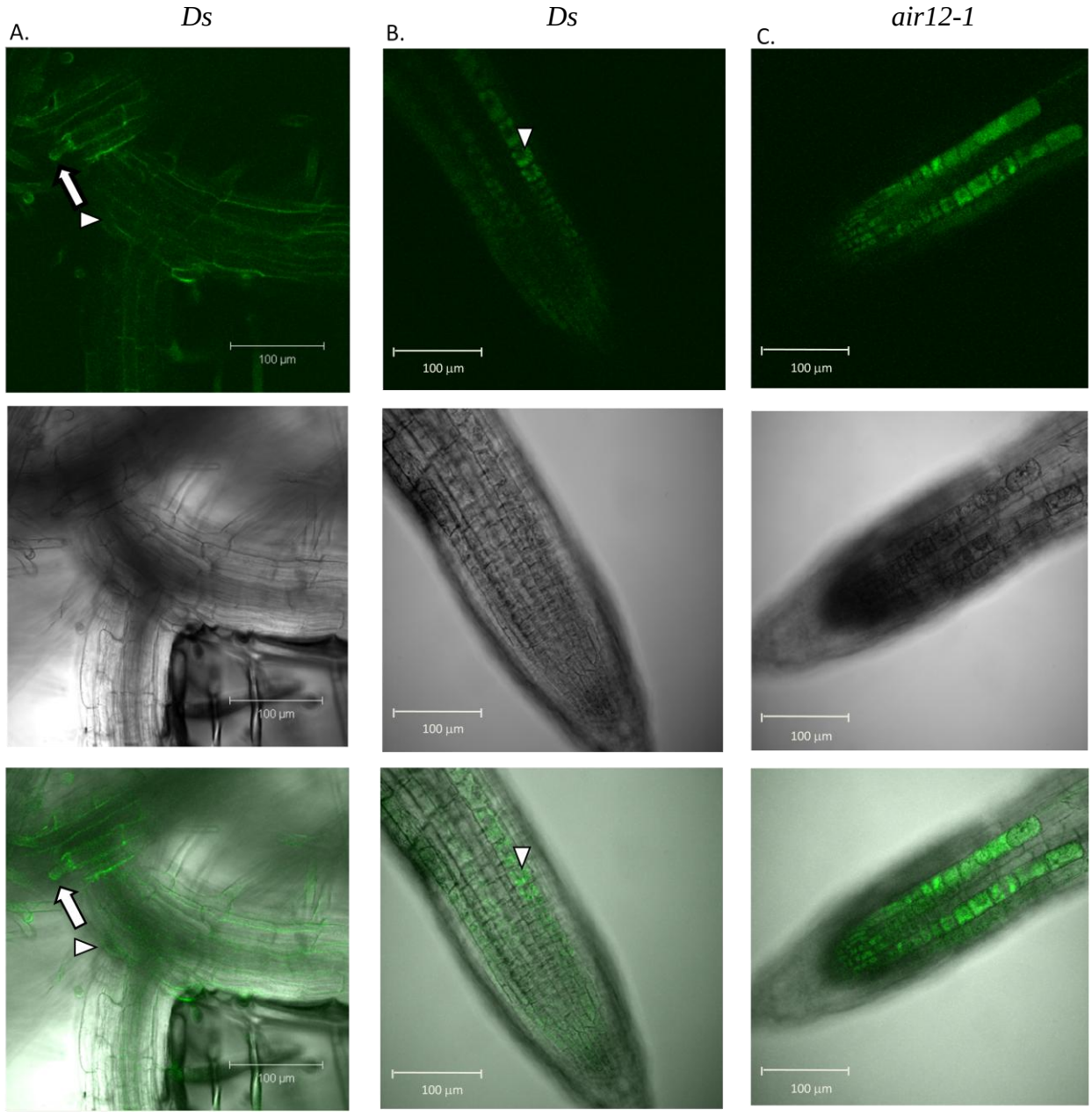

Figure 4.18. Localization of GFP-AIR12 in Arabidopsis *Ds* (A, B) and *air12-1* (C) stably transformed with *pAIR12::GFP-AIR12*. Seedlings were grown on ½ MS, 1% sucrose (w/v) supplemented with 1 mM H_2O_2 for 8 days. A, GFP-AIR12 localizes to the cell margins near *Ds* lateral (arrow) and second order lateral roots (arrowhead). B, GFP-AIR12 is absent from the apical pole (arrowhead) of epidermal cells in *Ds* lateral roots of the third independent line examind. C, GFP-AIR12 was observed throughout *air12-1* epidermal cells in the primary root. Top panel, fluorescence channel, bottom channel, DIC. A piece of agar (bottom panel under scale bar in (A) represents an artifact. Identical capture settings were used for all images.

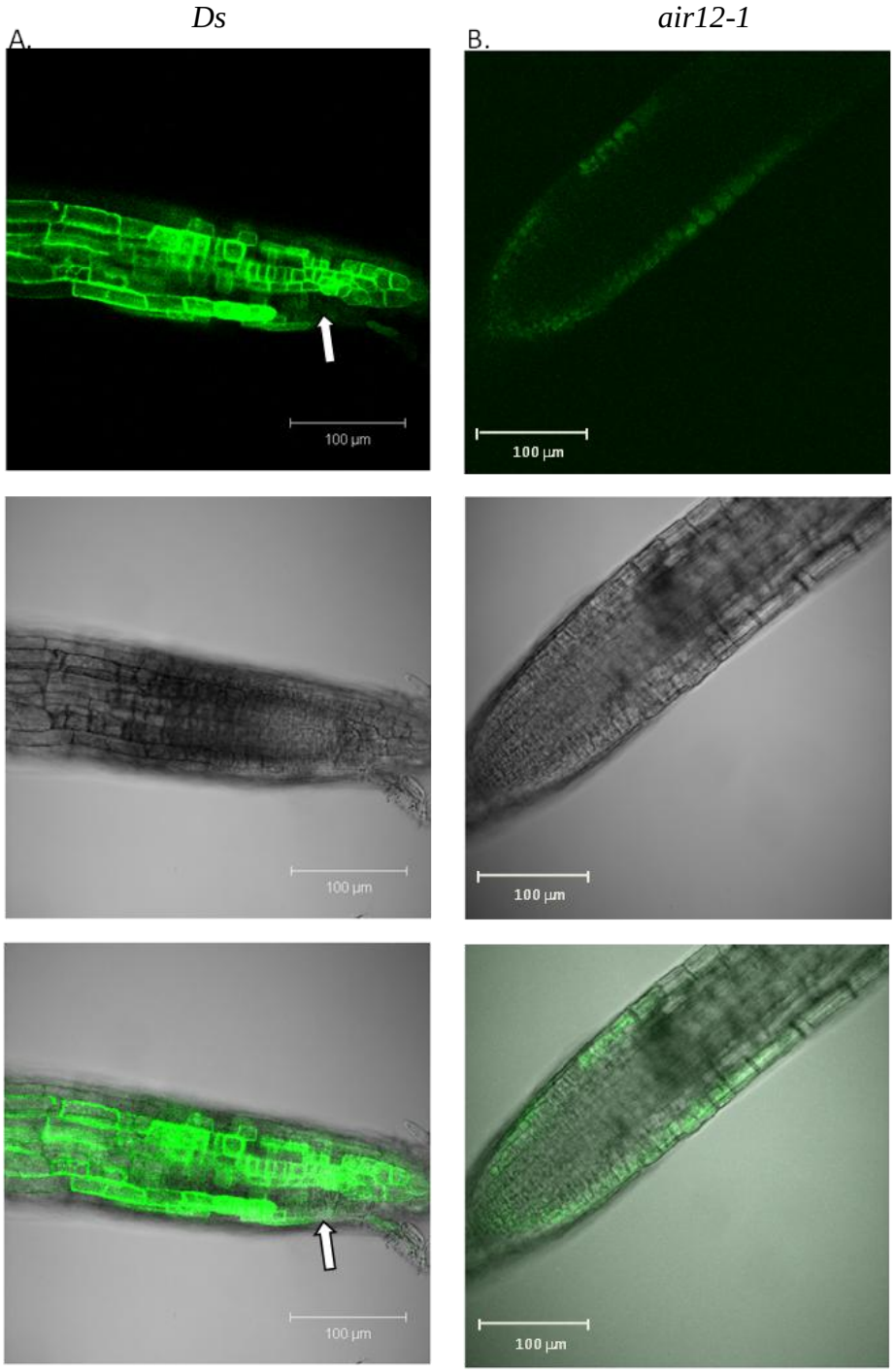

Figure 4.19. Affect of H_2O_2 on localization of GFP-AIR12 in Arabidopsis *Ds* (A) and *air12-1* (B) stably transformed with *pAIR12::GFP-AIR12*. Seedlings were grown on ½ MS, 1% sucrose (w/v) supplemented with 1 mM H_2O_2 for 8 days. Strong, uniform GFP-AIR12 was seen throughout *Ds* lateral root tips, with the exception of a small area of exclusion (arrow) (A), and in *air12-1* lateral root tips, GFP-AIR12 displayed punctate subcellular localization (B).Top panel, fluorescence channel; middle panel, DIC; bottom panel, merged image. Identical capture settings were used for all images.

4.7.3 GFP-AIR12 localization on medium supplemented with auxin

AIR12 was originally isolated from auxin-treated Arabidopsis roots. Treatment with auxin correlates with increases in *AIR12* expression during lateral root development (Laskowski et al., 2006). I hypothesized that seedling treatment with auxin would correlate with increased GFP-AIR12 accumulation in the primary and lateral roots. To test this hypothesis, seeds from both the *Ds* and *air12-1* background containing the *pAIR12::GFP-AIR12* construct were placed on medium containing 400 nM α-NAA and examined after 8 days of growth.

Ds seedlings grown on 400 nM α-NAA showed GFP-AIR12 localization to the tip of primary and elongating lateral roots, displaying a scattered pattern of fluorescence with one side of the root tip lacking fusion protein (Figure 4.20). This pattern of fluorescence resembled that of *Ds* seedlings grown on control medium or medium supplemented with 1 mM H_2O_2. Examination of developing lateral roots revealed GFP-AIR12 fusion protein on both sides of emerging root primrodia, flanking the organ (Figure 4.20B). These cells appeared endodermal in origin, and unlike with the control medium, consisted of more than one cell file in both lateral and secondary order lateral roots (Figure 4.20B and Figure 4.21B). Vascular localization of the GFP-AIR12 fusion was also detected in the primary and lateral roots (Figure 4.20C) and in root hairs of the primary root (Figure 4.22A). This may be the result of auxin stimulating cell division or because a slightly different-staged lateral root was observed relative to other treatments. GFP-AIR12 fusion protein was also visible in emerging primordial (Figure 4.21B), a phenomenon not observed when seedlings were grown on media lacking auxin (Data not shown).

When seedlings with the same construct from the *air12-1* background were examined, almost no GFP-AIR12 fusion protein could be detected in any organ examined. Extremely weak signal was found throughout lateral root tips (Figure 4.21C). Additional signal was found in the root hairs of the seedlings, similar to the *Ds* background (Figure 4.22B).

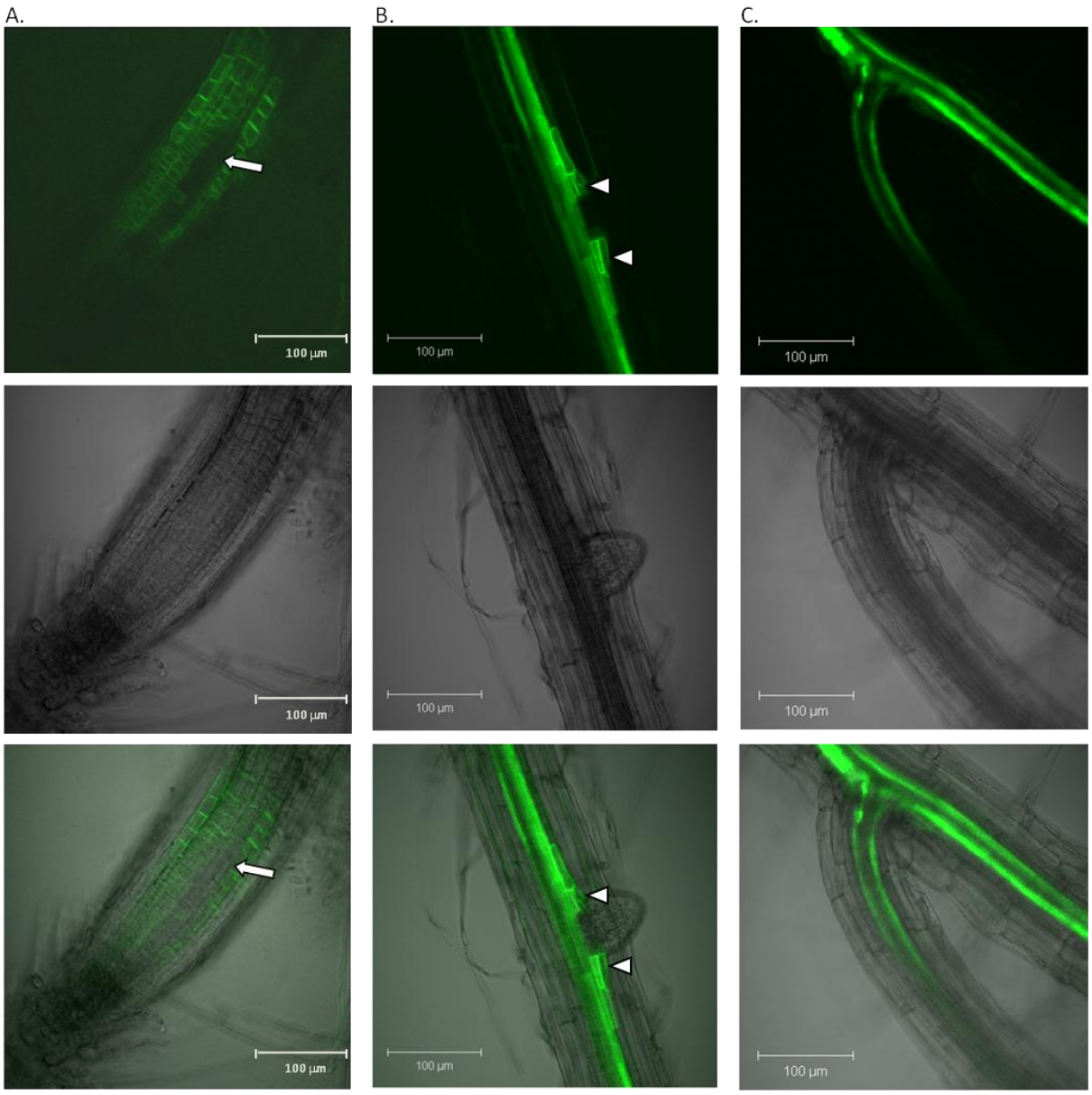

Figure 4.20. Localization of GFP-AIR12 in Arabidopsis (*Ds*) stably transformed with *pAIR12::GFP-AIR12*. Seedlings were grown on ½ MS, 1% sucrose (w/v) supplemented with 400 nM α-NAA for 8 days. A, GFP-AIR12 localization to margins of the epidermal cell file in primary roots, with the exception of a small area of exclusion (arrow). B, GFP-AIR12 localizes to the vascular tissue in the primary root and in endodermal cells flanking an emerging lateral root (arrowheads). C, GFP-AIR12 localizes to the vascular tissue of primary and lateral roots. Top panel, fluorescence channel; Middle panel, DIC; Bottom channel, merged image. Identical capture settings were used for all images.

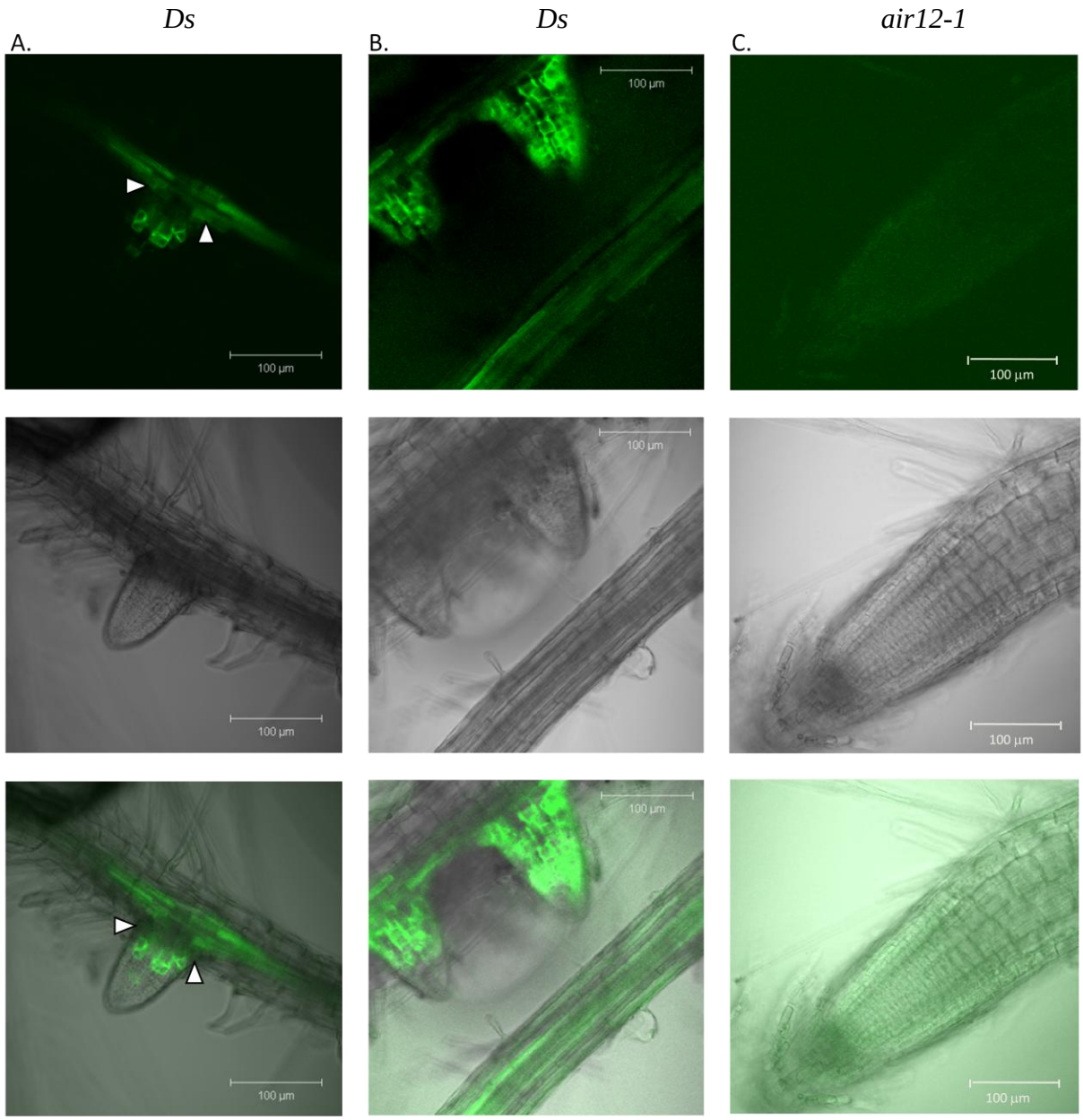

Figure 4.21. Localization of GFP-AIR12 in Arabidopsis *Ds* (A, B) and *air12-1* (C) stably transformed with *pAIR12::GFP-AIR12*. Seedlings were grown on ½ MS, 1% sucrose (w/v) supplemented with 400 nM α-NAA for 8 days. A, GFP-AIR12 localizes to the vascular tissue in *Ds* lateral roots, to cells flanking (arrowhead) and within a post-emergent second order lateral root. B, GFP-AIR12 localizes to the margins of *Ds* post-emergent lateral root cells. C, Faint localization of GFP-AIR12 in *air12-1* lateral roots. Top panel, fluorescence channel; Middle panel, DIC; Bottom panel, merged image. Identical pinhole settings used for all images. For *Ds* seedlings, a gain of 12.9% was used while with *air12-1* seedlings a gain of 15.9% was used.

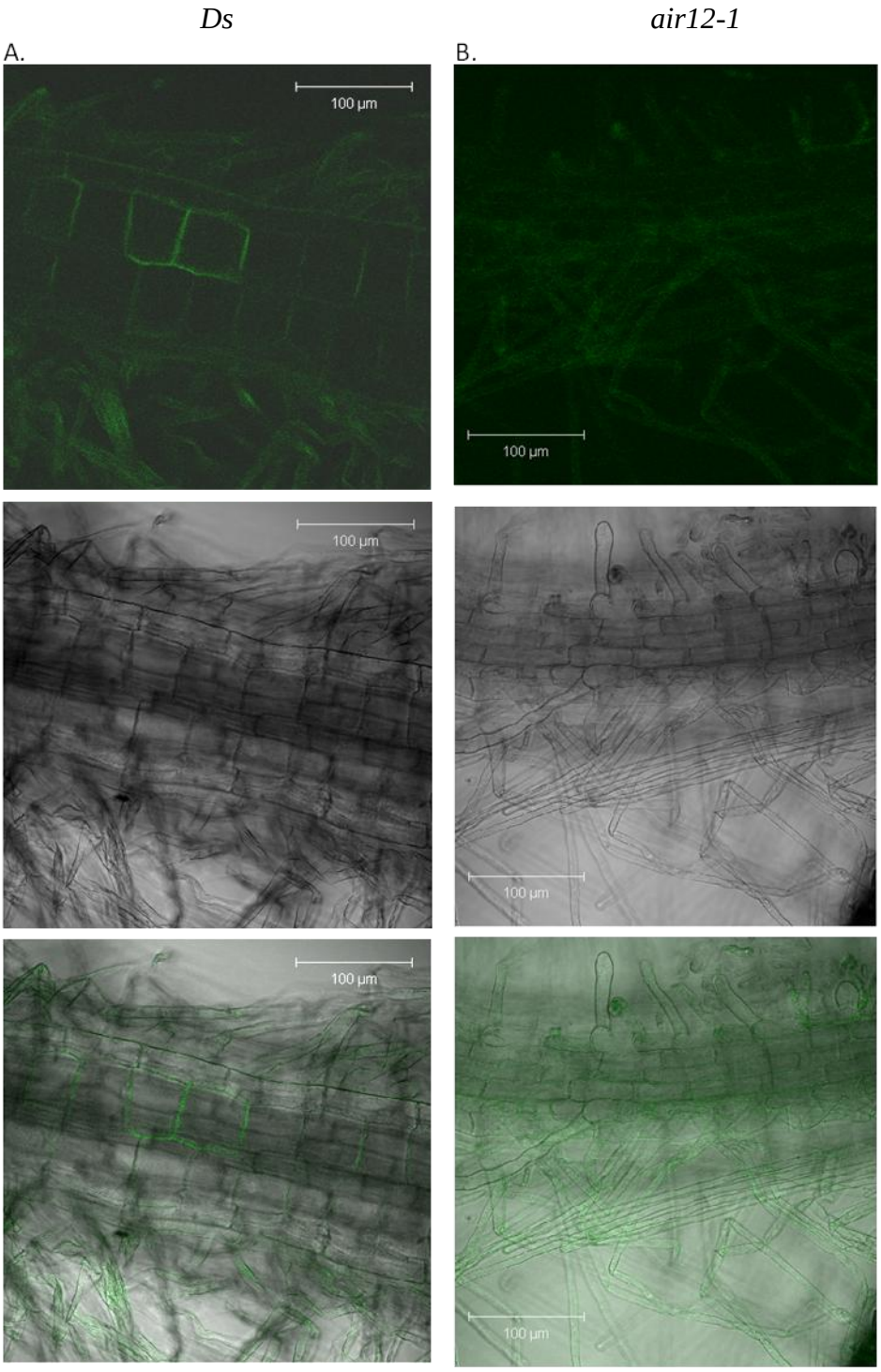

Figure 4.22. Localization of GFP-AIR12 to root hairs of stably transformed *pAIR12::GFP-AIR12 Ds* (A) and *air12-1* (B) 8 day old seedlings grown on ½ MS, 1% sucrose (w/v) supplemented with 400 nM α-NAA. Top panel, fluorescence channel; Middle panel, DIC; Bottom panel, merged image. Identical capture settings were used for all images.

4.7.4 GFP-AIR12 localization on control medium supplemented with KCl

As previously outlined, AIR12 contains DUF568, a domain thought to be involved with electron transfer during biochemical reactions (Iyer et al., 2007). This possible electron interaction role could be realized through cycling of reactive oxygen species, a type of free radical often found when plants are challenged with an abiotic stress. *AIR12* expression increases in response to a number of environmental stressors (Zeller et al., 2009). The Bio-Array Resource (Winter et al., 2007) was used to illustrate increased *AIR12* expression in response to salinity stress (Figure 4.23). Because of the similarities between AIR12 and CIL1 both at the amino acid level, I wanted to examine the localization of GFP-AIR12 during the response to salt stress in *Ds* and *air12* lines. Seeds from the *Ds* and *air12-1* background containing the *pAIR12::GFP-AIR12* construct were germinated on ½ MS supplemented with 1% sucrose (w/v) and 30 mM KCl, as outlined by Deak and Malamy (2005). After 8 days, seedlings were examined using confocal laser-scanning microscopy.

In the primary root tip of *Ds* seedlings the fusion protein was localized to the margins of epidermal cells in the MZ, similar to the localization pattern seen on control and auxin-supplemented media (Figure 4.24A). Approximately 600 μm proximal to the tip, GFP-AIR12 shifted from MZ margin localization to vascular localization (Figure 4.25A). The vascular localization ran almost the entire length of the primary root, from 600 μm basipetally of the root apex to the root base (Data not shown).

In medium supplemented with KCl, as in all other media examined, GFP-AIR12 in *Ds* seedlings was present in a scattered localization pattern in elongating lateral roots (Figure 4.26A), with the exception of a small region of the MZ that lacked fusion protein. Emerging lateral roots were characterized by GFP-AIR12 protein present in flanking cells with fluorescence constrained to the margins of the individual cells, similar to the localization pattern seen in control medium (Figure 4.25B).

Like seedlings in the *Ds* background, *air12-1 pAIR12::GFP-AIR12* seedlings demonstrated GFP-AIR12 localization in both the primary root tip and in lateral root tips. In the primary root, weak GFP-AIR12 signal was present near the elongation zone and was confined to the epidermal cell file (Figure 4.24B). No vascular fluorescence was observed in these lines, though root hair margins were fluorescent (Figure 4.26C). In lateral root tips, GFP-AIR12 localized to the epidermal cell file confined to a region behind the elongation zone only 6 cells in

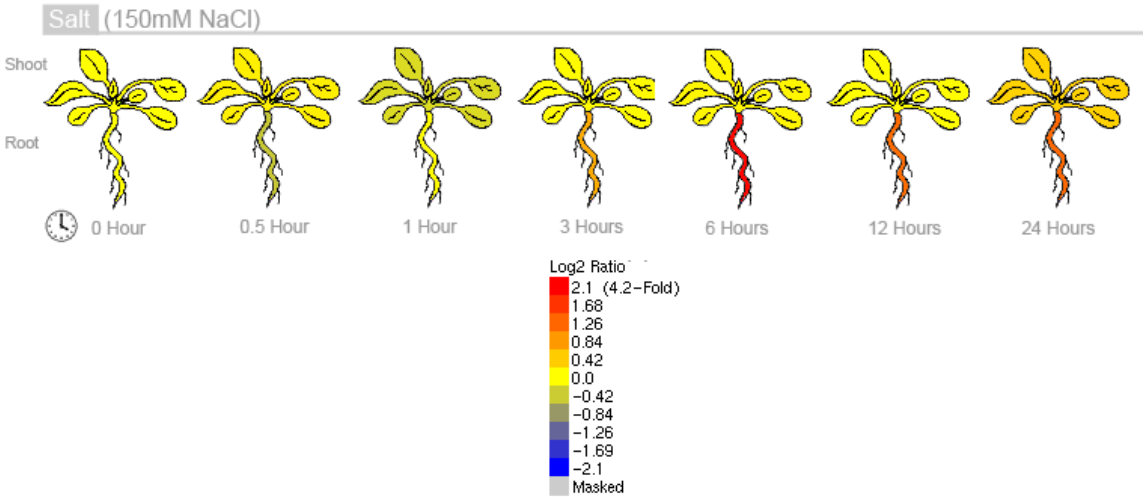

Figure 4.23. *AIR12* expression after treatment with 150 mM NaCl using the eFP browser from the Bio-Array Resource (http://bar.utoronto.ca/efp/cgi-bin/efpWeb.cgi). Heatmap values displayed below the plant images represent the fold-change in expression over the time course.

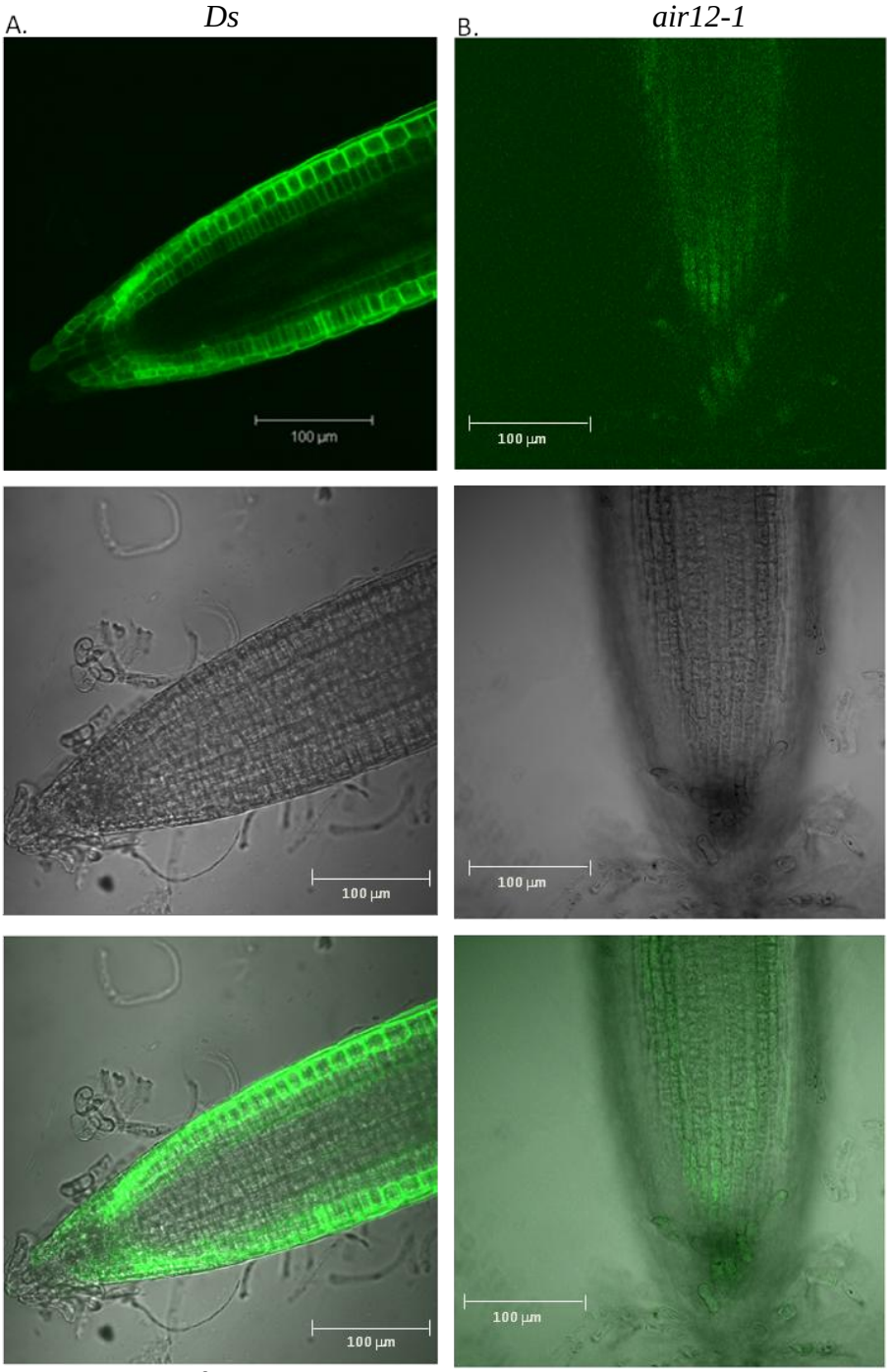

Figure 4.24. Localization of GFP-AIR12 in Arabidopsis *Ds* (A) and *air12-1* (B) stably transformed with *pAIR12::GFP-AIR12*. Seedlings were grown on ½ MS, 1% sucrose (w/v) supplemented with 30 mM KCl for 8 days. A, GFP-AIR12 localizes to the margins of the epidermal cell file in *Ds* primary root tips. B, GFP-AIR12 is present throughout *air12-1* epidermal cells in the elongating region of the primary root. Top panel, fluorescence channel; Middle panel, DIC; Bottom panel, merged image. Identical capture settings were used for all images.

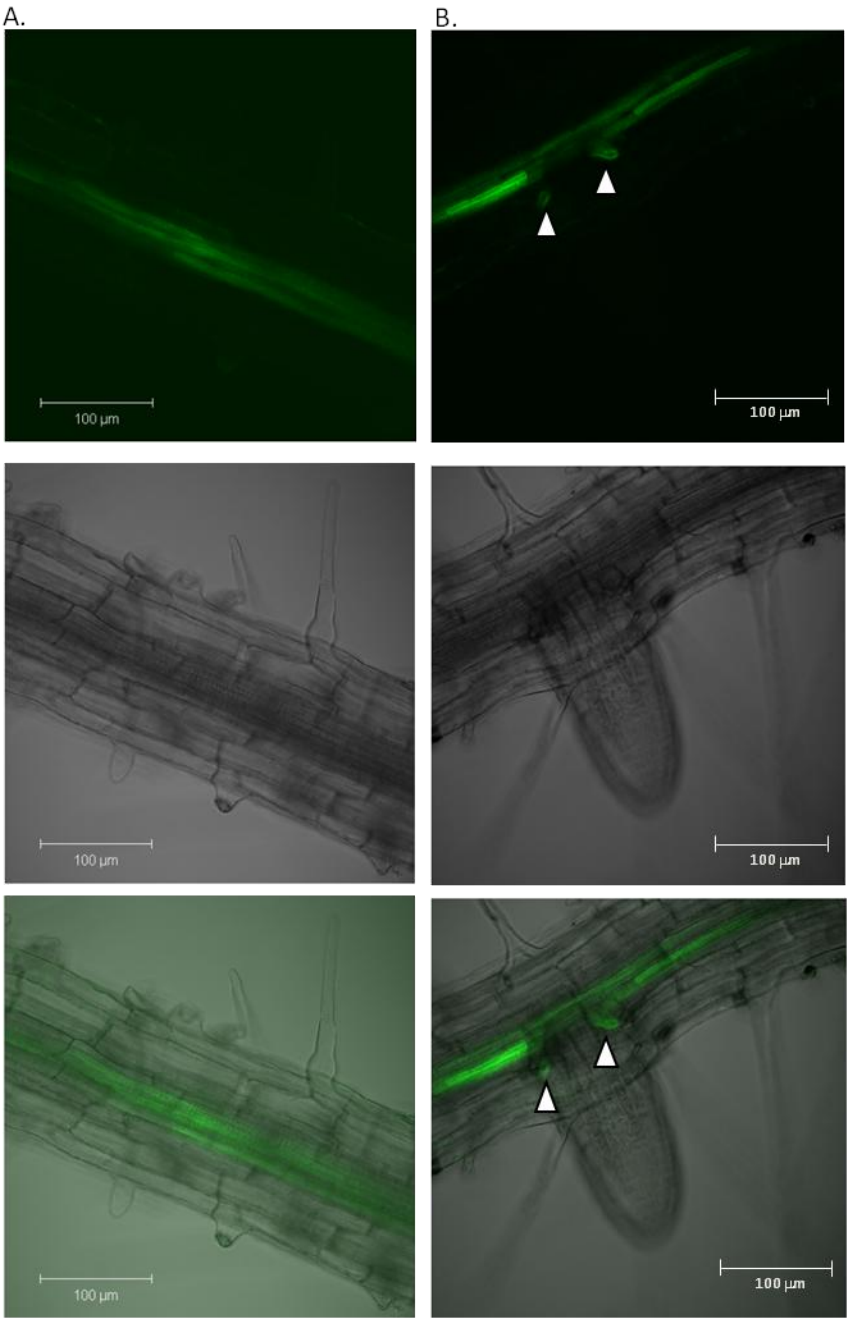

Figure 4.25. Localization of GFP-AIR12 in Arabidopsis (*Ds*) stably transformed with *pAIR12::GFP-AIR12*. Seedlings were grown on ½ MS, 1% sucrose (w/v) supplemented with 30 mM KCl for 8 days. A, Vascular localization of GFP-AIR12 in the primary root. B, Localization of AIR12-GFP to pericycle cells flanking a post-emergent lateral root (arrowheads). Top panel, fluorescence channel; Middle panel, DIC; Bottom channel, merged image. Identical capture settings were used for all images.

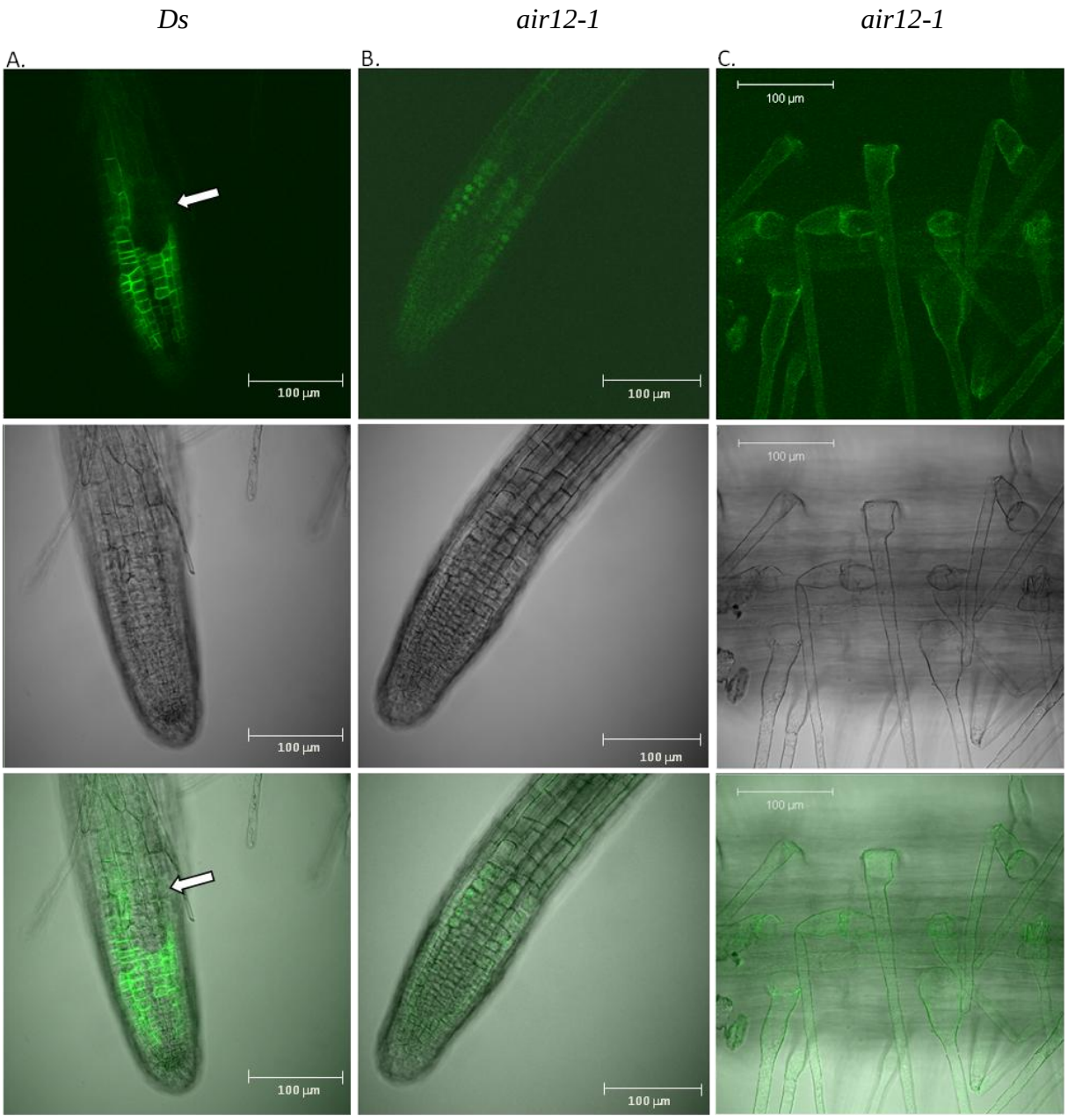

Figure 4.26. Localization of GFP-AIR12 in Arabidopsis *Ds* (A) and *air12-1* (B, C) stably transformed with *pAIR12::GFP-AIR12*. Seedlings were grown on ½ MS, 1% sucrose (w/v) supplemented with 30 mM KCl for 8 days. A, GFP-AIR12 localizes to the epidermal cell in *Ds* lateral roots, with the exclusion of a small area (arrow). B, Punctate localization of AIR12-GFP to the epidermal cell file of *air12-1* lateral roots. C, AIR12-GFP localizes to *air12-1* root hair cell margins with limited localization to cell margins in the primary root. Top panel, fluorescence channel; Middle panel, DIC; Bottom panel, merged image. For *Ds* images, pinhole and gain were 488 µm and 12.9%, respectively. For *air12-1* images, pinhole and gain were 590 µm and 15.9%, respectively.

length, and appeared predominantly localized to lateral poles of individual cells (Figure 4.26C). Proximal of this was a region consisting of GFP-AIR12 localization confined to cell margins after which no fluorescent signal could be observed.

4.8 *AIR12* expression is induced by auxin

All *air12* lines used in this study were mutagenized using the *Ac*/*Ds* system (Figure 4.8). As outlined previously, this system, in conjunction with the *uidA* (GUS) reporter gene is used to "trap" a gene or enhancer element. When the *Ds* cassette is inserted into a gene, it disrupts expression of that gene. The promoter of the disrupted gene however is still active and transcription of *uidA* will occur in place of the native gene. By staining seedlings or plant tissues with (X-Gluc), it is possible to localize expression of transcript of the interrupted gene. The location of the *uidA* transcript under untreated or treated conditions can be used to predict where the native gene transcript will accumulate after the same treatment, however, the position of the T-DNA insertion relative to the *AIR12* promoter (Figure 4.8) will affect the degree of *uidA* that is transcribed. *Ds* and *air12* seedlings were grown on vertical plates for 6-12 days, stained with X-gluc, processed through an ethanol series, and visualized under a compound microscope. When supplemented with 400 nM α-NAA precipitate was found in elongating lateral roots, lateral root tips, and vascular tissue of cotyledons in all lines, confirming the transcriptional activation after auxin treatment that led to the isolation of this gene by Neuteboon et al. (1998). On seedlings from *air12-2,* and *-3,* no GUS accumulation was evident when grown on ½ MS, 1% sucrose (w/v; Data not shown). A description of transcript accumulation in *air12-1* with or without auxin is summarized in Table 4.2. Seedlings from *air12-1* (Figure 4.27) grown on ½ MS, 1% sucrose (w/v) demonstrated GUS accumulation. In mature plants, GUS was observed in stipules and reproductive structures such as the stigma, young silique, and filament (Figure 4.27). When *air12-1* seedlings were grown on 400 nM α-NAA, GUS accumulation was visible in emerging lateral roots, the tip of elongating lateral roots, and in the vascular tissue of cotyledons in *air12-1* (Figure 4.28A-C). GUS-staining of 6-day old *air12-3* resulted in an almost identical pattern of *AIR12* transcript accumulation as 12-day old *air12-1* (Figure 4.28D). No GUS accumulation was visible in any *Ds* tissue (Figure 4.29). When GUS stain was present, it localized to lateral root tips, as in the *air12-1* seedlings.

Organ	Medium	- NAA	+ NAA
Stipule		Throughout	ne
Reproductive organs		Throughout stigma, style, and filament	ne
Cotyledon		ns	Throughout veins
Stele		ns	Faint staining visible
Lateral root		ns	Throughout emerging LR, root cap in elongating LR

Table 4.2. Summary of X-Gluc accumulation in Arabidopsis *AIR12*/*air12-1* heterozygous plants stained for 16 hours at 37 ^{o}C; ns, none seen; ne, not examined.

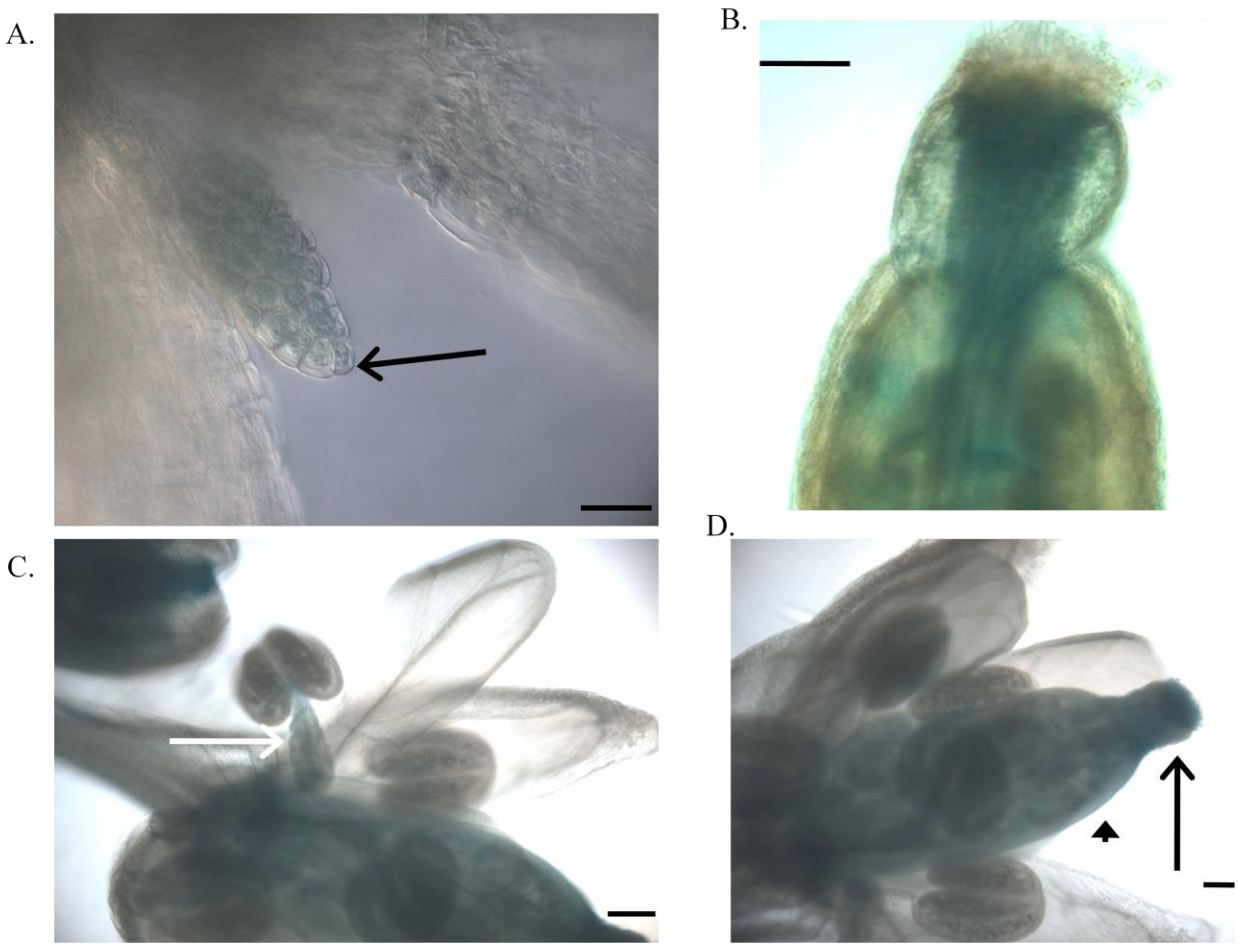

Figure 4.27. Transcript accumulation of GUS in *AIR12*/*air12-1* heterozygous Arabidopsis. Seeds were grown on ½ MS, 1% sucrose (w/v) and stained with X-Gluc for 16 hours at 37 ^{o}C after 45 days of growth. *AIR12* transcript is present (A) throughout stipules (arrow), to the remainder of the style in young siliques (B), to anther filaments (arrow, C), and to the stigma (D) (arrow) and style (arrowhead) of a mature carpel. In all figures, the scale bar represents 100 μm.

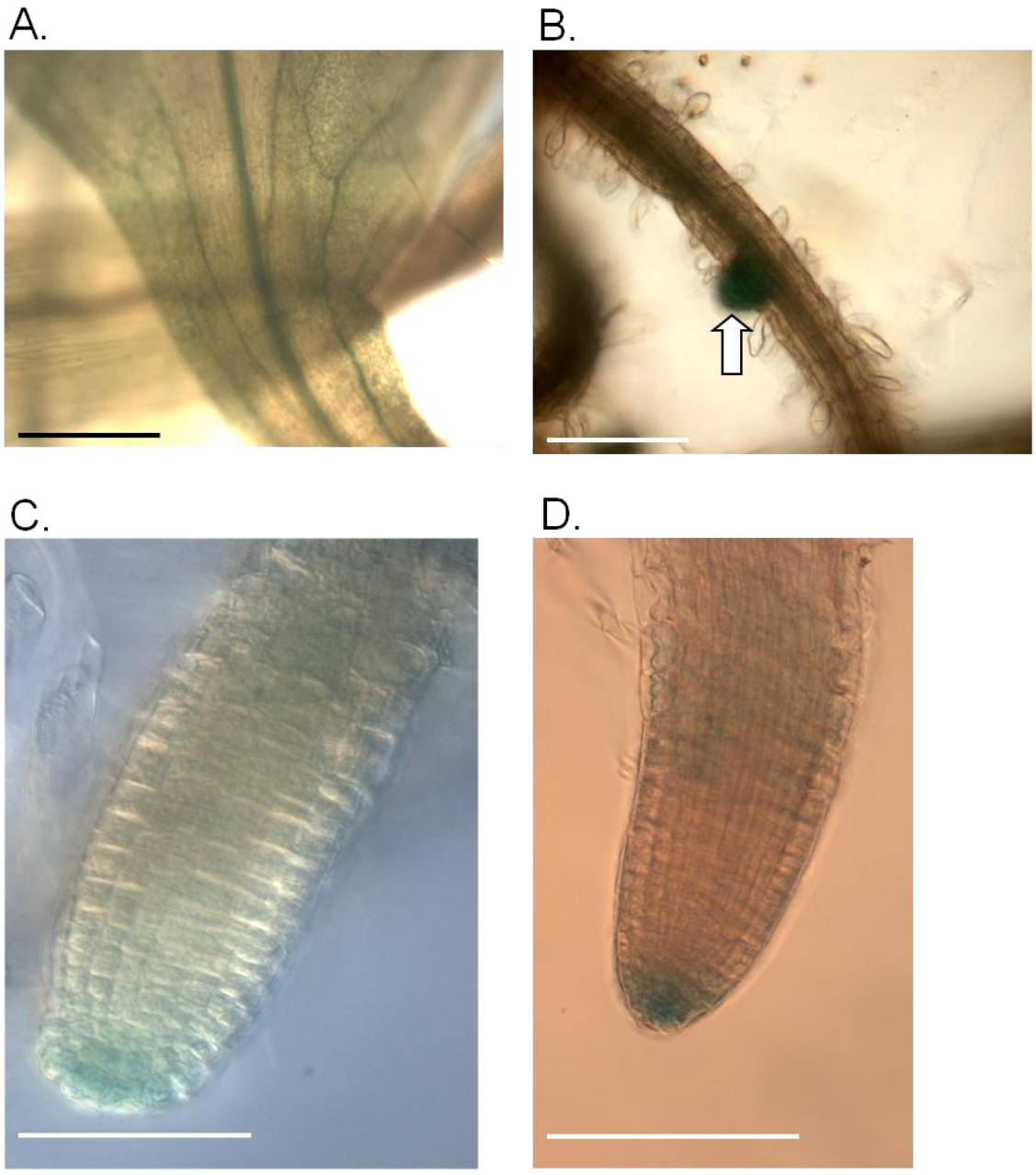

Figure 4.28. Transcript accumulation of GUS in 12-day old *AIR12*/*air12-1* heterozygous (A-C) and 6-day old *AIR12*/*air12-3* heterozygous (D) Arabidopsis. Seedlings were grown on ½ MS, 1% sucrose (w/v) supplemented with 400 nM α-NAA and stained with X-Gluc for 16 hours at 37 ^{o}C. Transcript localizes to vascular tissue of cotyledons (A), throughout emerging lateral roots (B, arrow), and to the cap of elongating lateral root (C, D). Scale bars represent 100 μm in A, and B and and 50 μm in C and D.

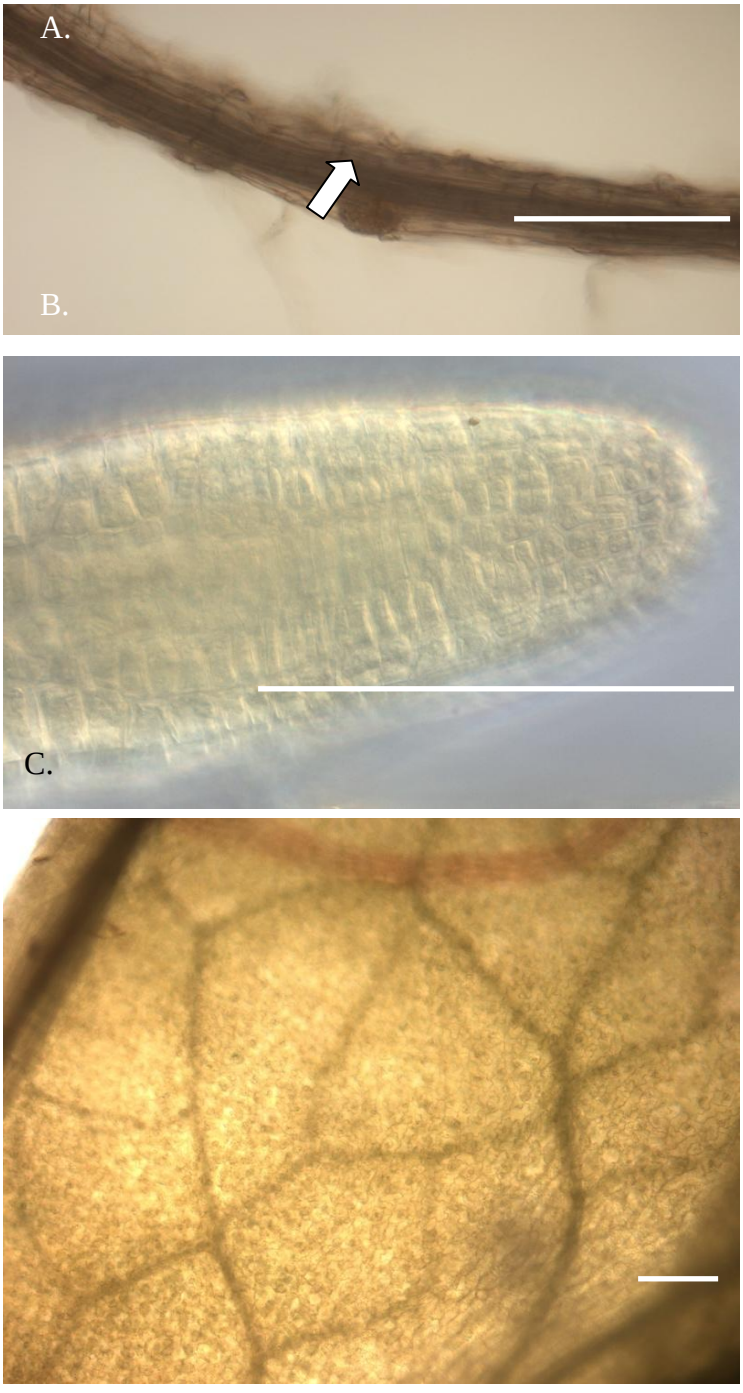

Figure 4.29. X-Gluc-stained 12-day old Arabidopsis *Ds*. *S*eedlings were grown on half strength MS supplemented with 1% sucrose (w/v) and 400 nM α-NAA shows no GUS accumulation in any of the tissues examined after staining with X-Gluc for 16 hours at 37 ^{o}C. A, Emerging lateral root (arrow); B, Elongating lateral root; C, Vascular tissue of cotyledon. Scale bars represent 50 μm (A, B) and 100 μm (C).

Attempts were made to stain *air12-4* after growth on ½ MS supplemented with either 1% sucrose (w/v) or 1% sucrose (w/v) and 400 nM α-NAA, however the line germinated very poorly. Only 1 seed out of the 40 plated germinated on control medium and no X-gluc precipitate was visible after staining (Data not shown). No GUS precipitate was visible in any of the four lines when grown on control medium.

Transcript abundance in different tissues for *AIR12* has been compiled by the Biological Array Resource (http://bar.utoronto.ca/), using data from a variety of microarray experiments. According to the electronic fluorescence browser (eFP), *AIR12* transcript accumulates in the lateral root cap, and very strongly in the spongy mesophyll and guard cells after growth for 6 days on ½ MS, 4.5% sucrose (w/v) or grown in soil for 5 weeks, respectively. GUS staining of the *air12* lines did not result in precipitate in either the mesophyll or guard cells, possibly because the promoter trap may prevent *AIR12* expression at wild type amounts.

4.9 Root development is reduced in *air12* seedlings

Since both *AIR12* transcript and GFP-AIR12 fusion protein localized to roots, after auxin treatment, and auxin and ABA interact during germination, the ability of *Ds* and *air12-1* seedlings to germinate under a series of treatments was assessed. Homozygous *Ds* and *air12-1* seed were surface sterilized and placed on media containing ½ MS, 1% sucrose (w/v), or on media composed of ½ MS, 1% sucrose + 60 mM mannitol, + 30 mM KCl, + 40 mM Nitrate (20 mM each of KNO_3 and NH_4NO_3), + 400 nM α-NAA, + 100 nM 2,4-D, 3.5 μM ± ABA, 1 mM H_2O_2, or + 3.5% sucrose (w/v). After 3 days at 4 ^oC the plates were placed vertically in a growth chamber. Auxin (α-NAA) was used because *AIR12* is an auxin induced gene, while ABA and salt were used because AC seedlings showed decreased sensitivity to ABA, and altered salt tolerance, respectively. Hydrogen peroxide was used because the DUF568 domain common to both AIR12 and CIL1 have been hypothesized to have electron transfer roles (Iyer et al., 2007)

Originally, the germination/root growth assay experiments were to be completed according to the methods of Deak and Malamy (2005); allowing seedlings to germinate and grow on control medium for 5 days, followed by transplantation to the abiotic stress or control medium and monitoring root growth for 8 additional days. This was attempted multiple times however upon attempting to remove the *air12* seedlings from the control media, the hypocotyl would often detach from the primary root. Further attempts were made removing seedlings from the

media by the root rather than the hypocotyl. In all attempts, the *air12-1* seedlings were firmly anchored to the media near the root-hypocotyl interface. To identify the reason for this anchoring, *Ds* and *air12-1* seedlings were germinated on filter paper flooded with water and allowed to grow for 5 days. *Ds* seedlings were removed with ease, while *air12-1* seedlings were again difficult to remove. Examination of the basal region of the primary root of *Ds* and *air12-1* seedlings showed a marked difference between root morphology of the two lines. *Ds* seedlings appeared normal with regular lateral roots and an elongating primary root (Figure 4.30A). *air12-1* seedlings produced short primary roots with a large base and an increased number of irregularly spaced lateral roots (Figure 4.30B).

The final experimental conditions consisted of seed sterilization followed by plating of the seed on media (control media or media supplemented with hormone or abiotic stressors) and incubated for three days at 4 ^{o}C. Plates were then placed vertically in a growth chamber and germination was monitored for 9 days with one observation per day. After 13 days, roots were measured.

In this study, seeds were designated as "germinated" once radicle protrusion was visible under a dissecting microscope. After 13 days growth seedlings were examined under a dissecting microscope and lateral root number was counted and lengths of the primary root and all lateral roots were measured manually using a ruler.

On all media, except that containing 3.5 μM ± ABA, *air12-1* seeds germinated more rapidly than *Ds*. On control medium 70% of *air12-1* seedlings germinated, compared to 20% of *Ds* seedlings (Figure 4.31A) after two days. By the third day, approximately 70% of the *air12-1* and *Ds* seedlings had germinated. On medium supplemented with 60 mM mannitol there was no significant initial germination difference, though by day 3 nearly 90% of *air12-1* seedlings were germinated compared to only 60% of *Ds* (Figure 4.31B). Germination rate of *air12-1* seedlings on medium supplemented with 30 mM KCl was more rapid than on control medium with 80% germination by day 2 compared to 20% of *Ds* (Figure 4.31C). Like the germination rate on control medium, the majority of *Ds* seedlings germinated one day later than *air12-1* and by day 8 the number of germinated *Ds* seedlings was equivalent to *air12-1*.

When medium was supplemented with 40 mM nitrate (20 mM each of KNO_3 and NH_4NO_3), 65% of *air12-1* seedlings had germinated by day 2 compared with 15% *Ds* seedlings (Figure 4.31D). By day 3 the number of germinated *Ds* seedlings was equivalent to *air12-1*.

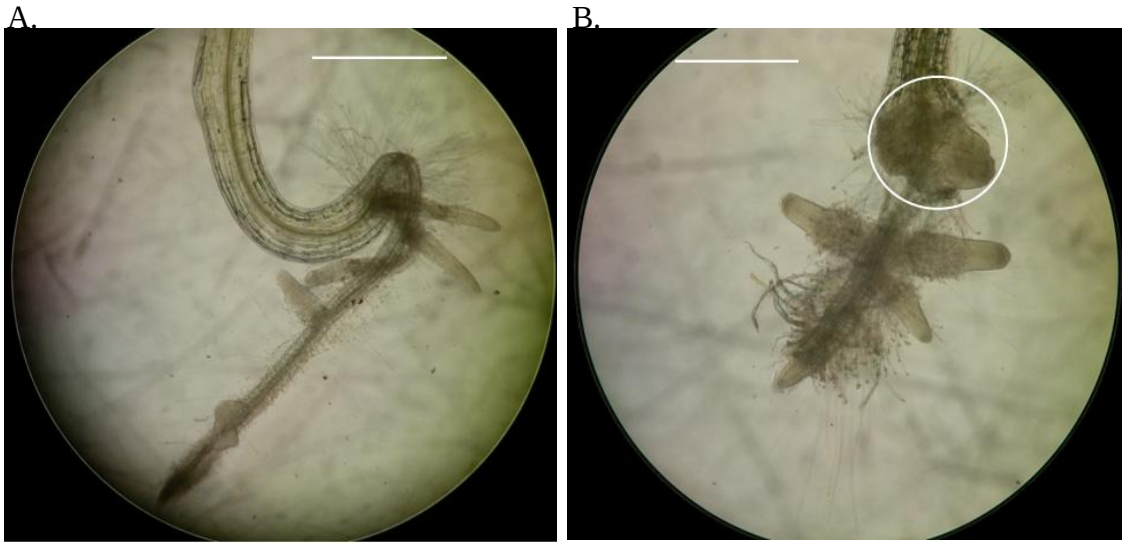

Figure 4.30. Appearance of *Ds* (A) and *air12-1* (B) roots after growth on water-flooded filter paper for 5 days. *air12-1* seedlings developed irregular lateral roots and a mass of root tissue near the primary root base (circled). Fibres are artifacts from the filter paper. Scale bars represent 5 mm.

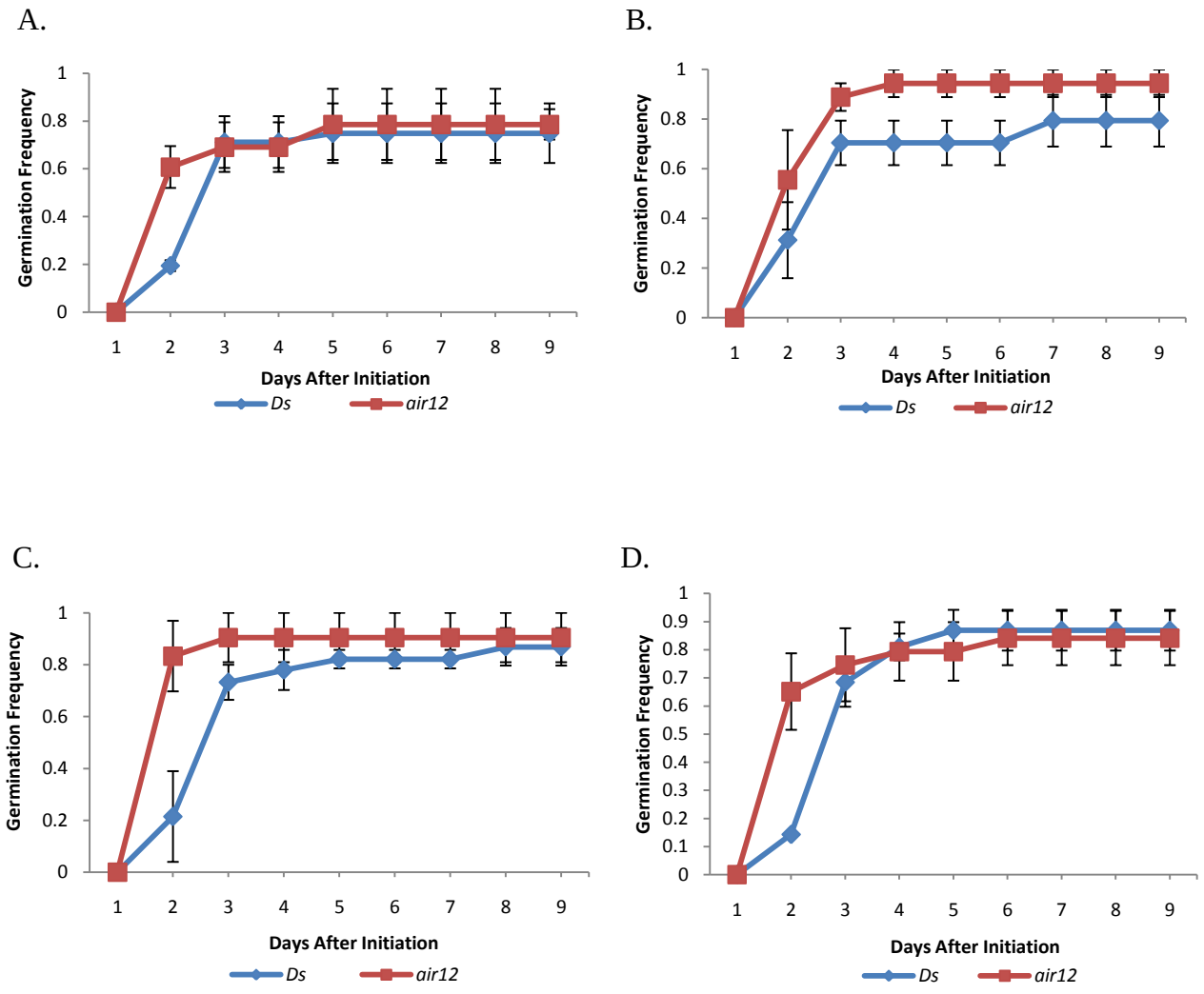

Figure 4.31. Germination frequency of Arabidopsis *Ds* and *air12-1* seeds over a 9 day period. Seeds were germinated on control medium (½ MS, 1% sucrose) (A), or control medium supplemented with 60 mM mannitol (B), 30 mM KCl (C), 40 mM Nitrate (20 mM each of KNO_3 and NH_4NO_3) (D). For all graphs, n=3, bars represent SE. No significance was found between *Ds* and *air12-1* using a two-tailed Student's t-test at $\rho < 0.05$.

The greatest differences in seed germination occurred on media supplemented with auxin (α-NAA or 2,4-D; Figures 4.32A and 4.32B) or media supplemented with H_2O_2 (Figure 4.32C). By day 2 on α-NAA, 75% of *air12-1* seedlings had germinated compared with less than 10% of *Ds* (Figure 4.32A). By day 3, approximately 60% of *Ds* seedlings had germinated, and by day 4, germination reached a maximum for both *air12-1* and *Ds* at 90% and 75%, respectively. Germination of greater than 80% of *air12-1* seedlings on medium supplemented with 2,4-D occurred by day 2, whereas it took until day 4 for this to occur with the *Ds* seedlings (Figure 4.32B). In addition, the total number of seedlings germinated on this synthetic auxin for *Ds* was reduced compared to α-NAA (Figure 4.32A). When supplemented with hydrogen peroxide, the seedling germination rate resembled that of control medium with 80% of *air12-1* seedlings germinated by day 2 compared with 20% *Ds* seedlings. (Figure 4.32C). Unlike control medium, total germinated *Ds* seedlings did not reach *air12-1* levels until day 4. Both *air12-1* and *Ds* seedlings grown on control medium supplemented with 3.5% sucrose displayed reduced germination rate, but a greater effect was observed in *air12-1* seedlings, showing a reduced initial germination frequency of almost 50% compared to control (Figure 4.32D). On medium supplemented with + 3.5 μM ± ABA, the germination frequency was opposite compared to other treatments, with *Ds* seeds germinating more rapidly than *air12-1* (Figure 4.33A). The germinated *Ds* seedlings, however, were incapable of primary root elongation and arrested soon after germination unlike *air12-1* seedlings, which continued to develop (Figure 4.33B).

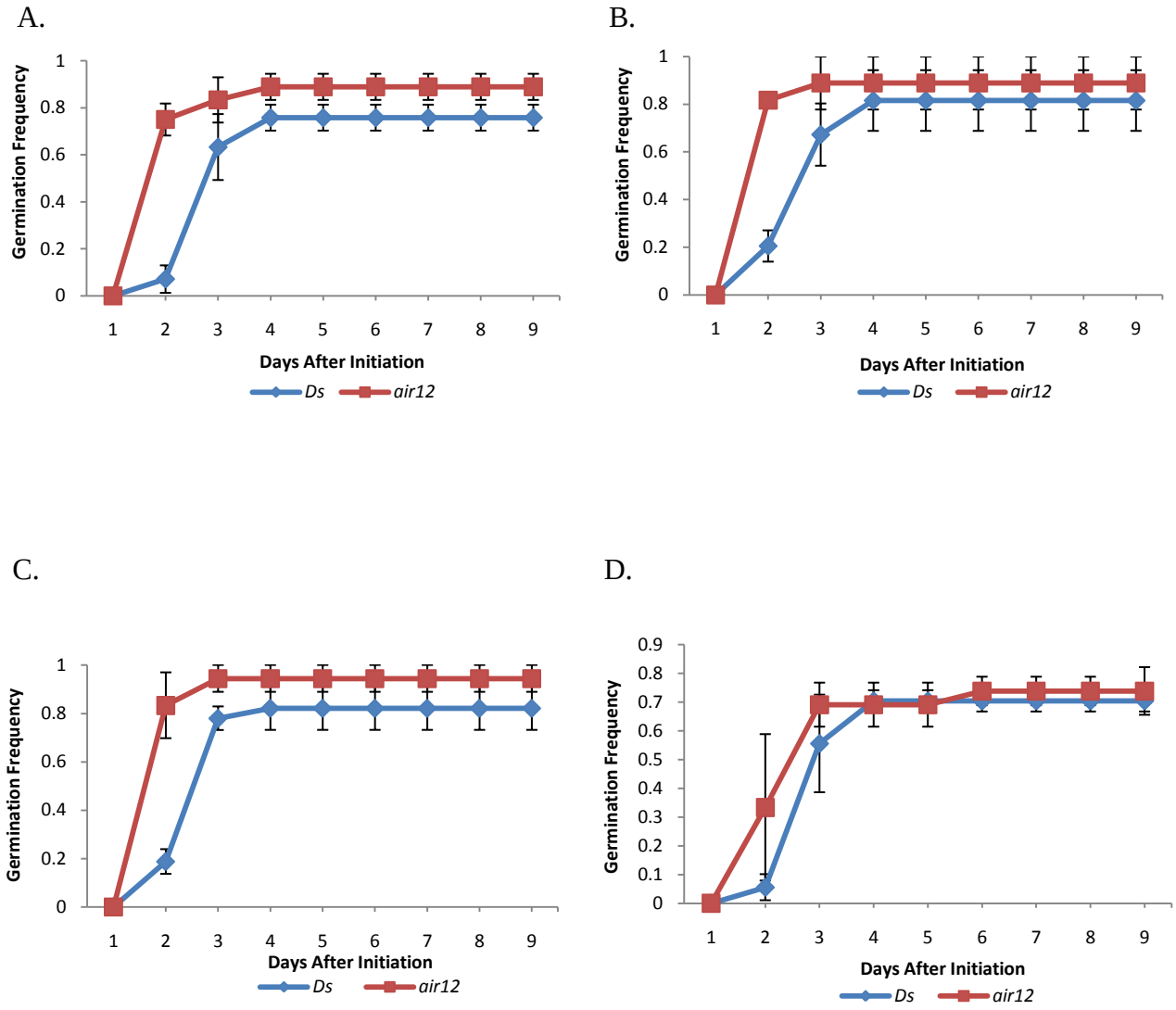

Figure 4.32. Germination frequency of Arabidopsis *Ds* and *air12-1* seeds over a 9 day period. Seeds were germinated on ½ MS, 1% sucrose supplemented with 400 nM α-napthaleneacetic acid (A), 100 nM 2,4-dichlorophenoxyacetic acid (B), 1 mM hydrogen peroxide (C), or 3.5% sucrose (D). For all graphs, n=3, bars represent SE. No significance was found between *Ds* and *air12-1* using a two-tailed Student's t-test at $\rho < 0.05$.

A.

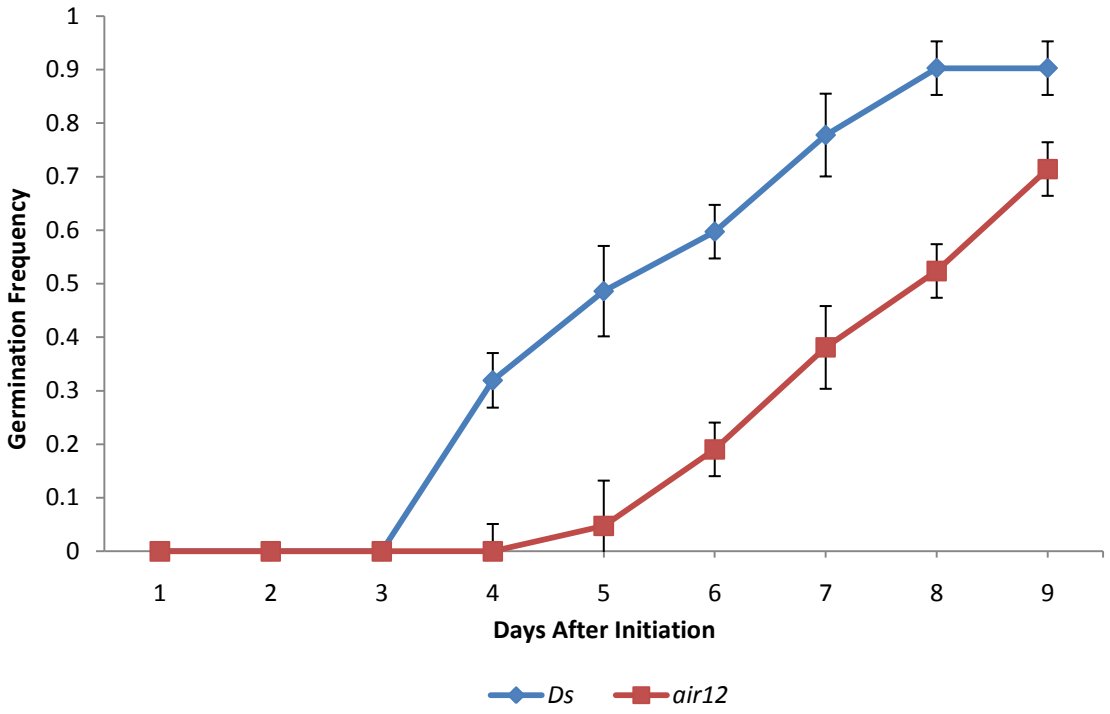

B.

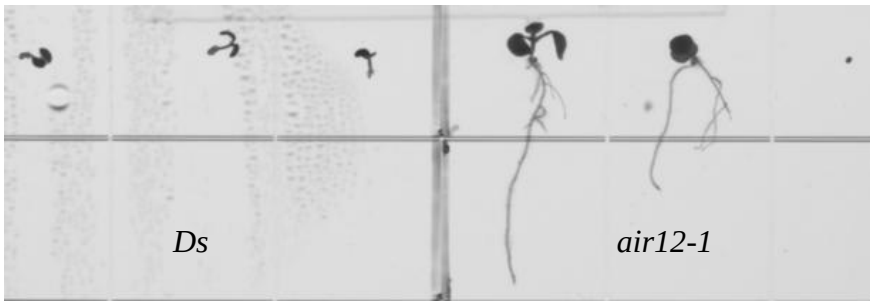

Figure 4.33. Germination of Arabidopsis *Ds* and *air12-1* on ½ MS, 1% sucrose supplemented with 3.5 μM ± abscisic acid. (A). Germination frequency of Arabidopsis *Ds* and *air12-1* seeds over 9 days, n=3, bars represent SE. After germination *Ds* seedlings arrested while *air12-1* seedlings continued to develop. (B) Representative image of *Ds* and *air12-1* seedlings after 13 days. No significance was found between *Ds* and *air12-1* using a two-tailed Student's t-test at $\rho < 0.05$.

4.9.1 Effect of media composition on primary root growth

Comparison of mean primary root length between treatments shows different trends between *air12-1* and *Ds* seedlings. In general, seedlings grown on auxin, specifically 2,4-D showed the greatest reduction in primary root length where the roots of *air12-1* and *Ds* seedlings were 14% and 10% of their control equivalent, respectively. (Figure 4.34). Comparison of *Ds* and *air12-1* primary root length for each treatment showed the greatest significant differences occurred on 40 mM nitrate, 1 mM H_2O_2, and 400 nM α-NAA, where the *air12-1* primary root was 67, 55, and 54% the length of the *Ds* root, respectively. No other treatments had a significant effect on primary root length.

On control medium a difference between *air12-1* and *Ds* mean primary root length was observed (Figure 4.35) however it was not significant given the experimental sample size (n=3). No difference was observed in seedlings grown on medium supplemented with mannitol (Figure 4.36). A trend was observed in seedlings grown on medium supplemented with KCl (Figure 4.37), and H_2O_2 (Figure 4.38), similar to the seedlings grown on control medium. On control medium supplemented with 3.5% sucrose the trend was opposite that of control medium alone, with *air12-1* primary roots longer than *Ds* (Figure 4.39). On nitrate, however, *air12-1* primary root length was reduced 40% compared to that of *Ds* seedlings (Figure 4.40). On medium supplemented with α-NAA *air12-1* primary root length was reduced almost 50% compared to *Ds* seedlings (Figure 4.41). In contrast, *air12-1* primary root length was only slightly reduced compared to *Ds* on 2,4-D (Figure 4.42).

The relationship between treatment and its effect on primary root length within a genotype was also compared. Relative percentages were used to compare mean primary root length between treatment and control for each genotype by dividing the mean primary root length per treatment per replicate by the mean primary root length for all replicates of that genotype on control media. Within both *Ds* and *air12-1* genotypes, the greatest reductions in primary root length were observed on 2,4-D, α-NAA, where a 90% and 25% reduction in primary root length was observed relative to control seedlings, respectively (Figure 4.43). In contrast, growth of *air12-1* on additional sucrose and nitrate had a slight inhibitory effect, decreasing primary root length by 45% and 35% relative to control, respectively, while *Ds* seedlings grown on the same media displayed a 60% and 45% reduction in primary root length relative to control seedlings, respectively (Figure 4.43). Neither genotype showed a significant

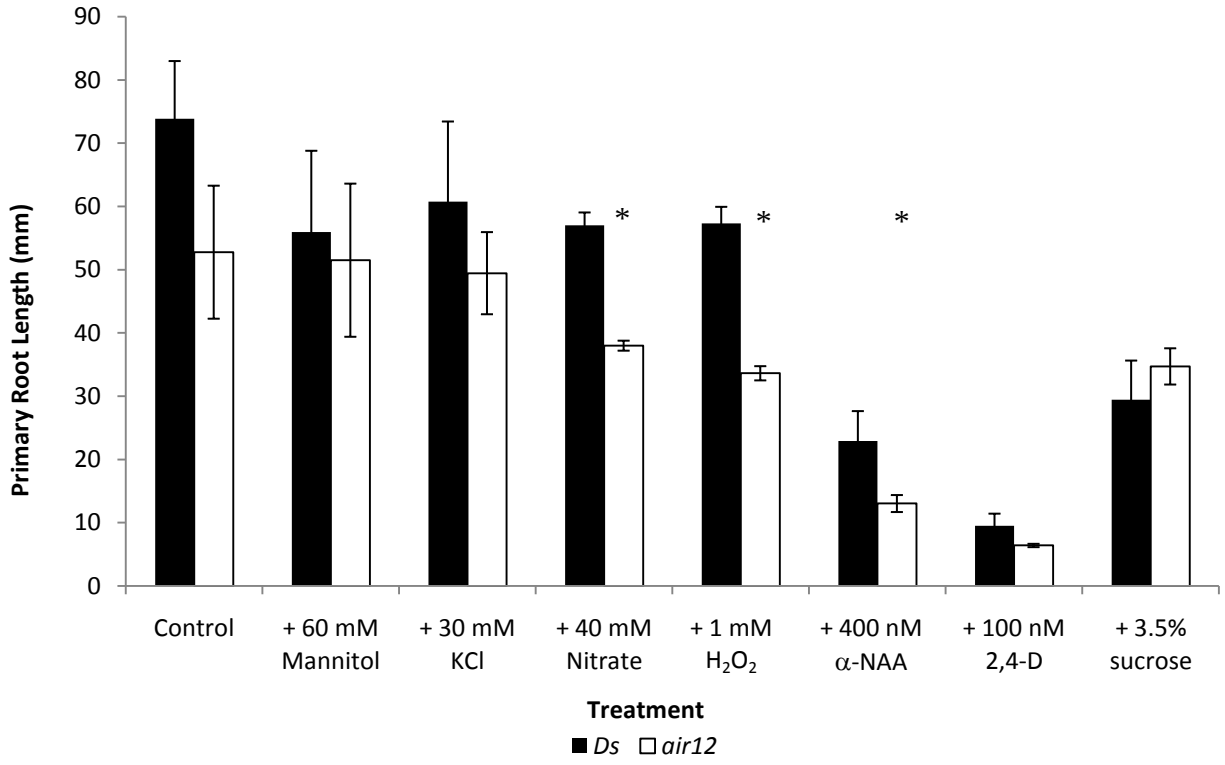

Figure 4.34. Mean primary root length of vertically grown Arabidopsis *Ds* and *air12-1* seedlings. Seedlings were grown for 13 days on ½ MS, 1% sucrose (w/v; control) plus indicated media; n=3, bars represent standard error. * denotes significance at $\rho < 0.05$ using a two-tailed Student's t-test.

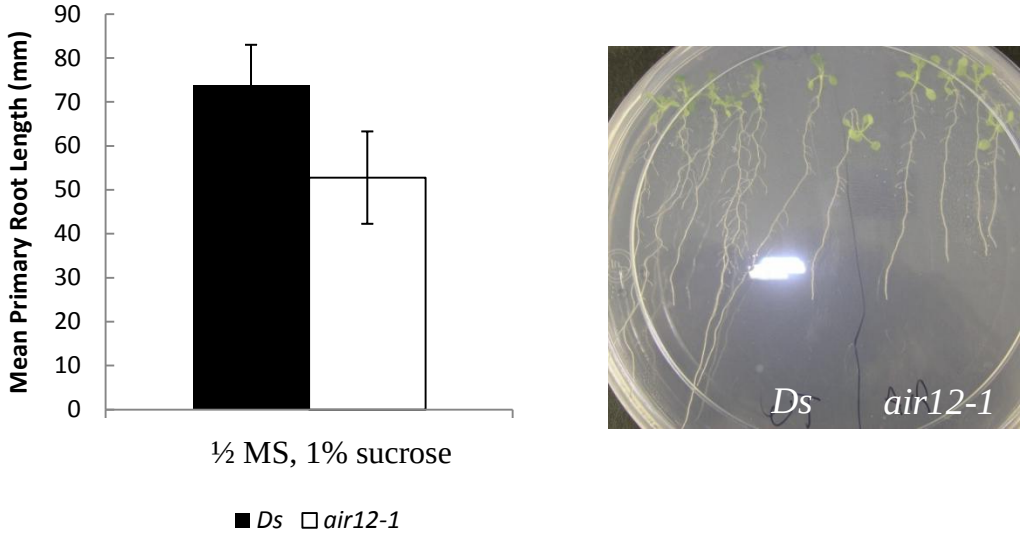

Figure 4.35. Effect of control medium on vertically grown Arabidopsis *Ds* and *air12-1* mean primary root length. Seedlings were grown on ½ MS, 1% sucrose (w/v) for 13 days; n=3, bars represent SE. Representative image shown on right. No significance was found between *Ds* and *air12-1* using a two-tailed Student's t-test at $\rho < 0.05$.

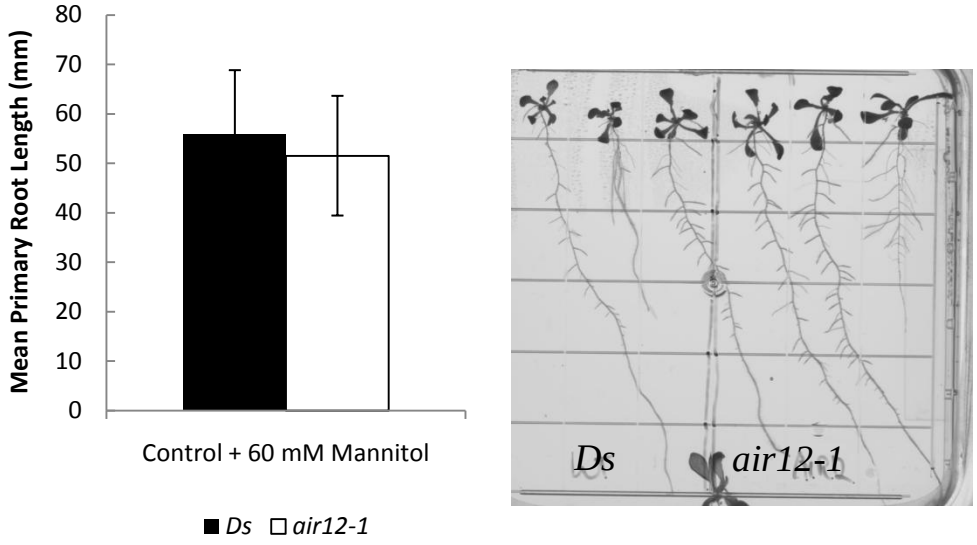

Figure 4.36. Effect of 60 mM mannitol on mean primary root length on vertically grown Arabidopsis *Ds* and *air12-1*. Seedlings were grown for 13 days; control represents ½ MS, 1% sucrose, n=3, bars represent SE. Representative image shown on right. No significance was found between *Ds* and *air12-1* using a two-tailed Student's t-test at $\rho < 0.05$.

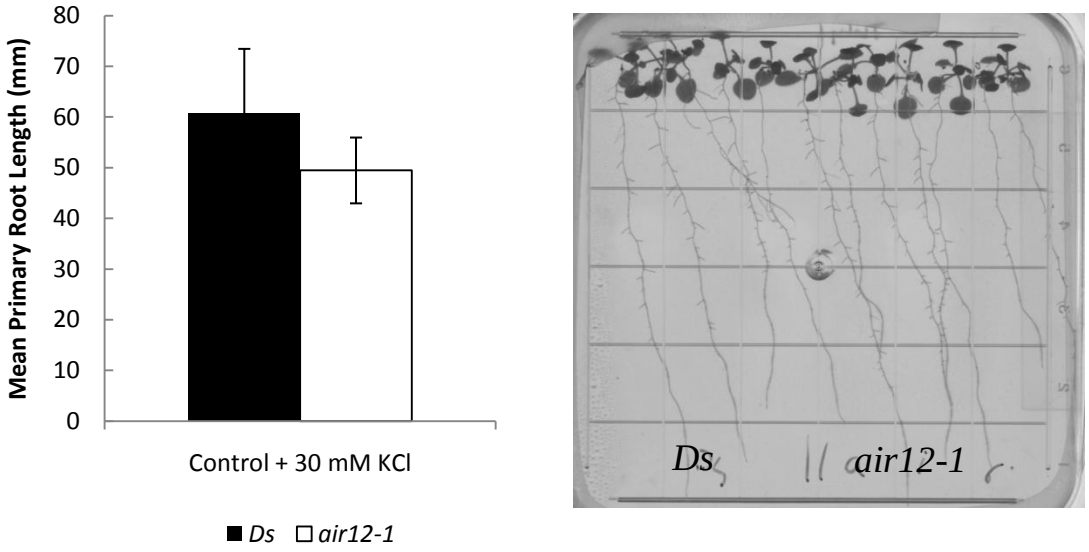

Figure 4.37. Effect of 30 mM KCl on mean primary root length of vertically grown Arabidopsis *Ds* and *air12-1*. Seedlings were grown for 13 days; control represents ½ MS, 1% sucrose, n=3, bars represent SE. Representative image shown on right. No significance was found between *Ds* and *air12-1* using a two-tailed Student's t-test at $\rho < 0.05$.

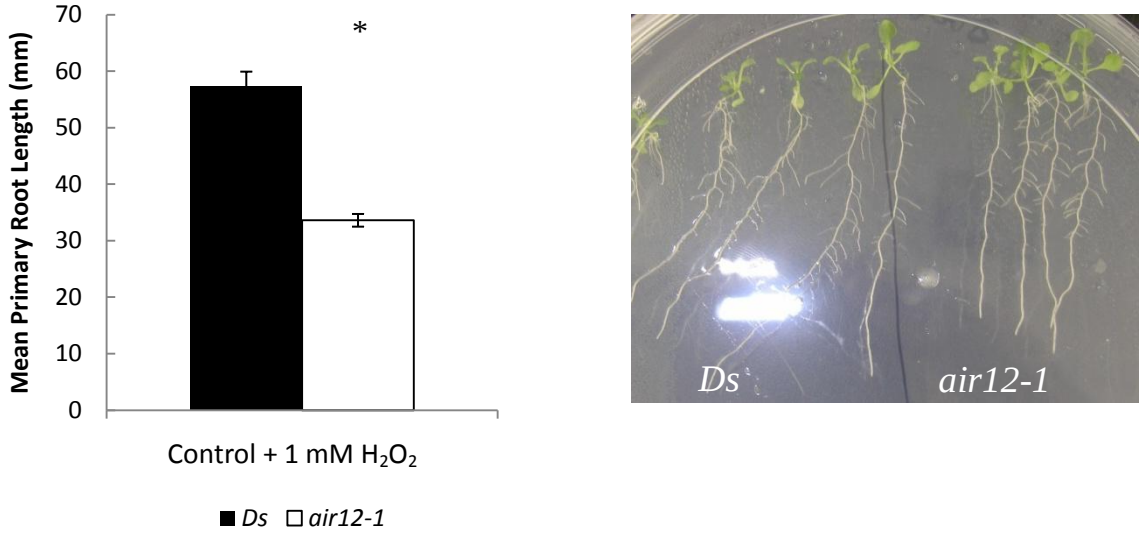

Figure 4.38. Effect of 1 mM H_2O_2 on mean primary root length of vertically grown Arabidopsis *Ds* and *air12-1*. Seedlings were grown for 13 days; control represents ½ MS, 1% sucrose, n=3, bars represent SE. Representative image shown on right. * denotes significance at $\rho < 0.05$ using a two-tailed Student's t-test.

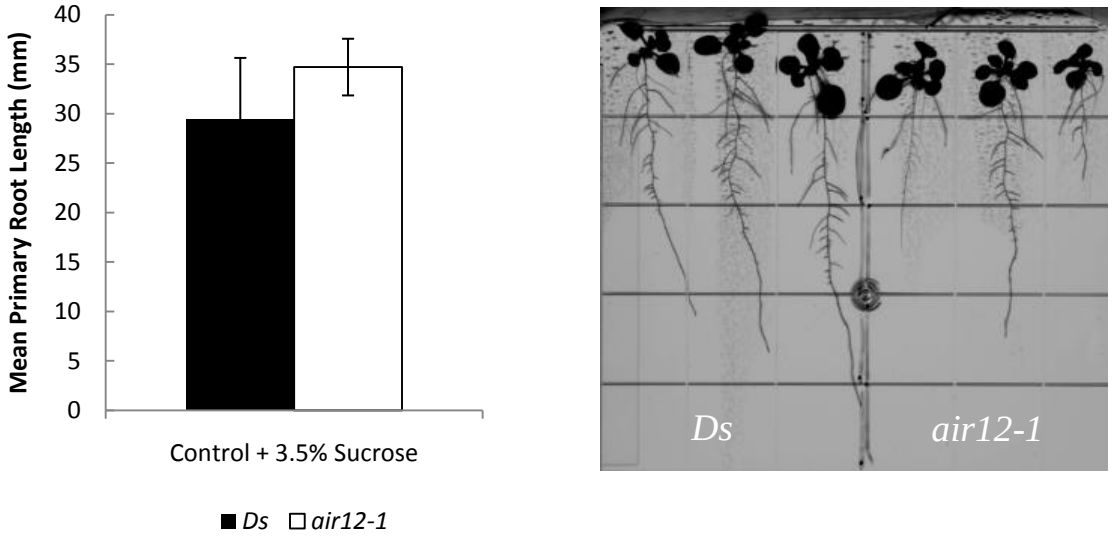

Figure 4.39. Effect of control medium supplemented with 3.5% sucrose (w/v) on mean primary root length of vertically grown Arabidopsis *Ds* and *air12-1*. Seedlings were grown for 13 days; control represents ½ MS, 1% sucrose, n=3, bars represent SE. Representative image shown on right. No significance was found between *Ds* and *air12-1* using a two-tailed Student's t-test at $\rho < 0.05$.

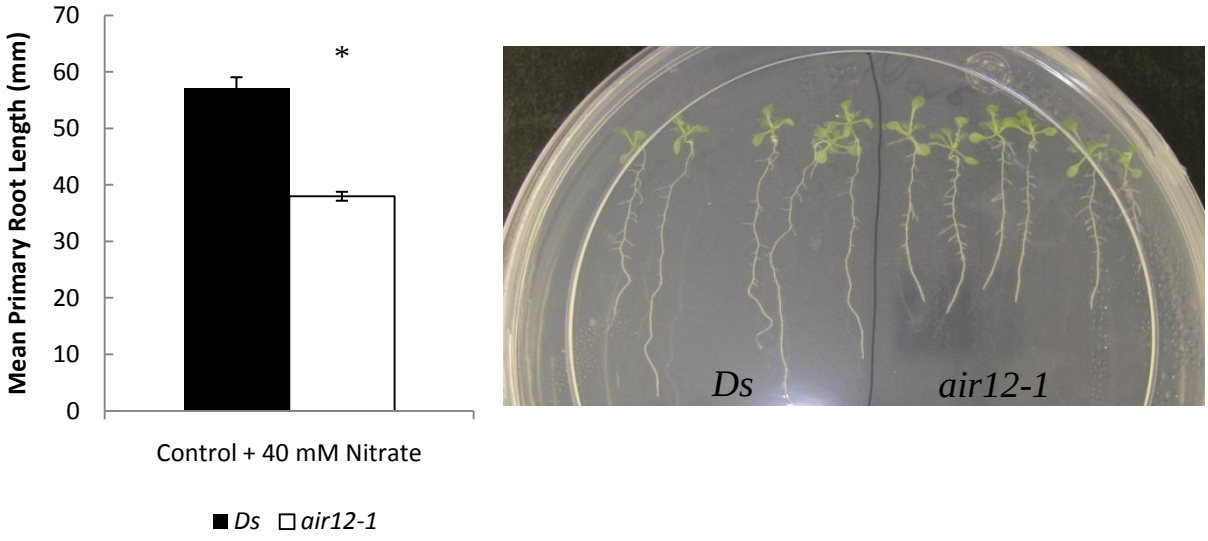

Figure 4.40. Effect of 40 mM nitrate (20 mM each of KNO_3 and NH_4NO_3) on mean primary root length of vertically grown Arabidopsis *Ds* and *air12-1*. Seedlings were grown for 13 days; control represents ½ MS, 1% sucrose, n=3, bars represent SE. Representative image shown on right. * denotes significance at $\rho < 0.05$ using a two-tailed Student's t-test.

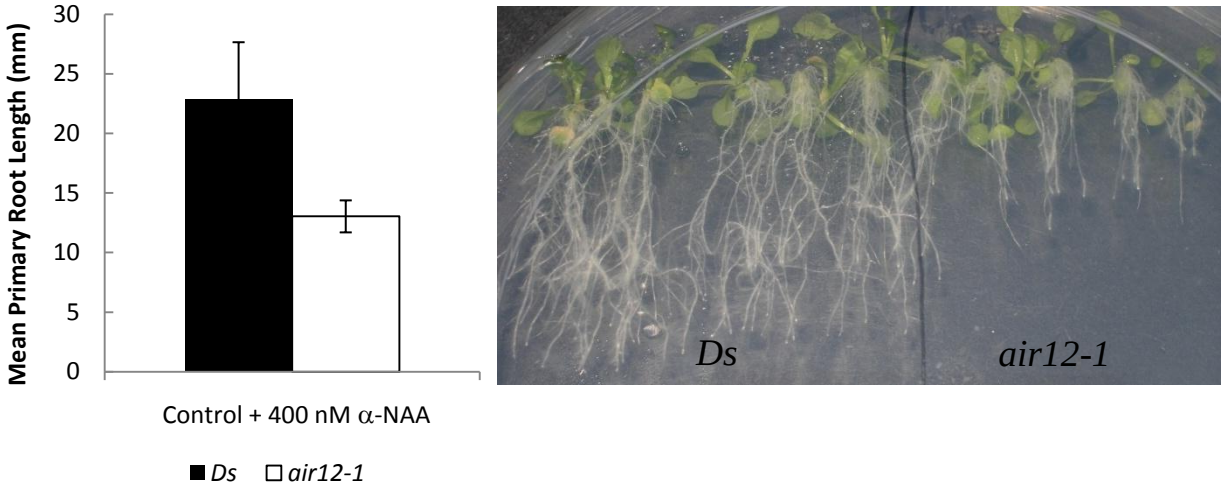

Figure 4.41. Effect of 400 nM α-naphthaleneacetic acid (α-NAA) on mean primary root length of vertically grown Arabidopsis *Ds* and *air12-1*. Seedlings were grown for 13 days; control represents ½ MS, 1% sucrose, n=3, bars represent SE. Representative image shown on right. No significance was found between *Ds* and *air12-1* using a two-tailed Student's t-test at $\rho < 0.05$.

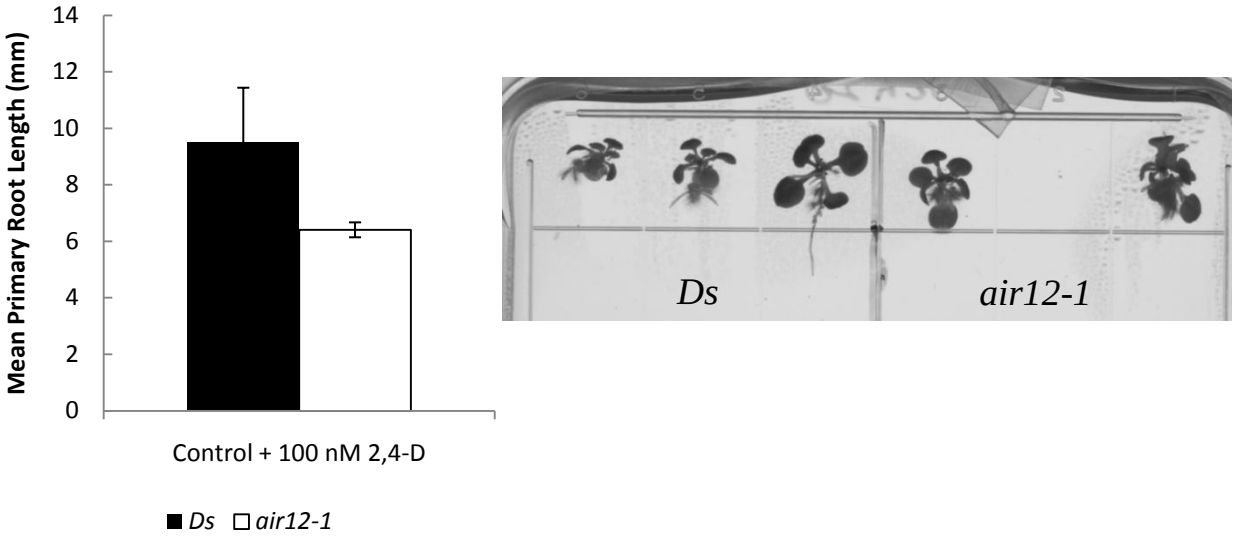

Figure 4.42 . Effect of 100 nM 2,4-D on mean primary root length of vertically grown Arabidopsis *Ds* and *air12-1*. Seedlings were grown for 13 days; control represents ½ MS, 1% sucrose , n=3, bars represent SE. Representative image shown on right. No significance was found between *Ds* and *air12-1* using a two-tailed Student's t-test at $\rho < 0.05$.

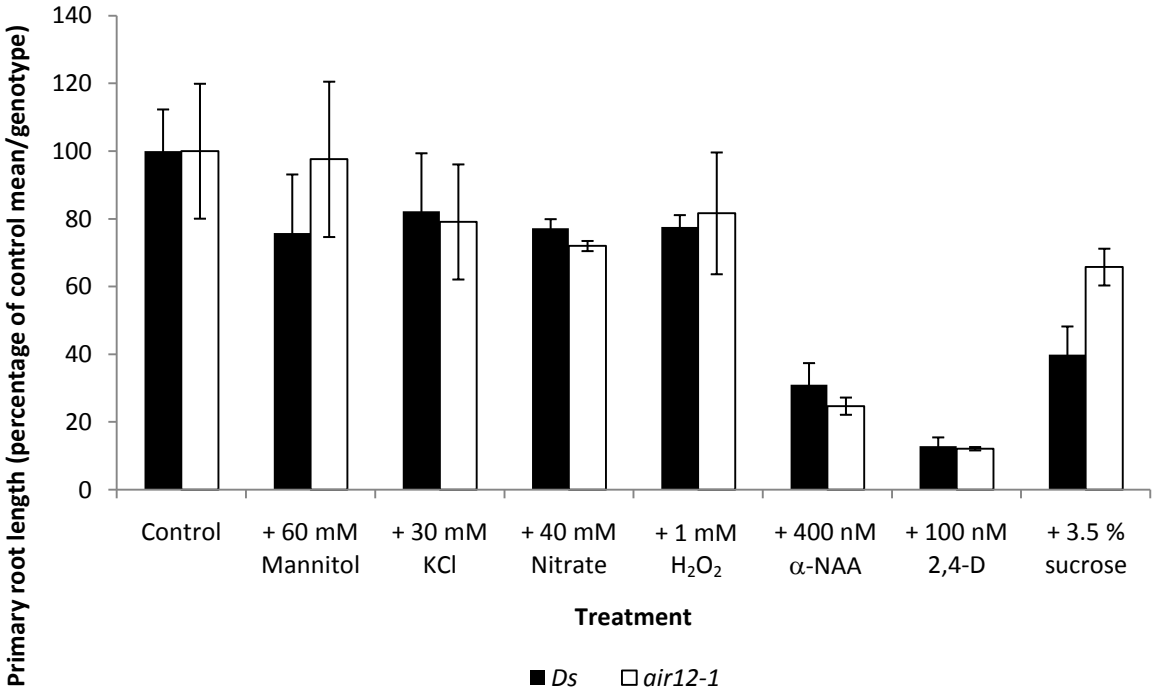

Figure 4.43. Comparison between control (½ MS, 1% sucrose [w/v]) and treatment and the effect on primary root growth of Arabidopsis *Ds* and *air12-1* seedlings. Relative percentages were used to compare mean primary root length between treatment and control for each genotype by dividing the mean primary root length per treatment per replicate by the mean primary root length for all replicates of that genotype on control media. Arabidopsis seedlings were vertically grown for 13 days on the indicated media; n=3, bars represent standard error. No significance was found between *Ds* and *air12-1* using a two-tailed Student's t-test at $\rho < 0.05$.

reduction in primary root length compared to their respective control when grown on mannitol, KCl, or H_2O_2.

4.9.2 Effects of treatment on lateral root number

Comparison between genotype shows the lateral root number of both *Ds* and *air12-1* seedlings on medium supplemented with 100 nM 2,4-D were 25 and 30% of control medium (Figure 4.44). On control medium a slight lateral root number decrease was observed in *air12-1* seedlings compared to *Ds* (Figure 4.44), while no difference in lateral root number was evident on medium supplemented with mannitol (Figure 4.44).

Supplementing the medium with H_2O_2 did not affect lateral root number, while the greatest difference in lateral root number was from seedlings grown on media supplemented with 30 mM KCl, where *air12-1* seedlings produced only 25% the lateral root number compared to growth on control medium. In contrast, *Ds* lateral root production was unaffected by growth on KCl in comparison to control medium. An even greater difference was present on medium supplemented with KCl, where *air12-1* lateral root number was diminished by 80% that of *Ds* seedlings (Figure 4.44). No difference in lateral root number was observed between *air12-1* and *Ds* seedlings grown on medium supplemented with nitrate, H_2O_2, 2,4-D, or 3.5% sucrose (Figure 4.44).

Comparison between treatment in both *air12-1* and *Ds* seedlings grown on 2,4-D showed a 75% and 70% reduction in lateral root number relative to control, respectively (Figure 4.45). In *air12-1* seedlings grown on KCl, a 70% reduction in lateral root number was also observed when compared to control seedlings (Figure 4.45). No other medium affected *air12-1* lateral root number relative to control seedlings. In contrast, *Ds* seedlings grown on nitrate showed a 40% reduction relative to control seedlings, while growth on mannitol, KCl, and H_2O_2 resulted in a 20% decrease in lateral root production. Growth on additional sucrose appeared to have an affect on *Ds* lateral root number, but the error is too great to draw conclusions from this data (Figure 4.45).

The mean lateral root density in the *Ds* genotype was increased by 220% following growth on 2,4-D compared to seedlings grown on control medium (Figure 4.46). Growth of *Ds* seedlings on other media did not affect lateral root density. Mean lateral root density of *air12-1* was increased by 260% and 170% following growth on 2,4-D and additional sucrose,

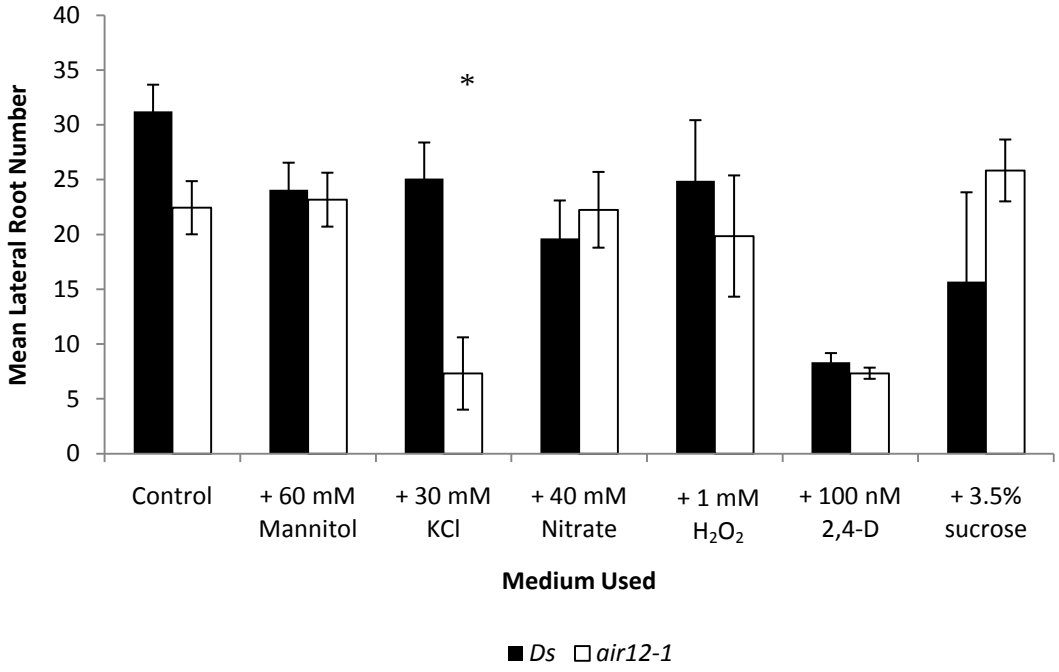

Figure 4.44. Mean lateral root number of vertically grown Arabidopsis *Ds* and *air12-1* seedlings. Seedlings were grown for 13 days on the indicated media with control media composed of ½ MS, 1% sucrose; n=3, bars represent standard error. * denotes significance at $\rho < 0.05$ using a two-tailed Student's t-test.

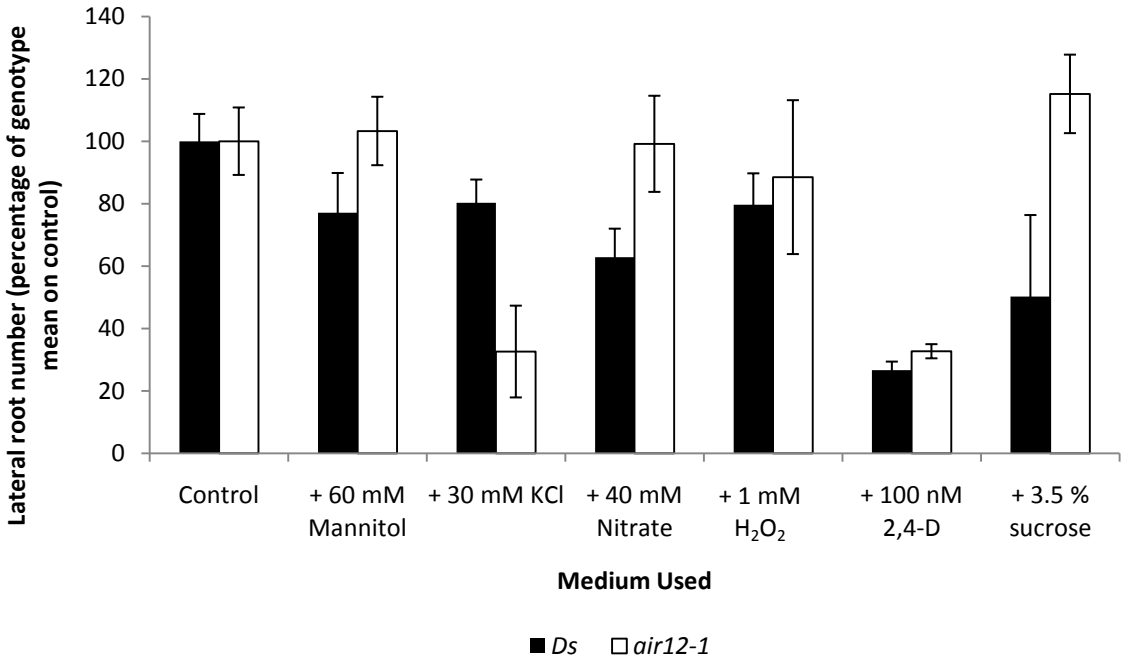

Figure 4.45. Comparison between control (½ MS, 1% sucrose [w/v]) and treatment and the effect on lateral root production of Arabidopsis *Ds* and *air12-1* seedlings. Relative percentages were used to compare mean lateral root number between treatment and control for each genotype by dividing the mean lateral root number per treatment per replicate by the mean lateral root number for all replicates of that genotype on control media. Arabidopsis seedlings were vertically grown for 13 days on the indicated media; n=3, bars represent standard error. No significance was found between *Ds* and *air12-1* using a two-tailed Student's t-test at $\rho < 0.05$.

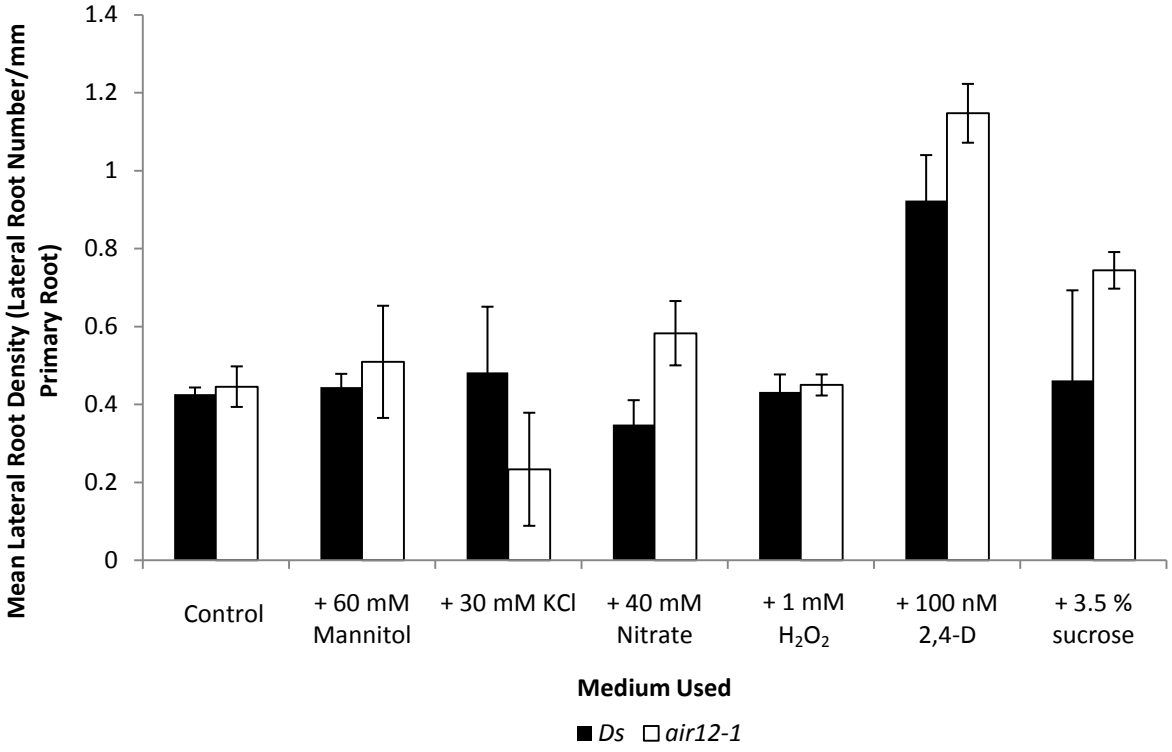

Figure 4.46. Mean lateral root density of vertically grown Arabidopsis *Ds* and *air12-1* seedlings. Seedlings were grown for 13 days on the indicated media with control medium composed of ½ MS, 1% sucrose (w/v). Mean lateral root density was calculated by dividng mean lateral root number by mean primary root number per treatment, per replicate, per line; n=3, bars represent standard error. No significance was found between *Ds* and *air12-1* using a two-tailed Student's t-test at $\rho < 0.05$.

respectively, compared to seedlings grown on control medium (Figure 4.46). No other treatment affected mean lateral root density. The mean lateral root density of *air12-1* seedlings was increased relative to *Ds* seedlings following growth on medium containing nitrate. No other media formulation showed a genotypic effect on mean lateral root density.

4.9.3 Lateral root elongation is reduced in *air12-1* seedlings

On control medium, *air12-1* lateral roots were 40% shorter than *Ds* lateral roots (Figure 4.47). However, *air12-1* lateral root length was not significantly different from *Ds* lateral root length on any other medium. The greatest inhibitory effect of treatment on the *Ds* lateral root length was observed after growth on 40 mM nitrate and 100 nM 2,4-D, where lateral roots, were, on average reduced 50% in length on both media. Length of *air12-1* lateral roots, on the other hand, was not reduced by these media. After growth on media containing 1 mM H_2O_2 *air12-1* lateral roots grew as long as *Ds* lateral roots grown on control medium.

Genotypic differences in lateral root length were also compared by calculating the mean after summing the total length of all lateral roots per seedling, resulting in the measurement of cumulative mean lateral root length. *air12-1* was unaffected by mannitol or nitrate while *Ds* cumulative mean lateral root length was reduced after growth on media containing these compounds (Figure 4.48). *Ds* cumulative mean lateral root length was unaffected by KCl, while *air12-1* cumulative mean lateral root length was reduced 66% compared to *air12-1* seedlings grown on control medium. On medium supplemented with H_2O_2, no difference in *Ds* cumulative mean lateral root length was observed while *air12-1* seedlings developed cumulative mean lateral roots with a length equivalent to *Ds*, almost twice as long compared to the cumulative mean measured lateral roots of *air12-1* seedlings grown on control medium. Similar to the effect of H_2O_2, the addition of 3.5% sucrose corresponded with a reduction of *Ds* cumulative mean lateral root length by 45% while *air12-1* cumulative mean lateral root length increased by 20%. No difference in cumulative mean lateral root length was observed between *Ds* and *air12-1* seedlings on 2,4-D (Figure 4.48).

On control medium, the cumulative mean measurement of *air12-1* lateral roots was 60% shorter than the *Ds* cumulative mean measurement (Figure 4.48). In the presence of mannitol *air12-1* cumulative mean lateral root length was, on average 55% shorter than *Ds* lateral roots (Figure 4.48). The greatest reduction in *air12-1* cumulative mean lateral root length was seen on

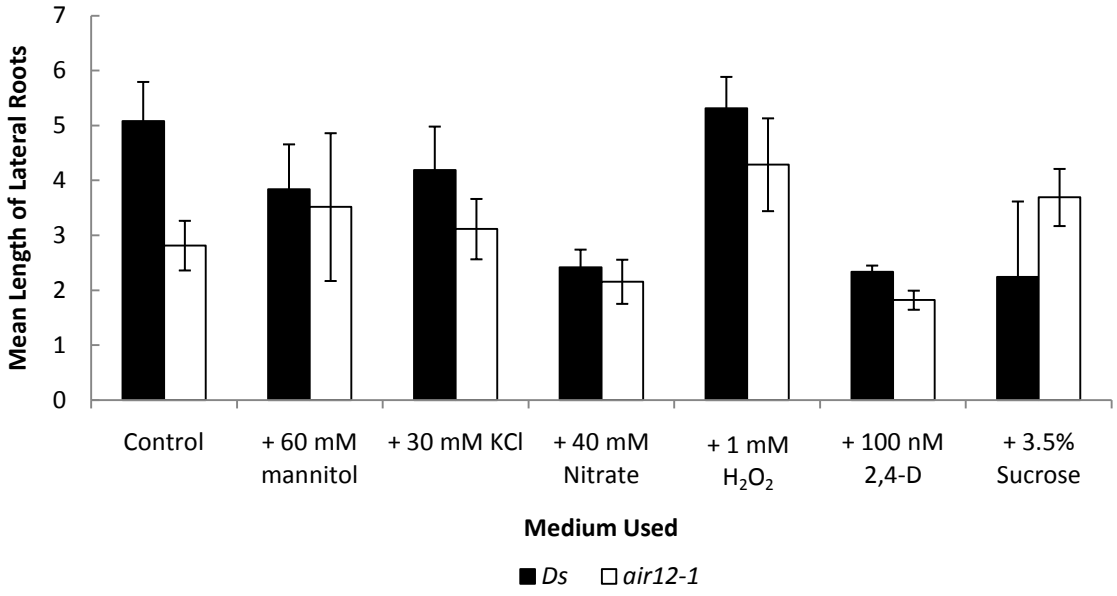

Figure 4.47. Mean lateral root length of vertically grown Arabidopsis *Ds* and *air12-1* seedlings. Seedlings were grown for 13 days on the indicated media with control media composed of ½ MS, 1% sucrose; n=3, bars represent standard error. No significance was found between *Ds* and *air12-1* using a two-tailed Student's t-test at $\rho < 0.05$.

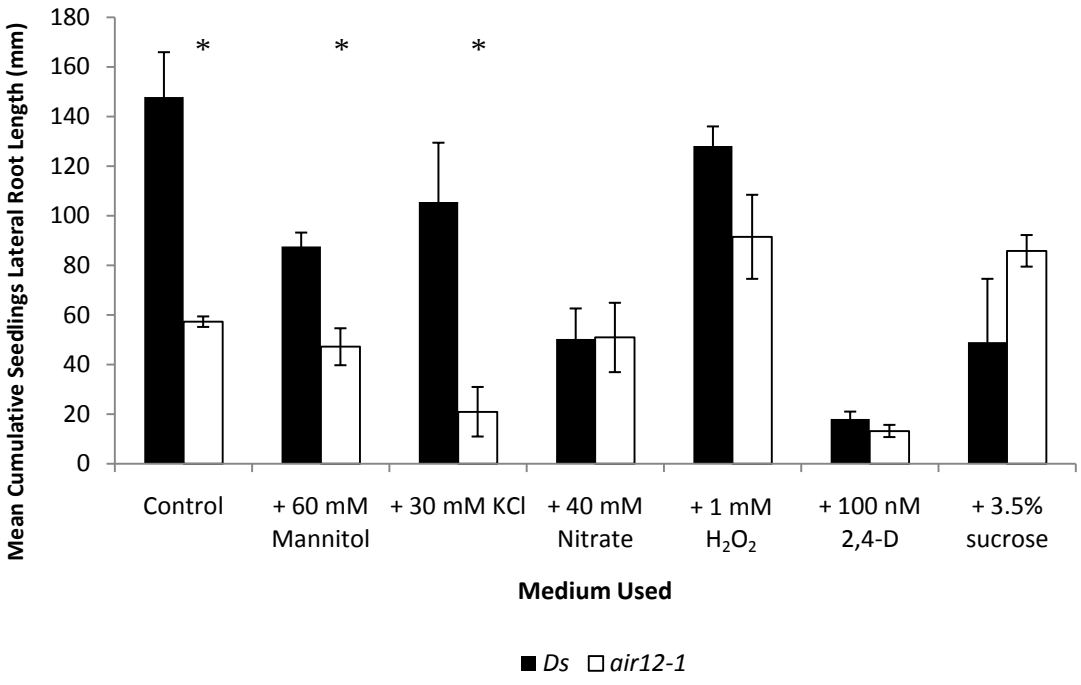

Figure 4.48. Mean cumulative seedling lateral root length of vertically grown Arabidopsis *Ds* and *air12-1* seedlings. Seedlings were grown for 13 days on the indicated media with control media composed of ½ MS, 1% sucrose; n=3, bars represent standard error. * denotes significance at $\rho < 0.05$ using a two-tailed Student's t-test.

KCl, where *air12-1* cumulative mean lateral root length was only 20% the length of the *Ds* cumulative mean lateral root length (Figure 4.48).

The largest decreases in *air12-1* mean cumulative lateral root length were observed on 2,4-D and KCl, where cumulative lateral root length was reduced 80% and 63% of *air12-1* seedlings grown on control medium, respectively (Figure 4.49). Interestingly, growth of *air12-1* seedlings on H_2O_2 and additional sucrose appeared to have a stimulatory effect on lateral root elongation and increased mean cumulative lateral root length to 160% and 145% of control, respectively (Figure 4.49). Growth of *air12-1* seedlings on nitrate had no effect. While growth of *air12-1* seedlings on mannitol appeared to have positive effect on lateral root elongation, the error is too great to draw conclusions from the data.

Similar to *air12-1*, growth of *Ds* seedlings on 2,4-D resulted in the greatest reduction of mean cumulative lateral root length, with a reduction of 90% relative to control (Figure 4.49). Reductions in the mean cumulative lateral root length of *Ds* seedlings were also observed when grown on additional sucrose, nitrate, mannitol, and KCl at 75%, 74%, 40%, and 35% relative to control, respectively (Figure 4.49).

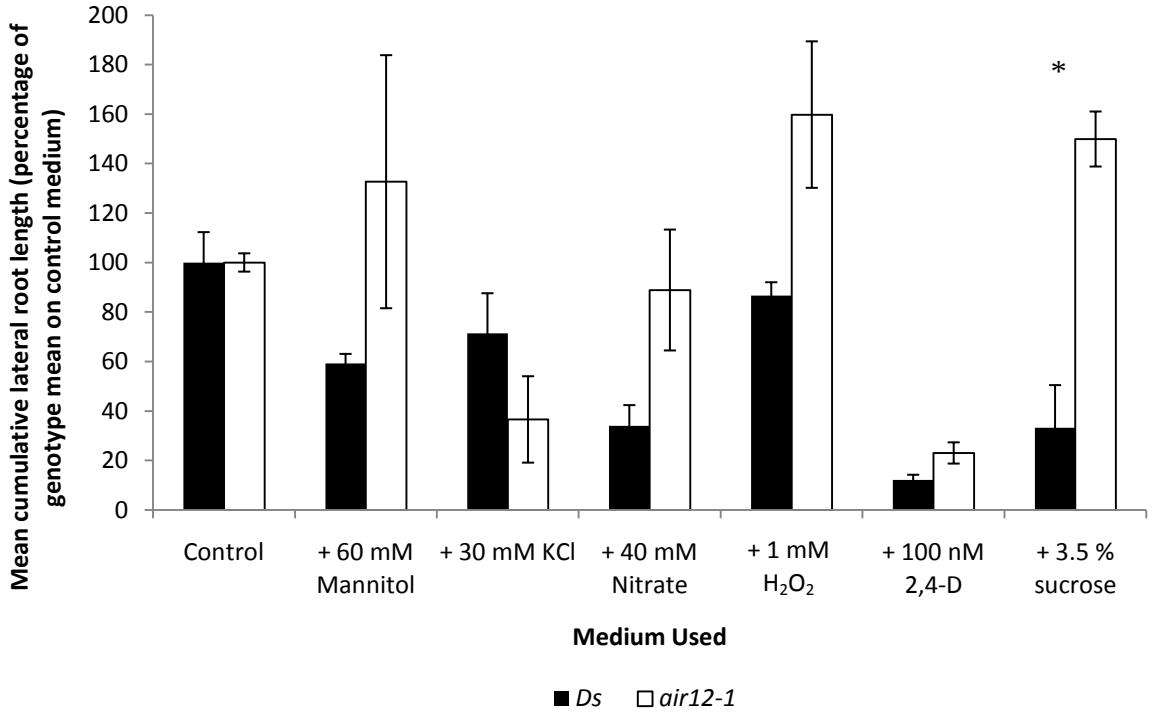

Figure 4.49. Comparison between control (½ MS, 1% sucrose [w/v]) and treatment and the effect on mean cumulative lateral root length of Arabidopsis *Ds* and *air12-1* seedlings. Relative percentages were used to compare mean cumulative lateral root length between treatment and control for each genotype by dividing the mean cumulative lateral root length per treatment per replicate by the mean cumulative lateral root length for all replicates of that genotype on control media. Arabidopsis seedlings were vertically grown for 13 days on the indicated media; n=3, bars represent standard error, * denotes significance at $\rho < 0.05$ using a two-tailed Student's t-test.

4.10 Catalase activity is increased and H_2O_2 concentration is decreased in *air12-1* plants

AIR12 is auxin-induced (Figure 4.28) and is involved in lateral root development (Figures 4.48 and 4.49). There is a demonstrated role for reactive oxygen species in root development (Joo et al., 2005). The data from AC *B. carinata* plants suggests there may be a decrease in steady-state ROS enzyme and molecule activity and concentration, respectively in *air12-1* seedlings. Due to time constraints, all redox constituents could not be determined. Instead, a series of experiments was designed to analyze the activity of catalase and hydrogen peroxide concentration of *air12-1* and *-2* plants in comparison to *Ds* and wild type Landsberg *erecta* (Ler) plants. Hydrogen peroxide concentration and catalase activity were assessed using the amplex red system (Shin et al., 2005). In the presence of an oxidase, generally HRP, amplex red (10-acetyl-3,7-dihydroxyphenoxazine), the reduced and colourless form of resorufin, reacts with H_2O_2 with a 1:1 stoichiometry producing oxidized fluorescent resorufin. The degree of fluorescence is directly propotional to the concentration of H_2O_2. Catalase is an enzyme responsible for converting H_2O_2 into H_2O, thus higher catalase activity will result in less H_2O_2 available to react with horseradish peroxidase (HRP) reducing oxidation of amplex red to resorufin. Therefore, higher fluorescence counts correspond to higher H_2O_2 concentration. For analysis of catalase activity, a saturating amount of H_2O_2 was added to control and experimental samples. After incubating for 30 minutes an amplex red mixture was added and fluorescence was determined. Unlike the H_2O_2 assay, catalase activity is inversely propotional to the intensity of fluorescence. In this case, reduced fluorescence corresponds to higher catalase activity.

4.10.1 Catalase activity is altered in *air12* mutants

Catalase activity was first assessed in 13 day old vertically grown *air12-2* and Ler seedlings grown vertically for 13 days on ½ MS, 1% sucrose, or media supplemented with 400 nM α-NAA or 1 mM H_2O_2. Prior to full-scale analysis, a small-scale assay was completed to determine the effect sample freezing had, if any, on catalase activity. Comparison of catalase activity in frozen versus unfrozen samples showed no difference in activity (Data not shown). Following the small-scale assay, catalase activity was assessed comparing *Ds* to *air12-1* and Ler to *air12-2* on three different media compositions: 1) control; 2) medium supplemented with 1 mM H_2O_2; 3) medium supplemented with 400 nM α-NAA. Catalase activity is expressed in terms of fresh weight and in terms of total soluble protein concentration.

Definite trends in catalase activity were present in both *air12* mutant lines relative to the wild type equivalent. When grown on control medium, specific catalase activity (U μg^{-1} soluble protein) of *air12-1* seedlings was significantly reduced to 50% of *Ds* (Figure 4.50). This trend was reversed when seedlings were grown on medium supplemented with 1 mM H_2O_2, however, with *air12-1* seedlings having significantly greater catalase activity than *Ds*. Supplementing medium with 400 nM α-NAA decreased catalase activity of *Ds* seedlings to *air12-1* levels. When examined in terms of catalase activity per mg fresh weight, *air12-1* seedlings had a significantly higher activity than *Ds* seedlings on 1 mM H_2O_2 (Figure 4.50 B). Growth on 400 nM α-NAA showed no significant difference in catalase activity of *Ds* and *air12-1* seedlings while *air12-1* seedlings showed a decrease in catalase activity compared to *Ds* seedlings on control medium.

When catalase activity was examined in Ler and *air12-2* seedlings, the trends were less consistent between U $(mg\ fw)^{-1}$ and specific activity (U μg^{-1} soluble protein) than they were with *Ds* and *air12-1*. On the control medium, *air12-2* seedlings had reduced catalase activity compared to Ler when analysed in terms of fresh weight, however this decrease was not significant (Figure 4.51). No significant difference in any treatment between the two lines was seen in U $(mg\ fw)^{-1}$. Comparing specific activity, *air12-2* appeared to have reduced catalase activity on both control and medium supplemented with 1 mM H_2O_2, however, these reductions were not significant using a student's t-test. No difference in catalase activity between Ler and *air12-2* was present after growth on media supplemented with 400 nM α-NAA. Curiously, comparisons between *Ds* and *air12-1* or wild type Ler and *air12-2* yielded different trends (Figures 4.50 and 4.51), though there were some general similarities, for example, the *air12* mutants showed reductions in specific catalase activity compared to their wild type equivalent on control medium.

4.10.2 Hydrogen peroxide concentration is not significantly altered in *air12-1*

Hydrogen peroxide concentrations were assessed in control and *air12* seedlings to determine if changes in catalase activity influenced accumulation of ROS. Similar to the initial catalase assay, a hydrogen peroxide assay was completed using both fresh and frozen plant material to determine if total concentration would be affected by the freezing treatment. Like the catalase activity, hydrogen peroxide concentration was unaffected by freezing (Data not shown).

Hydrogen peroxide concentration was then determined. Data were analyzed in terms of hydrogen peroxide concentration per μg soluble protein or per mg fresh weight.

Less defined trends of hydrogen peroxide concentration were apparent compared to catalase activity. Examining *Ds* and *air12-1*, there were small differences in hydrogen peroxide concentration (μM μg^{-1} soluble protein) on control medium and control medium supplemented with α-NAA (Figure 4.52A). In both of these treatments, *air12-1* displayed less hydrogen peroxide than *Ds*.

Almost no differences were present in hydrogen peroxide concentrations between the Landsberg *erecta* lines. Only a small increase in hydrogen peroxide concentration (nM μg^{-1} soluble protein) in *air12-2* was present on α-NAA compared to wild type (Figure 4.53A). Examination of hydrogen peroxide concentration in terms of fresh weight yielded a different trend for seedlings grown on medium supplemented with 1 mM H_2O_2. In this treatment, *air12-2* seedlings showed a reduction in hydrogen peroxide concentration compared to the wild type control, though this difference was not significant using a two-tailed student's t-test (Figure 4.53B).

A.

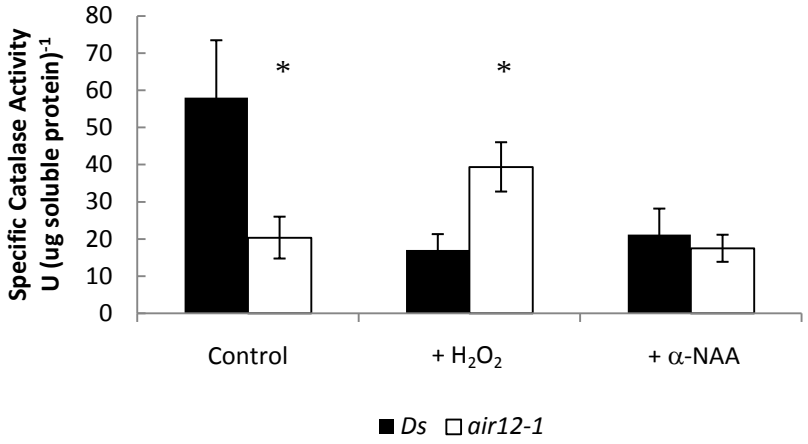

B.

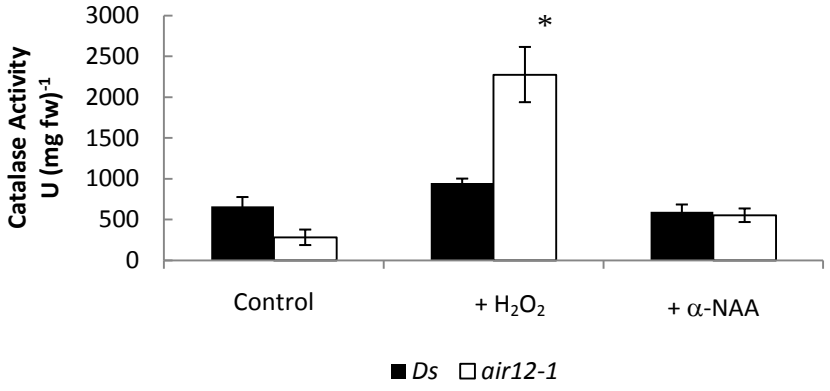

Figure 4.50. Catalase activity in Arabidopsis *Ds* and *air12-1* seedlings. A, Specific catalase activity; B, Catalase activity per mg fresh weight. n=3, bars represent standard error. * denotes significance at $\rho < 0.05$ using a two-tailed Student's t-test.

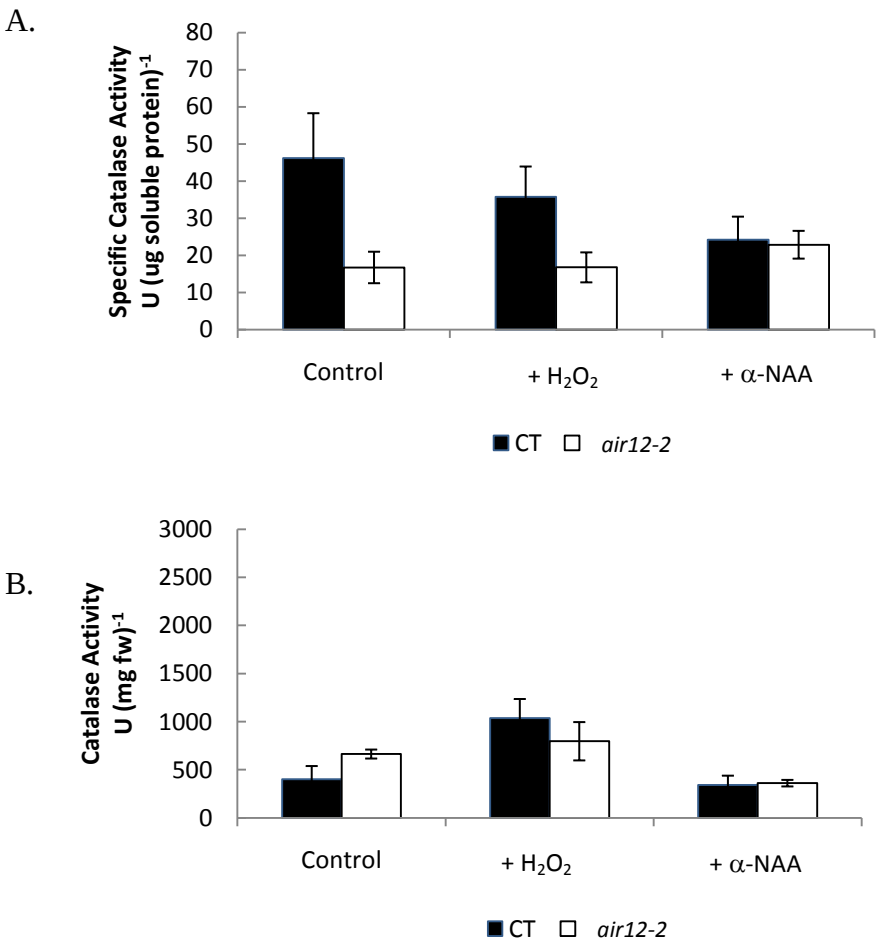

Figure 4.51. Catalase activity in Arabidopsis Landsberg *erecta* control (CT) and *air12-2* seedlings. A, Specific catalase activity; B, Catalase activity per mg fresh weight. n=3, bars represent standard error. No significance was found between *Ds* and *air12-2* using a two-tailed Student's t-test at $\rho < 0.05$.

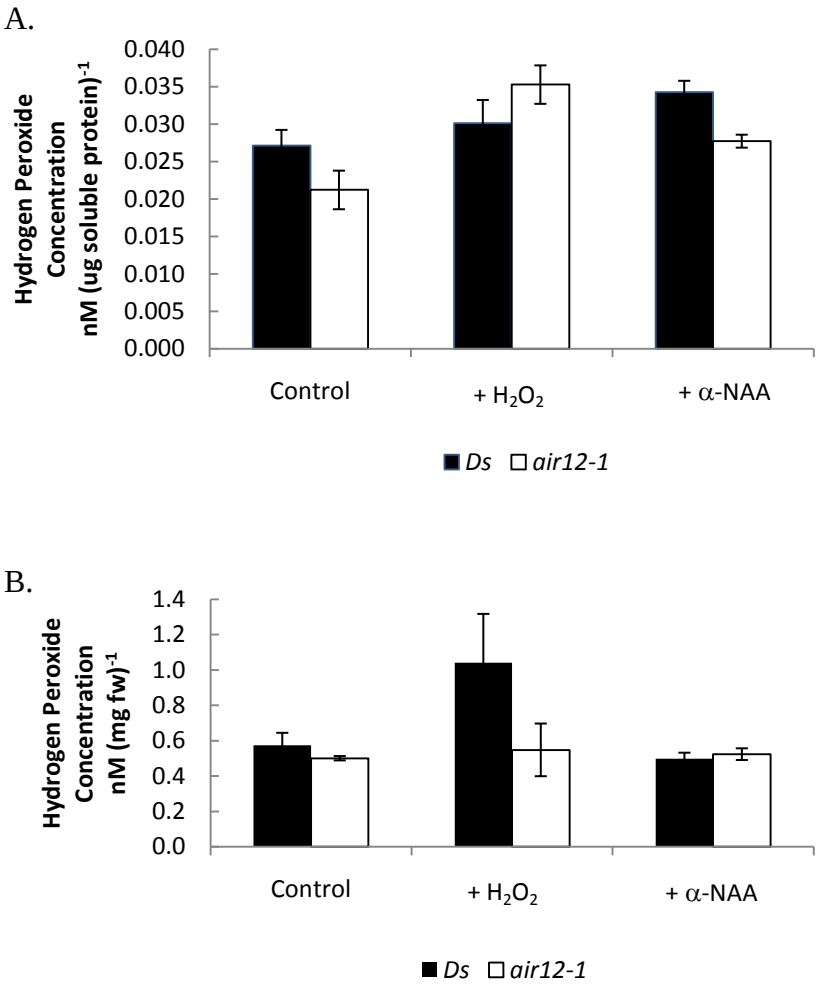

Figure 4.52. Hydrogen peroxide concentration in Arabidopsis *Ds* and *air12-1* seedlings. A, Hydrogen peroxide concentration per µg soluble protein. B, Hydrogen peroxide concentration per mg fresh weight. n=3, bars represent standard error. No significance was found between *Ds* and *air12-1* using a two-tailed Student's t-test at $\rho < 0.05$.

A.

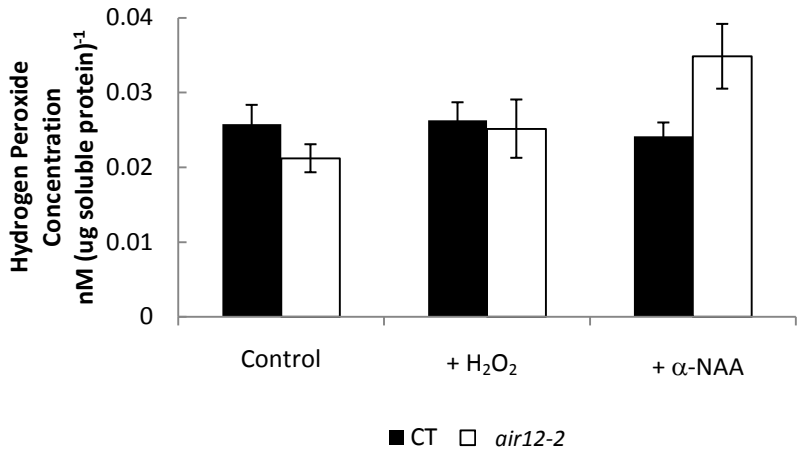

B.

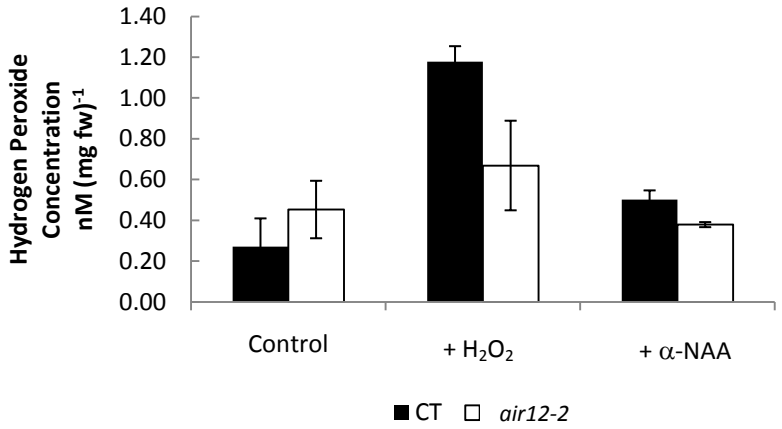

Figure 4.53. Hydrogen peroxide concentration in Arabidopsis Landsberg *erecta* control (CT) and *air12-2* seedlings. A, Hydrogen peroxide concentration per μg soluble protein. B, Hydrogen peroxide concentration per mg fresh weight. n=3, bars represent standard error. No significance was found between *Ds* and *air12-2* using a two-tailed Student's t-test at $\rho < 0.05$.

4.11 *air12* plants display reductions in extra- and intracellular ROS

Because of the differences in catalase activity and previously discussed involvement of ROS in lateral root development I wanted to ascertain the amount of superoxide present in developing roots. This set of experiments was designed to survey the extra- and intracellular superoxide of *air12* plants through the superoxide green fluorescent probes H_2DFFDA (5-(and-6)-carboxy-2',7'-difluorodihydrofluorescein diacetate) and Oxyburst (Invitrogen, Carlsbad CA, USA) according to Monshausen et al. (2007).

Oxyburst (dihydro-2′,4,5,6,7,7′-hexafluorofluorescein) and H_2DFFDA are fluorinated derivatives of fluorescein. Oxyburst is also conjugated to bovine serum albumin (BSA) to prevent the probe from crossing membranes and thus can be used to determine extracellular superoxide content. H_2DFFDA is capable of crossing membranes and can be used to assess intracellular superoxide. Both probes exhibit improved stability compared to the carboxy derivative, DCF (2′,7′-dichlorofluorescein; Molecular Probes), and are chemically reduced and acetylated, remaining colourless until the acetate groups are removed by esterases. Following esterase cleavage of the acetate group, in the presence of superoxide the molecules are oxidized and become fluorescent. Using these probes, a picture of wild type and *air12* Arabidopsis superoxide content can be constructed.

Vertically grown, 8 day old Arabidopsis was used in the following experiments. Each Arabidopsis line was grown on control media or control supplemented with either 1 mM H_2O_2 or 400 nM α-NAA. The entire seedling was removed from the media and incubated in an Oxyburst or H_2DFFDA solution for 15 minutes, followed by confocal laser-scanning microscopic analysis. To standardize lateral root imaging, all microscopic analysis began at the primary root apex. From the root apex, the root was scanned basipetally (toward root base) until an emerging lateral root was found. The first emerging lateral root was then imaged. An emerging lateral root is classified as a lateral root primordium that has grown at least one cell width, but not more than 5 cell widths beyond the epidermal cell file of the primary root. All of the data presented below were not quantified – they are representative qualitative observations. A summary of all fluorescence experiments can be found in Table 4.3 and describes the fluorescence of control seedlings relative to *air12*.

A.

	Medium	Intracellular	Extracellular
Nössen	Control	+	+++
	400 nM α-NAA	++	+++
	1 mM H_2O_2	+	+

B.

	Medium	Intracellular	Extracellular
Ler	Control	+	++
	400 nM α-NAA	++	+
	1 mM H_2O_2	+	++

Table 4.3. Summary of qualitative determination of superoxide accumulation in Nössen (A) and Landsberg *erecta* (B) Arabidopsis ecotypes. Fluorescence of control seedlings is described relative to *air12* using a "+","++", or "+++" to represent the intensity.

4.11.1 of intra- and extra-cellular O_2^- accumulation in *air12-1* relative to *Ds*

Initial comparisons of O_2^- accumulation were made between *Ds* and *air12-1* seedlings grown for 8 days on control medium, control medium supplemented with 400 nM α-NAA, or control medium supplemented with 1 mM H_2O_2. On the control medium, reduced fluorescence was visible in the elongating lateral roots from *air12-1* stained with Oxyburst compared to *Ds* (Figure 4.54A, B). However no difference was observed in fluorescence intensity between *air12-1* and *Ds* using H_2DFFDA (Figure 4.54C, D). Punctate fluorescence was visible in some Oxyburst-stained samples. Consultation with Molecular Probes revealed that the punctate fluorescence likely corresponds to localized regions of superoxide.

When stained with Oxyburst or H_2DFFDA, fluorescence in *air12-1* seedlings grown on medium supplemented with 400 nM α-NAA is markedly reduced compared to *Ds* seedlings (Figure 4.55). This pattern of fluorescence in Oxyburst-stained *air12-1* seedlings is indicative of decreased extracellular ROS generation compared to *Ds*.

No differences in fluorescence using both Oxyburst and H_2DFFDA, could be detected when seedlings were grown on 1 mM H_2O_2. The intensity of the fluorescent signal was extremely weak in most cases with small punctate regions of fluorescence distributed through the primary root (Figure 4.56). It is interesting that fluorescence was absent around emerging lateral roots.

4.11.2 Comparison of intra- and extra-cellular O_2^- accumulation in *air12-2* relative to control

Identical O_2^- accumulation experiments were completed in the Landsberg *erecta* ecotype of Arabidopsis comparing Ler to *air12-2* seedlings after 8 days of vertical growth on control medium, or medium supplemented with 400 nM α-NAA.

On control medium almost no emerging lateral roots could be identified after 8 days, examining at least 6 plants per line. As a result, junctions between the youngest elongating lateral root and the primary root were imaged using Oxyburst, while the tips of elongating lateral roots were imaged after H_2FFDA staining. Like the Nössen seedlings, there was a slight reduction in fluorescence from *air12-2* seedlings compared to wild type when stained with Oxyburst (Figure 4.57A, B). Like the Nössen seedlings, *air12-2* seedlings showed reduced fluorescence when stained with H_2DFFDA compared to wild type (Figure 4.57C, D).

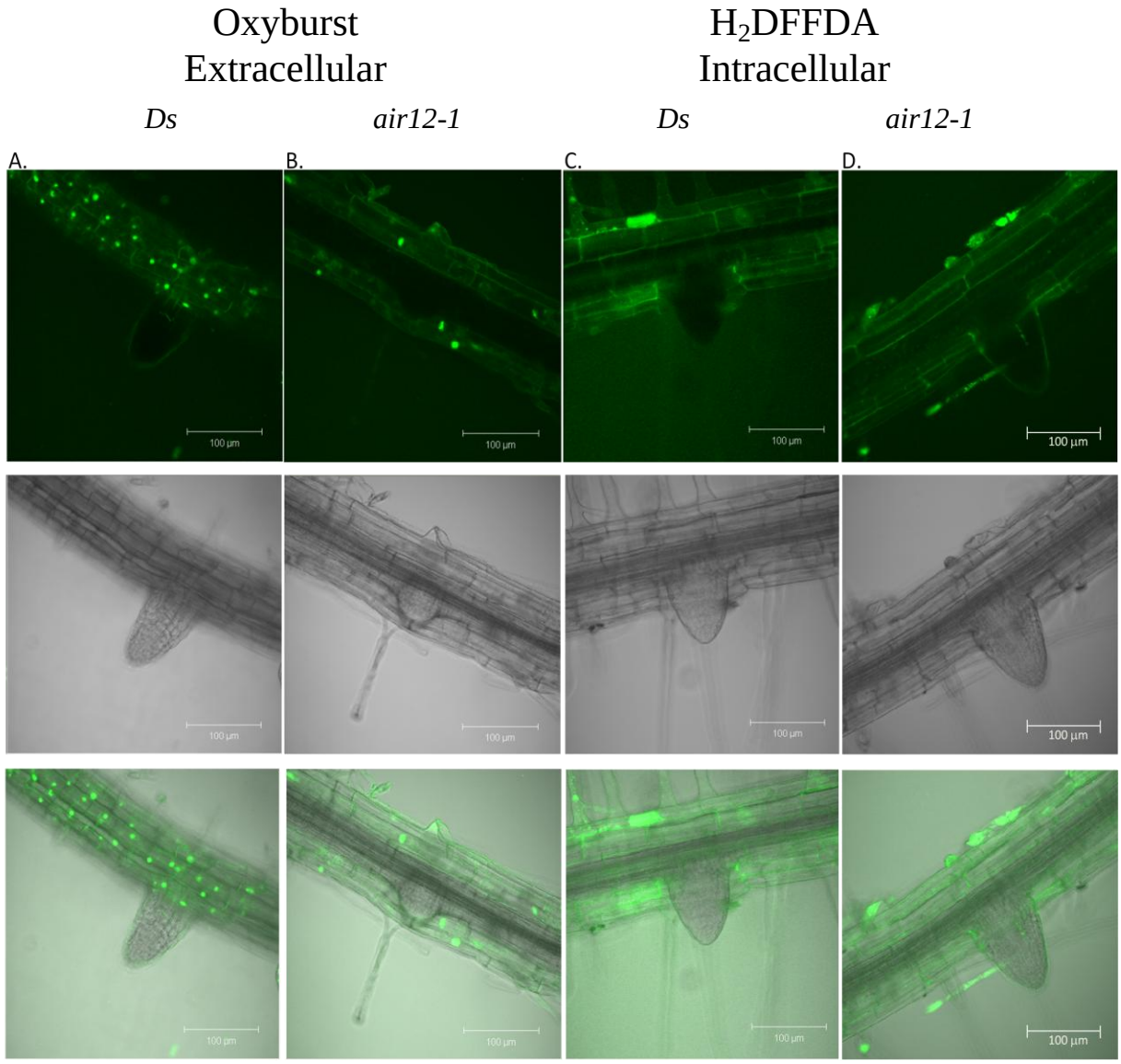

Figure 4.54. Qualitative analysis of extra- and intracellular superoxide in the Arabidopsis Nössen ecotype on control medium shown in fluorescence (top), DIC (middle), and merged images (bottom). Oxyburst (A, B) and H_2DFFDA (C, D) were used to stain 8-day old *Ds* (A, C) and *air12-1* (B, D) seedlings. Intensity of fluorescence is proportional to the amount of superoxide present. Identical capture settings were used for all images.

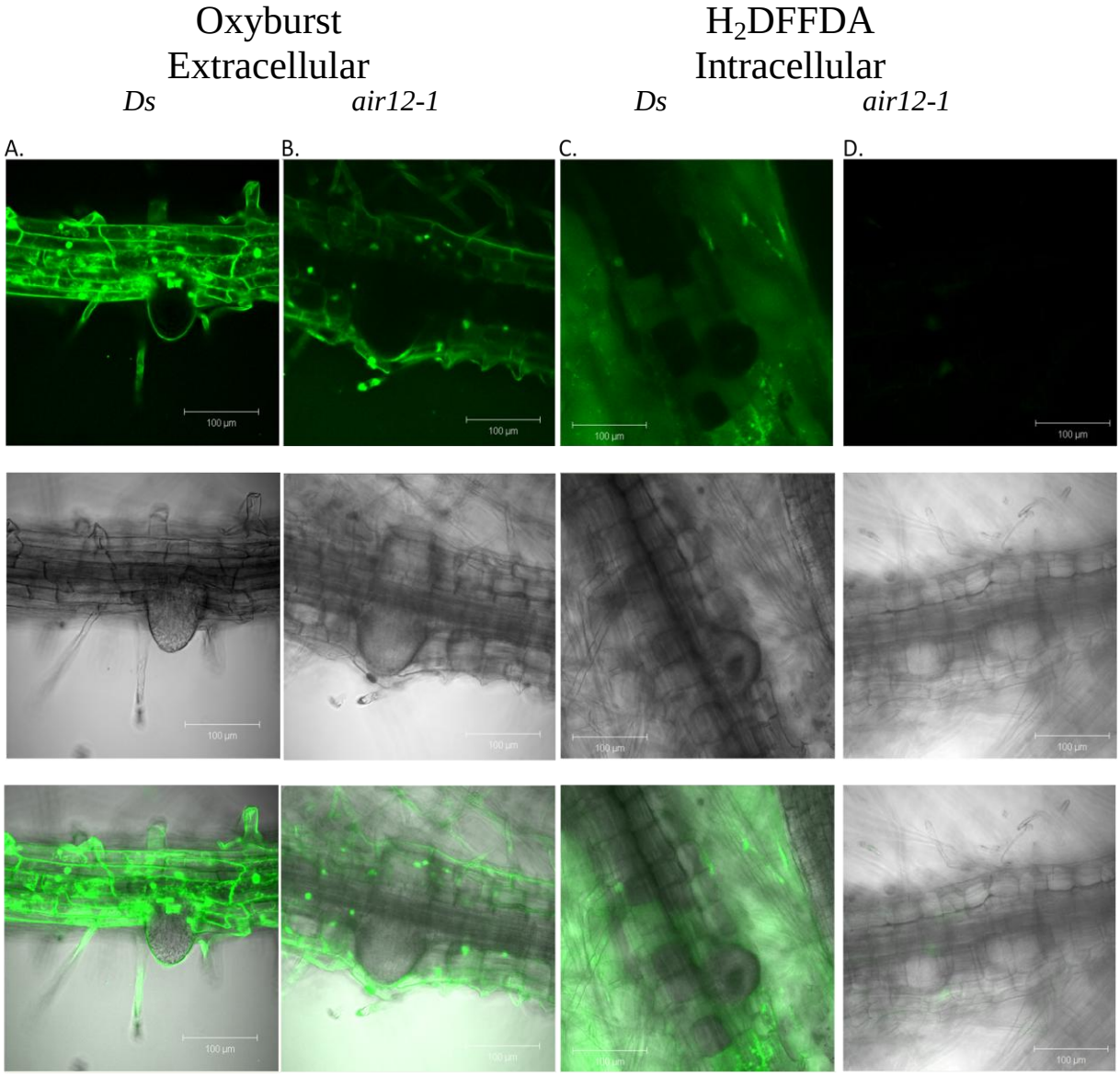

Figure 4.55. Qualitative analysis of extra- and intracellular superoxide in the Arabidopsis Nössen ecotype on medium with 400 nM α-NAA shown in fluorescence (top), DIC (middle), and merged images (bottom). Oxyburst (A, B) and H_2DFFDA (C, D) were used to stain 8-day old *Ds* (A, C) and *air12-1* (B, D) seedlings. Intensity of fluorescence is proportional to the amount of superoxide present. Identical capture settings were used for all images.

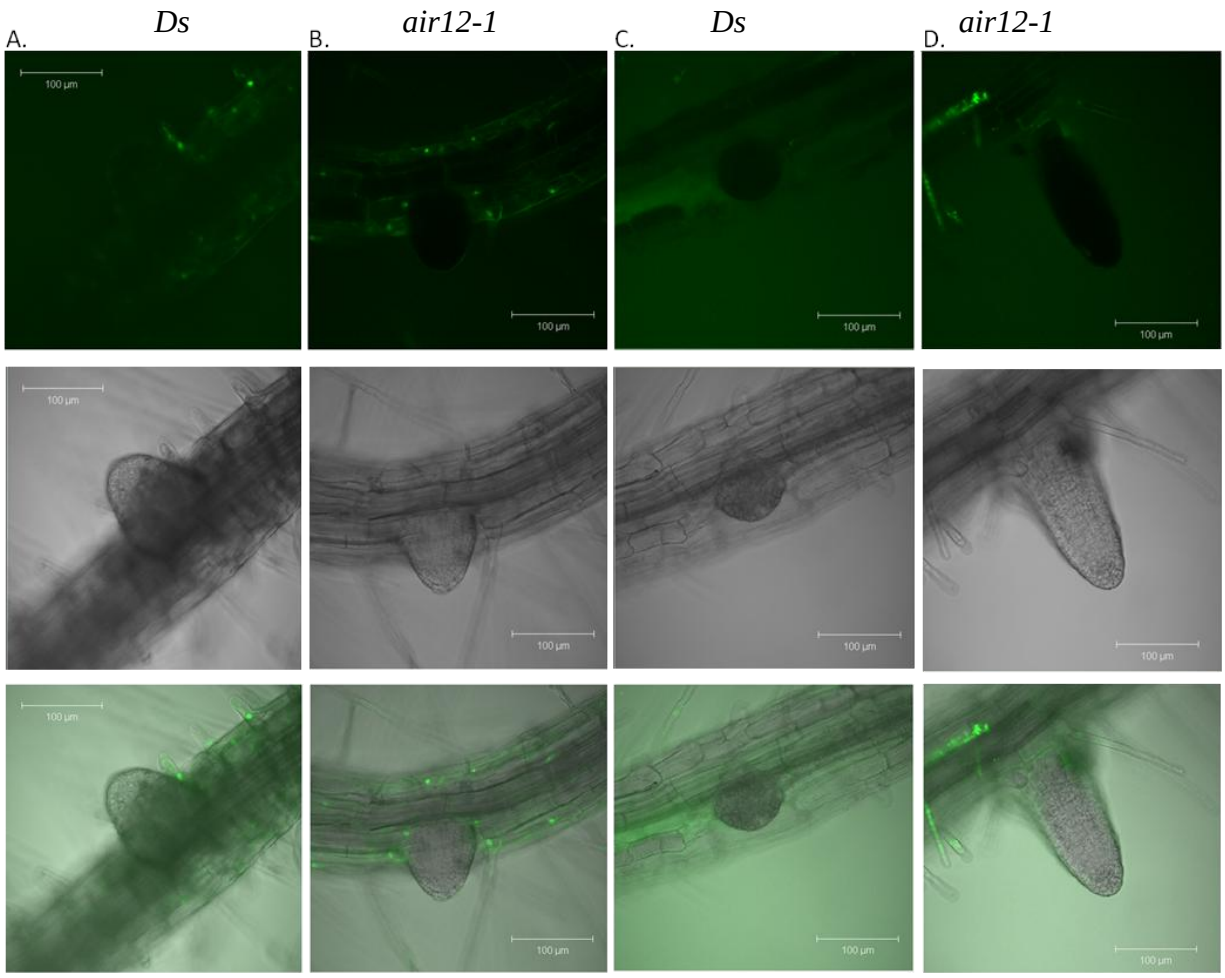

Figure 4.56. Qualitative analysis of extra- and intracellular superoxide in the Arabidopsis Nössen ecotype on 1 mM H_2O_2 shown in fluorescence (top), DIC (middle), and merged images (bottom). Oxyburst (A, B) and H_2DFFDA (C, D) were used to stain 8-day old *Ds* (A, C) and *air12-1* (B, D) seedlings. Intensity of fluorescence is proportional to the amount of superoxide present. Identical capture settings were used for all images.

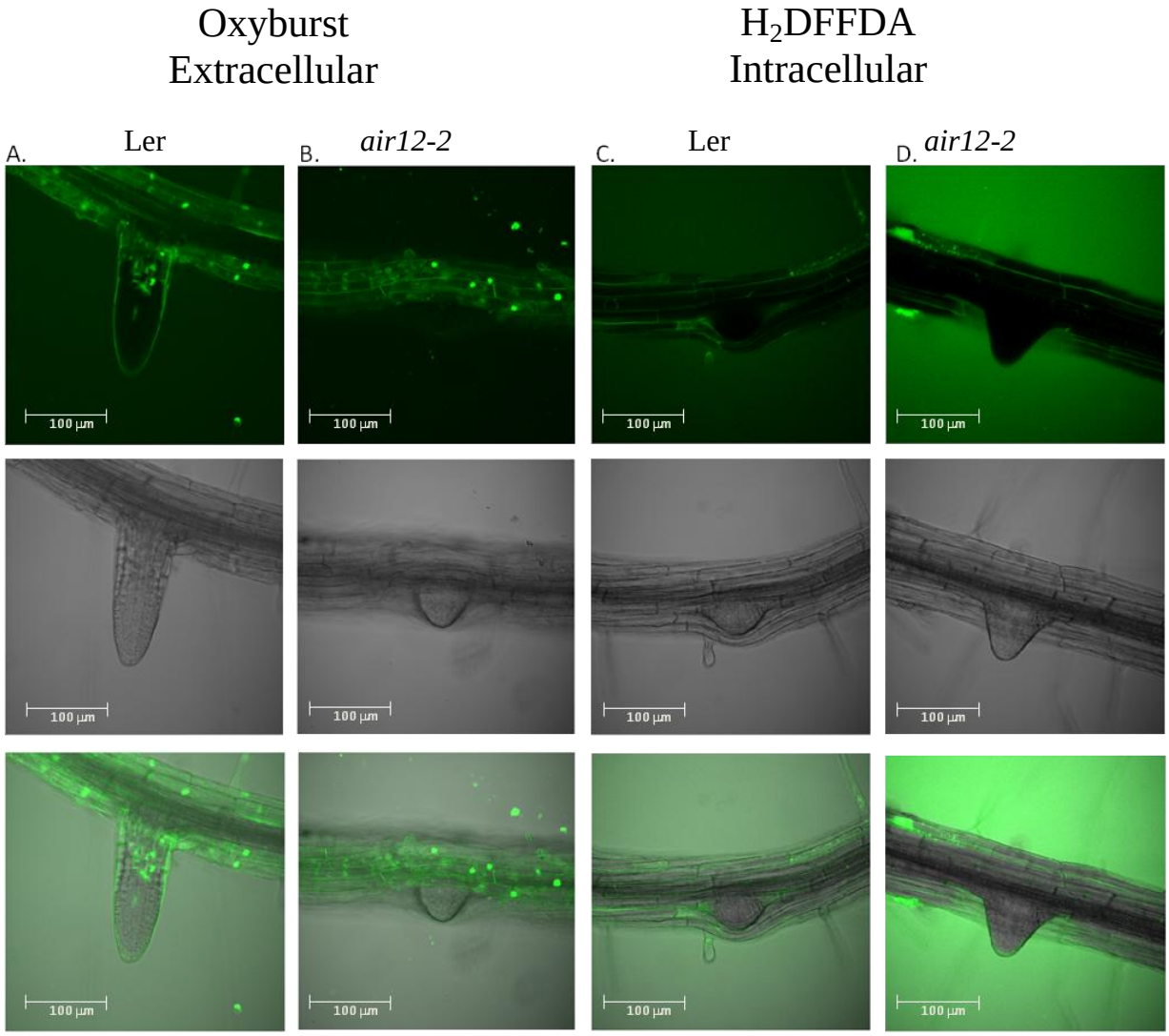

Figure 4.57. Qualitative analysis of extra- and intracellular superoxide in the Arabidopsis Landsberg *erecta* ecotype on control medium shown in fluorescence (top), DIC (middle), and merged images (bottom). Oxyburst (A, B) and H_2DFFDA (C, D) were used to stain 8-day old *Ds* (A, C) and *air12-1* (B, D) seedlings. Intensity of fluorescence is proportional to the amount of superoxide present. Identical capture settings were used for all images..

Examination of seedlings from the Ler background grown on medium supplemented with 400 nM α-NAA showed similarities when stained with Oxyburst; *air12-2* seedlings displayed slight reductions in superoxide levels relative to wild type Ler (Figure 4.58A, B). Similarly, staining with H_2DFFDA showed reduced superoxide accumulation in *air12-2* seedlings relative to wild type Ler (Figure 4.58C, D).

Analysis of seedlings grown on 1 mM H_2O_2 stained with Oxyburst again showed reduced superoxide in *air12-2* relative to wild type Ler (Figure 4.59) as opposed to H_2DFFDA staining, which showed no difference between lines.

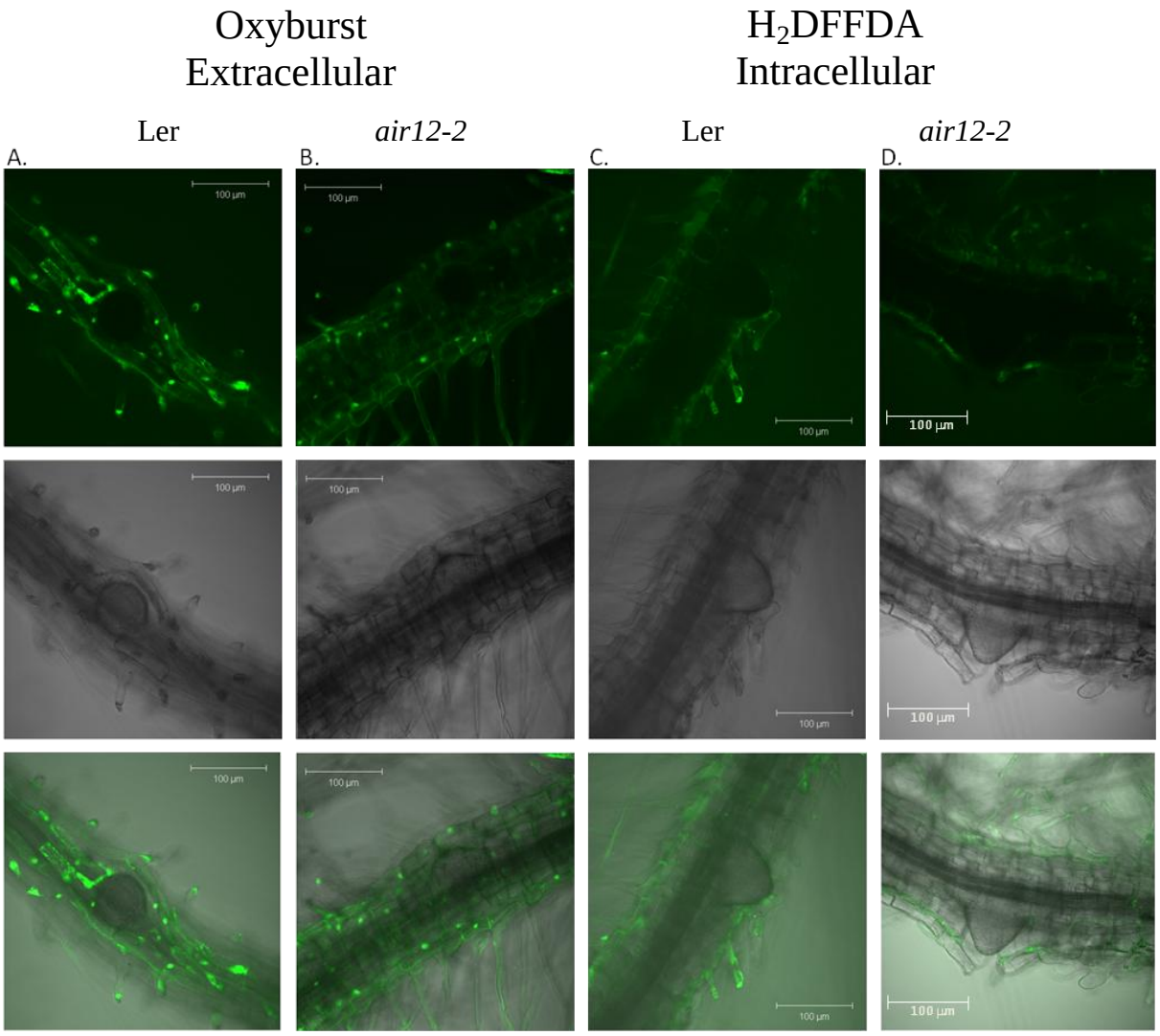

Figure 4.58. Qualitative analysis of extra- and intracellular superoxide in the Arabidopsis Landsberg *erecta* ecotype on 400 nM α-NAA shown in fluorescence (top), DIC (middle), and merged images (bottom). Oxyburst (A, B) and H_2DFFDA (C, D) were used to stain 8-day old *Ds* (A, C) and *air12-1* (B, D) seedlings. Intensity of fluorescence is proportional to the amount of superoxide present. Identical capture settings were used for all images.

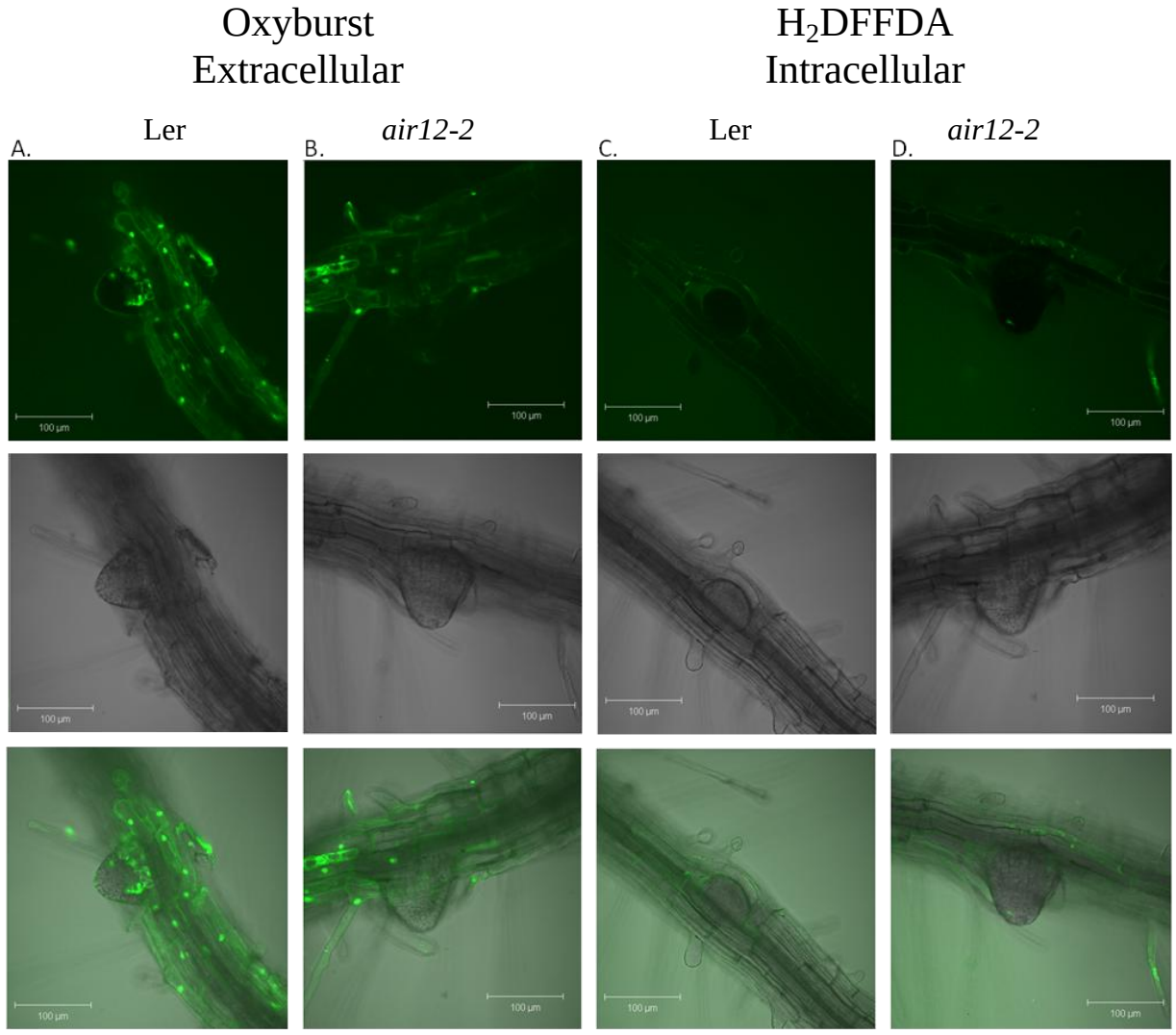

Figure 4.59. Qualitative analysis of extra- and intracellular superoxide in the Arabidopsis Landsberg *erecta* ecotype on 1 mM H_2O_2 shown in fluorescence (top), DIC (middle), and merged images (bottom). Oxyburst (A, B) and H_2DFFDA (C, D) were used to stain 8-day old *Ds* (A, C) and *air12-1* (B, D) seedlings. Intensity of fluorescence is proportional to the amount of superoxide present. Identical capture settings were used for all images.

5. DISCUSSION

The ambitious task of understanding root development in the context of hormonal or abiotic stress response can be approached from multiple angles, integrating information from physiological, molecular, and genetic studies to build a more complete model of this phenomenon. Two proteins, AIR12 and CIL1, isolated from Arabidopsis and *Brassica carinata*, respectively, were examined with the goal of elucidating their function. When working with seedlings, the main challenge in data interpretation comes from the large difference in seed size between Arabidopsis and *B. carinata*, representing small and large seeded species, respectively. The larger seed represents a larger energy reserve; this reserve also provides the seedling with a larger reserve of metabolic building blocks and the ability to withstand a potential stressor for a longer period of time than a small seeded species.

5.1 *AIR12* and *CIL1* play a role in root development

Root development is a dynamic process, integrating plant-wide signals in response to changing environmental and physiological conditions to grow vertically, as seen in primary roots, or laterally, as in lateral roots. Initiation and growth of lateral root primordia are stimulated by plant hormones. The present study examined the link between lateral root development and *AIR12*/*CIL1*. Decreases in lateral root development were observed when expression of functional copies of these genes was eliminated by insertion of a T-DNA (*AIR12*), or reduced using antisense technology (*CIL1*). In both cases, root development in response to the hormones auxin and abscisic acid was altered in the mutants. The hormone treatments used in this study act through discrete and separate pathways; however, the response to both hormones was attenuated in mutants. A possible intersection point lies with reactive oxygen species, a class of molecules containing unpaired electrons capable of acting as membrane-transmissible signals (Schopfer et al., 2002; Liszkay et al., 2004; Foreman et al., 2003; Li et al., 2005; Lin et al., 2009).

AIR12 and *CIL1* code for proteins containing a signal peptide and a GPI modification signal. Investigation of subcellular localization required fusing the open reading frame of *AIR12* with the gene coding for green fluorescent protein. However, the N-terminus of the translated protein is required for ER localization (Figure 4.5) and the C-terminus is required for extracellular targeting. These limitations were overcome using a fusion method similar to Sun et al. (2004), placing *GFP* directly downstream of the *AIR12* or *CIL1* signal peptide. The resulting

construct contains intact termini, a fusion between the *AIR12* open reading frame and the gene coding for green fluorescent protein, placed under the control of the *AIR12* promoter. Initially, both fusion proteins were detected at the cell margins in stably transformed Arabidopsis. This pattern of marginal localization is similar to that observed by Sun et al. (2004) in onion protoplasts. After plasmolysis with 800 mM sorbitol however extracellular and plasma membrane localization of the proteins was visible and distinct from the cell wall (Figure 4.13). This validates the Big-PI analysis and supports that both proteins are GPI anchored. One of the defining features of GPI-APs is the potential for activity in two positions: 1) anchored to the extracellular leaflet of the plasma membrane or, 2) free extracellular protein (Sherrier et al., 1999; Borner et al., 2002). In addition, these proteins can be cleaved from the anchor by phospholipase C (Borner et al., 2003), a protein produced following an ABA-mediated abiotic stress response (Hunt et al., 2003).

Investigation of organ-specific localization of GFP-AIR12 was completed first in *Ds* Arabidopsis seedlings stably transformed with *pAIR12::GFP-AIR12* and grown on control medium for 8 days. In these seedlings, fusion protein was present in every organ examined including the primary root, lateral root, hypocotyl, and leaves (Figures 4.14-4.16, Figure 4.17A). The presence of fusion protein throughout vegetatively growing Arabidopsis closely matches available transcript accumulation data, determined using a large number of microarray data sets at the Bio-Array Resource. As an additional validation of microarray data, *air12-1* seedlings were grown on different media formulations and stained with X-Gluc, utilizing the promoter trap construct interrupting *AIR12*. Using this assay, *AIR12* expression was seen in anther filaments, the stigma, style, carpel, and in stipules (Figures 4.27). *AIR12* expression was also seen in the tips of lateral roots and young leaves in 12 day old *air12-1* seedlings (Figure 4.28A-C) and in the lateral roots of *air12-3* seedlings grown on 400 nm α-NAA (Figure 4.28D). Interestingly, the pattern of GUS accumulation in *air12-1* seedlings grown on α-NAA often did not match the pattern of GFP-AIR12 fusion detected in *pAIR12::GFP-AIR12 air12-1* seedlings. Since the promoter trap in *air12-1* is inserted approximately halfway into *AIR12*, its position may be too far from the *AIR12* promoter to effectively trap its activity. However, the pattern of GFP-AIR12 accumulation matches that predicted from the Bio-Array Resource eFP browser, which shows high expression of *AIR12* in the epidermis of the primary root and in the leaves. Investigation of fluorescence accumulation in *pAIR12::GFP* seedlings grown on α-NAA presents an alternative

method to assess expression and would be able to confirm that the microarray data from the Bio-Array Resource as well as the GFP-AIR12 fluorescence patterns represent valid expression and fusion protein accumulation patterns, respectively.

Because *AIR12* was initially isolated from auxin-treated Arabidopsis roots, localization of GFP-AIR12 fusion protein was examined in this organ 8 days after germination in seedlings from the *Ds* background. Fusion protein was present throughout the primary root tip and appeared to localize to epidermal cells (Figure 4.14A). Curiously, however, one region of the primary root tip lacked fusion protein. Since AIR12 appears to have a promotive effect on lateral root development based on over-proliferative lateral root production in *p35S::GFP-AIR12* seedlings (Data not shown), AIR12 may be involved with lateral root emergence or elongation, but it is not clear what the significance is, if any, of the presence of GFP-AIR12 in the root apex.

In the primary root tip, AIR12 localized to the margins of epidermal cells approximately 100 μm in the meristematic zone (Dolan et al., 1993; Figure 4.14). Basipetally of this region, fusion protein localization shifted from the cell margins to predominantly vascular. The amount of fusion protein steadily increased, as regions farther from the primary root tip were examined until a maximum intensity approximately 1400 μm from the root tip (Figure 4.14). Throughout this region sparse localization was visible in the margins of epidermal cells and in some regions there appeared to be fluorescent cells flanking emerging or elongating, non-fluorescent lateral roots (Figures 4.16A, Figure 4.20B, and Figure 4.24B). This localization pattern superficially resembles LAX3 localization, an auxin influx carrier involved with cell separation during lateral root emergence (Swarup et al., 2008). Though this has not been tested to date, a construct was prepared containing a fusion between the synthetic ARE *DR5* and the mCherry red fluorescence protein to co-localize auxin patterning with GFP-AIR12 and *AIR12* using a *pAIR12::GFP* construct. This will allow me to test the hypothesis that GFP-AIR12 localization correlates with auxin patterning during lateral root development.

In lateral root tips, similar to primary root tips AIR12 fusion protein localized to the margin of epidermal cell files (Figure 4.17A). The fluorescence intensity however, was greater in lateral root tips and appeared restricted to a single epidermal layer. A shift in fluorescence from dermal to vascular cells also occurred, but was much less marked than in the primary root. The shifting dermal to vascular localization of the fusion protein in both primary and lateral roots suggests protein transport or tissue-specific expression patterns. The possibility exists that AIR12

synthesis occurs in elongating regions of root tips and is translocated to the stele, where intercellular transport can occur, similar to the SHORT-ROOT (SHR) transcription factor from Arabidopsis (Gallagher et al., 2004). Limited evidence exists in mammalian systems that GPI-APs can be transferred to adjacent cells (Premkumar et al., 2001). It is possible a similar mechanism exists in plants and that after transferring to vascular cells the anchor is cleaved. Alternatively, vascular GFP-AIR12 could be the direct effect of *AIR12* expression in the vascular tissue.

Examination of GFP-AIR12 localization in independent *pAIR12::GFP-AIR12* seedlings in the *air12-1* background showed similar patterns to lateral roots of the *Ds* background, though only in this organ. At the subcellular level, GFP-AIR12 appeared intercellular near the meristematic zone. Interestingly, this fluorescence pattern was evident solely in seedlings in the *air12-1* background suggesting these mutant plants are not capable of producing a similar amount of fusion protein as the *Ds* seedlings, there is a reduction in *GFP-AIR12* expression, the fusion produced is unstable, or export of GFP-AIR12 to the plasma membrane is impaired. Though this has not been tested, co-localization of GFP-AIR12 using Golgi-specific fluorescent markers may help answer the question of proper GFP-AIR12 export. The lack of visible fusion protein in the vascular tissue is also curious, suggesting the fusion protein is incapable of translocating from the epidermal cells to the vascular tissue supporting the hypothesis that the fusion protein is unstable. Alternatively, the lack of vascular localization could be the result of GFP-AIR12 degredation. In addition to lateral roots, GFP-AIR12 was present in the hairs of the primary root close to the apex. Root hair localization of GFP-AIR12 was not observed in any independent *Ds pAIR12::GFP-AIR12* lines grown on control medium, but GFP-AIR12 localization was observed in the margins of root hairs grown on α-NAA.

5.1.1 Action of *AIR12*/*CIL1* during auxin-induced root development

In the present study, growth of *air12-1* and AC seedlings on control medium was shown to have in a decrease in lateral root number while leaving the primary root length unaffected (Figures 4.1, 4.2, 4.34, and 4.44). The phenotype observed in *air12-1* and AC seedlings does not match any described auxin mutant.

Root development is a process primarily controlled by the plant hormone auxin. The most physiologically active form of auxin in plants, indole-3-acetic acid (IAA), is a membrane impermeable compound requiring active transport to cross the plasma membrane. Normally,

when Arabidopsis is grown on auxin, primary root development is greatly reduced while lateral proliferation increases (Casimiro et al., 2001; Christian et al., 2008). Reduction in lateral root number and length is indicative of reduced auxin biosynthesis or perception. Mutation of the Arabidopsis auxin influx transporter *AUX1* results in IAA insensitivity (Marchant, 1999). *aux1* seedlings are unaffected by IAA and 2,4-D, a synthetic auxin, and appear similar to control treatments. Only with α-NAA, a membrane permeable synthetic auxin, is the primary root growth of *aux1* seedlings inhibited, matching the phenotype of wild type seedlings. Mutation of auxin efflux carriers produces plants that develop an inflorescence almost completely devoid of flowers, causing the shoot to appear "pin-like", the phenotype from which the *PIN* family of genes derives its name (Goto et al., 1987; Okada et al., 1991; Bennett et al., 1995). Because of this requirement for auxin uptake via specific mechanisms, in this study, seeds were grown on medium containing either 2,4-D or α-NAA to investigate the possibility of lateral root growth restoration in mutant seedlings. The synthetic auxin α-NAA can be used to rescue influx mutants (Marchant et al., 1999; Morris, 2000). Both *air12-1* and AC appeared to have reduced sensitivity to α-NAA during primary root development, relative to wild type. Antisense *CIL1* seedlings retained primary root identity (Figure 4.2) while *air12-1* seedlings did not show a large increase in lateral root proliferation (Figure 4.42). On medium containing 2,4-D however, primary root growth of *air12-1* seedlings matched that of *Ds* seedlings (Figure 4.42). The differential response of *air12-1* seedlings to the two synthetic auxins may be due to a concentration effect of transported auxin. Since α-NAA is membrane diffusible, it may cycle through cells more quickly, having less effect than 2,4-D which follows the same influx/efflux pathway as IAA.

Auxin, produced in the shoot apex and young leaves is transported basipetally down the stem to the primary root apex where re-distribution occurs, regulated by PIN, PID, and PLT (Brady et al., 2007; Galinha et al., 2007; Grieneisen et al., 2007; Laskowski et al., 2008). At the root apex, cells rapidly divide in the meristematic zone. Distal to this region is the elongation zone, where cells elongate in size along a single plane. When treated with auxin, the region of *Ds pAIR12::GFP-AIR12* primary root tips containing fusion protein localized to cell margins was greater than that of seedlings grown on control medium, suggesting an expansion of the meristematic zone (Figure 4.20A). However, this perceived expansion could be the result of increased cell divisions, stimulated by auxin, or by observing slightly different staged roots. Distal to the meristematic zone of untreated seedlings, fusion protein appeared to localize to the

vascular tissue. The interface between the meristematic and elongation zones is the region where future lateral root primordia are defined (De Smet et al., 2007). Lateral roots develop from the pericycle, a layer of cells adjacent to two xylem poles (Casimiro et al., 2003). In this region, local abundance and position of an auxin influx carrier, AUX1 increases local auxin abundance. In cells containing high amounts of auxin, PIN proteins promote lateral transport of auxin, defining pericycle founder cells destined to become lateral root primordia. Once cell division begins, LAX3, another auxin influx protein, regulates the expression of several extracellular cell wall remodeling enzymes including a subtilisin-like protease (AIR3), an expansin (EXP17), pectate lyase (PLA2), polygalacturonase (PG), xyloglucan:xyloglucosyl transferase (XTR6), and a glucosyl hydrolase (GLH17), enabling the growing primordia to emerge from the pericycle (Swarup et al., 2008). Growth of *pAIR12::GFP-AIR12* seedlings from the *Ds* background on α-NAA showed strong fusion protein localization to the stele and pericycle cells of the primary root, flanking emerging and newly emerged lateral roots but not inside the lateral roots (Figure 4.20B). This suggests that AIR12 is involved with lateral emergence, assisting in endodermal cell separation. Following increases in LAX3-mediated auxin influx, repression of ARF7 and ARF19 is removed, allowing transcription of auxin-regulated genes and cell wall remodeling enzymes. It is possible that increased AIR12 activity is a downstream result of auxin-regulated gene transcription in emerging lateral roots. Alternatively AIR12 may act following local auxin maxima necessary for lateral root emergence and elongation to occur. As well, phloem transport represents one of the two methods of auxin transport (Cambridge and Morris, 1996; Swarup et al., 2001; Kramer and Bennett, 2006).

Previously documented auxin patterning using DR5::YFP, PIN7:GFP fusions detected auxin and auxin efflux carriers in the meristematic, basal, and elongation zones (Laskowski et al., 2008). Furthermore, a model presenting an overview of local auxin maxima controlled by PIN localization in the primary root during development showed presence of auxin in the three zones (Grieneisen et al., 2007). The observed GFP-AIR12 patterning occurs in regions overlapping the auxin maxima, suggesting a possible link between auxin transport and GFP-AIR12 patterning, though this has not been confirmed experimentally. Furthermore, the number of cells containing fusion protein in the primary root were greatly increased when grown on α-NAA compared to control-grown *pAIR12::GFP-AIR12* seedlings. Vascular localization of GFP-AIR12 appeared much more specific than seedlings grown on control medium and localized to

two discrete strands in the primary root, extending into mature lateral roots (Figure 4.20C). This is similar to that seen in the auxin patterning model proposed by Lakowski et al. (2008) suggesting that in this tissue auxin is driving *pAIR12*.

The pattern of GFP-AIR12 accumulation in mature lateral roots of the *Ds* background (Figure 4.16 and Figure 4.17A) appeared similar to primary roots on control medium (Figure 4.14A) supporting the hypothesis that lateral root development recapitulates primary root development (Malamy and Benfey, 1997). However, as described by Malamy and Benfey (1997), there are genes that are specifically active in lateral roots exclusively. In lateral roots of the *Ds* background, GFP-AIR12 accumulated in the vascular tissue of α-NAA treated Arabidopsis seedlings (Figure 4.20C). Auxin causes increased lateral and second order lateral root proliferation (Marchant et al., 1999; Casimiro et al., 2001; De Smet et al., 2007). GFP-AIR12 was detected in the pericycle cells of lateral roots and in the second order lateral roots themselves (Figure 4.21A,B), a phenomenon not seen on any other treatment. This raises the possibility that AIR12 has different activity in lateral roots, perhaps not being solely regulated by auxin, but by additional signals originating from other pathways, such as ABA. This may result in a shift of AIR12 patterning from being defined or enhanced by local auxin maxima to another role, such as the initiation of lateral roots, meristematic maintenance, or regulation of cell expansion.

Examination of *pAIR12::GFP-AIR12* seedlings grown on α-NAA from the *air12-1* background showed similar localization as when the lines were grown on control medium. Fluorescent signal was extremely weak and was only present in the lateral root tips and root hairs of the primary root. Although *Ds pAIR12::GFP-AIR12* seedlings grown on α-NAA showed very specific fusion protein localization to the pericycle (Figure 4.20B and Figure 4.21A,B), this was not present in *air12-1* seedlings (Figure 4.21C), suggesting that a basal level of AIR12 is required to positively regulate *AIR12* transcription. In this case, the basal AIR12 levels may have been too low for α-NAA to have an effect. Complementation studies of *air12-1* plants with *p35S::GFP-AIR12* have been initiated and from preliminary results, overexpression of *GFP-AIR12* correlates with increased lateral root elongation (Data not shown), supporting the hypothesis that AIR12 is involved with lateral root elongation possibly during emergence and post-emergence.

5.1.2 Interplay between auxin and abscisic acid during lateral root development

While auxin is a major regulator of root development, hormones do not act alone to drive development amongst the myriad signals present in plant cells; they often interact with each other to modulate growth in response to external (or internal) stimuli. Root development in particular, is regulated by antagonistic action of auxin and abscisic acid (ABA) in Arabidopsis (De Smet et al., 2003; Deak and Malamy, 2005; Guo et al., 2009). Growth on medium containing auxin showed that AC displayed reduced sensitivity to auxin, as these seedlings were able to retain primary root identity relative to wild type (Figure 4.2). It is possible the same trend was not observed in *air12-1* seedlings relative to *Ds* grown on medium containing auxin because of the difference in constructs used to reduce gene expression in *B. carinata* and Arabidopsis. The antisense construct in AC plants does not completely disrupt *CIL1* expression while the T-DNA insertion in *air12-1* plants does disrupt *AIR12* expression. Comparison of the response to auxin in multiple *air12* T-DNA insertion lines should allow a more complete picture of the *AIR12* auxin response during germination to be assembled. Since ABA and auxin interact synergistically to inhibit germination, crosstalk between ABA and auxin were examined by first investigating seed response to ABA, followed by ABA and α-NAA simultaneously.

When germinated on medium containing ABA, *air12-1* demonstrated increased sensitivity while AC seedlings demonstrated reduced sensitivity to the hormone. Following germination, *air12-1* demonstrated reduced sensitivity to ABA and both it and AC seedlings were capable of primary root elongation compared to wild type seedlings, which arrested after germination (Figures 4.2 and 4.33). In addition, *air12-1* seedlings demonstrated increased sensitivity to ABA during germination. The pattern of development demonstrated by these seedlings resembled that of other Arabidopsis ABA-insensitive mutants, *abi1*, *abi2*, and *abi3* (Finkelstein and Somerville, 1990) in *B. carinata* (Figure 4.2) and Arabidopsis mutants (Figure 4.33). Comparative root measurements between *air12-1* mutants and *Ds* seedlings could not be completed because seedlings from the *Ds* background did not develop these organs. In *B. carinata*, primary root length of AC seedlings was significantly increased compared to control seedlings (Figure 4.2). Control seedlings failed to develop lateral roots after three weeks of growth, therefore lateral root number and mean lateral root length were not compared between the two lines (Figure 4.1). During development of lateral root primordia, antagonistic action of ABA occurs through ENHANCED RESPONSE to ABA (ERA), a farnesyl transferase that acts

as a negative regulator of ABI3, a transcription factor required for correct ABA and auxin signaling (Brady et al., 2003). It is possible that AIR12 is a member of a similar pathway, and that reduced sensitivity to ABA following germination alters the resulting downstream signals, though this has not been tested experimentally.

When placed on medium containing either α-NAA or ABA alone, both wild type and mutant seedlings germinated (Figures 4.1, 4.32, and 4.33). However, on medium containing both hormones, wild type seeds failed to germinate (Data not shown), in agreement with previous experiments examining interactions between auxin and ABA during seed germination (Brady et al., 2003). Mutant *air12-1* and AC seedlings were capable of germination and primary root development, albeit slower than on either hormone alone. This supports the hypothesis of Brady et al. (2003) that both auxin and ABA interact to repress seed germination through a synergistic mechanism. MicroRNA 160 targets *ARF10*, an auxin response factor involved in recognition of an auxin signal, and acts as a negative regulator of germination in response to ABA (Liu et al., 2007; Nonogaki, 2008). *air12-1* and AC seedlings show reduced sensitive to both ABA and α-NAA following germination, but to a lesser degree than mutants insensitive to exogenously applied auxin, such as *abi1* and *aux1* (Finkelstein and Somerville, 1990; Marchant et al., 1999). AIR12 and CIL1 action likely occurs downstream of perception of both auxin and ABA during germination and lateral root development because mutant Arabidopsis seedlings deficient in hormone perception, such as the auxin receptor *tir1* or the ABA receptor *pyr1* display severe and often lethal phenotypes.

5.1.3 Involvement of ROS during auxin and ABA-induced lateral growth

A major tradeoff of all organisms that utilize oxygen is the potential for harmful radical formation. Oxygen radicals, commonly referred to as reactive oxygen species (ROS) are molecules containing oxygen with unpaired electrons in their pi orbital (Halliwell, 2006). Although ROS can be detrimental to cells in high concentrations causing formation of lipid radicals that can compromise the plasma membrane (Halliwell and Gutteridge, 1984; Halliwell and Gutteridge, 1992), in low concentrations they are used as signaling molecules in such processes as root hair development (Foreman et al., 2003), axillary branching of aerial tissue (Sagi et al., 2004; Sagi and Fluhr, 2006), and guard cell aperture control (Li et al., 2006). Because root growth of *air12-1* and AC seedlings displayed moderate insensitivity to both auxin

and abscisic acid, signaling molecules downstream of perception were examined as a possible intersection point between the two hormones.

In the current study, *Ds* seedling lateral roots were unaffected by H_2O_2 while *air12-1* lateral roots appeared to grow longer (Figures 4.47-4.49). This suggests that H_2O_2 is able to compensate for a deficiency in the *air12-1* mutant, though has little effect on seedlings with functional *AIR12*. Reactive oxygen species represent an important component of root development, and act as signals following auxin perception regulating processes such as gravitropism in Arabidopsis (Joo et al., 2001; Joo et al., 2005), adventitious root formation in cucumber (Xuan et al., 2008), and cell elongation in maize (Schopfer, 2001; Schopfer et al., 2002). The longer lateral roots of *air12-1* seedlings grown on H_2O_2 may be a direct effect of H_2O_2, stimulating an increased rate of cell elongation. However H_2O_2 can also reduce primary root length in wheat, presumably by prematurely stimulating secondary cell wall growth (Hameed, et al., 2004).

Treatment of Arabidopsis seedlings with hydrogen peroxide decreased lateral root production (Figure 4.44), similar to the effect of auxin (Figures 4.2 and 4.44). Proliferation in lateral root production may stem from weakening the pericycle cell wall polymers and stimulating the development of LR primordia. Growth of *pAIR12::GFP-AIR12* seedlings from two independent *Ds* lines on H_2O_2 produced unique localization patterns not observed with other treatments. Fusion protein was visible throughout specific regions of the primary, lateral, and second-order lateral roots, predominantly around the interface of these organs. Very high amounts of fusion protein were detected in lateral root tips as well (Figure 4.19A). Despite the distribution of GFP-AIR12 throughout the root tip, there was an area of exclusion in the meristematic zone lacking fusion protein. Currently the significance of this exclusionary zone is unknown.

In addition, an independent *Ds* line transformed with AIR12-GFP, that previously exhibited strong fluorescence localization on control medium and medium supplemented with 400 nM α-NAA showed a different pattern of localization when the medium was supplemented with 1 mM H_2O_2 (Figure 4.18B). In this line, fusion protein localized to all cellular poles with the exception of the apex, suggesting basipetal localization, transport of GFP-AIR12 fusion protein, or protein degredation. Subcellular localization of the fusion protein may be intercellular possibly indicating transport between cells. Curiously, the *air12-1 pAIR12::GFP-AIR12* lines

exhibited similar localization patterns to this single *Ds* line (Figure 4.18C). As previously hypothesized, it is possible that AIR12 biosynthesis or translocation from the epidermis to vascular tissue is dependent on the presence of a basal amount of AIR12, positively regulating its own biosynthesis, transport, storage, or secretion. In this case, complementing *air12-1* seedlings with a fusion between GFP-AIR12 may block or impede proper AIR12 activity, if the N-terminus of the *in vivo* protein is required for activity, or the GFP fusion alters the protein's ability to function. Or, the fusion protein may fold in such a way to exclude PLC from being able to access the GPI anchor for proper cleavage to occur. Currently, the cause of the shift from marginal to what appeared to be intercellular localization in the single *Ds* line is unknown. Lateral roots did not generally contain GFP-AIR12 fusion protein until the emergence or post-emergent stage, with the exception of seedlings grown on α-NAA (Figure 4.20B and Figure 4.21A,B).

To ascertain if the loss of *AIR12* or *CIL1* function affected steady state redox cycling and root development in the *air12-1* T-DNA knockout and AC seedlings, catalase activity and H_2O_2 concentration were investigated. It is compelling to note that a large difference was observed between catalase activity of *air12-1* and *Ds* seedlings grown on both control medium and medium supplemented with 1 mM H_2O_2 (Figure 4.50). In *air12-1* seedlings, neither catalase activity nor H_2O_2 concentration was affected by growth on medium containing α-NAA (Figures 4.50 and 4.52). These results run counter to the increased catalase transcript correlated with IAA or 2,4-D treatment of maize coleoptiles found by Guan and Scandalios (2002). However, sensitivity of plant cells to hormones is dependent on their developmental stage (Weyers and Paterson, 2001 and references therein); these results may be indicative of reduced sensitivity to auxin-induced catalase expression in 8-day old Arabidopsis seedlings. Alternatively, expression of catalase in response to auxin does not guarantee translation of the transcript to a functional enzyme. A third possibility is that the α-NAA concentration used in this study may have been below a threshold required to enhance catalase transcription. Previous studies used 1 mM IAA or 2,4-D and demonstrated an effect on catalase expression (Guan and Scandalios, 2002; Tyburski et al., 2009), however, *in planta* the concentration of IAA is magnitudes lower, and measured in nM (Bhalerao et al., 2002). Despite the reduced catalase activity in *air12-1* seedlings compared to *Ds* seedlings on control medium and increased activity on 1 mM H_2O_2, concentration of *in vivo* H_2O_2 was unchanged between the two lines on either treatment. The increased catalase

activity of *air12-1* seedlings grown on medium containing 1 mM H_2O_2 may also indicate higher seedling tolerance to long-term exposure of oxidative stress. This suggests that increased catalase activity is a consequence of elevated H_2O_2 and that despite exogenous H_2O_2 application steady state H_2O_2 levels were mantained.

Measurement of redox enzyme activity and molecule abundance was completed by Janet Taylor and Alix Conway and presented here as evidence supporting the hypothesized role of *AIR12* and *CIL1* in root development (Figure 4.4). Analysis of these compounds showed a decrease in O_2^- and H_2O_2 concentration accompanied by an increase in ascorbate (Asc), SOD, and CAT activity in leaves. As with *air12-1* seedlings, this could represent an overall increase in redox detoxification and tolerance to oxidative stressors. Alternatively, the loss of the putative cytochrome *b*561 CIL1 may prevent proper extracellular electron generation or scavenging, leaving a larger pool of Asc and preventing developmental responses that rely on extracellular redox cycling. In addition, recent research has highlighted the possibility that glutathione homeostasis plays a role in auxin transport (Bashandy et al., 2010), which in turn would affect the priming of xylem pole pericycle cells towards lateral root development (De Smet et al., 2007). GFP-tagged CIL1 localizes to the plasma membrane and in plasmolyzed cells is present in the apoplast. GPI-anchored proteins are capable of being cleaved from the GPI anchor inserted in the plasma membrane by phospholipase C (Borner et al., 2003; Eisenhaber et al., 2003), providing a possible mechanism for CIL1 localization. It is possible that CIL1 affects electron generation or scavenging in either its membrane-bound or free state, possibly exerting different effects on scavenging or generation depending on the presence of the GPI anchor.

The enzymatic assays provide a "snapshot" of redox conditions present in the plants at the early stages of development in *air12-1* seedlings, and during vegetative growth in AC plants. As such, the challenge comes from interpretation of the snapshot and integration into a model. Conserved domains present in AIR12 and CIL1, along with cytochrome *b*561-like activity demonstrated by Preger et al. (2009), predicts that the proteins possess electron transfer activity, similar to the N-terminal region of dopamine-β-monooxygenase, as postulated by Aravind (2001). Both *air12-1* roots and AC leaves displayed altered steady state ROS levels. Growth of *air12-1* seedlings on medium containing H_2O_2 correlated with increased catalase activity and greater lateral root length. This implies that increased catalase activity is a direct result of increased H_2O_2, and that absence of *AIR12* may have altered the rate of H_2O_2 turnover. Since

there was no significant difference in H_2O_2 concentration between *Ds* and *air12-1* roots grown on H_2O_2 but there was a significant increase in *air12-1* catalase activity relative to *Ds* when grown on H_2O_2, the H_2O_2 concentrations observed in *air12-1* roots are likely the result of increased turnover of H_2O_2 by catalase. As well, GFP-AIR12 fusion protein was present in greater amounts in *Ds pAIR12::GFP-AIR12* seedlings grown on medium containing H_2O_2 versus control medium suggesting AIR12 responds directly to H_2O_2 or other ROS. In the meristematic zone of the primary root tip localized regions of increased H_2O_2 correspond with local auxin maxima (Tyburski et al., 2009). The regions include where GFP-AIR12 is strongly localized to cell margins (Figures 4.16, 4.17A, 4.19A, and 4.20A,B).

The *Glycine max* orthologue of AIR12 and CIL1 was identified as a cytochrome *b*561 isoform that was postulated to interact with members of the plasma membrane redox system (Preger et al. 2009; Iyer et al. 2007; Aravind, 2001). In mammals, cytochrome *b*561 is involved with ascorbate regeneration across membranes (Su et al. 2006) during the conversion of dopamine to norepinephrine in the chromaffin granules of adrenal glands (Aravind, 2001). In plants, ascorbate plays a role in scavenging ROS generated through photosynthetic electron transport (Bowler et al., 1991; Smith and Veitch, 1998; Scandalios, 2005). The extracellular localization of AIR12 and CIL1 may lead to association with complexes on the plasma membrane.

5.2 Role of ROS in plant development

Reactive oxygen species, a class of molecules once thought to be only involved in photosynthesis and respiration as well as response to pathogen attack and environmental challenge, are now recognized as important factors in multiple stages of plant development. From germination (Guan and Scandalios, 2002) to senescence (Jing et al., 2008), plants appear to take advantage of ROS. Plant cells capitalize on the ability of hydrogen peroxide, a relatively stable ROS, to freely diffuse across the plasma membrane, acting as a membrane diffusible signaling molecule (Levine et al., 1994) to control root development (Joo et al., 2001; Guo et al., 2009), thigmomorphogenesis (Chehab et al., 2009), and guard cell closure (Song et al., 2009). Evidence from the current study provides additional insights regarding the role of ROS during lateral root patterning and emergence. The question remains, however; how does extracellular AIR12 or CIL1 interact with ROS, auxin, and ABA to affect lateral root development? This

question may be answered by examining NADPH oxidase (NOX), a plasma membrane-spanning enzyme complex that utilizes intracellular NADPH to reduce extracellular O_2, forming superoxide (Sagi and Fluhr, 2006).

5.2.1 The NOX enzyme complex and *air12*/AC

Generation of extracellular O_2^- signals is mediated by the NOX enzyme complex and represents a method of transmitting intracellular signals to the apoplast of plants. Altered catalase activity observed in the *air12-1* T-DNA knockout and AC seedlings may be the result of changes in the rate of O_2^- production from O_2 via NOX. Following extracellular O_2^- production, it can be detoxified using SOD, resulting in H_2O_2 which can be used as a membrane-transmissible signal. The catalase enzyme acts on H_2O_2, converting it into water and oxygen, detoxifying it. This pathway was examined using two different methods: qualitative observation of O_2^- accumulation in *air12-1* mutants Figures 4.54-4.59; Table 4.3) and enzymatic analysis of NOX activity and O_2^- concentration in AC plants (Figure 4.4). Since O_2^- cannot cross membranes (Takahashi and Asada, 1983), the effect of intracellular superoxide would be manifested after being converted to H_2O_2 by intracellular SODs. The resulting intracellular H_2O_2 could then cross the plasma membrane or activate intracellular signaling pathways. As such, involvement of AIR12 with intracellular-derived O_2^- is likely minimal.

Using the fluorescent dyes Oxyburst and H_2DFFDA, extra- and intracellular O_2^- accumulation was observed in *air12-1* and *air12-2* mutant seedlings. Using H_2DFFDA, differences in cellular fluorescence were seen only in *air12-1* seedlings grown on control medium supplemented with α-NAA. Auxin has a promotive effect on ROS production, stimulating cell elongation in maize coleoptiles (Rodriguez et al., 2002). As the major enzyme complex involved in the production of extracellular ROS, NOX may be the central component required for cell elongation. Indeed, elongation of root hairs specifically requires NOX activity, mediated by RHD2 (Foreman et al., 2003) and then spatially regulated by SCN1 (Carol and Dolan, 2006). Interestingly, there appeared to be no difference in O_2^- accumulation on control medium or control medium supplemented with H_2O_2 between *Ds* and *air12-1* seedlings, suggesting that the *air12-1* allele affects catalase and NOX activities differently, depending on the environmental stress the seedling perceives.

Extracellular O_2^- provided the most pertinent data with respect to the *air12-1* phenotype, as O_2^- cannot readily cross the plasma membrane in significant amounts (Takahashi and Asada, 1983). On control medium and on α-NAA there was greater fluorescence in *Ds* seedlings relative to *air12-1* (Figures 4.54 and 4.55). These fluctuations in O_2^- may reflect regulation of the NOX enzyme complex by α-NAA, and in turn may reflect a reduction in activity due to the mutation of *AIR12*, or, may be the result of induced changes in ROS scavenging or turnover in enzymes and compounds other than catalase, though this was not examined. Curiously, supplementing medium with H_2O_2 did not affect O_2^- accumulation (Figure 4.56), suggesting that H_2O_2 concentration does not regulate NOX activity but instead may stimulate ROS scavenging.

Visualization of O_2^- in *air12-2* seedlings of the Landsberg *erecta* ecotype presented a slightly different picture of ROS steady state accumulation compared to *air12-1*. The main differences in intracellular O_2^- accumulation were present in control medium and on H_2O_2, where it was greater in wild type Ler compared to control seedlings, and no difference was observed when grown on α-NAA (Figures 4.57 and 4.58). Extracellular O_2^- patterns matched *air12-1* for all treatments except on 1 mM H_2O_2, where Ler appeared to contain a higher level than *air12-2* (Figure 4.59). Overall, O_2^- levels in the *air12* mutants were very similar. Differences between the two lines can likely be attributed to the position of the *Ds* cassette in the 3' UTR of *air12-2* mutant plants, perhaps because functional AIR12 protein was produced in this line.

Integrating the *B. carinata* and Arabidopsis data suggests that changes to NOX and SOD activity may result in altered O_2^- patterns in *air12-1* T-DNA knockout and AC seedlings. Increased NOX activity leads to increased O_2^- production (Sagi and Fluhr, 2001), which in turn may lead to increased SOD activity, similar to Arabidopsis plants challenged with an oxidative stress (Alscher et al., 2002). In response to an oxidative stress, conversion from O_2^- to H_2O_2 mediated by SOD also increases. In both the *air12-1* T-DNA knockout and AC plants, little difference was observed in H_2O_2 concentration compared to control plants. However catalase activity was significantly increased in the mutants. Though NOX and/or SOD activity were not monitored and O_2^- concentration not quantitatively determined in the *air12* mutants, it seems reasonable based on phenotypic, localization, and sequence similarity to hypothesize that *air12* mutants exhibit increased NOX activity, and that increased SOD activity is a direct result of

increased production of O_2. Following increased H_2O_2 production, catalase activity would also increase to detoxify the excess catalase, as seen in *air12-1* roots isolated from media containin H_2O_2 (Figure 4.50). Given the magnitude of increased catalase activity compared to SOD in mutant plants, the total pool of H_2O_2 may appear similar to wild type while actually indicating a more rapid turnover of H_2O_2 into H_2O and O_2. These data may indicate that both AIR12 and CIL1 modify, through an unknown mechanism, the first step involving the reduction of extracellular O_2, and that this modification has an effect on ROS scavenging and turnover.

5.3 Induced developmental changes by hormonal or abiotic stress treatment

As sessile organisms, plants cannot move to avoid stressful environmental conditions like animals. Environmental challenges such as heat, cold, or soil salinity stimulate signaling pathways allowing a plant to endure the stress, avoid the stress by reproduction, or direct root growth away from the stress (Hodge et al., 2009), among other responses. Responses to abiotic stressors are generally mediated by ABA (Koornneef et al., 1998; Zhu, 2002; Havlová et al., 2008), a hormone both the *air12-1* T-DNA knockout and AC plants demonstrated reduced sensitivity to during primary root elongation following germination. Investigations focused on the overexpressed fusion GPI-anchored proteins, GFP-AIR12 and GFP-CIL1. Some GPI-APs, such as SKU5 (Sedbrook et al., 2002) are cleaved from their anchor by phospholipase C (PLC), leaving the protein free to associate with extracellular structures such as the cell wall (Borner et al., 2003). Furthermore, PLC biosynthesis increased in response to abiotic stress mediated by ABA in Arabidopsis plants (Hirayama et al., 1995). Therefore, it seems possible that AIR12 and CIL1 may be released from their anchor following PLC digestion during abiotic stress.

In this study, two different abiotic stressors were applied to the plant cells, simulating a salt (NaCl) or osmotic (sorbitol) stress. In both cases, fusion protein was clearly localized to the plasma membrane (Figures 4.12 and 4.13). Large amounts of additional fusion protein were present in the apoplast of cells as well, likely resulting from the cleavage of fusion protein from the GPI anchor by PLC. Application of stressors, such as salt, or pathogens elicits ABA-mediated PLC biosynthesis (Hirayama et al., 1995). Oxidative bursts resulting from abiotic stress elicit PLC-mediated release of intracellular Ca^{2+} from internal stores which can stabilize the NOX complex by binding to its EF-hands (Legendre et al., 1993; Hunt et al., 2003). A secondary function of PLC during stress responses is cleavage of GPI-APs (Borner et al., 2003). The

pattern of subcellular localization seen with both GFP-AIR12 and GFP-CIL1 is indicative of GPI anchoring and that these specific proteins are cleaved during abiotic salt or osmotic stress. However, using this experimental system it is impossible to determine if the proteins are preferably membrane-associated or free in non-stress conditions. It is possible that under non-stress conditions, AIR12 and CIL1 are primarily localized to the extracellular leaflet of the plasma membrane, held in place by their GPI anchor. When exposed to an abiotic stressor, an oxidative burst, mediated by ABA would cause an increase in PLC biosynthesis resulting in the release of intracellular Ca^{2+} cleaving AIR12 and CIL1 from their GPI anchor and releasing them into the apoplast. A secondary effect of cytosolic Ca^{2+} increase is the stabilization of NOX, by the binding of Ca^{2+} to the EF hands of the complex, as observed during salinity responses (Chung et al., 2008). Increased NOX stability may enable AIR12 and CIL1 to affect NOX activity, either directly or indirectly.

The *air12-1* seeds germinated more rapidly than *Ds* on all media examined, with the exception of media containing ABA (Figure 4.33). On all media except mannitol and H_2O_2, *Ds* seeds were able to reach *air12-1* germination levels by day 3 indicating sensitivity toward osmotic stress that was not seen in *air12-1* seeds (Figure 4.31). This indicates that AIR12 may be a negative regulator of response to osmotic stressors during seed germination, and that AIR12 may act downstream of ABA-mediated GPI anchor cleavage by PLC. Germination and subsequent development under environmental stress reduces seed yield while increasing plant mortality (Wan et al., 2009). Inhibition of germination can allow a seed to remain dormant until stressful conditions have ceased, when it can then complete its lifecycle under more optimal conditions resulting in greater seed production and fitness. The mannitol concentration used in this study not only reduced the germination rate of *Ds* seedlings, but reduced cumulative mean lateral root length as well (Figures 4.31 and 4.48). In contrast, mean lateral root length and cumulative mean lateral root length of *air12-1* seedlings was unaffected by mannitol, compared to control medium (Figures 4.47-4.49). However the additional 3.5% sucrose used in this study, corresponding to 100 mM sucrose, represents a higher osmotic stress. The higher osmotic stress of sucrose reduced the mean cumulative lateral root length of *Ds* seedlings relative to seedlings grown on control medium, while *air12-1* seedlings displayed increased lateral root length when grown on sucrose relative to control medium, further supporting the hypothesis that *air12-1* seedlings are deficient in a mechanism that either perceives or responds to osmotic stress.

Though germination rate was not significantly altered by growth on media containing KCl (Figure 4.31), lateral root number and length was severely reduced in *air12-1* seedlings while *Ds* seedlings were largely unaffected (Figure 4.44). This indicates AIR12 is a positive regulator of the resistance to salt stress during lateral root development. Examination of GFP-AIR12 localization in response to KCl supports this hypothesis as fusion protein is distributed throughout the entire meristematic zone of the primary root, lacking the zone of exclusion seen with other treatments (Figure 4.25A). Examining *air12-1* seedlings transformed with *pAIR12::GFP-AIR12,* no vascular accumulation of GFP-AIR12 was observed. Fusion protein in the *air12-1* background was faintly present in the meristematic zone of the primary root and appeared to be intercellular, while in the lateral root tip it appeared it punctate, localizing to lateral poles of epidermal cells possibly indicating areas of future cell expansion in response to the stress.

Response of Arabidopsis seedlings to the treatments examined all utilize signaling pathways mediated by ABA to adapt to abiotic stressors (Zhang et al., 2006; Hodge et al., 2009; Jiang et al., 2009). Furthermore, these stressors initially have a negative effect on lateral root development, indirectly diminishing the plant's photosynthetic output and fecundity if the stress persists. Response to an abiotic stress occurs after local accumulation of ABA at the initial site of environmental challenge (Nambara and Marion-Poll, 2005). Following accumulation, ABA is perceived by a receptor, activating signaling pathways leading to a stress response. Recently, ABI2, a protein phosphatase 2C involved in ABA signaling (Finkelstein et al., 2002) was shown to interact directly with Glutathione peroxidase3 (Miao et al., 2006), providing a direct link between ABA signaling and ROS detoxification. When challenged with an osmotic stress or high nitrogen concentrations, perception occurs through ABA followed by redox cascades mediated by ABI2, finally resulting in repression of lateral root elongation. In *air12-1* mutants the response to nitrate and mannitol was attenuated and no adverse effect on cumulative lateral root length was observed, relative to *air12-1* seedlings grown on control medium (Figures 4.47-4.49).

The decrease in cumulative lateral root length of *Ds* seedlings grown on nitrate may represent different nitrogen usage strategies: instead of below-ground lateral branching to locate nitrogen and other micronutrients, the plant may invest solely in primary root growth until a high nitrogen region is exhausted, relying on root hairs for absorption. Following exhaustion of local nitrogen and micronutrients, the plant would likely invest in lateral root growth to find new

sources of metabolic building blocks. Similarly, the decrease in cumulative lateral root length of *Ds* seedlings grown on control medium supplemented with 3.5% sucrose relative to control seedlings (Figures 4.47-4.49) may represent different carbon usage strategies, or, as previously hypothesized, susceptibility to higher the osmotic stress pressure of 100 mM sucrose. It is possible that high concentrations of carbon inhibits lateral because of an alteration of developmental pathways. It is interesting that in *air12-1* seedlings grown on control medium supplemented with 3.5% sucrose, cumulative mean lateral root length increased substantially compared to seedlings grown on control medium; an inverse trend compared to *Ds* seedlings. It is possible that loss of *AIR12* prevents a carbon-sensing mechanism from properly responding to the increased carbon source in the medium and instead hyper-responds by producing longer lateral roots.

Responses to salinity stress, unlike osmotic and nitrogen stress, utilizes both ABA-dependent and -independent pathways acting through ROS intermediates (Lim et al., 2010; Guo et al., 2009; Mahajan and Tuteja, 2005; Zhu, 2002). Based on the *air12-1* seedlings response to KCl compared with either nitrate or mannitol, the KCl response appears to proceed through pathways not mediated by ABA. Involvement of ABA in the salinity response pathway is not a complete "all or nothing" response; some responses to salinity show partial involvement of ABA while other salinity responses show no ABA involvement. Arabidopsis *NAC* (*AtNAC*; *NAM, ATAF1,2, and CUC2* [a helix-turn-helix structure that directly binds DNA]) is induced by ABA and α-NAA after stress perception however does not utilize the ABA-signaling intermediates ABI2, 3, or 4 during the response. The SALT OVERLY SENSITIVE (SOS) proteins are Na^+/H^+ antiporters in the plasma membrane that use NOX-generated extracellular ROS to convey salinity tolerance to plants (Kamei et al., 2005; Chung et al., 2008). Reduced extracellular O_2^- concentration (Figure 4.54) correlated with increased KCl susceptibility in *air12-1* seedlings (Figure 4.44). The increased localization of fusion protein in the primary and lateral roots of *Ds pAIR12::GFP-AIR12* seedlings implies that AIR12 acts in multiple pathways during the abiotic stress response including salinity and osmotic stress, and is affected by the stress-regulating hormone ABA. Development of lateral roots in *air12-1* seedlings is more severely affected under salinity stress than osmotic stress. Additionally, plant development in response to ABA appears to occur in two stages: increased sensitivity during germination and reduced sensitivity during vegetative development. Given that AIR12 appears to interact with ABA-specific and

nonspecific stress responses during root development, and that ABA, auxin, and abiotic stress responses all utilize ROS, AIR12 may act at an intersection point of the three pathways; possibly at or close to the NOX enzyme complex based on enzymatic data from both the *air12-1* T-DNA knockout seedlings and AC plants.

Similar to *air12-1* seeds, AC seeds germinated more readily than wild type under saline conditions and were resistant to salinity during vegetative development (Figure 4.3). An increased catalase activity and reduced O_2^- in AC plants matched the patterns observed in *air12-1* mutants, supporting the hypothesis that these genes are involved in regulation of ROS in response to hormone or stress perceptions representing an intersection point at or near the NOX enzyme complex. From these data I conclude that *CIL1* is the *B. carinata* orthologue of Arabidopsis *AIR12*.

5.4 A model for AIR12/CIL1 GPI-APs in ROS signaling

Based on the evidence collected in this study I propose models describing how AIR12 and CIL1 functions during root development. The models outline the hormones (Figure 5.1) and stressors (Figures 5.2 and 5.3) used to initiate signal cascades followed by induction/repression of gene expression to control plant development.

During root development, auxin and ABA act as antagonists (De Smet et al., 2003; Deak and Malamy, 2005). *AIR12* and *CIL1* are auxin-responsive and increased auxin concentrations correlate with increased expression of these genes (Gibson, 2005; Laskowski et al., 2006; Lee et al., 2007; Chen et al., 2008). Root development of *air12-1* and AC plants show reduced sensitivity to ABA, suggesting that during normal development ABA inhibits AIR12 and CIL1 indirectly, though this has not been examined. Direct inhibition of AIR12 and CIL1 by ABA would likely result in much stronger inhibition of root development similar to a hormone receptor response such as with *tir1* auxin receptor (Dharmasiri et al., 2005a; Kepinsky et al., 2005) or *pyr* ABA receptor (Ma et al., 2009; Park et al., 2009) mutants . At this point, the pathway diverges, depending on whether an environmental stress is being perceived, which may alter ABA regulation of AIR12 and CIL1. Under non-stress conditions PLC biosynthetic activity is lower than during stress conditions (Figure 5.1). This will reduce the total amount of PLC available to cleave AIR12, CIL1, and other GPI-anchored proteins from their anchor. As a result, AIR12 and CIL1 localize to the extracellular leaflet of the plasma membrane, bound to their

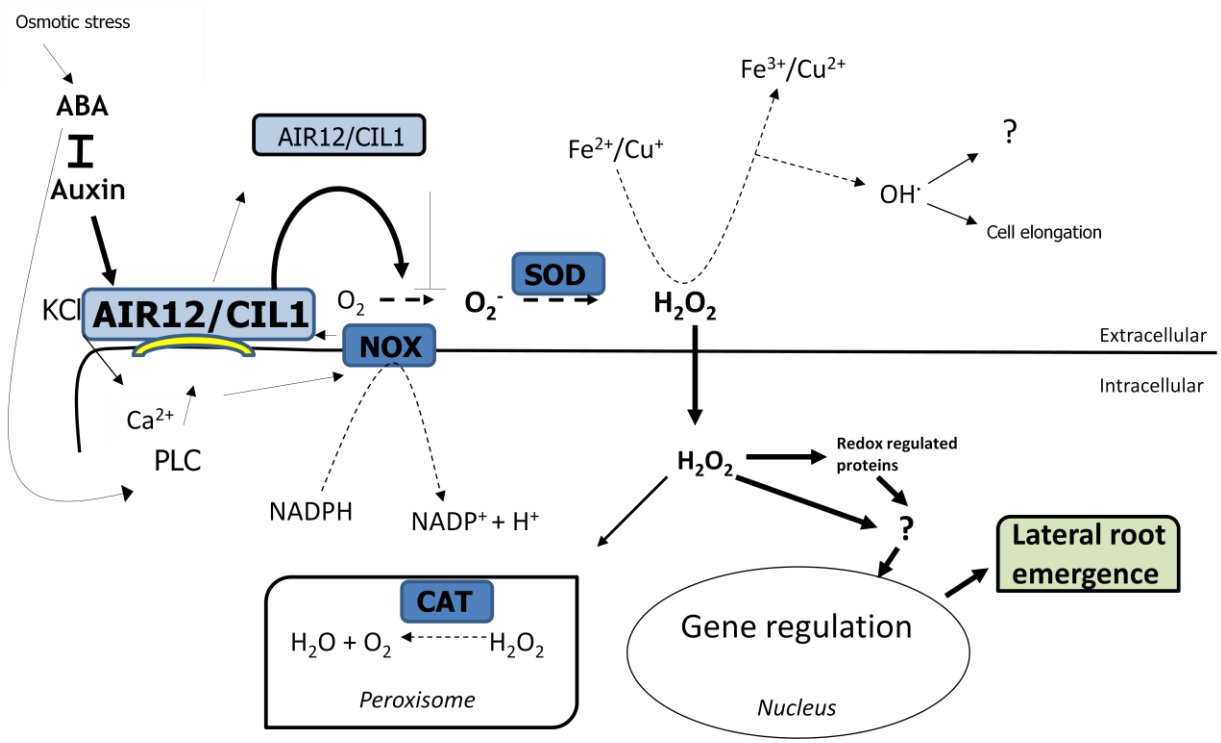

Figure 5.1. Hypothetical model describing interactions between ABA and auxin that show the early signaling and downstream signal transduction regulating AIR12 and CIL1 that in turn regulate lateral root emergence. Under normal developmental conditions, AIR12/CIL1 bound at the plasma membrane increases NOX and SOD, culminating with production of $OH^·$ radicals by Fenton reactions that break cross-links in cell walls. Hydrogen peroxide, acting as a membrane diffusible signal, may cross the plasma membrane to trigger gene regulation. NOX, NADPH oxidase; SOD, superoxide dismutase; CAT, catalase.

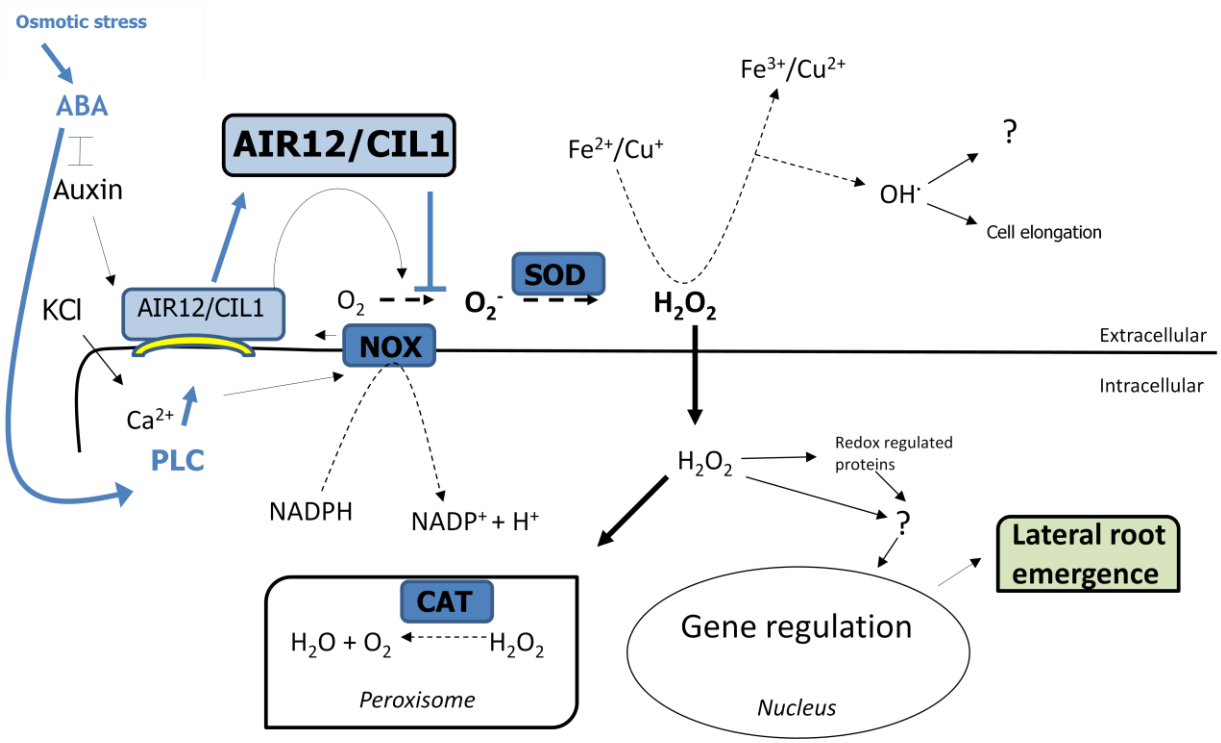

Figure 5.2. Hypothetical model describing early signaling and downstream signal transduction regulating AIR12/CIL1. Osmotic or nitrogen stress increase ABA accumulation and activate ABA signaling pathways resulting in PLC biosynthesis which can cleave GPI-APs from the plasma membrane. Released AIR12/CIL1 would then interact with NOX and SOD, reducing enzyme activity and preventing lateral root emergence.

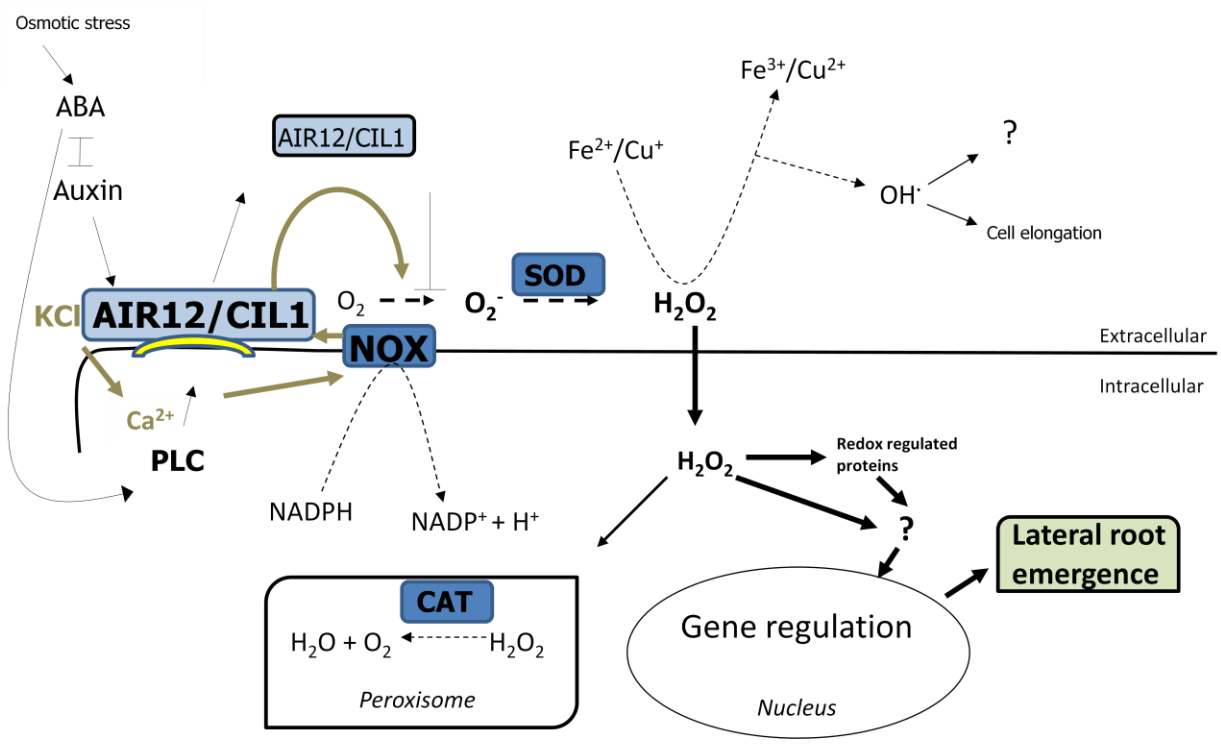

Figure 5.3. Hypothetical model describing early and downstream signaling in response to a salt stress. After perception of a salt stress, Ca^{2+} activates/stabilizes NOX, increasing O_2^- production. Increased NOX activity may in turn feedback into AIR12, perhaps increasing transcription, allowing AIR12/CIL1 to associate with NOX and SOD to enhance lateral root initiation or elongation. An intracellular component likely proceeds through membrane transmissible H_2O_2 signals causing shifts in gene regulation toward salt resistance, further increasing salt tolerance.

GPI-anchor. Under normal developmental conditions *air12-1* roots displayed reductions in O_2^- and catalase activity (Figures 4.50 and 4.54), and AC leaves displayed reductions in O_2^- and NOX activity (Figure 4.4). From these data, it appears as though AIR12 and CIL1 may be required to maintain extracellular ROS, specifically O_2^- at some above-threshold level that results in lateral root initiation or elongation. The effect of AIR12 and CIL1 on catalase activity is compelling; how do AIR12 and CIL1, extracellular proteins, affect catalase, an intracellular enzyme compartmentalized in peroxisomes? It seems likely that in this model, the reduction in catalase activity is an indirect result of reduced extracellular O_2^- accumulation and SOD activity, leading to a lower concentration of the membrane-transmissible H_2O_2. Because of this, I suggest that the overall effect of AIR12 and CIL1 on development is to positively regulate lateral root emergence or elongation. A possible intersection point between hormonal and ROS pathways lies with the NOX enzyme complex, which converts extracellular O_2 to O_2^- using intracellular NADPH (Sagi and Fluhr, 2006). Following this conversion, O_2^- is dismuted by extracellular SOD, evidence for which has been found in developing cotton fibers (Kim et al., 2008), resulting in H_2O_2. H_2O_2 then interacts with free Fe^{2+}/Cu^+ in the cell wall (Becker et al., 1995) forming $OH^\cdot$ radicals through Fenton reactions (Halliwell and Gutteridge, 1992). Extracellular hydroxyl radicals, being short-lived signal molecules likely act along with cell wall permeases during lateral root emergence (Swarup et al., 2008) to break cross-linked glycans in the cell wall (Schopfer, 2002; Liszkay et al., 2004) or possibly act alone to break cross-linked glycans in the cell walls of elongation lateral roots. Alternatively, H_2O_2 could diffuse across the plasma membrane (Levine et al., 1994) where it may interact with free cytosolic Fe^{2+}/Cu^+ forming $OH^\cdot$ to regulate gene expression and control lateral root initiation or can be detoxified by cellular catalases. This hypothesized branch of the model imposes several difficulties however; H_2O_2 is normally detoxified in peroxisomes (Oshima et al., 2008), while iron and copper sequestration is under tight control in chloroplasts, mitochondria, and the vacuole (Palmer and Guerinot, 2009). Under physiologically normal conditions it seems unlikely that H_2O_2 would be exposed to intracellular iron or copper, reducing the likelihood of gene regulation by intracellularly-derived $OH^\cdot$. Additionally, detoxification of intracellular H_2O_2 may occur through a hypothesized cytosolic catalase (Beffagna and Lutzu, 2007) though it is more likely detoxified solely through peroxisomal catalase. It is possible that the produced H_2O_2 could interact with proteins that form

disulfide bonds through cysteine groups, similar to the acylphosphatase in vertebrate muscles that dimerizes after exposure to hydrogen peroxide (Paoli et al., 2001). Oxidizing disulfide bonds of cysteine-containing proteins such as transcription factors could activate gene transcription leading to transcription of genes involved in lateral root emergence or elongation similar to the activation of the NPR-TGA1 system in Arabidopsis by nitric oxide to activate the plant defence responses system (Lindermayr et al., 2010). Alternatively, H_2O_2 may activate gene regulatory pathways through an as of yet undescribed mechanism, perhaps similar to how NOX-derived H_2O_2 was hypothesized to function during salt stress (Chung et al., 2008). From the examination of both *Ds* and *air12-1* seedlings transformed with *pAIR12::GFP-AIR12* it seems that some basal level of AIR12 is required either for increased *AIR12* expression or increased AIR12 production. Perhaps this occurs through AIR12 positively regulating its own expression, leading to direct AIR12 translation in the vascular tissue.

Exposure to abiotic stressors can cause remobilization of plant resources to ensure plant survival. Integral to the proper response to environmental challenges is intact ABA signaling (Mahajan and Tuteja, 2005; Munns and Tester, 2008 and references therein; Cousson, 2009). *air12* and AC seedlings showed reduced responses to abiotic stressors (Figures 4.2, and 4.32). From the abiotic stress experiments two different response pathways became apparent and depended on whether the challenge applied was a saline one or not. Regardless of the perceived stress both models rely on the hypothesis that AIR12 and CIL1 have either reduced activity when anchored to the extracellular leaflet of the plasma membrane compared to the free form, or that the proteins function differently when bound. In the case of a non-saline challenge, ABA accumulates at the site of osmotic or nitrogen accumulation (Nambara and Marion-Poll, 2005) followed by activation of ABA signal cascades (Verslues and Zhu, 2007) proceeding through the ABI protein phosphatase 2Cs (Finkelstein et al., 2002). Growth of *Ds* seedlings on medium containing nitrogen, mannitol, or 100 mM sucrose resulted in reduced mean cumulative lateral root length (Figures 4.47-4.49) and did not affect root length lateral or primary root number (Figures 4.35 and 4.44). Furthermore, sucrose and mannitol had no effect on *air12-1* mean cumulative lateral root length (Figures 4.47-4.49), suggesting that AIR12 is involved with either emergence or elongation of lateral roots during osmotic stressors. Interestingly, 100 mM sucrose had a positive effect on *air12-1* mean cumulative lateral root length, significantly increasing elongation (Figure 4.49) demonstrating that *air12-1* seedlings respond opposite of *Ds* seedlings,

which displayed large reductions in mean cumulative lateral root length relative to seedlings grown on control medium. One component of ABA signaling is the activation of messengers such as phytate via PLC that increase accumulation of Ca^{2+} resulting in the activation of phosphorylation/dephosphorylation cascades and calmodulin accumulation (Munnik and Testerink, 2009). In addition, PLC cleaves certain GPI-APs inserted in the outer leaflet of the plasma membrane from their anchor, releasing these proteins into the apoplast (Borner et al., 2003). Release of AIR12/CIL1 from the plasma membrane may allow the proteins to interact with NOX, either directly or indirectly, decreasing its activity. As a result, the rate of extracellular O_2^- production would be reduced, decreasing available H_2O_2 to interact with Fe^{2+} and Cu^+ in the cell wall. The reduction in H_2O_2 would also decrease the oxidation cystein-containing proteins by H_2O_2, thereby limiting lateral root emergence or elongation (Figure 5.2). The question remains: why would a plant decrease lateral root development during osmotic stress? During an osmotic stress, dicotyledenous plants such as Arabidopsis may invest more of their resources into primary root growth to grow away from the source of osmotic stress. Once a suitable location is reached, lateral root development would then resume, minimizing the expended energy to escape the osmotic stress.

In *air12-1* seedlings and AC plants, the response to salt stress appeared to be additive with ABA responses and may proceed through a third pathway (Figure 5.3). The ABA-dependent pathway proceeds as previously described. As outlined by Chung et al. (2008), ABA-independent salt perception results in Ca^{2+} mobilization to NOX, activating or stabilizing the complex, resulting in extracellular conversion of O_2 to O_2^-. The significant decrease in *air12-1* lateral root production upon growth in KCl (Figure 4.44) strongly suggests as with normal development, that NOX activity increases, and promotes the generation of hydroxyl radicals accelerating lateral root initiation and emergence. AIR12 may increase SOD activity as well, further accelerating lateral root development to escape stressful conditions. At the same time, the increased O_2^- generated by NOX would be able to synergistically increase *SOS1* stability leading to the production and activation of the Na^+/H^+ antiporter (Chung et al., 2008). A further possibility is that salt stress incorporates both extracellular and intracellular cascades. Intracellular signals mediated by H_2O_2 could result in oxidation of cysteine-containing proteins forming disulfide bonds, leading to protein activation and increased transcription of genes involved in lateral root initiation or emergence, causing a shift in metabolism toward the

production of compounds such as proline that raise the water potential of the plant (Verslues and Bray, 2006) or remove salt from cells (Chung et al., 2008).

The above models are predictions based on available data but could be validated using a number of methods. Enzymatic assays examining NOX and SOD activity in control and *air12* mutant plants in stress, non-stress conditions as well as following growth on hormones would provide increased support for the proposed models. Examination of lateral root development and response to abiotic stressors could also be examined in *air12*/*rboh* (*respiratory burst oxidative homologue*) double mutants, to determine if AIR12 acts before or after NOX in extracellular O_2^- generation. Treatment of control and *air12* plants with the NOX inhibitor diphenylene iodonium (DPI; Bedard and Crause, 2007) would yield additional information regarding at what position AIR12 acts in relation to NOX in the generation of extracellular ROS. As well, yeast two-hybrid analysis using systems designed for use with membrane proteins could reveal interacting proteins. Following yeast two-hybrid, co-immunoprecipitation could be conducted to confirm AIR12-interacting proteins *in planta*.

5.5 Significance

The results described in this study represent the first description of two plant glucosylphosphatidylinositol-anchored proteins involved in root development, seed germination, and abiotic stress response. Furthermore, these results lead to the hypothesis that there is an intersection point between auxin and ABA signaling during root development and the response to abiotic stressors and that this intersection point is dependent on the generation of extracellular O_2^-. Within the past three years, focus on uncharacterized auxin-responsive genes thought to be involved with lateral root development identified *AIR12* as a gene of possible interest (De Smet et al., 2006b). This research advances knowledge of how hormonal signals integrate with ROS signals to direct lateral root development in dicotyledenous plants.

6. CONCLUSIONS

In plants, roots represent the major organ used for both water and mineral uptake. Despite the tremendous advances over the past decade in understanding how roots develop, we still do not understand how interplay between plant hormones modulates the myriad signals present in cells to regulate development. This study focused on two uncharacterized genes: *AIR12* and *CIL1* from Arabidopsis and *B. carinata*, respectively, and their role as glucosylphosphatidylinositol-anchored proteins in root development. Loss-of-function mutation of *AIR12* and reduction of *CIL1* transcript by antisense technology resulted in plants that produced a reduced number of lateral roots with reduced length, reduced sensitivity to the hormones auxin and abscisic acid, and displayed reduced responses to abiotic stressors. Ectopic expression of *p35S::GFP-AIR12* or *p35S::GFP-CIL1* in stably transformed Arabidopsis showed fusion protein at the cell margins in leaves and roots. After treatment with NaCl or sorbitol, the fusion proteins localized to the plasma membrane and apoplast, showing they were extracellular. At the organ level, GFP-AIR12 fusion protein was present in the epidermis of primary and lateral root tips in the meristematic zone, localizing at the subcellular level to the margins in stably transformed *pAIR12::GFP-AIR12* Arabidopsis. The majority of root tips contained a zone of exclusion, where fusion protein was absent. The results suggest the fusion protein is either synthesized within the vascular tissue of the primary root or translocated into the vasculature of the primary root and transported toward sites of lateral root emergence and/or elongation. Further, AIR12 and CIL1 may act to promote lateral root initiation, emergence, and elongation during normal development and salt stress, while inhibiting elongation and emergence during osmotic stress. From this study, the following conclusions can be drawn:

1. AIR12 and CIL1 are extracellular proteins that function in lateral root development.
2. *AIR12* and *CIL1* are orthologous genes in Arabidopsis and *B. carinata*, respectively.
3. AIR12 is present at the margins of epidermal cells of both the primary and lateral root tips restricted specifically to the meristematic zone.
4. GFP-AIR12 fusion protein accumulates both in the meristematic zone of the primary root and in the vascular tissue of the differentiation and elongation zones.

Prior to this study, the involvement of AIR12 and CIL1 in root development was unknown. These results show that extracellular proteins can not only affect lateral root development, but that they also play a role in the responses to abiotic stressors. Prior to this study, AIR12 localization during root development was unknown. This study adds another piece to the network of proteins integral for auxin-mediated lateral root development.

Furthermore, both developmental and stress response pathways appear to involve a suite of ROS, both intracellular and extracellular in origin. These signals from different pathways are then integrated togther to modulate root development. Involvement of signals downstream of hormone perception is not well understood. This study provides evidence that AIR12, an extracellular protein acts downstream of hormone perception and mediates ROS signals to drive lateral root development.

7. FUTURE DIRECTIONS

Though the initial work has been completed proposing how AIR12 and CIL1 interact with plant hormones and extracellular ROS, much work remains to completely describe the function of these proteins. As outlined above, the proposed models could be experimentally validated through a combination of enzymatic analysis, inhibitor treatments, yeast two-hybrid, and *air12/rboh* double mutant analysis. To characterize the activity of enzymes involved in ROS generation and detoxification, NOX and SOD activity could be confirmed by isolating plasma membranes and apoplastic fluid, respectively, from primary and lateral roots during normal development and abiotic stress treatment. Further work could focus on identification of AIR12-interacting proteins, using yeast two-hybrid or co-immunoprecipitation. *In vitro* interactions could be validated by raising antibodies to AIR12 and conducting co-immunoprecipitation assays or by a pull down assay using the *p35S::GFP-AIR12* stably transformed Arabidopsis plants with GFP-specific antibodies.

To determine if localization of GFP-AIR12 to the vascular tissue was the result of tissue-specific expression or translocation, additional transcript profiling could be completed using stably transformed *pAIR12::GFP* lines that would be more sensitive than GUS-staining of activation or enhancer tagged *air12* mutants because of the proximity of the *AIR12* promoter to the reporter gene. Examination of AIR12 and auxin interactions could be completed by co-localizing auxin patterning using a *pDR5::mCherry*/*pAIR12::GFP* or *pDR5::mCherry*/*pAIR12::GFP-AIR12* with either the *AIR12* transcript or AIR12 protein, respectively. Data from these experiments would test whether auxin patterning has a direct effect on *AIR12* expression or AIR12 production. Ultimately, knowledge of how AIR12 acts during lateral root development and in abiotic stress responses will contribute to our understanding of how roots develop and why certain environmental conditions impede development more than others.

8. REFERENCES

Abel S and Theologis A, 1995. A polymorphic bipartite motif signals nuclear targeting of early auxin-inducible proteins related to PS-IAA4 from pea (*Pisum sativum*). Plant J. 8:87-96.

Abel S and Theologis A, 1996. Early genes and auxin action. Plant Physiol. 111:9-17.

Able AJ, Guest DI, and Sutherland MW, 1998. Use of a new tetrazolium-based assay to study the production of superoxide radicals by tobacco cell cultures challenged with avirulent zoospores of *Phyophthora parasitica* var *nicotianae*. Plant Physiol. 117: 491-499.

Aida M, Ishida T, Fukaki H, Fujisawa H, and Tasaka M, 1997. Genes involved in organ separation in Arabidopsis: an analysis of the cup-shaped cotyledon mutant. Plant Cell 9:841-857.

Addicott FT, Lyon JL, Ohkuma K, Thiessen WE, Carns HR, Smith OE, Cornforth JW, Milborrow BV, Ryback G, and Wareing PF, 1968. Abscisic acid: a new name for abscisin II (dormin). Science 159:1493.

Ainley WM, Walker JC, Nagao RT, and Key JL, 1988. Sequence and characterization of two auxin-regulated genes from soybean. J. Biol. Chem. 263:10658-10666.

Ali-Rachedi S, Bouinot D, Wagner M, Bonnet M, Sotta B, Grappin P, and Jullien M, 2004. Changes in endogenous abscisic acid levels during dormancy release and maintenance of mature seeds: studies with the Cape Verde Islands ecotype, the dormant model of Arabidopsis. Planta 219:479-488.

Alscher RG, Donahue JL, and Crammer CL, 1997. Reactive oxygen species and antioxidants: relationships in green cells. Physiol. Plant. 100:224-233.

Anderson RGW, 1993. Caveolae: where incoming and outgoing messengers meet. Proc. Natl. Acad. Sci. USA 90:10909-10913.

Arakawa N, Tsutsumi K, Sanceda NG, Kurata T, and Inagaki C, 1981. A rapid and sensitive method for the determination of ascorbic acid using 4,7-diphenyl-1,10-phenathroline. Agric. Biol. Chem. 45:1289-1290.

Aravind L, 2001. DOMON: an ancient extracellular domain in dopamine beta-monooxygenase and other proteins. Trends Biochem. Sci. 26:524–526.

Asada K, 2006) Production and scavenging of reactive oxygen species in chloroplasts and their functions. Plant Physiol. 141:391-396.

Bai C, Sen P, Hofmann K, Ma L, Goebl M, Harper JW, and Elledge SJ, 1996. SKP1 connects cell cycle regulators to the ubiquitin proteolysis machinery through a novel motif, the F-box. Cell 86:263-274.

Bainbridge K, Guyomarc'h S, Bayer E, Swarup R, Bennett M, Mandel T, and Kuhlemeier C, 2008. Auxin influx carriers stabilize phyllotactic patterning. Genes Dev. 22:810-823.

Baker CJ and Orlandi EW, 1995. Active oxygen in plant pathogenesis. Annu. Rev. Phytopathol. 33:299-321.

Ballas N, Wong LM, and Theologis A, 1993. Identification of the auxin-responsive element, AuxRE, in the primary indoleacetic acid-inducible gene, PS-IAA4/5, of pea (Pisum sativum). J. Mo1. Biol. 233: 580-596.

Bashandy T, Guilleminot J, Vernoux T, Caparros-Ruiz D, Ljung K, Meyer Y, and Reichheld J-P, 2010. Interplay between the NADPH-linked thioredoxin and glutathione systems in *Arabidopsis* auxin signaling. Plant Cell 22:376-391.

Bartel B, LeClere S, Magidin M, and Zolman BK, 2001. Inputs to the active indole-3-acetic acid pool: de novo synthesis, conjugate hydrolysis, and indole-3-butyric acid β-oxidation. J. Plant Growth Regul. 20:198-216.

Bedard K and Krause K-H, 2007. The NOX family of ROS-generating NADPH oxidases: physiology and pathophysiology. Phyiol. Rev. 87:245-313.

Beemster GTS, Fiorani F, and Inzé D, 2003. Cell cycle: The key to plant growth control? Trends Plant Sci. 8:154–158.

Beck E, Fettig S, Knake C, Hartig K, and Bhattarai T, 2007. Specific and unspecific responses of plants to cold and drought stress. J. Biosci. 32:501-510.

Bendtsen J D, Nielsen H, von Heijne G, and Brunak S, 2004. Improved prediction of signal peptides: SignalP 3.0. J. Mol. Biol. 340:783–795.

Benjamins R and Scheres B, 2008. Auxin: the looping star in plant development. Ann. Rev. Plant Biol. 59:443-465.

Bennett SRM, Alvarez J, Bossinger G, and Smyth DR, 1995. Morphogenesis in *pinoid* mutants of Arabidopsis. Plant J. 8:505–520.

Bennett MJ, Marchant A, Green HG, May ST, Ward SP, Millner PA, Walker AR, Schulz B, and Feldmann KA, 1996. Arabidopsis AUX1 gene: a permease-like regulator of root gravitropism. Science 273:948-950.

Bethke PC and Jones RL, 2001. Cell death of barley aleurone protoplasts is mediated by reactive oxygen species. Plant J. 25:19-29.

Bhalerao RP, Eklöf J, Ljung K, Marchant A, Bennett M, Sandberg G, 2002. Shoot-derived auxin is essential for early lateral root emergence in Arabidopsis seedlings. Plant J. 29: 325–332.

Bhat RA and Panstruga R, 2005. Lipid rafts in plants. Planta 223, 5-19.

Bialek K and Cohen JD, 1989. Free and conjugated indole-3-acetic acid in developing bean seeds. Plant Physiol. 91:775-779.

Blatt MR, and Grabov A, 1997. Signalling gates in abscisic acid-mediated control of guard cell ion channels. Physiol. Plant. 100:481–490.

Blilou I, Xu J, Wildwater M, Willemsen V, Paponov I, Friml J, Heldstra R, Aida M, Palme K, and Scheres B, 2005. The PIN auxin efflux facilitator network controls growth and patterning in Arabidopsis roots. Nature 433:39-44.

Boccuni P, Del Vecchio L, Di Noto R, and Rotoli B, 2000. Glycosyl phosphatidylinositol (GPI)-anchored molecules and the pathogenesis of paroxysmal nocturnal hemoglobinuria. Crit. Rev Onc/Hem. 33:25-43.

Boerjan W, Cervera MT, Delarue M, Beeckman T, Dewitte W, Bellini C, Caboche M, Van Onckelen H, Van Montagu M, and Inzé D, 1995. superroot, a recessive mutation in Arabidopsis, confers auxin overproduction. Plant Cell 7: 1405-1419.

Borner GH, Sherrier DJ, Stevens TJ, Arkin IT, and Dupree P, 2002. Prediction of glycosylphosphatidylinositol-anchored proteins in Arabidopsis. A genomic analysis. Plant Physiol. 129:486-499.

Borner GH, Lilley KS, Stevens TJ, and Dupree P, 2003. Identification of glycosylphosphatidylinositol-anchored proteins in Arabidopsis. A proteomic and genomic analysis. Plant Physiol. 132:568-577.

Borner GH, Sherrier DJ, Weimar T, Michaelson LV, Hawkins ND, Macaskill A, Napier JA, Beale MH, Lilley KS, and Dupree P, 2005. Analysis of detergent-resistant membranes in Arabidopsis. Evidence for plasma membrane lipid rafts. Plant Physiol. 137:104-116.

Borsani O, Zhu J, Verslues PE, Sunkar R, and Zhu JK, 2005. Endogenous siRNAs derived from a pair of natural cisantisense transcripts regulate salt tolerance in Arabidopsis. Cell 123:1279–1291.

Bowler C, Slooten L, Vandenbranden S, De Rycke R, Botterman J, Sybesma C, Van Montagu M, and Inzé D, 1991. Manganese superoxide dismutase can reduce cellular damage mediated by oxygen radicals in transgenic plants. EMBO J. 10:1723–1732.

Boysen-Jensen P, 1913. Uber die leitung des phototropischen reizes in der Avenakoleoptile. Ber Deut Bot Ges 31:559-566.

Blakely LM, Durham M, Evans TA, and Blakely RM, 1982. Experimental studies on lateral root formation in radish seeling roots. I. General methods, developmental stages, and spontaneous formation of laterals. Bot. Gaz. 143: 341–352.

Brady SM, Sarkar SF, Bonetta D, and McCourt P, 2003. The Abscisic Acid Insensitive 3 (ABI3) gene is modulated by farnesylation and is involved in auxin signaling and lateral root development in Arabidopsis. Plant J. 34:67–75.

Brady SM, Orlando DA, Lee J-Y, Wang JY, Koch J, Dinneny JR, Mace D, Ohler U, and Benfey PN, 2007. A high-resolution root spatiotemporal map reveals dominant expression patterns. Science 2:801-806.

Braun N, Wyrzykowska J, Muller P, David K, Couch D, Perrot-Rechenmann C, and Fleming AJ, 2008. Conditional Repression of AUXIN BINDING PROTEIN1 Reveals That It Coordinates Cell Division and Cell Expansion during Postembryonic Shoot Development in Arabidopsis and Tobacco. Plant Cell 20:2746-2762.

Brown DA, and Rose JK, 1992. Sorting of GPI-anchored proteins to glycolipid-enriched membrane subdomains during transport to the apical cell surface. Cell 68:533-544.

Cambridge AP and Morris DA, 1996. Transfer of exogenous auxin from the phloem to the polar auxin transport pathway in pea (*Pisum sativum* L.). Planta 199**:** 583-588.

Campbell GS, 1977. Growth hormone signal transduction, J. Ped. 131: 42–44.

Capell T, Bassie L, and Christou P, 2004. Modulation of the polyamine biosynthetic pathway in transgenic rice confers tolerance to drought stress, Proc. Natl. Acad. Sci. U.S.A. 101:9909–9914.

Carol RJ and Dolan L, 2006. The role of reactive oxygen species in cell growth: Lessons from root hairs. J. Exp. Bot. 57:1829–1834.

Casimiro I, Marchant A, Bhalerao RP, Beeckman T, Dhooge S, Swarup R, Graham N, Inze D, Sandberg G, Casero PJ, and Bennett M, 2001. Auxin transport promotes Arabidopsis lateral root initiation. Plant Cell 13:843-852.

Casano LM, Lascano HR, and Trippi VS, 1994. Hydroxyl radicals and a thylakoid-bound endopeptidase are involved in a light- and oxygen-induced proteolysis in oat chloroplasts, Plant Cell Physiol. 35:145–152.

Charles SA, and Halliwell B, 1981. Light activation of fructose bisphosphatase in isolated spinach chloroplasts and deactivation by hydrogen peroxide. A physiological role for the thioredoxin system. Planta 151, 242–246.

Chatterjee S and Mayor S, 2001. The GPI-anchor and protein sorting. Cell. Mol. Life. Sci. 58:1969-1987.

Chehab EW, Eich E, and Braam J, 2009. Thigmomorphogenesis: a complex plant response to mechano-stimulation. J. Exp. Bot. 60:43-56.

Chen JG, Ullah H, Young JC, Sussmann MR, Jones AM, 2001. ABP1 is required for organized cell elongation and division in Arabidopsis embryogenesis. Genes Dev.15:902–911.

Chen H, Zhang J, Neff MM, Hong SW, Zhang H, Deng XW, and Xiong L, 2008. Integration of light and abscisic acid signaling during seed germination and early seedling development. Proc. Natl. Acad. Sci. USA 105:4495-4500.

Christian M, Hannah WB, Luthen H, and Jones AM, 2008. Identification of auxins by a chemical genomics approach. J. Exp. Bot. 59:2757-2767.

Chung JS, Zhu JK, Bressan RA, Hasegawa PM, and Shi H, 2008. Reactive oxygen species mediate Na+-induced SOS1 mRNA stability in Arabidopsis. Plant J. 53:554-565.

Clough S and Bent AF, 1998. Floral dip: a simplified method for Agrobacterium-mediated transformation of Arabidopsis. Plant J. 16: 735-743.

Cosgrove DJ, 2000. Loosening of plant cell walls by expansins. Nature 407:321–326.

Coruzzi G and Last RL, 2000. Amino acids. In BB Buchanan, W Gruissem, and RL Jones (Eds.), Biochemistry and molecular biology of plants (pp.358-401), Rockville, USA: American Society of Plant Physiologists.

Cousson A, 2009. Involvement of phospholipase C-independent calcium-mediated abscisic acid signalling during Arabidopsis response to drought. Biologia Plantarum 53:53-62.

Crozier A, Kamiya Y, Bishop G, and Yokota T, 2000. Biosynthesis of hormones and elicitor molecules. In BB Buchanan, W Gruissem, and RL Jones (Eds.), Biochemistry and molecular biology of plants (pp. 850-901), Rockville, USA: American Society of Plant Physioloists.

Darwin CR, 1880. The power of movement in plants. London: Murray.

Damveld RA, Arentshorst M, VanKuyk PA, Klis FM, vand den Hondel CAMJJ, and Ram AFJ, 2005. Characterisation of CwpA, a putative glucosylphosphatidylinositol-anchored cell wall mannoprotein in the filamentous fungus Aspergillus niger. Fungal Genet. Biol. 42:873-885.

Dasharath Prasad L, Jennifer ES, James GL, Joseph JK, Kristin DB, and David Mc KB, 2004. Cytokinins play opposite roles in lateral root formation, and nematode and Rhizobial symbioses. Plant J. 38:203-214.

Datla RSS, Bekkaoui F, Hammerlindl JK, Pilate G, Dunstan DI, and Crosby WL, 1993.

Improved high-level constitutive foreign gene expression in plants using an AMV RNA4 untranslated leader sequence. Plant Sci. 94:139-149.

Datla RSS, Hammerlindl JK Panchuk B, Pelcher LE, and Keller W, 1992. Modified binary plant transformation vectors with the wild-type gene encoding NPTII. Gene 122:383-384.

De Groot, PW, Ram AF, and Klis FM, 2005. Features and functions of covalently linked proteins in fungal cell walls. Fungal Genet. Biol. 42:657-675.

DeRidder BP, Dixon DP, Beussman DJ, Edwards R, and Goldsbrough PB, 2002. Induction of glutathione S-transferases in Arabidopsis by herbicide safeners. Plant Physiol. 130: 1497-1505.

De Smet I, Signora L, Beeckman T, Inze D, Foyer CH, and Zhang H, 2003. An abscisic acid-sensitive checkpoint in lateral root development of Arabidopsis. Plant J. 33:543-555.

De Smet I, Vanneste S, Inzé D, Beeckman T, 2006a. Lateral root initiation or the birth of a new meristem. Plant Mol. Biol. 60:871–887.

De Smet I, Zhang H, Inzé D, and Beeckman T, 2006b. A novel role for abscisic acid emerges from underground. Trends Plant Sci. 11: 434-439.

De Smet I, Tetsumura T, De Rybel B, Frey NF, Laplaze L, Casimiro I, Swarup R, Naudts R, Vanneste S, Audenaert D, Inzé D, Bennett MJ, and Beeckman T, 2007. Auxin-dependent regulation of lateral root positioning in the basal meristem of Arabidopsis, Development 134:681–690.

Deak KI and Malamy J, 2005. Osmotic regulation of root system architecture. Plant J. 43:17-28.

Dellaporta SL, Wood J, and Hicks JB, 1983. A plant DNA minipreparation: version II. Plant Mol. Biol. Rep. 1:19-21.

Dengler NG and Kang J, 2001. Vascular patterning and leaf shape. Curr. Op. Plant Biol. 4:50-56.

Deshaies RJ and Jacks T, 1999. Cell multiplication peering in and peering out: regulation of and by the cell cycle. Curr. Op. Cell Biol. 11:705-707.

Dharmasiri S and Estelle M, 2002. The role of regulated protein degradation in auxin response. Plant Mol. Biol. 49, 401–409.

Dharmasiri N, Dharmasiri S, and Estelle M, 2005a. The F-box protein TIR1 is an auxin receptor. Nature 435:441-445.

Dharmasiri N, Dharmasiri S, Weijers D, Lechner E, Yamada M, Hobbie L, Ehrismann JS, Jürgens G, and Estelle M, 2005b. Plant development is regulated by a family of auxin receptor F Box proteins. Dev. Cell 9:109-119.

Dhonukshe P, Aniento F, Hwang I, Robinson DG, Mravec J, Stierhof Y-D, and Friml J, 2007. Clathrin-mediated constitutive endocytosis of PIN auxin efflux carriers in Arabidopsis. Curr. Biol. 17:520-527.

Dolan L, Janmaat K, Willemsen V, Linstead P, Poethig S, Roberts K, and Scheres B, 1993. Cellular organisation of the Arabidopsis root. Development 119:71-84.

Drazkiewicz M, Skorzynska-Polit E, and Krupa Z, 2007. The redox state and activity of superoxide dismutase classes in Arabidopsis under cadmium or copper stress. Chemosphere 67:188-193.

Dubrovsky JG, Sauer M, Napsucialy-Mendivil S, Ivanchenko MG, Friml J, Shishkova S, Celenza J, and Benkova E, 2008. Auxin acts as a local morphogenetic trigger to specify lateral root founder cells. Proc. Natl. Acad. Sci. USA 105:8790-8794.

Eagles CF and Wareing PF, 1964. The role of growth substances in the regulation of bud dormancy. Physiol. Plant. 34:201–203.

Eisenhaber B, Bork P, and Eisenhaber F, 1998. Sequence properties of GPI-anchored proteins near the omega-site: Constraints for the polypeptide binding site of the putative transamidase. Protein Eng. 11:1155-1161.

Eisenhaber B, Bork P, and Eisenhaber F, 1999. Prediction of potential GPI-modification 16 sites in proprotein sequences. J. Mol. Biol. 292:741-758.

Eisenhaber F, Eisenhaber B, Kubina W, Maurer-Stroh S, Neuberger G, Schneider G and Wildpaner M, 2003. Prediction of lipid posttranslational modifications and localization signals from protein sequences: Big-pi, nmt and pts1. Nucleic Acids Res. 31:3631-3634.

Elortza F, Mohammed S, Bunkenborg J, Foster LJ, Nuhse TS, Brodbeck U, Peck SC, and Jensen ON, 2006. Modification-specific proteomics of plasma membrane proteins: identification and characterization of glycosylphosphatidylinositol-anchored proteins released upon phospholipase D treatment. J. Prot. Res. 5:935-943.

Evans RJ, Derkach V, and Surprenant A, 1992. ATP mediates fast synaptic transmission in mammalian neurons. Nature 357: 503-505.

Evans ML, Ishikawa H, and Estelle MA, 1994. Responses of Arabidopsis roots to auxin studied with high temporal resolution: comparison of wild type and auxin response mutants. Planta 194:215-222.

Fankhauser N, Maser P, 2005. Identification of GPI anchor attachment signals by a Kohonen self-organizing map. Bioinformatics 21: 1846-1852.

Faure J, Lachenal G, Court M, Hirrlinger J, Chatellard-Causse C, Blot B, Grange J, Schoehn G, Goldberg Y, Boyer V, Kirchhoff F, Raposo G, Garin J, and Sadoul R, 2006. Exosomes are released by cultured cortical neurones. Mol. Cell. Neurosci. 31:642-648.

Fedoroff NV and Smith DL, 1993. A versatile system for detecting transposition in Arabidopsis. Plant J. 3:273-289.

Fink RC and Scandalios JG, 2002. Molecular evolution and structure--function relationships of the superoxide dismutase gene families in angiosperms and their relationship to other eukaryotic and prokaryotic superoxide dismutases. Arch. Biochem. Biophys. 399:19-36.

Finkelstein R and Somerville C, 1990. Three classes of abscisic acid (ABA)–insensitive mutations of Arabidopsis define genes that control overlapping subsets of ABA responses. Plant Physiol. 94:1172–1179.

Finkelstein RR, Gampala SSL, and Rock CD, 2002. Abscisic acid signaling in seeds and seedlings. Plant Cell 14:S15-S45.

Fontaine T, Smith TK, Crossman A, Brimacombe JS, Latge JP, and Ferguson MAJ, 2004. In vitro biosynthesis of glucosylphosphatidylinositol in *Aspergillus fumigatus*. Biochemistry 43:15267-15275.

Foreman J, Demidchik V, Bothwell JH, Mylona P, Miedema H, Torres MA, Linstead P. Costa S, Brownlee C, Jones JD, Davies JM, and Dolan L, 2003. Reactive oxygen species produced by NADPH oxidase regulate plant cell growth. Nature 422:442-446.

Freemont PS, 2000. Ubiquitination: RING for destruction? Curr. Biol. 10:R84-R87.

Friml J, Wisniewska J, Benkova E, Mendgen K, and Palme K, 2002a. Lateral relocation of auxin efflux regulator PIN3 mediates tropism in Arabidopsis. Nature 415L806-809.

Friml J, Benková E, Blilou I, Wisniewska J, Hamann T, Ljung K, Woody S, Sandberg G, Scheres B, Jürgens G, and Palme K, 2002b. AtPIN4 Mediates Sink-Driven Auxin Gradients and Root Patterning in Arabidopsis. Cell 108:661-673.

Friml J and Palme K, 2002. Polar auxin transport – old questions and new concepts? Plant Mol. Biol. Rep. 49:273-284.

Friml J, 2003. Auxin transport – shaping the plant. Curr. Op. Plant Biol. 6:7-12.

Friml J, Vieten A, Sauer M, Weijers D, Schwarz H, Hamann T, Offringa R, and Jurgens G 2003. Efflux-dependent auxin gradients establish the apical-basal axis of Arabidopsis. Nature 426:147-153.

Friml J, Yang,X, Michniewicz M, Weijers D, Quint A, Tietz O, Benjamins R, Ouwerkerk PBF, Ljung K, Sandberg G, Hooykaas PJJ, Palme K, and Offringa R, 2004. A PINOID-

Dependent Binary Switch in Apical-Basal PIN Polar Targeting Directs Auxin Efflux. Science 306:862-865.

Fujita Y, Fujita M, Satoh R, Maruyama K, Parvez MM, Seki M, Hiratsu K, Ohme-Takagi M, Shinozaki K, and Yamaguchi-Shinozaki K, 2005. AREB1 Is a Transcription Activator of Novel ABRE-Dependent ABA Signaling That Enhances Drought Stress Tolerance in Arabidopsis. Plant Cell 17:3470-3488.

Fukaki H, Tameda S, Masuda H, and Tasaka M, 2002. Lateral root formation is blocked by a gain-of-function mutation in the SOLITARY-ROOT/IAA14 gene of Arabidopsis. Plant J. 29: 153–168.

Fukaki H, Nakao Y, Okushima Y, Theologis A, Tasaka M (2005) Tissue-specific expression of stabilized SOLITARY-ROOT/IAA14 alters lateral root development in Arabidopsis. Plant J 44: 382–395.

Fukaki H and Tasaka M, 2009. Hormone interactions during lateral root formation. Plant Mol. Biol. 69:437-449.

Galinha C, Hofhuis H, Luijten M, Willemsen V, Blilou I, Heidstra R, and Scheres B, 2007. PLETHORA proteins as dose-dependent master regulators of Arabidopsis root development. Nature 449:1053–1057.

Gallagher KL, Paquette AJ, Nakajima K, and Benfey PN, 2004. Mechanisms regulating SHORT-ROOT intercellular movement. Curr. Biol. 14:1847–1851.

Galweiler L, Guan C, Muller A, Wisman E, Mendgen K, Yephremov A, and Palme K, 1998. Regulation of polar auxin transport by AtPIN1 in Arabidopsis vascular tissue. Science 282:2226-2229.

Garcia-Mata C, Gay R, Sokolovski S, Hills A, Lamattina L, and Blatt MR, 2003. Nitric oxide regulated K+ and Cl– channels in guard cells through a subset of abscisic acid-evoked signaling pathways. Proc. Natl. Acad. Sci. USA 100:11116–11121.

Gaspar TH, Kevers C, Faivre-Rampant O, Crevecoeur M, Penel CL, Greppin H, and Dommes J, 2003. Changing concepts in plant hormone action. In Vitro Cell Dev. Biol-Plant 39:85-106.

Geldner N, Friml J, Stierhof Y-D, Jurgens G, and Palme K, 2001. Auxin transport inhibitors block PIN1 cycling and vesicle trafficking. Nature 413:425-428.

Gibson SW, 2005. The role of CIL1 in Brassica carinata lateral meristem development. Master's thesis. University of Saskatchewan, Canada.

Gillmor CS, Lukowitz W, Brininstool G, Sedbrook JC, Hamann T, Poindexter P, and Somerville C, 2005. Glycosylphosphatidylinositol-anchored proteins are required for cell wall synthesis and morphogenesis in Arabidopsis. Plant Cell 17:1128-1140.

Goto N, Starke M, and Kranz AR, 1987. Effect of gibberellins on flower development of the*pin-formed* mutant ofArabidopsis. Arabidopsis Inf. Serv. 23 66–71.

Gray WM, del Pozo JC Walker L, Hobbie L, Risseeuw E, Banks T, Crosby WL, Yang M, Ma H, and Estelle M, 1999. Identification of an SCF ubiquitin-ligase complex required for auxin response in Arabidopsis. Genes Dev. 13: 1678–1691.

Gray WM, Kepinski S, Rouse D, Leyser O, and Estelle M, 2001. Auxin regulates SCFTIR1-dependent degradation of AUX/IAA proteins. Nature 414:271-276.

Grieneisen VA, Xu J, Maree AF, Hogeweg P, and Scheres B, 2007. Auxin transport is sufficient to generate a maximum and gradient guiding root growth. Nature 449:1008–1013.

Griffith OW, 1980. Determination of glutathione and glutathione disulfide using glutathione reductase and 2-vinylpyridine. Anal. Biochem. 106: 207-212.

Gonzalez-Carranza ZH, Elliott KA, and Roberts JA, 2007. Expression of polygalacturonases and evidence to support their role during cell separation processes in Arabidopsis. J. Exp. Bot. 58:3719–3730.

Guilfoyle T, Hagen G, Ulmasov T, and Murfett J, 1998. How does auxin turn on genes? Plant Physiol. 118:341-347.

Guilfoyle TJ and Hagen G, 2007. Auxin response factors. Curr. Op. Plant Biol. 10:453-460.

Guan LM and Scandalios JG, 2002. Catalase gene expression in response to auxin-mediated developmental signals. Physiol. Plant.114:288–295.

Guo D, Liang J, and Li L, 2009. Abscisic acid (ABA) inhibition of lateral root formation involves endogenous ABA biosynthesis in *Arachis hypogaea* L. Plant Growth Regul. 58:173-179.

Hagar H, Ueda N, Shah SV, 1996. Role of reactive oxygen metabolites in DNA damage and cell death in chemical hupoxic injury to LLC-PK1 cells. Am. J. Physiol. 271: 209-215.

Hagen G, Kleinschmidt A, and Guilfoyle T, 1984. Auxin-regulated gene expression in intact soybean hypocotyl and excised hypocotyl sections. Planta 162:147-153.

Hagen G, Martin G, Li Y, and Guilfoyle TJ, 1991. Auxin-induced expression of the soybean GH3 promoter in transgenic tobacco plants. Plant Mol. Biol. 17:567-579.

Halliwell B and Gutteridge JMC, 1984. Oxygen toxicity, oxygen radicals, transition metals and disease. Biochem. J. 219:1-14.

Halliwell B and Gutteridge JM, 1992. Biologically relevant metal ion-dependent hydroxyl radical generation. An update. FEBS Lett. 307:108-12.

Halliwell B, 2006. Reactive species and antioxidants. Redox biology is a fundamental theme of aerobic life. Plant Physiol. 141:312-322.

Hardtke CS, Ckurshumova W, Vidaurre DP, Singh SA, Stamatiou G, Tiwari SB, Hagen G, Guilfoyle TJ, Berleth T, 2004. Overlapping and non-redundant functions of the Arabidopsis auxin response factors MONOPTEROS and NONPHOTOTROPIC HYPOCOTYL 4. Development 131:1089–1100.

Havlová M, Dobrev PI, Motyka V, Štorchová H, Libus J, Dobrá J, Malbeck J, Gaudinová A, and Vanková R, 2008. The role of cytokinins in responses to water deficit in tobacco plants over-expressing trans-zeatin O-glucosyltransferase gene under 35S or SAG12 promoters. Plant Cell Environ. 31:341-353.

He XJ, Mu RL, Cao WH, Zhang ZG, Zhang JS, and Chen SY, 2005. AtNAC2, a transcription factor downstream of ethylene and auxin signaling pathways, is involved in salt stress response and lateral root development. Plant J. 44, 903-916.

Hetherington AM 2001. Guard cell signaling. Cell 107:711-714.

Henzler and Steudle E, 2000. Transport and metabolic degradation of hydrogen peroxide in Chara corallina: model calculations and measurements with the pressure probe suggest transport of H2O2 across water channels. J. Exp. Bot. 51: 2053–2066.

Higo K, Ugawa Y, Iwamoto M, and Korenaga T, 1999. Plant cis-acting regulatory DNA elements (PLACE) database. Nucleic Acids Res. 27:297-300.

Himanen K, Boucheron E, Vanneste S, de Almeida Engler J, Inze D, and Beeckman T, 2002. Auxin-mediated cell cycle activation during early lateral root initiation. Plant Cell 14:2339-2351.

Hirayama T, Ohto C, Mizoguchi T, and Shinozaki K, 1995. A gene encoding a phosphatidylinositol-specific phospholipase C is induced by dehydration and salt stress in Arabidopsis. Proc. Natl. Acad. Sci. USA 92:3903-3907.

Hodge A, 2009. Root decisions. Plant Cell Environ. 32:628–640.

Hooper NM, 2001. Determination of glycosyl-phosphatidylinositol membrane protein anchorage. Proteomics 1:748-755.

Horton P, Park KJ, Obayashi T, and Nakai K, 2006. Protein subcellular localization prediction withWoLF PSORT. Jiang T, Yang U-C, Chen Y-PP, eds. (2006) Proc. 4th Ann. Asia Pacific Bioinformatics Conference, APBC06. London: Imperial College Press. 39–48.

Horton P, Park KJ, Obayashi T, Fujita N, Harada H, Adams-Collier CJ, and Nakai K, 2007. WoLF PSORT: protein localization predictor. Nucleic Acids Res. 35:W585–W587.

Huang D, Wu W, Ambrose SD, Ross AR, Abrams SR, and Cutler AJ, 2007. Comparing the effects of (+)-ABA and ABA analogs on Arabidopsis gene expression in relation to ABA metabolism. Plant J. 50:414-428.

Huang D, Wu W, Abrams SR, and Cutler AJ, 2008. The relationship of drought-related gene expression in Arabidopsis to hormonal and environmental factors. J. Exp. Bot. 59:2991-3007.

Hunt L, Mills LN, Pical C, Leckie CP, Aitken FL, Kopka J, Mueller-Roeber B, McAinsh MR, Hetherington AM, and Gray JE. 2003. Phospholipase C is required for the control of stomatal aperture by ABA. Plant J. 34:47–55.

Iyer K, Bürkle L, Auerbach D, Thaminy S, Dinkel M, Engles K, and Stangljar I, 2005. Utilizing the split-ubiquitin membrane yeast two-hybrid system to identify protein-protein interactions of integral membrane proteins. Science Sig. 275:p13.

Iyer LM, Anantharaman V, and Aravind L, 2007. The DOMON domains are involved in heme and sugar recognition. Bioinformatics 23:2660-2664.

Jiang WS, Liu DH, Xu P, 2009. Cd-induced system of defence in the garlic root meristematic cells. Biol. Plant. 53:369–372.

Jing H-C, Hebeler R, Oeljeklaus S, Sitek B, Stühler K, Meyer HE, Sturre MJG, Hille J, Warscheid B, and Dijkwel PP, 2008. Early leaf senescence is associated with an altered cellular redox balance in Arabidopsis *cpr5*/*old1* mutants. Plant Biol. 10: 85–98.

Jones MA, Raymond MJ, and Smirnoff N, 2006. Analysis of the root-hair morphogenesis transcriptome reveals the molecular identity of six genes with roles in root-hair development in Arabidopsis. Plant J. 45:83-100.

Jones-Rhoades MW, Bartel DP, and Bartel B, 2006. MicroRNAs AND THEIR REGULATORY ROLES IN PLANTS. Ann. Rev. Plant Biol. 57:19-53.

Joo JH, Bae YS, and Lee JS, 2001. Role of auxin-induced reactive oxygen species in root gravitropism. Plant Physiol. 126:1055-1060.

Joo JH, Wang S, Chen JG, Jones AM, and Fedoroff NV, 2005. Different signaling and cell death roles of heterotrimeric G protein alpha and beta subunits in the Arabidopsis oxidative stress response to ozone. Plant Cell 17:957-970.

Kamei A, Seki M, Umezawa T, Ishida J, Satou M, Akiyama K, Zhu J-K, and Shinozaki K, 2005. Analysis of gene expression profiles in Arabidopsis *salt overly sensitive* mutants sos2-1 and sos3-1. Plant Cell Environ. 28:1267-1275.

Kampfenkel K, Van Montagu M, and Inze D, 1995. Extraction and determination of ascorbate and dehydroascorbate from plant tissue. Analyt. Biochem. 225:165-167.

Kaplinsky NJ and Barton MK, 2004. Plant acupuncture: sticking PINs in the right places. Science 306:822-823.

Kasuga M, Liu Q, Miura S, Yamaguchi-Shinozaki K, and Shinozaki K, 1999. Improving plant drought, salt, and freezing tolerance by gene transfer of a single stress-inducible transcription factor. Nat. Biotechnol. 17:287–291.

Kay R, Chan A, Daly M, and McPherson J, 1987. Duplication of CaMV 35S promoter sequences creates a strong enhancer for plant genes. Science 236:1299-1302.

Kepinski S, and Leyser O, 2005. The Arabidopsis F-box protein TIR1 is an auxin receptor. Nature 435:446-451.

Keller T, Abbott J, Moritz T, and Doerner P, 2006. Arabidopsis REGULATOR OF AXILLARY MERISTEMS1 controls a leaf axil stem cell niche and modulates vegetative development. Plant Cell 18:598-611.

Kinoshita and Inoue N, 2000. Dissecting and manipulating the pathway for glycosylphosphatidylinositol-anchor biosynthesis, Curr. Opin. Chem. Biol. 4:632–638.

Kim J, Harter K, Theologis A, 1997. Protein-protein interactions among the Aux/IAA proteins. Proc. Natl. Acad. Sci. USA 94: 11786-11791.

Kim HJ, Kato N, Kim S, and Triplett B, 2008. Cu/Zn superoxide dismutases in developing cotton fibers: evidence for an extracellular form. Planta 228:281-292.

Kipreos E T and M Pagano, 2000. The F-box protein family. Genome Biol. 1:REVIEWS3002.

Kliebenstein DJ, Monde RA, and Last RL, 1998. Superoxide dismutase in Arabidopsis: an eclectic enzyme family with disparate regulation and protein localization. Plant Physiol. 118:637-650.

Konopka-Postupolska D, Clark G, Goch G, Debski J, Floras K, Cantero A, Fijolek B, Roux S, Hennig J, 2009. The role of annexin 1 in drought stress in Arabidopsis. Plant Physiol. 150:1394–1410.

Koornneef M, Léon-Kloosterziel KM, Schwartz SH, and Zeevaart JAD, 1998. The genetic and molecular dissection of abscisic acid biosynthesis and signal transduction in Arabidopsis. Plant Physiol. Biochem. 36:83-89.

Kovács I, Ayaydin F, Oberschall A, Ipacs I, Bottka S, Pongor S, Dudits D, and Toth EC, 1998. Immunolocalization of a novel annexin-like protein encoded by a stress and abscisic acid responsive gene in alfalfa. Plant J.15:185–197.

Kramer EM and Bennett MJ, 2006. Auxin transport: a field in flux. Trends. Plant Sci. 11:382–386.

Kwak JM, Mori IC, Pei ZM, Leonhardt N, Torres MA, Dangl JL, Bloom RE, Bodde S, Jones JD, and Schroeder JI, 2003. NADPH oxidase AtrbohD and AtrbohF genes function in ROS-dependent ABA signaling in Arabidopsis. EMBO J. 22:2623-2633.

Lalanne E, Honys D, Johnson A, Borner GH, Lilley KS, Dupree P, Grossniklaus U, and Twell D, 2004. SETH1 and SETH2, two components of the glycosylphosphatidylinositol anchor biosynthetic pathway, are required for pollen germination and tube growth in Arabidopsis. Plant Cell 16:229-240.

Laplaze L, Benkova E, Casimiro I, Maes L, Vanneste S, Swarup R, Weijers D, Calvo V, Parizot B, Herrera-Rodriguez MB, Offringa R, Graham N, Doumas P, Friml J, Bogusz D, Beeckman T, and Bennett M, 2007. Cytokinins act directly on lateral root founder cells to inhibit root initiation. Plant Cell 19:3889-3900.

Laskowski M, Biller S, Stanley K, Kajstura T, and Prusty R, 2006. Expression profiling of auxin-treated Arabidopsis roots: toward a molecular analysis of lateral root emergence. Plant Cell Physiol. 47:788-792.

Laskowski M, Grieneisen VA, Hofhuis H, Hove CA, Hogeweg P, Mare AF, and Scheres B, 2008. Root system architecture from coupling cell shape to auxin transport. PLoS Biol. 6: e307.

Lee S, Lee EJ, Yang EJ, Lee JE, Park AR, Song WH, Park OK, 2004. Proteomic identification of annexins, calcium-dependent membrane binding proteins that mediate osmotic stress and abscisic acid signal transduction in Arabidopsis. Plant Cell 16:1378–1391.

Lee J, He K, Stolc V, Leeh, Figueroa P, Gao Y, Tongprasit W, Zhao H, Lee I, and Deng XW, 2007. Analysis of transcription factor HY5 genomic binding sites revealed its hierarchical role in light regulation of development. Plant Cell 19:731-749.

Lemtiri-Chlieh F, MacRobbie EAC, Webb AAR, Manison NF, Brownlee C, Skepper JN, Chen J, Prestwich GD, Brearley CA, 2003. Inositol hexakisphosphate mobilizes an endomembrane store of calcium in guard cells. Proc. Natl. Acad. Sci. USA 100:10091–10095.

Levine A, Tenhaken R, Dixon R, and Lamb C, 1994. H2O2 from the oxidative burst orchestrates the plant hypersensitive disease resistance response. Cell 79:583-593.

Leyser HMO, Lincoln CA, Timpte C, Lammer D, Turner J, and Estelle M, 1993. Arabidopsis auxin-resistance gene AXR1 encodes a protein related to ubiquitin-activating enzyme E1. Nature 364:161-164.

Leyser O, 2005. Auxin distribution and plant pattern formation: How many angels can dance on the point of PIN? Cell 121:819–822.

Lucas M, Godin C, Jay-Allemand C, and Laplaze L, 2008. Auxin fluxes in the root apex co-regulate gravitropism and lateral root initiation. J. Exp. Bot. 59: 55–66.

Li Y and Trush MA, 1993. Oxidation of hydroquinone by copper: chemical mechanism and biological effects. Arch. Biochem. Biophys. 300:346-355.

Li J, Wang XQ, Watson MB, and Assmann SM, 2000. Regulation of abscisic acid-induced stomatal closure and anion channels by guard cell AAPK kinase. Science 287:300–303.

Li J, Yang H, Ann Peer W, Richter G, Blakeslee J, Bandyopadhyay A, Titapiwantakun B, Undurraga S, Khodakovskaya M, Richards EL, Krizek B, Murphy AS, Gilroy S, and Gaxiola R, 2005. Arabidopsis H+-PPase AVP1 Regulates Auxin-Mediated Organ Dev. Sci. 310:121-125.

Li S, Assmann SM, and Albert R, 2006. Predicting essential components of signal transduction networks: a dynamic model of guard cell abscisic acid signaling. PLoS Biol. 4:e312.

Liang Y, Mitchell DM, and Harris JM, 2007. Abscisic acid rescues the root meristem defects of the Medicago truncatula latd mutant. Dev. Biol. 304:297-307.

Lin F, Ding H, Wang J, Zhang H, Zhang A, Zhang Y, Tan M, Dong W, and Jiang M, 2009. Positive feedback regulation of maize NADPH oxidase by mitogen-activated protein kinase cascade in abscisic acid signalling. J. Exp Bot. 60:3221-3238.

Lindermayr C, Sell S, Müller B, Leister D, and Durner J, 2010. Redox regulation of the NPR1-TGA1 system of *Arabidopsis thaliana* by nitric oxide. Plant Cell Advance Online Publication, Aug. 17, 2010.

Lingqiang MG and Scandalios JG, 2002. Catalase gene expression in response to auxin-mediated developmental signals. Physiol. Plant. 114:288-295.

Linding R, Jensen LJ, Diella F, Bork P, Gibson TJ, and Russell RB, 2003. Protein disorder prediction: implications for structural proteomics. Structure 11:1453–1459.

Lisanti MP, Scherer PE, Tang ZL, and Sargiacomo M, 1994. Caveolaer, caveolin and caveolin-rich membrane domains: a signalling hypothesis. Trends Cell Biol 4:231-235.

Liszkay A, van der Zalm E, and Schopfer P, 2004. Production of reactive oxygen intermediates (O(2)(.-), H(2)O(2), and (.)OH) by maize roots and their role in wall loosening and elongation growth. Plant Physiol. 136:3114-3123.

Liu Q, Kasuga M, Sakuma Y, Abe H, Miura S, Yamaguchi-Shinozaki K, and Shinozaki K, 1998. Two Transcription Factors, DREB1 and DREB2, with an EREBP/AP2 DNA Binding Domain Separate Two Cellular Signal Transduction Pathways in Drought- and Low-Temperature-Responsive Gene Expression, Respectively, in Arabidopsis. Plant Cell 10:1391-1406.

Liu J and Zhu J-K, 1998. A calcium sensor homolog required for plant salt tolerance. Science 280:1943-1945.

Liu J P, Ishitani M, Halfter U, Kim C S, and Zhu J K, 2000. The Arabidopsis SOS2 gene encodes a protein kinase that is required for salt tolerance. Proc. Natl. Acad. Sci. USA. 97:3730–3734.

Liu X, Yue Y, Li B, Nie Y, Li W, Wu WH and Ma L, 2007a. A G protein-coupled receptor is a plasma membrane receptor for the plant hormone abscisic acid. Science 315:1712–1716.

Liu PP, Montgomery TA, Fahlgren N, Kasschau KD, Nonogaki H, and Carrington JC, 2007b. Repression of AUXIN RESPONSE FACTOR10 by microRNA160 is critical for seed germination and post-germination stages. Plant J. 52:133-146.

Ljung K, Bhalerao RP, and Sandberg G, 2001. Sites and homeostatic control of auxin biosynthesis in Arabidopsis during vegetative growth. Plant J. 28:465-474.

Long JA, Woody S, Poethig S, Meyerowitz EM, and Barton MK. Transformation of shoots into roots in Arabidopsis embryos mutant at the TOPLESS locus. Development 129:2797–2806.

Ma Y, Szostkiewicz I, Korte A, Moes D, Yang Y, Christmann A, and Grill E, 2009. Regulators of PP2C phosphatase activity function as abscisic acid sensors. Science 324:1064–1068.

Maeda Y, Tashima Y, Houjou T, Fujita M, Yoko-o T, Jigami Y, Taguchi R, and Kinoshita T, 2007. Fatty acid remodeling of GPI-anchored proteins is required for their raft association. Mol. Biol. Cell 18:1497-1506.

Mahajan S and Tuteja N, 2005. Cold, salinity and drought stresses: an overview. Arch. Biochem. Biophys. 444:139-158.

Maher EP and Martindale SJB, 1980. Mutants of Arabidopsis with altered responses to auxins and gravity. Biochem. Genet. 18:1041-1053.

Malamy JE and Benfey PN, 1997. Organization and cell differentiation in lateral roots of Arabidopsis. Development 124:33-44.

Mäntylä E, Lang V, and Palva ET, 1995. Role of abscisic acid in drought-induced freezing tolerance, cold acclimation, and accumulation of LT178 and RAB18 proteins in Arabidopsis. Plant Physiol. 107:141-148.

Marchant A, Kargul J, May ST, Muller P, Delbarre A, Perrot-Rechenmann C, and Bennett MJ, 1999. AUX1 regulates root gravitropism in Arabidopsis by facilitating auxin uptake within root apical tissues. EMBO J. 18:2066-2073.

Marchler-Bauer A, Anderson JB, DeWeese-Scott C, Fedorova ND, Geer LY, He S, Hurwitz DI, Jackson JD, Jacobs AR, Lanczycki CJ, Liebert CA, Liu C, Madej T, Marchler GH, Mazumder R, Nikolskaya AN, Panchenko AR, Rao BS, Shoemaker BA, Simonyan V, Song JS, Thiessen PA, Vasudevan S, Wang Y, Yamashita RA, Yin JJ, and Bryant SH, 2003. CDD: a curated Entrez database of conserved domain alignments. Nucleic Acids Res. 31:383–387.

Marchler-Bauer A, Anderson JB, Chitsaz F, Derbyshire MK, DeWeese-Scott C, Fong JH, Geer LY, Geer RC, Gonzales NR, Gwadz M, He S, Hurwitz DI, Jackson JD, Ke Z, Lanczycki CJ, Liebert CA, Liu C, Lu F, Lu S, Marchler GH, Mullokandov M, Song JS, Tasneem A, Thanki N, Yamashita RA, Zhang D, Zhang N, and Bryant SH, 2009. CDD: specific functional annotation with the Conserved Domain Database. Nucleic Acids Res. 37:205-10.

Martienssen RA, 1998. Functional genomics: probing plant gene function and expression with transposons. Proc. Natl. Acad. Sci. USA 95:2021-2026.

Marin-Rodriguez MC, Orchard J, and Seymour GB, 2002. Pectate lyases, cell wall degradation and fruit softening. J. Exp. Bot. 53:2115–2119.

Martin SW, Glover BJ, and Davies JM, 2005. Lipid microdomains--plant membranes get organized. Trends Plant Sci. 10:263-265.

Matsui A, Ishida J, Morosawa T, Mochizuki Y, Kaminuma E, Endo TA, Okamoto M, Nambara E, Nakajima M, Kawashima M, Satou M, Kim J-M, Kobayashi N, Toyoda T, Shinozaki K, and Seki M, 2008. Arabidopsis transcriptome analysis under drought, cold, high-salinity and ABA treatment conditions using a tiling Array. Plant Cell Physiol. 49:1135-1149.

Meyer U, Benghezal M, Imhof I, and Conzelmann A, 2000. Active site determination of Gpi8p, a caspase-related enzyme required for glycosylphosphatidylinositol anchor addition to proteins. Biochemistry 39:3461-3471.

Miao Y, Lv D, Wang P, Wang X-C, Chen J, Miao C, and Song C-P, 2006. An Arabidopsis glutathione peroxidase functions as both a redox transducer and a scavenger in abscisic acid and drought stress responses. Plant Cell 18:2749-2766.

Michniewicz M, Zago MK, Abas L, Weijers D, Schweighofer A, Meskiene I, Heisler MG, Ohno C, Zhang J, Huang F, Schwab R, Weigel D, Meyerowitz EM, Luschnig C, Offringa R, and Friml J, 2007. Antagonistic regulation of PIN Pposphorylation by PP2A and PINOID directs auxin flux. Cell 130:1044-1056.

Miedema H and Assmann SM, 1996. A membrane-delimited effect of internal pH on the K+ outward rectifier of Vicia faba guard cells. J. Membr. Biol. 154: 227-237.

Mittler R, 2002. Oxidative stress, antioxidants and stress tolerance. Trends Plant Sci. 7:405-410.

Monshausen GB, Bibikova TN, Messerli MA, Shi C, and Gilroy S, 2007. Oscillations in extracellular pH and reactive oxygen species modulate tip growth of Arabidopsis root hairs. Proc. Natl. Acad. Sci. USA 104:20996-21001.

Moon JY, Henzler-Wildman KA, and Ramamoorthy A, 2006. Expression and purification of a recombinant LL-37 from Escherichia coli. Biochimica Biophys. Acta 1758:1351-1358.

Morgan KE, Zarembinski TI, Theologis A, and Abel S, 1999. Biochemical characterization of recombinant polypeptides corresponding to the predicted [beta][alpha][alpha] fold in Aux/IAA proteins. FEBS Lett. 454:283-287.

Morris DA, 2000. Transmembrane auxin carrier systems — dynamic regulators of polar auxin transport. Plant Growth Regul. 32:161-172.

Müller A, Guan C, Gälweiler L, Tänzler P, Huijser P, Marchant A, Parry G, Bennett M, Wisman E, and Palme K, 1998. AtPIN2 defines a locus of Arabidopsis for root gravitropism control. Embo J. 17:6903-6911.

Müller B. and Sheen J, 2008. Cytokinin and auxin interaction in root stem-cell specification during early embryogenesis. Nature 453:1094-1097.

Muller AH and Hansson M, 2009. The barley magnesium chelatase 150-kd subunit is not an abscisic acid receptor. Plant Physiol. 150:157–166.

Munnik T and Testerink C, 2009. Plant phospholipid signaling: “in a nutshell”. J. Lipid Res. 50:S260-S265.

Munns R and Tester M, 2008. Mechanisms of salinity tolerance. Ann. Rev. Plant Biol. 59:651-681.

Munro S, 2003. Lipid rafts: elusive or illusive? Cell 115:377-388.

Naderi M, Caplan A, and Berger PH, 1997. Phenotypic characterization of a tobacco mutant impaired in auxin polar transport. Plant Cell Rep. 17:32-38.

Nakanomyo I, Kost B, Chua NH, and Fukuda H, 2002. Preferential and asymmetrical accumulation of a Rac small GTPase mRNA in differentiating xylem cells of Zinnia elegans. Plant Cell Physiol. 43:1484-1492.

Nambara E and Marion-Poll M, 2005. Abscisic acid biosynthesis and catabolism. Ann. Rev. Plant Biol. 56:165–185.

Napier RM, David KM, and Pettot-Rechenmann C, 2002. A short history of auxin binding proteins. Plant Mol. Biol. 49:339-348.

Napier R, 2004. Plant hormone binding sites. Ann. Bot. 93:227–33.

Narusaka Y, Nakashima K, Shinwari ZK, Sakuma Y, Furihata T, Abe H, Narusaka M, Shinozaki K, and Yamaguchi-Shinozaki K, 2003. Interaction between two cis-acting elements, ABRE and DRE, in ABA-dependent expression of Arabidopsis rd29A gene in response to dehydration and high-salinity stresses. Plant J. 34:137–148.

Neuteboom LW, Ng JM, Kuyper M, Clijdesdale OR, Hooykaas PJ, and van der Zaal B,J 1999. Isolation and characterization of cDNA clones corresponding with mRNAs that accumulate during auxin-induced lateral root formation. Plant Mol. Biol. 39:273-287.

Nielsen H, Engelbrecht J, Brunak S, and von Heijne G, 1997. Identification of prokaryotic and eukaryotic signal peptides and prediction of their cleavage sites. Protein Eng. 10:1-6.

Nielsen H, Krogh A,1998. Prediction of signal peptides and signal anchors by a hidden Markov model. Proceedings of the Sixth International Conference on Intelligent Systems for Molecular Biology (ISMB98), 122-130.

Nishimura N, Hitomi K, Arvai AS, Rambo RP, Hitomi C, Cutler SR, Schroeder JI, and Getzoff ED, 2009. Structural Mechanism of Abscisic Acid Binding and Signaling by Dimeric PYR1. Science 326:1373-1379.

Nonogaki H, 2008. Repression of transcription factors by microRNA during seed germination and postgermination: another level of molecular repression in seeds. Plant Sig. Behav. 3:65-67.

Normanly J and Bartel B, 1999. Redundancy as a way of life – IAA metabolism. Curr. Op. Plant Biol. 2:207-213.

Normanly J, 2010. Approaching cellular and molecular resolution of auxin biosynthesis and metabolism. Cold Spring Harb Perspect. Biol. 2:a001594.

Nothnagel EA, 1997. Proteoglycans and related components in plant cells. Int. Rev. Cytol. 174:195-291.

Nowacki J, Bandurski RS, 1980. Myo-inositol esters of indole-3-acetic acid as seed auxin precursors of Zea mays L. Plant Physiol. 65:422–427.

Ohishi K, Inoue N, Maeda Y, Takeda J, Riezman H, and Kinoshita T, 2000. Gaa1p and gpi8p are components of a glycosylphosphatidylinositol (GPI) transamidase that mediates attachment of GPI to proteins. Mol. Biol. Cell 11:1523-1533.

Ohkuma K, Lyon JL, Addicott FT, Smith OE, 1963. Abscisin II, an abscission-accelerating substance from young cotton fruit. Science 142:1592–1593.

Oka M, Miyamoto K, Okada K, and Ueda J, 1999. Auxin polar transport and flower formation in Arabidopsis transformed with indoleacetamide hydrolase (iaaH) gene. Plant Cell Physiol. 40:231-237.

Okada K, Ueda J, Komaki MK, Bell CJ, and Shimura Y, 1991. Requirement of the auxin polar transport system in early stages ofArabidopsis floral bud formation. Plant Cell 3 677–684.

Okushima Y, Fukaki H, Onoda M, Theologis A, and Tasaka M, 2007. ARF7 and ARF19 regulate lateral root formation via direct activation of LBD/ASL genes in Arabidopsis. Plant Cell 19:118–130.

Oshima Y, Kamigaki A, Nakamori C, Mano S, Hayashi M, Nishimura M, and Esaka M, 2009. Plant catalase is imported into peroxisomes by Pex5p but is distinct from typical PTS1 import. Plant Cell Physiol. 49:671-677.

Ouellet F, Overvoorde PJ, Theologis A, 2001. IAA17/AXR3. Biochemical insight into an auxin mutant phenotype. Plant Cell 13:829–842.

Paal A, 1918. Uber phototropische. Reizleitung Jahrb Wiss Bot 58:406-458.

Palmer CM and Guerinot ML, 2009. Facing the challenges of Cu, Fe and Zn homeostasis in plants. Nature Chem. Biol. 5 :333–340.

Pandey S, Nelson DC, and Assmann SM, 2009. Two novel GPCR-type G proteins are abscisic acid receptors in Arabidopsis. Cell 136:136–148.

Parizot B, Laplaze L, Ricaud L, Boucheron-Dubuisson E, Bayle V, Bonke M, De Smet I, Poethig SR, Helariutta Y, Haseloff J, Chriqui D, Beeckman T, and Nussaume L, 2008. Diarch symmetry of the vascular bundle in Arabidopsis root encompasses the pericycle and is reflected in distich lateral root Initiation. Plant Physiol. 146:140-148.

Park S-Y, Fung P, Nishimura N, Jensen DR, Fujii H, Zhao Y, Lumba S, Santiago J, Rodrigues A, Chow T-FF, Alfred SE, Bonetta D, Finkelstein R, Provart NJ, Desveaux D, Rodriguez PL, McCourt P, Zhu J-K, Schroeder JI, Volkman BF, and Cutler SR, 2009. Abscisic acid inhibits type 2C protein phosphatases via the PYR/PYL family of START proteins. Science 324:1068-1071.

Parton RG and Simons K, 1995. Digging into caveolae. Science 269:1398-1399.

Parry G, Marchant A, May S, Swarup R, Swarup K, James N, Graham N, Allen T, Martucci T, Yemm A, Napier R, Manning K, King G, and Bennett M, 2001. Quick on the uptake: characterization of a family of plant auxin influx carriers. J. Plant Growth Regul. 20:217-225.

Paoli P, Giannoni E, Pescitelli R, Camici G, Manao G, and Ramponi G, 2001. Hydrogen peroxide triggers the formation of a disulfide dimer of muscle acylphosphatase and modifies some functional properties of the enzyme. J. Biol. Chem. 276:41863-41869.

Pei ZM, Murata Y, Benning G, Thomine S, Klusener B, Allen GJ, Grill E, and Schroeder JI, 2000. Calcium channels activated by hydrogen peroxide mediate abscisic acid signalling in guard cells. Nature 406:731-734.

Péret B, De Rybel B, Casimiro I, Benková E, Swarup R, Laplaze L, Beeckman T, and Bennet MJ, 2009. Arabidopsis lateral root development: an emerging story. Trends Plant Sci. 14:399-408.

Penkner A, Tang L, Novatchkova M, Ladurner M, Fridkin A, Gruenbaum Y, Schweizer D, Loidl J, and Jantsch V, 2007. Dev. Cell 12:873–885.

Pernas M, Garcia-Casado G, Rojo E, Solano R, and Sanchez-Serrano JJ, 2007. A protein phosphatase 2A catalytic subunit is a negative regulator of abscisic acid signalling. Plant J. 51:763-778.

Peskan T, Westermann M, and Oelmuller R, 2000. Identification of low-density Triton X-100-insoluble plasma membrane microdomains in higher plants. European J. Biochem. 267:6989-6995.

Petrasek J, Mravec J, Bouchard R, Blakeslee JJ, Abas M, Seifertova D, Wisniewska J, Tadele Z, Kubes M, Covanova M, Dhonukshe P, Skupa P, Benkova E, Perry L, Krecek P, Lee OR, Fink GR, Geisler M, Murphy AS, Luschnig C, Zazimalova E, and Friml J, 2006. PIN proteins perform a rate-limiting function in cellular auxin efflux. Science 312:914-918.

Pickett FB, Wilson AK, and Estelle M, 1990. The aux1 mutation of Arabidopsis confers both auxin and ethylene resistance. Plant Physiol. 94:1462-1466.

Preger V, Tango N, Marchand C, Lemaire SD, Carbonera D, Di Valentin M, Costa A, Pupillo P, and Trost P, 2009. Auxin-responsive genes AIR12 code for a new family of plasma membrane b-type cytochromes specific to flowering plants. Plant Physiol. 150:606-620.

Premkumar DRD, Fukuoka Y, Sevlever D, Brunschwig E, Rosenberry TL, Tykocinski ML, and Medof ME, 2001. Properties of exogenously added GPI-anchored proteins following their incorporation into cells. J. Cell Biochem. 82:234-245.

Queval G and Noctor G, 2007 A plate reader method for the measurement of NAD, NADP, glutathione and ascorbate in tissue extracts: application to redox profiling during Arabidopsis rosette development. Anal. Biochem. 363: 58–69.

Quint M and Gray WM, 2006. Auxin signaling. Curr. Op. Plant Biol. 9: 448-453.

Rodriguez AA, Grunberg KA, and Taleisnik EL, 2002. Reactive oxygen species in the elongation zone of maize leaves are necessary for leaf extension. Plant Physiol. 129:1627-1632.

Rapparini F, Tam YY, Cohen JD, and Slovin JP, 2002. Indole-3-acetic acid metabolism in Lemna gibba undergoes dynamic changes in response to growth temperature. Plant Physiol. 128:1410-1416.

Raumann BE, Brown BM, and Sauer RT, 1994. Major groove DNA recognition by beta-sheets: The ribbon-helix-helix family of gene regulatory proteins. Curr. Opin. Struct. Biol. 4:36-43.

Razem FA and Bernards MA, 2003. Reactive oxygen species production in association with suberization: evidence for an NADPH-dependent oxidase. J. Exp. Bot. 54:935-941.

Razem FA and El-Kereamy A, Abrams SR, and Hill RD, 2006. The RNA-binding protein FCA is an abscisic acid receptor. Nature 439:290–294.

Reese MG, 2001. Application of a time-delay neural network to promoter annotation in the Drosophila melanogaster genome. Comput. Chem. 26:51-56.

Remington DL, Vision TJ, Guilfoyle TJ, and Reed JW, 2004. Contrasting modes of diversification in the Aux/IAA and ARF gene families. Plant Physiol. 135:1738–1752.

Ribnicky DM, Cohen JD, Hu W-S, and Cooke TJ, 2002. An auxin surge following fertilization in carrots: a mechanism for regulating plant totipotency. Planta 214:505-509.

Risk JM, Macknight RC, and Day CL, 2008. FCA does not bind abscisic acid. Nature 456:E5–E6.

Risk JM, Day CL, and Macknight RC, 2009. Reevaluation of abscisic acid-binding assays shows that G-Protein-Coupled Receptor2 does not bind abscisic acid. Plant Physiol. 150:6–11.

Romanov GA, 2002. The phytohormone receptors. Russ. J. Plant Physiol. 49:552-560.

Ruegger M, Dewey E, Hobbie L, Brown D, Bernasconi P, Turner J, Muday G, and Estelle M, 1997. Reduced naphthylphthalamic acid binding in the tir3 mutant of Arabidopsis is associated with a reduction in polar auxin transport and diverse morphological defects. Plant Cell 9:745-757.

Ruegger M, Dewey E, Gray WM, Hobbie L, Turner J, and Estelle M, 1998. The TIR1 protein of Arabidopsis functions in auxin response and is related to human SKP2 and yeast Grr1p. Genes Dev. 12:198–207.

Sagi M, Davydov O, Orazova S, Yesbergenova Z, Ophir R, Stratmann JW, and Fluhr R, 2004. Plant respiratory burst oxidase homologs impinge on wound responsiveness and development in Lycopersicon esculentum. Plant Cell 16:616-628.

Sagi M and Fluhr R, 2006. Production of reactive oxygen species by plant NADPH oxidases. Plant Physiol. 141:336-340.

Sakamoto H, Matsuda O, and Iba K, 2008. ITN1, a novel gene encoding an ankyrin-repeat protein that affects the ABA-mediated production of reactive oxygen species and is involved in salt-stress tolerance in Arabidopsis. Plant J. 56:411–422.

Salin ML, 1991. Chloroplast and mitochondrial mechanism for protection against oxygen toxicity. Free Radical Res. Commun. 12-13:851–858.

Santner A, Calderon-Villalobos LIA, and Estelle M, 2009. Plant hormones are versatile chemical regulators of plant growth. Nature Chem. Biol. 5:301-307.

Sauer M, Balla J, Luschnig C, Wiśniewska J, Reinöhl V, Friml J, and Benková E, 2006. Canalization of auxin flow by Aux/IAA-ARF-dependent feed-back regulation of PIN polarity, Genes Dev. 20:2902–2911.

Scandalios JG, 2005. Oxidative stress: molecular perception and transduction of signals triggering antioxidant gene defenses. Braz. J. Med. Biol. Res. 38:995-1014.

Scarpella E, Marcos D, Friml J, and Berleth T, 2006. Control of leaf vascular patterning by polar auxin transport, Genes Dev. 20:1015–1027.

Scheres B, Wolkenfelt H, Willemsen V, Terlouw M, Lawson E, Dean C and Weisbeek P, 1994. Embryonic origin of the Arabidopsis primary root and root meristem initials. Development 120:2475-2487.

Schopfer P, 2001. Hydroxyl radical-induced cell-wall loosening in vitro and in vivo: implications for the control of elongation growth. Plant J. 28:679-688.

Schopfer P, Liszkay A, Bechtold M, Frahry G, and Wagner A, 2002. Evidence that hydroxyl radicals mediate auxin-induced extension growth. Planta 214:821-828.

Schroeder JI, Kwak JM, and Allen GJ, 2001. Guard cell abscisic acid signalling and engineering drought hardiness in plants. Nature 410:327-330.

Schurr U, Gollan T, Schulze E-D, 1992. Stomatal response to soil drying in relation to changes in the xylem sap composition of *Helianthus annuus*. II. Stomatal sensitivity to abscisic acid imported from the xylem sap. Plant Cell Environ. 15:561–567.

Sedbrook JC, Carroll KL, Hung KF, Masson PH, and Somerville CR, 2002. The Arabidopsis SKU5 gene encodes an extracellular glycosyl phosphatidylinositol-anchored glycoprotein involved in directional root growth. Plant Cell 14:1635-1648.

Seki M, Umezawa T, Urano K, and Shinozaki K, 2007. Regulatory metabolic networks in drought stress responses. Curr. Op. Plant Biol. 10:296-302.

Shin R, Berg RH, and Schachtman DP, 2005. Reactive oxygen species and root hairs in Arabidopsis root response to nitrogen, phosphorous, and potassium deficiency. Plant Cell Physiol. 46:1350-1357.

Shen YY, Wang XF, Wu FQ, Du SY, Cao Z, Shang Y, Wang XL, Peng CC, Yu XC, Zhu SY, Fan RC, Xu YH, and Zhang DP, 2006. The Mg-chelatase H subunit is an abscisic acid receptor. Nature 443:823–826.

Sherrier DJ, Prime TA, and Dupree P, 1999. Glycosylphosphatidylinositol-anchored cell-surface proteins from Arabidopsis. Electrophoresis 20:2027–2035.

Shi H, Ishitani M, Kim C, and Zhu J-K, 2000. The Arabidopsis salt tolerance gene SOS1 encodes a putative Na+/H+ antiporter. Proc. Natl. Acad. Sci. USA 97:6896-6901.

Shi H, Quintero FJ, Pardo JM, and Zhu J-K, 2002. The Putative Plasma Membrane Na+/H+ Antiporter SOS1 Controls Long-Distance Na+ Transport in Plants. Plant Cell 14:465-477.

Shi H, Lee B-H, Wu S-J, and Zhu J-K, 2003. Overexpression of a plasma membrane Na+/H+ antiporter gene improves salt tolerance in Arabidopsis. Nat. Biotech. 21:81-85.

Shi S, Wang G, Wang Y, Zhang L, and Zhang L, 2005. Protective effect of nitric oxide against oxidative stress under ultraviolet-B radiation. Nitric Ox. 13:1-9.

Shimomura S, 2006. Identification of a glycosylphosphatidylinositol-anchored plasma membrane protein interacting with the C-terminus of auxin-binding protein 1: a photoaffinity crosslinking study. Plant Mol. Biol. 60:663-677.

Showalter AM, 2001. Arabinogalactan-proteins: structure, expression and function. Cell Mol. Life Sci. 58:1399-1417.

Simoes T, Teixeira MC, Fernandes AR, and Sa-Correia I, 2003. Adaptation of Saccharomyces cerevisiae to the herbicide 2,4-dichlorophenoxyacetic acid, mediated by Msn2p- and Msn4p-regulated genes: important role of SPI1. App. Environ. Microbiol. 69:4019-4028.

Simons K and Ikonen E, 1997. Functional rafts in cell membranes. Nature 387:569-572.

Smith AT and Veitch NC, 1998. Substrate binding and catalysis in heme peroxidases. Curr. Op. Chem. Biol. 2:269-278.

Somerville C, Browse J, Jaworski JG, and Ohlrogge JB, 2000. Lipids. In BB Buchanan, W Gruissem, and RL Jones (Eds.), Biochemistry and molecular biology of plants (pp.358-401), Rockville, USA: American Society of Plant Physiologists.

Sorefan K, Girin T, Liljegren SJ, Ljung K, Robles P, Galván-Ampudia CS, Offringa R, Friml J, Yanofsky MF, and Østergaard L, 2009. A regulated auxin minimum is required for seed dispersal in Arabidopsis, Nature 459:583–586.

Sparkes IA, Runions J, Kearns A, Hawes C, 2006. Rapid, transient expression of fluorescent fusion proteins in tobacco plants and generation of stably transformed plants. Nature Prot. 1:2019–2025.

Stone BB, Stowe-Evans EL, Harper RM, Celaya RB, Ljung K, Sandberg G, and Liscum E, 2008. Disruptions in AUX1-dependent auxin influx alter hypocotyl phototropism in Arabidopsis. Mol. Plant. 1:129-144.

Su D, May JM, Koury MJ, and Asard H, 2006. Human erythrocyte membranes contain a cytochrome *b*561 that may be involved in extracellular ascorbate recycling. J. Biol. Chem. 281**:**39852–39859.

Sudo E, Itouga M, Yoshida-Hatanaka K, Ono Y, and Sakakibara H, 2008. Gene expression and sensitivity in response to copper stress in rice leaves. J. Exp. Bot. 59:3465-3474.

Sun W, Zhao ZD, Hare MC, Kieliszewski MJ, and Showalter AM, 2004a. Tomato LeAGP-1 is a plasma membrane-bound, glucosylphosphatidylinositol-anchored arabinogalactan-protein. Physiol. Plant. 120:319-327.

Sun W, Kieliszewski MJ, and Showalter AM, 2004b. Overexpression of tomato LeAGP-1 arabinogalactan-protein promotes lateral branching and hampers reproductive development. Plant J. 40:870-881.

Sundaresan V, Springer P, Volpe T, Haward S, Jones JD, Dean C, Ma H, and Martienssen R, 1995. Patterns of gene action in plant development revealed by enhancer trap and gene trap transposable elements. Genes Dev. 9:1797-1810.

Szemenyei H, Hannon M, and Long JA, 2008. TOPLESS mediates auxin-dependent transcriptional repression during Arabidopsis embryogenesis. Science 319:1384-1386.

Swarup R, Friml J, Marchant A, Ljung K, Sandberg G, Palme K, and Bennett M, 2001. Localization of the auxin permease AUX1 suggests two functionally distinct hormone transport pathways operate in the Arabidopsis root apex. Genes Dev. 15:2648-2653.

Swarup K, Benkova E, Swarup R, Casimiro I, Peret B, Yang Y, Parry G, Nielsen E, De Smet I, Vanneste S, Levesque MP, Carrier D, James N, Calvo V, Ljung K, Kramer E, Roberts R, Graham N, Marillonnet S, Patel K, Jones JD, Taylor CG, Schachtman DP, May S, Sandberg G, Benfey P, Friml J, Kerr I, Beeckman T, Laplaze L, and Bennett MJ, 2008. The auxin influx carrier LAX3 promotes lateral root emergence. Nature Cell Biol. 10:946-954.

Taiz L and Zeiger E, 1998. Plant Physiology, 2nd ed., Massachusetts, USA: Sinauer Associates.

Takahashi MA and Asada K, 1983. Superoxide anion permeability of phospholipid membranes and chloroplast thylakoids. Arch. Bioch. Biophys. 226:558-566.

Tam YY, Epstein E, and Normanly J, 2000. Characterization of auxin conjugates in Arabidopsis. Low steady-state levels of indole-3-acetyl-glutamate, and indole-3-acetyl-glucose. Plant Physiol. 123:589-595.

Tanaka, H., Dhonukshe, P., Brewer, P., and Friml, J. (2006). Spatiotemporal asymmetric auxin distribution: a means to coordinate plant development. Cellular and Molecular Life Sciences 63, 2738-2754.

Tan X, Calderon-Villalobos LI, Sharon M, Zheng C, Robinson CV, Estelle M, and Zheng N, 2007. Mechanism of auxin perception by the TIR1 ubiquitin ligase. Nature 446:640-645.

Teerawanichpan P, Hoffman T, Ashe P, Datla R, and Selvaraj G, 2007. Investigations of combinations of mutations in the jellyfish green fluorescent protein (GFP) that afford brighter fluorescence, and use of a version (VisGreen) in plant, bacterial, and animal cells. Biochim. Biophys. Acta - General Subjects 1770:1360-1368.

Theologis A, Huynh TV, and Davis RW, 1985. Rapid induction of specific mRNAs by auxin in pea epicotyl tissue. J. Mol. Biol. 183:53-68.

Tiwari SB, Hagen G, and Guilfoyle T, 2003. The Roles of Auxin Response Factor Domains in Auxin-Responsive Transcription. Plant Cell 15:533-543.

Tiwari SB, Hagen G, and Guilfoyle TJ, 2004. Aux/IAA Proteins Contain a Potent Transcriptional Repression Domain. Plant Cell 16:533-543.

Tyburski J, Dunajska K, Mazurek P, Piotrowska B, and Tretyn A, 2009. Exogenous auxin regulated H_2O_2 metabolism in roots of tomato (*Lycopersicon esculentum* Mill.) seedlings affecting the expression and activity of CuZn-superoxide dismutase, catalase, and peroxidase. Acta Physiol. Plant. 31:249-260.

Udenfriend S and Kodukula K, 1995. How glycosylphosphatidylinositol-anchored membrane proteins are made. Ann. Rev. Biochem. 64:563-591.

Ulmasov T, Liu Z-B, Hagen G, and Guilfoyle TJ, 1995. Composite structure of auxin response elements. Plant Cell 7:1611-1623.

Ulmasov T, Hagen G, and Guilfoyle TJ, 1997a. ARF1, a transcription factor that binds to auxin response elements. Science 276:1865-1868.

Ulmasov T, Murfett J, Hagen G and Guilfoyle TJ, 1997b. Aux/IAA proteins repress expression of reporter genes containing natural and highly active synthetic auxin response elements. Plant Cell 9:1963-1971.

Ulmasov T, Hagen G, and Guilfoyle TJ, 1999. Dimerization and DNA binding of auxin response factors. Plant J. 19:309-319.

Vanneste S and Friml J, 2009. Auxin: trigger of change in plant development. Cell 136:1005–1016.

Vicete-Agullo F, Rigas S, Desbrosses G, Dolan L, Hatzopoulos P, and Grabov A, 2004. Potassium carrier TRH1 is required for auxin transport in Arabidopsis roots. Plant J. 40:523-535.

Verslues PE and Bray EA, and 2006. Role of abscisic acid (ABA) and Arabidopsis ABA-insensitive loci in low water potential-induced ABA and proline accumulation. J. Exp. Bot. 57:201-212.

Verslues P and Zhu J, 2007. New developments in abscisic acid perception and metabolism. Curr. Op. Plant Biol. 10:447-452.

Vinocur B and Altman A, 2005. Recent advances in engineering plant tolerance to abiotic stress: achievements and limitations. Curr. Op. Biotech. 16:123-132.

Vissenberg K, Fry SC, Pauly M, Hofte H, and Verbelen JP, 2005. XTH acts at the microfibril-matrix interface during cell elongation. J. Exp. Bot. 56:673–683.

Voetberg GS and Sharp RE, 1991. Growth of the maize primary root tip at low water potentials. III. Role of increased proline deposition in osmotic adjustment. Plant Physiol. 96:1125-1130.

Vogel JP, Raab TK, Schiff C, and Somerville SC, 2002. PMR6, a pectate lyase-like gene required for powdery mildew susceptibility in Arabidopsis. Plant Cell 14:2095-2106.

Voinnet O, Rivas S, Mestre P, and Baulcombe D, 2003. An enhanced transient expression system in plants based on suppression of gene silencing by the p19 protein of tomato bushy stunt virus. Plant J. 33:949-956.

Wan S, Wu J, Zhang Z, Sun X, Lv Y, Gao C, Ning Y, Ma J, Guo Y, Zhang Q, Zheng X, Zhang C, Ma Z, and Lu T, 2009. Activation tagging, an efficient tool for functional analysis of the rice genome. Plant Mol. Biol. 69:69–80.

Wang H, Ma L-G, Li J-M, Zhao Y-H, Deng XW, 2001. Direct interaction of Arabidopsis cryptochromes with COP1 in light control development. Science 294:154–158.

Wang S, Tiwari SB, Hagen G, and Guilfoyle TJ, 2005. AUXIN RESPONSE FACTOR7 restores the expression of auxin-responsive genes in mutant Arabidopsis leaf mesophyll protoplasts. Plant Cell 17:1979-1993.

Weijers D, Benkova E, Jager KE, Schlereth A, Hamann T, Kientz M, Wilmoth JC, Reed JW, and Jurgens G, 2005. Developmental specificity of auxin response by pairs of ARF and Aux/IAA transcriptional regulators. EMBO J. 24:1874-1885.

Weijers D, Schlereth A, Ehrismann JS, Schwank G, Kientz M, and Jürgens G, 2006. Auxin triggers transient local signaling for cell specification in Arabidopsis embryogenesis. Dev. Cell 10:265–270.

Went FW, 1926. On growth-accelerating substances in the coleoptile of Avena sativa. Proc. Kon. Ned. Akad. Wet. 30:10-19.

Winter D, Vinegar B, Nahal H, Ammar R, Wilson GV, Provart NJ, 2007. An "electronic fluorescent pictograph" browser for exploring and analyzing large-scale biological data sets. PLoS ONE 2: e718

Wisniewska J, Xu J, Seifertova D, Brewer PB, Ruzicka K, Blilou I, Rouquie D, Benkova E, Scheres B, and Friml J, 2006. Polar PIN localization directs auxin flow in plants. Science 312:858-860.

Wilmoth JC, Wang S, Tiwari SB, Joshi AD, Hagen G, Guilfoyle TJ, Alonso JM, Ecker JR, Reed JW, 2005. NPH4/ARF7 and ARF19 promote leaf expansion and auxin-induced lateral root formation. Plant J. 43:118–130.

Wu F-Q, Xin Q, Cao Z, Liu Z-Q, Du S-Y, Mei C, Zhao C-X, Wang X-F, Shang Y, Jiang T, Zhang X-F, Yan L, Zhao R, Cui Z-N, Liu R, Sun H-L, Yang X-L, Su Z, and Zhang D-P 2009. The Mg-chelatase H subunit binds abscisic acid and functions in abscisic acid signaling: new evidence in Arabidopsis. Plant Physiol. 150:1940–1954 .

Xuan W, Zhu FY, Xu S, Huang BK, Ling TF, Qi JY, Ye M-B, and Shen W-B, 2008. Heme oxygenase/carbon monoxide system is involved in auxin-induced cucumber adventitious rooting process. Plant Physiol. 148:881–893.

Yamamoto M and Yamamoto KT, 1998. Differential effects of 1-naphthaleneacetic acid, indole-3-acetic acid and 2, 4-dichlorophenoxyacetic acid on the gravitropic response of roots in an auxin-resistant mutant of Arabidopsis, aux1. Plant Cell Physiol. 39:660–664.

Yamaguchi-Shinozaki K and Shinozaki K, 1994. A novel cis-acting element in an Arabidopsis gene is involved in responsiveness to drought, low-temperature, or high-salt stress. Plant Cell 6:251–264.

Yang Y, Hammes UZ, Taylor CG, Schachtman DP, and Nielsen E, 2006. High-Affinity Auxin Transport by the AUX1 Influx Carrier Protein. Curr. Biol. 16:1123-1127.

Yu H, Wu J, Xu N, and Peng M, 2007. Roles of F-box proteins in plant hormone responses. Acta Biochim. Biophys. Sin. 39:915-922.

Zegzouti H, Anthony RG, Jahchan N, Bögre L, and Christensen SK, 2006. Phosphorylation and activation of PINOID by the phospholipid signaling kinase 3-phosphoinositide-dependent protein kinase 1 (PDK1) in Arabidopsis. Proc. Natl. Acad. Sci. USA 103:6404-6409.

Zeller G, Henz SR, Wildmer CK, Sachsenberg T, Rätsch G, Weigel D, and Laubinger S, 2009. Stress-induced changes in Arabidopsis transcriptome analyzed using whole-genome tiling arrays. Plant J. 58:1068-1082.

Zenser N, Ellsmore A, Leasure C, and Callis J, 2001. Auxin modulates the degradation rate of Aux/IAA proteins. Proc. Natl. Acad. Sci. USA 98:11795-11800.

Zenser N, Dreher KA, Edwards SR, Callis J. 2003. Acceleration of Aux/IAA proteolysis is specific for auxin and independent of AXR1. Plant J. 35:285–94.

Zhang X, Miao YC, An GY, Zhou Y, Shangguan ZP, Gao JF, and Song CP, 2001a. K+ channels inhibited by hydrogen peroxide mediate abscisic acid signaling in Vicia guard cells. Cell Res. 11:195-202.

Zhang X, Zhang L, Dong F, Gao J, Galbraith DW, and Song CP, 2001b. Hydrogen peroxide is involved in abscisic acid-induced stomatal closure in *Vicia faba*. Plant Physiol. 126:1438-1448.

Zhang J, Jia W, Yang J, and Ismail AM, 2006. Role of ABA in integrating plant responses to drought and salt stresses. Field Crops Res. 97:111–119.

Zhigang A, Cuijie L, Yuangang Z, Yejie D, Wachter A, Gromes R, and Rausch T, 2006. Expression of BjMT2, a metallothionein 2 from Brassica juncea, increases copper and cadmium tolerance in Escherichia coli and Arabidopsis, but inhibits root elongation in Arabidopsis seedlings. J. Exp. Bot. 57:3575–3582.

Zhao ZD, Tan L, Showalter AM, Lamport DT, and Kieliszewski, MJ, and 2002. Tomato LeAGP-1 arabinogalactan-protein purified from transgenic tobacco corroborates the Hyp contiguity hypothesis. Plant J. 31:431-444.

Zheng Z, Uchacz TM, and Taylor JL, 2001. Isolation and characterization of novel defence-related genes induced by copper, salicylic acid, methyl jasmonate, abscisic acid and pathogen infection in *Brassica carinata*. Mol. Plant Pathol. 2:159-169.

Zhu J-K, 2001. Cell signaling under salt, water and cold stresses. Curr. Opin. Plant Biol. 4:401–406.

Zhu JK, 2002. Salt and drought stress signal transduction in plants. Ann. Rev. Plant Biol. 53:247-273.